THE UNIVERSITY OF MANITOBA

EXTRACELLULAR ION FLUXES DURING GERM CELL DIFFERENTIATION AND OÖGENESIS IN *RHODNIUS PROLIXUS*

CHRISTOPHER STEPHEN BJORNSSON

A THESIS SUBMITTED TO THE FACULTY OF GRADUATE STUDIES

IN PARTIAL FULFILLMENT OF THE REQUIREMENTS FOR THE DEGREE

OF DOCTOR OF PHILOSOPHY

DEPARTMENT OF ZOOLOGY

WINNIPEG, MANITOBA

THE UNIVERSITY OF MANITOBA

FACULTY OF GRADUATE STUDIES

*****

COPYRIGHT PERMISSION PAGE

EXTRACELLULAR ION FLUXES DURING GERM CELL DIFFERENTIATION AND OÖGENESIS IN *RHODNIUS PROLIXUS*

BY

CHRISTOPHER STEPHEN BJORNSSON

A Thesis/Practicum submitted to the Faculty of Graduate Studies of The University of Manitoba in partial fulfillment of the requirements of the degree of

Doctor of Philosophy

ABSTRACT

The roles of extracellular ionic fluxes that accompany oögenesis are poorly understood. The telotrophic meroistic ovarioles of *Rhodnius prolixus* provide an excellent model to address this problem with the exaggerated morphological and physiological polarity between their syncytial nurse cells and oöcytes. In view of the cellular importance and pleiotropic effects of intracellular pH and Ca^{2+} dynamics, the corresponding extracellular H^+ and Ca^{2+} fluxes were measured non-invasively, at numerous positions along the ovariole throughout an entire oögenesis cycle, using a self-referencing ion-selective probe. Prominent H^+ efflux occurred at interfollicular stalks separating adjacent follicles, and changed over the course of oögenesis. This H^+ efflux appeared prior to vitellogenesis and stalk formation in the adjacent posterior follicle; efflux peaked during midvitellogenesis and declined during late vitellogenesis. H^+ efflux was also observed over follicle cells forming specialized regions of the chorion. Proton fluxes around 5^{th} instar ovarioles also undergo dynamic changes, which appear to correspond to germ cell differentiation events, as nurse cell and oöcyte fates are defined. Extracellular Ca^{2+} fluxes were also measured around individual ovarioles. Although steady, stage-specific Ca^{2+} fluxes significantly greater than background noise were not detected, increased variability in flux near the posterior surface of the T-1 follicle during later stages may indicate signalling activity related to interfollicular feedback regulation during this period. In order to understand the molecular basis of extracellular ion fluxes, immunofluorescent labelling of selected H^+ and Ca^{2+} pumps and channels was

performed. Expression was predominantly restricted to the somatic follicle cells. The proton pump, H^+/K^+-ATPase, was increasingly expressed by somatic cells as the follicle grew, although no qualitative differences were evident among different populations of cells. Ca^{2+} pumps and an L-type calcium channel were expressed differently by follicle cells during late previtellogenesis, in a pattern that became more complex as the follicle matured. Regional differences in calcium transport protein expression may mark areas of restricted intercellular communication. This is the first study describing extracellular H^+ and Ca^{2+} fluxes during an oögenesis cycle and during formation of the adult ovariole, providing greater understanding of the ionic and molecular basis of bioelectric currents during oögenesis.

ACKNOWLEDGMENTS

First and foremost, thank you Doc; everything I have become in the lab I owe to you. You took me on when I was ready to abandon science and revived my interest with your tireless enthusiasm. If I can part with a shadow of the example you've set I'll be extremely fortunate. Thank you for showing me the true face of the black dog, for the opportunity to teach, and for your patience. Thanks to Drs. Hara, Wiens, & Worobec for providing many helpful comments as well as a sense of direction throughout this project. Thanks as well to Dr. Woodruff; your comments on the thesis helped immensely and your papers were always an inspiration. I am grateful to Dr. Runtao He for the generous use of the confocal microscope and western blot equipment, and to Garrett Wong for his insight and expertise in troubleshooting western blots. I owe John Brubacher, Dr. Hare, and Dr. Gillis my sanity after they helped me navigate the statistical wasteland. Thanks as well to Roxane Graham for livening up the lab. I am grateful to Bill Diehl-Jones for much-appreciated conversations that helped me come to grips with the probe. I owe a great debt of gratitude to Al Shipley and Eric Karplus for helping me troubleshoot the probe, and for developing new software solutions to improve it. I am deeply indebted to Eric Johnson for his assistance in installing the isolation transformer that allowed me to see and eliminate system noise for the first time. I am grateful to Dr. Joe Kunkel for teaching me more about the proper application of the probe. Thanks to the old guard, for keeping me preoccupied and honest during the early years: Ian 'I'm your Daddy's Daddy' McIntyre, Ernie 'Clam Boy' Watson, 'Baybee' Bruce Adams, Fred 'Chachi' Laberge, and Mike 'Passport Party' Goodyear, who managed to collect every stamp and

still defend his thesis. I owe a special debt of gratitude to Ernie and Shannon, for enduring one more thesis-writing session under their roof. To my family, for getting me here, taking an interest in something completely foreign, and for always humouring and supporting me. Finally, to Cassey, for tolerating my constant distraction, for patience above and beyond the call of duty, and for giving me a reason to be; for sushi, rock climbing, covered bridges and braving the ocean in homebuilt kayaks. You're crazy!

TABLE OF CONTENTS

LIST OF FIGURES

CHAPTER 1

CHAPTER 2

CHAPTER 3

CHAPTER 4

LIST OF TABLES

LIST OF ABBREVIATIONS

ABP.....actin-binding protein

ADF.....actin depolymerizing factor

Ca^{2+}.....free calcium ion

cADPR.....cyclic adenosine diphosphate receptor

CaM.....calmodulin

CaMK.....calmodulin-dependent multiprotein kinase

cAMP.....cyclic adenosine monophosphate

CICR.....calcium-induced calcium release

CREB.....cAMP response element binding protein

DAG.....diacylglycerol

DHPR.....dihydropyridine receptor

dpf.....days post-feed

E_m.....membrane potential

ER.....endoplasmic reticulum

FC.....follicle cell

GJ.....gap junction

GVBD.....germinal vesicle breakdown

H^+.....hydrogen ion

IP_3.....inositol 1,4,5-trisphosphate

ISP.....ion-selective probe

LIX.....liquid ionophore exchanger

MAPK.....mitogen-activated protein kinase

MAPs.....microtubule-associated proteins

MDCK.....Madin-Darby canine kidney (epithelial cell line)

MPF.....maturation promoting factor

mRNA.....messenger ribonucleic acid

MTOC.....microtubule organizing centre

NC.....nurse cells

O.....oocyte

PIP_2.....phosphatidylinositol bisphosphate

PKC.....protein kinase C

PLC.....phospholipase C

PMCA.....plasma membrane calcium ATPase

RACC.....receptor-activated calcium channel

RNA.....ribonucleic acid

SERCA.....sarco-endoplasmic reticulum calcium ATPase

SOC.....store-operated channel

SR.....sarcoplasmic reticulum

V-ATPase.....vacuolar ATPase

VOCC.....voltage-operated calcium channel

GENERAL INTRODUCTION

This thesis presents an investigation of the ionic and molecular basis of bioelectric currents around 5th instar and adult ovarioles of the hemipteran, *Rhodnius prolixus*. It is hoped the results presented here will advance our understanding of the role these currents may play in regulating various aspects of ovarian development and oögenesis, including the establishment and maintenance of nurse cell-oöcyte polarity, nurse cell-oöcyte transport, follicle cell differentiation, and the physiological feedback mechanisms controlling oögenesis. Two key regulatory ions, H^+ and Ca^{2+}, were chosen because of their roles in modulating a number of cellular processes in oögenesis, particularly intercellular communication and cytoskeletal regulation. The literature review will focus on the importance of these ions to cell processes relevant to oogenesis, on the molecular basis for bioelectric currents, and on oogenesis in the model system, *Rhodnius prolixus*.

In the first chapter, the spatial and temporal patterns of extracellular H^+ fluxes around adult *Rhodnius* ovarioles are described. A number of potential roles for these fluxes are explored based on their location and the timing of their appearance during an oögenesis cycle. In addition, differences in H^+ flux according to orientation based on an early morphological marker of oöcyte polarity, the offset germinal vesicle, are discussed.

In the second chapter, the spatial and temporal dynamics of extracellular Ca^{2+} fluxes around adult *Rhodnius* ovarioles are described. The relationship of these fluxes to the establishment of a recently discovered steady intercellular Ca^{2+} gradient (Bjornsson,

Miller, & Huebner, submitted), and to transient Ca^{2+} events during oögenesis is considered.

In the third chapter, the presence and timing of extracellular H^+ and Ca^{2+} fluxes around 5th instar ovarioles, and the potential roles these fluxes play in nurse cell-oöcyte differentiation and formation of the adult ovariole are discussed. The initial differentiation of the syncytial germ tissue into nurse cells and oöcytes is central to *Rhodnius* oögenesis, and these experiments may help us to understand how nurse cell-oöcyte differences are established and regulated.

The fourth chapter describes an investigation of the molecular basis of transcellular H^+ and Ca^{2+} fluxes using antibodies against three ion transport proteins: H^+/K^+-ATPase, plasma membrane Ca^{2+} ATPase (PMCA), and an L-type Ca^{2+} channel, which previous studies by Diehl-Jones & Huebner (1992) and O'Donnell (1986) suggested is present in *Rhodnius* ovarioles. The relationship between observed extracellular fluxes and the distribution of ion transport proteins is considered.

THE BIOLOGY OF *RHODNIUS PROLIXUS*

This species is a member of a remarkable group of insects [Triatominae (Hemiptera, Reduviidae)] which on one hand provide excellent research material to investigate a host of cell biology problems, and on the other hand cause misery to some 15 million people in the America's who contract Chagas disease. These are blood-sucking insects found from the southern USA through Central America and into South America to central Argentina and Chile. They feed primarily on small terrestrial and arboreal mammals, some birds, and several species have colonized human habitations. These insects are a vector for the blood protozoan parasite, *Trypanosoma cruzi*, the causative agent for Chagas' disease, which is estimated to infect 15 million people in the Americas and to cause some 50,000 deaths annually.

The *Rhodnius* life cycle is as follows. There are 5 larval instars with a blood meal required to progress to the next moult. The 5th instar moults to the adult and subsequent blood meals provide for egg production and perpetuation of the life cycle. In *Rhodnius prolixus* the life cycle is about 90-120 days depending on temperature and humidity. Oogenesis is triggered by the blood meal and the subsequent hormonal cascade. Each ovary consists of 7 ovarioles, the functional unit of the ovary. *Rhodnius* ovarioles are an excellent model for studying the cell biology of oogenesis.

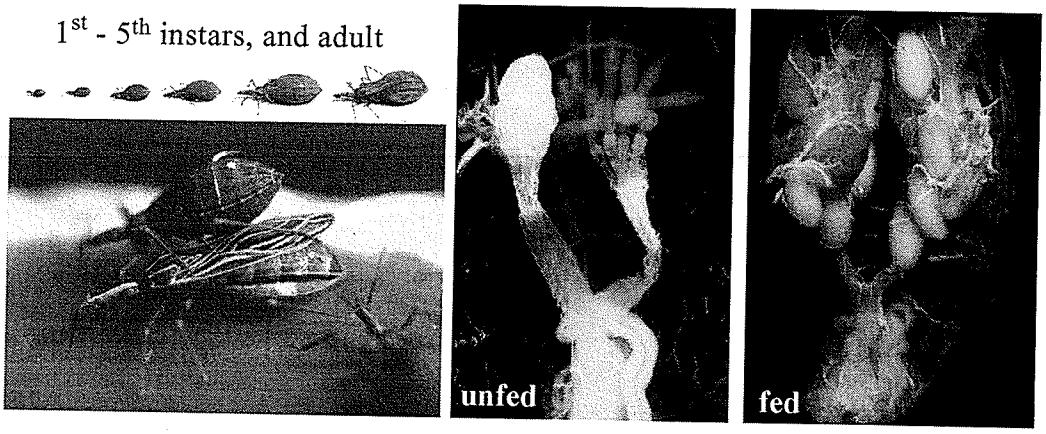

LITERATURE REVIEW

The oöcyte is a truly remarkable cell. During oögenesis the developing egg stockpiles enough synthetic material to last the future embryo through early development, and sets aside maternal determinants necessary to lay out the blueprint for the future organism, including body axes and initial segmentation patterns. While it is impressive enough that these stores and determinants are localized in the polarized oöcyte during oögenesis, it is perhaps even more so in insect meroistic ovarioles, where most of these products are not synthesized by the oöcyte itself; rather they are produced by nurse cells and transported to the growing oöcyte via intercellular bridges. The synthetically quiescent oöcytes undergo a considerable transformation during vitellogenesis, when yolk products synthesized by the fat body and ovarian follicle cells are actively endocytosed (Telfer, 1965; Huebner *et al.*, 1975; Isaac & Bownes, 1982; Telfer *et al.*, 1982; Melo *et al.*, 2000). Nurse cells and oöcytes stem from a common progenitor and retain cytoplasmic continuity with each other after undergoing incomplete cell divisions (Telfer, 1975; Lutz & Huebner, 1979; Deng & Lin, 2001). The intricate relationship between these two cell types raises a number of intriguing questions: How can nurse cells and oöcytes, sharing a common cytoplasm, establish and maintain such profound differences in structure and function? How is unidirectional transport accomplished? And what are the mechanisms regulating a follicle's entry into vitellogenesis?

The accentuated polarity between nurse cells and oöcytes in insect meroistic ovarioles extends to differences in transcriptional and synthetic activity (Telfer, 1975;

Woodruff & Telfer, 1998), cytoskeletal architecture (Huebner & Gutzeit, 1986; McPherson & Huebner, 1993; Riparbelli & Callaini, 1995), and cell membrane activity and bioelectrical properties (Woodruff *et al.*, 1986; Woodruff & Telfer, 1990, 1994; O'Donnell & Sharda, 1994). Research in each of these areas offers a unique perspective into the physiological state of these cells, and the establishment and maintenance of cell polarity. In particular, regional differences in intracellular ion activity possess the capability to regulate many of the other polarized elements typical of meroistic ovarioles. Furthermore, as second messengers involved in intracellular signalling, ions like Ca^{2+} may also be involved in coordinating nurse cell-oöcyte interactions and follicle growth. These factors make bioelectrical properties of insect meroistic ovarioles interesting candidates for the regulation and coordination of a number of events during oögenesis.

This thesis focuses on the extracellular dynamics of two key regulatory ions, hydrogen (H^+) and calcium (Ca^{2+}), during oögenesis in the telotrophic ovariole of *Rhodnius prolixus*. These extracellular ion movements are especially interesting because of what they can tell us about events inside the cells involved. As a result, the literature review will feature a selective review of the roles and regulation of H^+ and Ca^{2+} in a number of systems, following a brief overview of the model system: the telotrophic ovariole of the hemipteran, *Rhodnius prolixus*.

The Insect Ovariole

Insect Ovary Classification

Insect ovaries are classified as either panoistic, when germ cell progenitors give rise solely to oöcytes, or as meroistic when germ cells differentiate into two cell types, nurse cells and oöcytes (Telfer, 1975; King & Buning, 1985; Buning, 1994). In meroistic ovaries, mitochondria, ribosomes, various RNAs, and proteins are produced by endopolyploid nurse cells and transported to the oöcyte, typically arrested in metaphase I (Gilbert, 2000), via cytoplasmic bridges (Vanderberg, 1963; Davenport, 1974; Hyams & Stebbings, 1977; Huebner, 1981a). Meroistic ovaries are further divided into polytrophic and telotrophic types depending on how the nurse cells are organized. In polytrophic ovaries, nurse cells and oöcytes arising from incomplete cell division travel together in a single follicle as the oöcyte develops. Each germ cell cluster is surrounded by a simple follicular epithelium, which is in turn surrounded by a basal lamina that helps shape the growing follicle (Gutzeit & Haas-Assenbaum, 1991). In telotrophic ovaries, common to hemiptera, polyphagous coleoptera, and megaloptera (Buning, 1994), nurse cells form a syncytium occupying a common chamber, the tropharium, where they collectively synthesize material to supply developing oöcytes (Huebner & Anderson, 1972c). Oöcytes develop in a highly regulated fashion in an 'assembly line' at the posterior of the ovariole, and are connected to nurse cells throughout previtellogenesis and in some cases into vitellogenesis via extended intercellular bridges, the trophic cords. These cords are heavily enriched in microtubules, which facilitate transport (Vanderberg, 1963;

Macgregor & Stebbings, 1970; Telfer, 1975; Huebner, 1981b; Huebner, 1984; Hyams & Stebbings, 1977) of mitochondria (Harrison, 1997; Stebbings & Hunt, 1987), ribosomes (Stebbings, 1971), and RNAs (Stephen *et al.*, 1999; Hurst *et al.*, 1999; Stebbings, 2001). As in other meroistic types, morphological differences between nurse cells and oöcytes correspond to functional and physiological differences between these syncytial cells, even though they share a common cytoplasm. In contrast to polytrophic types, the polarity between nurse cells and oöcytes in telotrophic ovarioles spans the entire ovariole.

Germ Cell Differentiation in *Rhodnius prolixus*

Differences between nurse cells and oöcytes appear early in the development of telotrophic ovaries in comparison to polytrophic systems. In polytrophic ovaries, early signs of polarity between nurse cells and oöcytes develop in the adult, within each syncytial germ cell cluster, through coordinated divisions and somatic cell interaction as they move away from the germline stem cell from which they arose (reviewed by Deng & Lin, 2001). In the telotrophic ovarioles of a hemipteran, *Rhodnius prolixus*, nurse cell-oöcyte determination occurs during the last (5^{th}) larval instar (Lutz & Huebner, 1980).

Following a blood meal, germ cell compartments increase in cell number through mitotic division during the proliferative stage, which occurs 1-8 days post-feed (dpf)(Lutz & Huebner, 1980). Differences in nuclear structure and cytoplasmic composition between nurse cells and oöcytes appear during the early differentiation stage (9-15 dpf), when a posterior zone of cells lacking prominent nucleoli and possessing lighter cytoplasmic

staining than the anterior (nurse) cells can be identified. By the end of the early differentiation phase, three distinct zones of nurse cells can be distinguished, and some amount of nurse cell-oöcyte transport appears to have occurred (Lutz & Huebner 1980). During the late differentiation stage (16-21 dpf), posterior nurse cell cytoplasm becomes increasingly basophilic, and fusion of nurse cell membranes occurs (Lutz & Huebner, 1981). Somatic prefollicular cells begin to invade the oöcyte region, and several oöcytes initiate previtellogenic growth. During this period, the trophic core forms at the centre of the tropharium through growth and fusion of ring canals to form an F-actin mesh (Yeow, 1995; Huebner & Gutzeit, 1986), and microtubule arrays reorganize to form nutritive cords connecting nurse cells and oöcytes (Lutz & Huebner, 1980; Valdimarsson & Huebner, 1989). Once the 5th instar is ready to moult at approximately 21 dpf, the ovarioles present the appearance of the adult structure, and await the first adult blood meal and hormonal stimuli to initiate oögenesis (Wigglesworth, 1936; Davey, 1997). The initial differentiation of the syncytial germ tissue into nurse cells and oöcytes is central to *Rhodnius* oögenesis, and highlights the need to understand how nurse cell-oöcyte differences are established and regulated.

Oögenesis and Follicle Cell Differentiation in *Rhodnius prolixus*

Oögenesis is highly coordinated in *Rhodnius*, where only a single follicle, the posterior or terminal (T) follicle, enters vitellogenesis by initiating yolk uptake from the haemolymph and follicle cells (Huebner & Anderson, 1972b; Pratt & Davey, 1972;

Huebner, 1984). Anterior follicles are arrested in a previtellogenic state, until the T follicle completes vitellogenesis and begins chorionation (eggshell formation); at this point the follicle next in line is triggered to initiate vitellogenesis. The nature of this feedback suggests it likely originates from within the ovariole, and it has been suggested that the T oöcyte trophic cord may prevent further growth of more anterior follicles (Huebner, 1981a). Additionally, a bioelectrical feedback may be involved (Diehl-Jones, 1991).

As the oöcyte grows, the associated somatic follicular epithelium also undergoes considerable change. The initially uniform population of follicle cells differentiates giving rise to specialized groups that will determine the route of yolk uptake and later define specialized regions of the chorion essential to fertilization and hatching. Identification of the regulatory mechanisms responsible for coordinating these events would significantly advance our understanding of oögenesis in *Rhodnius* as well as in many other organisms. Intracellular ionic differences are a potential means by which ovarioles may coordinate oögenesis. In order to understand how this may be accomplished, an overview of the major stages of oöcyte growth and the time-course of potentially ion-regulated events must first be presented.

Previtellogenesis

In the prefollicular zone of the ovariole, follicles are established with the proliferation of follicle cells that form a simple epithelium surrounding the developing oöcyte (Huebner & Anderson, 1972a). When the previtellogenic oöcyte is 300-400 μm in length, an interfollicular stalk of cells derived from the follicular epithelium begins to

form between adjacent follicles. During this period, follicle cells express gap junctions (GJs) coupling them to the oöcyte and each other, permitting coordination of cell activity (Huebner, 1981a; Huebner & Injeyan, 1981; Telfer *et al.*, 1982). Although GJ plaques have only been found ultrastructurally when the oöcyte reaches about 400 μm in length, dye coupling can be demonstrated between follicle cells and oöcytes around 200 μm in diameter (Huebner, unpublished results). Previtellogenic oöcyte growth is the result of materials contributed by the nurse cells, including proteins, ribosomes, various RNAs, and mitochondria, which are transported to the oöcyte via elongate, microtubule-rich trophic cords (Vanderberg, 1963; Macgregor & Stebbings, 1970; Telfer, 1975; Huebner, 1981b; Huebner, 1984; Hyams & Stebbings, 1977).

Vitellogenesis

Vitellogenesis is marked by a number of changes in both oöcytes and follicle cells as the oöcyte begins to actively take up yolk precursors from the haemolymph via receptor-mediated endocytosis (Telfer, 1965; Telfer *et al.*, 1982). Follicle cells play an important role in regulating vitellogenesis by permitting vitellogenin access to the oölemma (Huebner & Anderson, 1972a; Pratt & Davey, 1972, Huebner & Injeyan, 1980). In fact, even previtellogenic oöcytes in the telotrophic ovarioles of another hemipteran, *Dysdercus intermedius*, are capable of yolk uptake if the follicle cell layer is mechanically removed (Dittmann & Bizcowski, 1995). In *Rhodnius*, columnar follicle cells at the anterior pole of the follicle form a layer that is relatively impermeable to larger molecules, and yolk uptake occurs across the lateral and posterior surfaces of the follicle where large spaces develop between cuboidal follicle cells (Huebner & Anderson,

1972a). Lateral follicle cell shape changes are a result of cytoskeletal rearrangements (Abu-Hakima & Davey, 1977b) and of volume changes caused by Na^+/K^+-ATPase activation via juvenile hormone (Abu-Hakima & Davey, 1977a, 1979; Huebner & Injeyan, 1980), in a process mediated by the Ca^{2+}-sensitive enzyme, protein kinase C (Sevala & Davey, 1989, 1993). Near the end of vitellogenesis the trophic cord closes, and the microtubule array begins to disassemble as the cord retracts towards the tropharium (Huebner, 1981).

Choriogenesis

Once vitellogenesis is complete the follicle cells restructure and initiate synthesis and secretion of the secondary egg coat, or chorion (Huebner & Anderson, 1972a). Specialized regions of the chorion, including the main body, neck, rim, micropyles, seal, and cap are laid down by specialized groups of follicle cells that become distinguishable during late vitellogenesis based on morphological features (Beament, 1946, 1947). Of these cell groups, the micropyle and pseudomicropyle cells are unique in that they create extended channels in the chorion by maintaining long, slender, actin-rich processes (Huebner & Bjornsson, 2002) that are withdrawn once the chorion is secreted. Once chorionation is complete, the mature egg leaves the ovariole and travels down the oviduct to be fertilized and deposited, while the follicle cells that were once associated with it begin to degenerate. The former T-1 follicle becomes the new T follicle, and a new oögenesis cycle begins.

Cytoskeletal Organization during Oögenesis in *Rhodnius prolixus*

Over the course of oögenesis, the cytoskeleton undergoes considerable change in both oöcytes and follicle cells. Dynamic restructuring of F-actin and microtubules has been studied in depth in *Rhodnius*, and deserves special attention here.

In *Rhodnius*, the oöcyte undergoes a dramatic restructuring of the cortex concomitant with vitellogenesis, affecting both the actin and microtubule cytoskeleton (McPherson & Huebner, 1993). While actin is barely detectable in early previtellogenic oöcytes (50-150 μm), a large G-actin pool is present in the cortex by mid-previtellogenesis (150-250 μm), and a limited meshwork of cortical actin develops (McPherson & Huebner, 1993). This presumably supports the growth of short microvilli that appear during late previtellogenesis (250-350 μm). During vitellogenesis, microvilli increase in size, and three distinct regions of the oölemma can be identified based on the observed microvillar pattern: anterior and lateral aspects of the oöcyte, separated by a band near the anterior pole (McPherson & Huebner, 1993). Regional differences in microvillar pattern appear to be influenced by the follicle cells. Longer microvilli are seen where follicle cells are not in close proximity to the oölemma, especially over the lateral surface, while short microvilli couple the oöcyte to follicle cells (McPherson & Huebner, 1993). F-actin bundles have also been observed in trophic cords near the plasma membrane (McPherson & Huebner, 1993), with a banding pattern reminiscent of sarcomeric structure (Huebner, unpublished results).

Oöcyte microtubules spread throughout the cortex, parallel to the surface (McPherson & Huebner, 1993). During vitellogenesis the number of microtubules in the lateral cortex declines, with a clear decline in microtubule number at the junction

between anterior and lateral regions (McPherson & Huebner, 1993). An increased number of microtubules, similar to that seen in the anterior pole, is also seen in the posterior pole of the oöcyte. As the trophic cord closes during late vitellogenesis and retracts towards the tropharium, the prominent microtubule array within the cord begins to disassemble (Hyams & Stebbings, 1979; Huebner, 1981a).

In the follicle cells, cytoskeletal reorganization accompanies the morphological changes observed during differentiation (Watson & Huebner, 1986). Microfilament arrays are not prominent in prefollicular cells, which develop short microtubules running parallel to the long axis of each cell along the lateral surfaces, and along the basal surface. In previtellogenic follicles, microtubules occupy the lateral cortex at the centre of the cell, parallel to the long axis. A subplasmalemmal band of microfilaments is present along the basal follicle cell surface, associated with the adherens junctions (Watson & Huebner, 1986). In vitellogenic follicles, cytoskeletal organization in the anterior columnar epithelium resembles that in previtellogenic follicles, while shorter microtubules in lateral follicle cells are restricted to discrete bundles in various orientations throughout the cytoplasm. Notably, microtubules in the anterior follicle cells in vitellogenic follicles are longer and denser than in any other stage (Watson & Huebner, 1986).

During choriogenesis, follicle cells exhibit a diffuse basolateral microtubule distribution, and microfilaments are generally not prominent (Watson & Huebner, 1986). However, one of the follicle cell populations involved in sculpting the specialized features of the cap edge and rim of the main body undergoes considerable rearrangement of its actin cytoskeleton coincident with H^+ efflux, becoming very long and narrow, with

a slender process rich in F-actin filaments (Huebner & Bjornsson, 2002) that occupy channels in the forming chorion (Beament, 1947, Huebner & Bjornsson, 2002). These cells are distributed within a single row completely encircling the rim, where they form the pseudomicropyles and true micropyles.

The Importance of Ions to Cell Physiology and Development

Among the physiological differences between nurse cell and oöcyte compartments, regional differences in intracellular ion activity possess the power to impact a broad spectrum of cellular functions relevant to oögenesis. Many cellular processes are influenced by ions in one way or another. Sodium and potassium ions commonly act as counter-ions and regulate volume changes and membrane properties; and Mg^{2+} is essential to stabilize the phosphate groups of nucleotides (Vogel, 1994). In contrast, H^{+} and Ca^{2+} are key regulators of myriad cellular events, often working in concert to coordinate these events. These ions were chosen as the subject of my research because of their involvement in a number of cell processes important to oögenesis; the following discussion will focus on how these ions are managed by cells, and their roles in physiology and development.

The Roles of pH in Cell Physiology & Development

By altering intracellular pH (pH_i) levels, hydrogen ion (H^+, proton) dynamics can coordinate a broad range of cellular events. While some proteins, purified actin for example, are relatively insensitive to pH, they are often affected by other interacting pH-sensitive proteins. Many of the processes involved in early development are influenced by changes in pH (ΔpH), and developmental models have proven to be ideal subjects for investigating the regulation and roles of ΔpH_i. Since these models are an integral part of research in this area, they are woven into the description of pH regulation of cellular events below.

Metabolic Activity

Hydrogen ions are an integral part of the metabolic activity of eukaryotes, since the electrochemical gradient established by H^+ transport across the inner mitochondrial membrane is fundamental to ATP production. For ions and other molecules smaller than about 5000 Da the intermembrane space is essentially continuous with the cytosol due to the presence of mitochondrial porin protein (Lodish *et al.*, 2000), although H^+ transported into this space does not alter cytosolic pH substantially. Similarly, the acidifying effects of metabolism are generally misunderstood; careful examination of the H^+ balance during aerobic respiration shows that H^+ are not generated, and anaerobic metabolism only generates H^+ when coupled with the downstream hydrolysis of ATP (see Busa & Nuccitelli, 1984, for an excellent review).

Nevertheless, H^+ does influence several aspects of metabolism. Sea urchin eggs provide one of the best-studied examples; in response to sperm binding, the egg releases 'fertilization acid' into the extracellular space, elevating pH_i from ~6.8 to 7.3 (Shen & Steinhardt, 1978). This event sets in motion a suite of changes collectively referred to as the 'late events' of fertilization (Busa & Nuccitelli, 1984). The rise in pH causes, among other things, an increased rate of protein synthesis (Winkler & Steinhardt, 1981; Winkler, 1982), as well as an increased amount of unmasked mRNA (Brandis & Raff, 1979). pH changes in a variety of systems have also been demonstrated to have direct bearing on basic metabolic pathways by modulating key rate-limiting enzymes including phosphofructokinase (Trivedi & Danforth, 1966; Fidelman *et al.*, 1982), glucose-6-phosphate dehydrogenase (Aune & Epel, 1978), phosphoglycerate mutase (Setlow & Setlow, 1980), and glycogen catabolism generally (Baginsky, 1981).

An extreme example of metabolic regulation via pH_i occurs in cryptobiotic organisms including bacterial spores (Setlow & Setlow, 1980), yeast (Barton *et al.*, 1980; Busa, 1982), and some crustacean embryos. In the brine shrimp *Artemia salina*, a pH_i increase of 1.6 units is observed, triggering a transition from dormancy to a metabolically active state (see Clegg & Conte, 1980, for review). Generally, lower pH_i is associated with decreased metabolic activity, and higher pH with increased metabolic activity.

During oögenesis in the polytrophic ovarioles of *Hyalophora*, a rise in pH_i accompanies the onset of vitellogenesis, where it may act to increase oöcyte metabolic activity in preparation for the active endocytosis of yolk precursors from the haemolymph (Woodruff & Telfer, 1990).

Gap Junction Activity

Gap junctions are hydrophilic channels between cells, allowing passage of small molecules including ions, signalling molecules (IP_3, cAMP), and small metabolites. Acidification of the cytosol leads to inactivation of gap junctions (GJs) in a range of vertebrate and invertebrate tissue by partially or completely closing the pore (Perrachia & Perrachia, 1980b; Giaume *et al.*, 1980; Bohrmann & Haas-Assenbaum, 1993; Rozental *et al.*, 2001; Levin, 2002; etc.). The effects of pH are conserved despite differences in protein structure between vertebrates and invertebrates (Liu *et al.*, 1993; reviewed by Levin, 2002; Stebbings *et al.*, 2002). Vertebrate gap junctions are aggregates (plaques) of connexons, each a hexamer of connexin subunits, forming intercellular channels between cells (Lodish *et al.*, 2000). Connexons may be homo- or heteromeric, and different connexins exhibit variation in pH-sensitivity, allowing for varied, tissue-specific, and often subtle modulation of gap junctional coupling by ΔpH_i (Munz, 1988; Liu *et al.*, 1993; Francis *et al.*, 1999). Invertebrate systems express innexins, which are functional homologs of connexins even though they do not bear any sequence similarities (Phelan *et al.*, 1998; Stebbings *et al.*, 2002). A second and unrelated protein, ductin, has been identified that is associated with GJ plaques in mouse liver (Finbow *et al.*, 1987), the arthropod *Nephrops norvegicus*, mollusc embryos (Serras *et al.*, 1988), *Manduca* (Finbow *et al.*, 1994), and various tissues in *Drosophila* (Bohrmann & Bonafede, 2000). This identification is based primarily on immunolocalization and inhibition of GJ coupling using a polyclonal antibody raised against an 18 kDa antigen from *Nephrops* (Leitch & Finbow, 1990; Finbow & Pitts, 1993; Bohrmann, 1993). Ductin leads a dual life, having also been identified as one of the subunits composing the vacuolar H^+

ATPase (V-ATPase) associated with the plasma and endosomal membranes (Finbow *et al.*, 1995). The evidence linking ductin to GJs is not entirely compelling, since polyclonal antibodies may cross-react with related proteins, and considering the pH-dependence of many GJs, it is quite possible that inhibition of GJ coupling could in fact result from acidification of the cytosol through inhibition of V-ATPase activity, thereby inhibiting connexin- or innexin-based GJ communication instead of directly inhibiting GJs composed of ductin. Regardless of which proteins constitute GJs, acidification suppresses intercellular communication in general and in insect ovarioles specifically; for example, lowering pH_i in the oöcyte affects dye coupling in *Oncopeltus* (Anderson & Woodruff, 2001) and *Drosophila* (Bohrmann & Haas-Assenbaum, 1993).

Microfilament Assembly and Dynamics

Purified actin polymerizes rapidly and completely under a wide range of physiological pH conditions (Hatano *et al.*, 1969; Pollard & Weihing, 1974; Spudich, 1974; Bray & Thomas, 1976). Dynamic turnover of actin filaments *in vitro* is primarily mediated by actin-binding proteins (ABPs)(Tilney *et al.*, 1978), some of which are pH-sensitive. For example, actin depolymerizing factor (ADF)/cofilin severs F-actin filaments, increasing the number of free F-actin ends and increasing disassembly, thereby enhancing actin turnover in motile nonmuscle cells (Southwick, 2000). Severing proteins are important not only for cell locomotion (Svitkina & Borisy, 1998; Chen *et al.*, 2001) but also for cytokinesis (Rappaport, 1996), and presumably likewise in regulating constriction of adherens junctions during epithelial morphogenesis. ADF/cofilin are pH-sensitive enzymes, with highest affinity for actin around pH 8.0 (Southwick, 2000). Even

gelsolin, known for its Ca^{2+}-sensitive severing activity, can be activated in the absence of Ca^{2+} by sufficiently low pH (Lamb *et al.*, 1993).

Profilin has been identified as the pH-sensitive activator of F-actin formation during the acrosomal reaction in echinoderms, where alkalinization causes an explosive polymerization of actin (Tilney *et al.*, 1978). Profilin promotes microfilament growth by binding G-actin monomers and preventing their incorporation into the less stable (-)-end of actin filaments (Machesky, 1998). In addition, profilin/actin dimers bound to Vasp or Mena, both cell membrane-associated signalling and cytoskeletal anchoring proteins, act as nucleation sites for filament formation (Welch *et al.*, 1997). This and other membrane-cytoskeletal associations, for example α-fodrin (spectrin) and actin binding in Madin-Darby canine kidney (MDCK) cells (Huotari *et al.*, 1996), may be disrupted by cytosolic acidification.

Sea urchin eggs provide an excellent model for studying the effects of pH on F-actin formation. Intracellular alkalinization due to release of 'fertilization acid' promotes extensive cortical actin reorganization and formation of numerous elongated microvilli (Begg & Rebhun, 1979; Tilney & Jaffe, 1980). A detailed examination of microvillar formation has revealed that Ca^{2+} is required to bring about changes in the plasma membrane and F-actin formation, while the rise in pH promotes microfilament bundling (Begg *et al.*, 1982; Carron & Longo, 1982). Fascin acts as an F-actin crosslinker in sea urchin oöcyte microvilli (Kane, 1976; Bryan & Kane, 1978; Kurieshy *et al.*, 2002), and the activity of human fascin is heavily dependent on pH: inactivation due to phosphorylation is greatly enhanced under acidic conditions (Yamakita *et al.*, 1996). Unfortunately, while Yamakita *et al.* (1996) studied the effects of pH ranging from 5 to 7,

the effects of more alkaline conditions, similar to those following fertilization in sea urchins, were not investigated.

Although the effects of pH_i changes on microfilament dynamics during insect oögenesis have not been investigated to my knowledge, the initiation of vitellogenesis in *Rhodnius* follicles shares a number of similarities with the events during sea urchin fertilization. Previtellogenic *Rhodnius* oöcytes possess a large G-actin pool, which presumably fuels the extensive formation of microvilli across the oöcyte surface as vitellogenesis progresses (MacPherson & Huebner, 1993). It is possible that microvillar formation during vitellogenesis in *Rhodnius* is regulated by pH_i, as it is in sea urchin eggs during fertilization.

Microtubule Assembly and Dynamics

Purified microtubule extracts display optimal stability around pH 6.9 (Olmsted & Borisy, 1975; Burton & Himes, 1978). Microtubule assembly kinetics can be described by a first-order equation, and the order of the equation does not change with ΔpH; however, the critical concentration of tubulin subunits necessary to initiate and sustain microtubule assembly increases with increasing pH due to accelerated disassembly (Barton *et al.*, 1987). Even so, a stable steady state can be achieved up to pH 8.3 (Galella & Smith, 1979; Regula *et al.*, 1981). In addition, the dynamics of tubulin-GTP interactions necessary for microtubule elongation and stability favour assembly at lower pH (Hamel *et al.*, 1986).

The situation *in vivo* is markedly different, however. During sea urchin fertilization, microtubule asters form in response to pH elevation from ~6.8 to 7.3

(Schatten *et al.*, 1985; Suprenant, 1989); the threshold for aster formation appears to be pH 7.0 (Harris & Clason, 1992; Hamaguchi & Hamaguchi, 2001). Suppression of elevated pH inhibits spindle pole formation, while a return to unfertilized pH levels results in microtubule disassembly. Schatten and coworkers (1985) attributed the disparity between *in vivo* and *in vitro* microtubule dynamics to the presence of microtubule organizing centres (MTOCs) that stabilize the microtubule (-)-ends most prone to disassembly under alkaline conditions. This was later confirmed by Suprenant (1991), who found that with the (-)-ends stabilized, (+)-ends are prone to regulation via subtle changes in pH.

Several microtubule-associated proteins (MAPs) are also affected by pH. Carr & Acott (1990) have identified a MAP2 protein from bovine sperm, whose phosphorylation is pH-regulated. In neurons and epithelial cells, low pH induces anterograde redistribution of late endocytic structures (Parton *et al.*, 1991) and fragmentation and dispersion of the Golgi apparatus in interphase cells (Yoshida *et al.*, 1999); transport of endosomes and lysosomes is inhibited by suppression of kinesin heavy chain expression in neurons, suggesting their activation may be pH-dependent (Feiguin *et al.*, 1994). Chromosomal movement, driven by (-)-end motors, is also inhibited by low pH during sea urchin fertilization (Ford & Roberts, 1983; Shatten *et al.*, 1985, 1986). Activation of sperm motility requires elevated pH_i to activate axonemal dynein (Shapiro *et al.*, 1990); a similar role for pH in activating cytoplasmic dynein has also been described (Parton *et al.*, 1991; etc.). In contrast, acidification (from pH 7.2 to 6.8) appears to activate kinesin (Verhey *et al.*, 1998). Thus, it seems that pH can coordinate the activity of these two opposing microtubule motors.

Cell Membrane Energization and Dynamics

In many insects, electrogenic H^+ pumps associated with the cell membrane contribute to the resting membrane potential (E_m) (Dittmann, 1997; Haley & O'Donnell, 1997; Harvey & Wieczorek, 1997; Weiczorek *et al.,* 1999). Similarly, an H^+-dependent pump helps establish E_m and regulates pH_i in vitellogenic follicles of *Rhodnius* ovarioles (O'Donnell & Sharda, 1994). H^+-pump activity may be linked to specific events during oögenesis; for example Woodruff & Telfer (1990) found that prior to visible accumulation of yolk spheres in *Hyalophora* ovarian follicles, oöcyte pH rose from 6.7 to 7.4, gap junctional coupling was established between follicle cells and the germ syncytium, and the membranes of both nurse cells and oöcytes hyperpolarized. Cell membranes hyperpolarized in nurse cells more than in oöcytes, creating a ~5 mV difference between the compartments and resulting in the charge-dependent restriction of protein transport. While the role of Ca^{2+} in establishing an ionic gradient between nurse cell and oöcyte compartments has been described (Woodruff & Telfer, 1994; Woodruff *et al.*, 1998), pH also plays a key role. Ovarioles treated with azide, a metabolic inhibitor, lose gap junctional coupling and membrane hyperpolarization, presumably due to inactivation of an H^+ extrusion mechanism (Stynen *et al.*, 1988).

In addition to the effects of H^+ pumps on E_m, changes in pH_i may also result in alterations in membrane structure and function in their own right. For example, the release of fertilization acid in sea urchins introduces an increase in cell membrane K^+ conductance (Steinhardt & Mazia, 1973; Shen & Stenhardt, 1980). The mechanisms underlying this event are still unknown, and may involve activation of channels already present, or increased expression through transcriptional or translational control.

Acidification of endosomal vesicles

While acidification of endosomal and lysosomal vesicles is a common feature of most eukaryotic cells, it is particularly important in oögenesis since it regulates the uptake and synthesis of yolk. Fusion of smaller yolk vesicles into larger, more membrane-efficient spheres requires acidification of the vesicle interior to release vitellogenin from its receptor, so that excess membrane can then return to the oöcyte surface (DiMario & Mahowald, 1986). This process appears to involve H^+-pump activity, likely a V-ATPase (DiMario & Mahowald, 1986; O'Donnell & Sharda, 1994), to move H^+ from the oöplasm into the yolk spheres. Intravesicular acidification is required for subsequent processing of the endosomal compartments in a number of species (Nordin *et al.*, 1990, 1991). In the blowfly, *Phormia regina*, acidification occurs as vitellogenin deposition diminishes, and chorionation begins (Nordin *et al.*, 1991). In other insects, including *Ornithodorus moubata* and *Blattella germanica* (Nordin *et al.*, 1991), yolk vesicle acidification is delayed until yolk degradation and utilization begin during embryogenesis.

Signalling

pH_i can modulate the activity of many conventional signalling pathways. The ubiquitous regulatory and signalling molecule, calmodulin, binds calcium in a pH-dependent manner (Busa & Nuccitelli, 1984; Danylovych & Tuhai, 2001; but see Ogawa & Tanokura, 1984), resulting in pH modulation of processes and pathways downstream of calmodulin activation. Cyclic AMP levels are also sensitive to pH (Reynolds & Haugaard, 1967; Yajima & Ui, 1975), due primarily to the pH-sensitivity of adenylate

cyclase (Johnson, 1982), affecting pathways that incorporate this second messenger. In addition, the JAK-STAT pathway is modulated by the cell's redox potential, through JAK inactivation via disulfide bond formation (reviewed in Duhe *et al.*, 2001), a reaction that may be regulated on pH.

The Roles of Calcium in Cell Physiology & Development

As stated by Loewi, 'calcium is everything' (Loewenstein, 1999). Calcium plays a role in fertilization, secretion, contraction, proliferation, differentiation, neural signalling, intercellular communication, learning, and cell death, by regulating a range of cellular events during each of these general processes (Berridge, 1997a). In response to hormonal and developmental cues (McDonald *et al.*, 1976; Bygrave, 1978a), calcium operates as a second messenger through activation of kinases, phosphatases, proteases, and transcription factors. Ca^{2+} also regulates motor protein activity, and is well known for its role in excitation/contraction coupling in contractile tissues, although its range in this regard extends to all cells.

Most intracellular Ca^{2+} ($[Ca^{2+}]_i$) is bound to cytosolic proteins, stored in intracellular compartments (primarily ER and mitochondria), or associated with oxyanionic phospholipids (PIP_2, etc.) and proteins along the inner face of the cell membrane (Berridge, 1997a). Free ionized calcium (free Ca^{2+}) accounts for only a minute fraction of the total calcium present in cells (Carafoli, 1987; Bygrave, 1978a). However, free Ca^{2+} is the biochemically active form, and as such will be the focus of this

discussion. Cytosolic Ca^{2+} levels are usually kept very low; resting $[Ca^{2+}]_c$ in many cells is approximately 100nM, although liver cells typically operate at around 1μM (Berridge, 1978), and some insect cells may be slightly higher (Woodruff & Telfer, 1994; Dittmann, 1996; Bjornsson *et al.*, submitted).

Cytoplasmic Ca^{2+} levels are closely monitored and highly regulated by cells, which have developed elaborate mechanisms to shuttle Ca^{2+} between compartments as needed. Each intracellular compartment is fundamentally affected by this ion, making the balance among all essential to normal cell function. Identification of the intracellular organelles involved in Ca^{2+} dynamics and their regulatory roles is necessary to appreciate how the extracellular space fits into the overall scheme of Ca^{2+} regulation. To this end, the compartments involved in Ca^{2+} regulation and the physiological roles of Ca^{2+} in these compartments are considered next.

Calcium Stores and Sinks

Most cells have two primary Ca^{2+} stores at their disposal, extracellular stores, and the endoplasmic reticulum (ER)(see Berridge *et al.*, 1998 for review). Calcium from the extracellular space may be used to initiate signals, through activation of receptor-activated, voltage-gated and stretch-operated Ca^{2+} channels. Cells also draw upon the extracellular Ca^{2+} pool to charge internal stores or replenish them after extended bursts of signalling activity (Berridge *et al.*, 1998), since some of the Ca^{2+} used in signalling is transported out of the cell. In this case, Ca^{2+} entry is mediated by store-operated channels that are present along the plasma membrane (SOCs; Barritt, 1999).

Extracellular Ca^{2+} can account for a significant amount of the total Ca^{2+} exchanged by a cell, depending on the cell type. Cardiac tissue is heavily reliant on extracellular Ca^{2+} levels for contraction (Bygrave, 1978a), and neurons similarly depend on extracellular Ca^{2+} for exocytosis of neurotransmitters and for long-term potentiation (Berridge *et al.*, 1998). Up to 60% of the total cell Ca^{2+} exchanged in hepatocytes comes from extracellular fluid (Claret-Berthon *et al.*, 1977). In contrast, contraction in skeletal and smooth muscle is regulated primarily by Ca^{2+} fluxes between the sarcoplasm and sacroplasmic reticulum (SR) in response to depolarization of the sarcolemma; as a consequence these tissues respond only slowly to changes in extracellular Ca^{2+} (Bygrave, 1978a). Differences in the dependence on extracellular Ca^{2+} are often a reflection of the distribution of Ca^{2+} transport proteins, which will be discussed further on.

ER stores are responsible for the explosive bursts of Ca^{2+} observed during signalling and exocytosis. A steep concentration gradient is maintained between ER and cytosol; in pancreatic acinar cells, $[Ca^{2+}]$ in the ER is 0.1-0.3 mM at rest, dropping to 20-40 μM Ca^{2+} during prolonged signalling bouts (Petersen *et al.*, 1999). Calcium release by two channels, the inositol 1,4,5-trisphosphate (IP_3) receptors and cyclic ADP-ribose (cADPr) receptors (a.k.a. ryanodine receptors), can elicit local or whole-cell response, depending on the intensity and duration of calcium release. cADPr receptors are stimulated further by elevated $[Ca^{2+}]_c$ levels, causing Ca^{2+}-induced Ca^{2+} release (CICR), and amplifying the cellular response to a signal. IP_3 receptors also exhibit CICR, but are inhibited by more extreme elevations in $[Ca^{2+}]_c$ (Rutter *et al.*, 1998). Following release, Ca^{2+} is rapidly sequestered from the cytosol by the sarco-endoplasmic calcium ATPase

(SERCA), aided by the presence of low-affinity, high capacity calcium-binding proteins like calsequestrin or calreticulin inside the ER (Koch, 1990; Milner *et al.*, 1992).

The distribution of ER pumps and channels and other transport proteins essential to ER Ca^{2+} homeostasis may be highly polarized. Pancreatic acinar cells have been studied extensively as a prototype for non-excitable cells; in these polarized secretory cells, the ER extends into apical and basal regions. ER channels are located near the apical zymogen granules, SERCA is found throughout, SOCs are restricted to the basal plasma membrane, and plasma membrane Ca^{2+} ATPase (PMCA) is located apically (Petersen *et al.*, 1999). Signalling occurs in the apical region, where PMCA activation helps modulate $[Ca^{2+}]_c$. SOCs are inactivated during signalling by the presence of elevated $[Ca^{2+}]_c$ (Petersen *et al.*, 1999), but as Ca^{2+} sinks reclaim the cytosolic calcium, SOC activation permits entry of extracellular Ca^{2+} into the cytosol to help recharge depleted ER stores by increasing the amount of cytosolic Ca^{2+} available (Petersen *et al.*, 1999). Mitochondria also play a crucial role in modulating signalling events, as discussed below. This example demonstrates how coordinated interaction between multiple sinks and stores can be implemented to achieve specific cellular responses.

Cytosolic Calcium

Many cytosolic macromolecules possess a number of Ca^{2+}-binding sites that are typically unoccupied, and rapidly bind Ca^{2+} introduced from stores or by microinjection (Allbritton & Meyer, 1993). $[Ca^{2+}]_c$ affects gap junctional coupling, endocytosis and exocytosis, microfilament and microtubule dynamics, and the activity of a number of ion

transport proteins, to name only a few of its effects. Each of these will be considered in more depth below.

Calcium is perhaps best known for its role as an intracellular messenger. Upon binding an extracellular ligand, cell membrane receptor tyrosine kinases activate phospholipase C, which cleaves PIP_2 to form IP_3 and diacylglycerol (DAG). Both of these molecules mobilize calcium-related events: IP_3 activates ER Ca^{2+} channels, while Ca^{2+} and DAG cooperatively activate any one of 12 isoforms of protein kinase C (PKC)(Toker, 1998). Ca^{2+}-binding by PKC causes it to move to the inner surface of the cell membrane, where PKC is activated by DAG. Activated PKC can in turn activate a number of downstream events important to early development, including activation of the mitogen-activated protein kinase (MAPK) pathway and remodeling of the cytoskeleton (Toker, 1998).

As demonstrated by interactions with PKC, Ca^{2+} rarely acts alone in the cytosol. More often, Ca^{2+} is bound by calmodulin (CaM), which contains four Ca^{2+}-binding sites that exhibit cooperative binding to allow maximal response with only small elevations in $[Ca^{2+}]_c$ (Vogel, 1994). The activated Ca^{2+}/CaM complex then interacts with proteins bearing CaM-binding domains. Five different serine/threonine kinases - CaM kinases I, II and III, phosphorylase kinase, and myosin light chain kinase (MLCK) - are among the cytosolic proteins affected by Ca^{2+}/CaM (Ganong, 1991). CaMKI regulates synaptic function, CaMKII regulates synaptic plasticity, neurotransmission, gene expression, secretion, cell shape, and cell cycle (DeKoninck & Shulman, 1998); CaMKIII modulates protein synthesis; phosphorylase kinase stimulates glycogen catabolism. MLCK activates myosin II through phosphorylation of the regulatory light chain, activating actomyosin-

based contraction in both motile and nonmotile cells. Other members of the myosin superfamily (I, V, VI) involved in vesicle transport and cytoskeleton-membrane interactions are activated by Ca^{2+}/CaM directly (Mooseker & Cheney, 1995). In addition, Ca^{2+}/CaM or Ca^{2+} alone regulate the activity of numerous ion transport proteins, including the plasma membrane Ca^{2+} ATPase (Guerini, 1998) and a variety of ion channels (Saini & Kung, 1994).

Signalling Dynamics: The Importance of Amplitude and Frequency Modulation

The range of effects that Ca^{2+}, a simple and ubiquitous ion, can achieve has been a source of fascination for many years. How cells interpret a change in $[Ca^{2+}]_i$ to mobilize one downstream response and not another is only beginning to be understood. Ca^{2+} signals are often transient and repetitive, and both their amplitude and frequency are used to encode signals that target specific cellular receptors by catering to their particular Ca^{2+}-binding characteristics. For example, CaMKII activity is regulated by changes in the amplitude and frequency of Ca^{2+} entry (DeKoninck & Shulman, 1998). Gene transcription can be affected by differences in the amplitude of $[Ca^{2+}]_c$ spikes in B lymphocytes (Dolmetsch *et al.*, 1997). Here, small rises in calcium activate NFAT and the ERK pathway inducing negative responses, whereas larger rises activate NF-kB and c-Jun kinase, inducing positive responses; this explains the different responses elicited by naive and self-tolerant B cells to antigens, and represents a general strategy employed by cells.

How do cells actually create differences in the amplitude of Ca^{2+} transients? Advances in imaging capability and molecular probes have provided the tools to observe

elementary events in calcium dynamics. CICR is necessary for contraction in cardiac muscle cells, and these should be all-or-nothing processes; however variations in cell membrane potential modulate the strength of contraction (Berridge, 1997b). Subtle modulation of CICR can be achieved by activating single IP_3 receptors (blips) or cADPRs (quarks) or group release of calcium 'puffs' and 'sparks' (Berridge, 1997b; Bootman *et al.*, 1997; Lipp & Bootman, 1997). Amplitude can therefore be adjusted through activation of different numbers of these elementary units.

Information may also be encoded by changing the duration and periodicity (frequency) of calcium transients. For example, sharp Ca^{2+} spikes were found to be necessary for neurotransmitter expression and channel maturation in developing *Xenopus* spinal neurons, whereas longer Ca^{2+} waves were required for neurite extension. Spikes and waves appear to operate through different cellular mechanisms, since PKC inhibition blocked spike-induced channel maturation but not neurite extension (Gu & Spitzer, 1995). There are a number of examples illustrating how Ca^{2+} encodes information through differences in amplitude, frequency, duration, and number of Ca^{2+} oscillations in epithelial pacemaker cells (Sanderson *et al.*, 1990; Leite, 2002), coupled oscillators in heart, pancreas, and brain (Cornell-Bell *et al.*, 1990; Cornell-Bell & Finkbeiner, 1991; Meyer & Streyer, 1991; Dani *et al.*, 1992; Strogatz & Stewart, 1993; Berridge, 1993, 1997a; Clapham, 1995), and in fertilized eggs (Stricker, 1999). Many of these examples involve intercellular communication, where coordinated Ca^{2+} signals are relayed via gap junctions. Typically the signal passing through the intercellular junctions is IP_3, not calcium itself; the Ca^{2+} signal resumes once IP_3 induces Ca^{2+} release from ER stores in the neighboring cell (Sanderson, 1994).

In addition to using amplitude and frequency modulation to elicit different responses, intracellular Ca^{2+} stores are often arranged to propagate Ca^{2+} signals so they are contained within or spread throughout specific regions of the cell. Smooth muscle cells provide a well characterized example, where Ca^{2+} sparks from ER-associated cADPRs located near the cell membrane specifically activate K^+ channels causing the cell to relax, while a deeper, global rise in Ca^{2+} stimulates contraction through Ca^{2+}/CaM activation of myosin light chain kinase (Nelson *et al.*, 1995). The confinement of Ca^{2+} signalling to discrete microdomains within cells is a common theme used to select specific downstream responses.

Calcium Spikes and Global Propagating Waves

Most global Ca^{2+} oscillations, including those described above, are in fact propagating waves. Jaffe & Creton (1998) have divided Ca^{2+} waves into four categories, according to the velocity of the wave front and their distinctive roles. Slow waves, moving at velocities of approximately 1 μm/s, are commonly associated with surface contractions, cell cleavage, and mitosis. These waves appear to operate through mechanical propagation between 'relay' points of calcium release. Fast calcium waves, which move at approximately 10-30 μm/s, appear to operate via a reaction-diffusion mechanism (Jaffe & Creton, 1998), likely involving Ca^{2+}-induced IP_3 production followed by diffusion of IP_3 (Allbritton & Meyer, 1993). Such waves have been observed in association with secretion and contraction. According to this classification scheme, calcium action potentials are considered 'ultrafast' calcium waves, although their speed has only been measured in a couple of systems (Jaffe & Creton, 1998). The fourth class

of waves is the 'ultraslow' class, which include the Ca^{2+} wave associated with the morphogenetic furrow in *Drosophila* eye imaginal discs (Heberlein & Moses, 1995).

One additional way in which cells modulate cellular activity is by establishing steady Ca^{2+} gradients (Jaffe, 1981). Intracellular Ca^{2+} gradients are generated by asymmetrical ion transport, involving movement of ions into one pole of the cell(s) coupled with ion flux out of another pole. Ca^{2+} influx results in a local increase in $[Ca^{2+}]$, causing ions to diffuse down their chemical gradient to the other pole, where efflux leaves a region of low $[Ca^{2+}]$. A stable gradient can be maintained so long as the transcellular fluxes move ions fast enough that homogeneity cannot be established.

Nuclear Calcium, $[Ca^{2+}]_n$

Ca^{2+} signalling is also an important part of nuclear regulation in many cells, although it is still unknown whether nuclear Ca^{2+} spikes and resting levels are independent of cytoplasmic events (Santella, 1996; Santella & Carafoli, 1997), or whether the nuclear pores are completely permeable to small molecules and ions (Brini *et al.*, 1993; Allbritton *et al.*, 1994). Nuclear permeability varies with cell type, as does the existence of active regulation. Cytosolic Ca^{2+} spikes do not affect $[Ca^{2+}]_n$ in pancreatic acinar cells; however sustained and global $[Ca^{2+}]_c$ elevations do include the nucleus (Petersen *et al.*, 1999). In some cases the permeability of nuclear pores to cytosolic Ca^{2+} appears to depend on the amplitude of cytosolic Ca^{2+} spikes (Al-Mohanna *et al.*, 1994), or to the concentration of Ca^{2+} in the ER/perinuclear space (Greber & Gerace, 1995).

Ca^{2+} signalling appears important enough to nuclear events that the nucleus possesses the machinery necessary for autonomous signalling, including a P-type Ca^{2+}

pump, IP_3 and cADPr receptors (Santella, 1996), enzymes for IP_3 production and turnover (Santella & Kyozuka, 1997), and CaM (Means, 1994). The perinuclear space, bounded by the inner and outer nuclear membranes, is an extension of the ER stores (Santella, 1996). Rutter (1998) argues that the inner membrane lacks sufficient numbers of SERCA pumps to facilitate nuclear signalling, suggesting that rapid Ca^{2+} decline seen after nuclear signalling is likely due to leaks through the nuclear pores. CaM associates with the inner membrane, where it interacts with nuclear actin-related proteins, protein phosphatase 2B (calcineurin) and CaMK II, which activates the transcription factor cAMP-response element binding (CREB) protein, and is responsible for resumption of meiosis and subsequent germinal vesicle breakdown (GVBD) in starfish oöcytes (Santella, 1996). Regardless of whether Ca^{2+} traffic is unrestricted between the nucleus and cytosol, there is definitely communication: during fertilization in starfish oöcytes (where $[Ca^{2+}]_n$ and $[Ca^{2+}]_c$ appear to be independent) an initial cytoplasmic Ca^{2+} transient elicits a nuclear transient, which in turn stimulates a second cytoplasmic transient (Santella, 1996).

Transcription can be modulated by $\Delta[Ca^{2+}]_n$; for example, Ca^{2+}-sensitive proteins in both cytosol (serum-response element, or SRE) and the nucleus (CREB) can be regulated to induce expression of the c-fos gene in a mouse pituitary cell line (Hardingham *et al.*, 1997, 1998; Hardingham & Bading, 1998, 1999). In addition, many of the cell cycle checkpoints are affected by Ca^{2+} levels, as will be discussed later on.

Mitochondrial Calcium

In healthy cells, minimal amounts of Ca^{2+} are stored by mitochondria, and little Ca^{2+} is released from mitochondria into the cytosol in unstimulated cells (Pozzan *et al.*, 2000). While the rate of Ca^{2+} accumulation by mitochondria can be quite high, it is no match for the ER's capacity to exchange vast quantities of Ca^{2+}. Three proteins present along the inner mitochondrial membrane mediate mitochondrial Ca^{2+} transport: a membrane-potential driven uniporter takes in Ca^{2+}, while two exchangers, a Na^+/Ca^{2+}-exchanger and a Ca^{2+}/H^+-exchanger, are responsible for efflux (Pozzan *et al.*, 1994; Gunter *et al.*, 2000). If $[Ca^{2+}]_m$ reached the equilibrium of the membrane-potential driven uniporter in a typical cell, it would hit 0.1M, but this is prevented by the exchangers, which slowly return calcium to the cytosol (Pozzan *et al.*, 2000).

While mitochondria appear to be less involved than the ER in the rapid exchange of $[Ca^{2+}]_c$ observed in signalling, they do participate, helping lower cytosolic Ca^{2+} levels during sustained bouts of signalling (Carafoli, 1987). In HeLa cells, when $[Ca^{2+}]_c$ peaked at ~2 μM, $[Ca^{2+}]_m$ reached 60-80 μM (Pozzan *et al.*, 2000), and $[Ca^{2+}]_m$ levels >300 μM have been reported for chromaffin cells (Montero *et al.*, 1995). During $[Ca^{2+}]_c$ oscillations, $[Ca^{2+}]_m$ also displays oscillating behaviour (Liu *et al.*, 2001). cADPr receptors (cADPrR) are stimulated by elevated $[Ca^{2+}]_c$ levels, while IP_3 receptors are stimulated by moderate elevations in $[Ca^{2+}]_c$ but are inhibited beyond a certain point. $[Ca^{2+}]_c$ buffering by mitochondria, and consequent suppression of cADPrR and sustained activation of IP_3R allow mitochondria to help pace Ca^{2+} oscillations (Jouaville *et al.*, 1995; Zimmermann, 2000). By taking up Ca^{2+} near hotspots along the ER and plasma membrane (Thayer & Miller, 1990; Rutter *et al.*, 1993; Werth & Thayer, 1994; Hoth *et*

al., 1997; Hajnoczky *et al.*, 2000; Colgrove *et al.*, 2000), mitochondria help shape the kinetics of Ca^{2+} release (Pozzan *et al.*, 2000). By lowering $[Ca^{2+}]_c$, mitochondrial buffering stimulates IP_3R, and plasma membrane channels to prolong Ca^{2+} entry and signalling (Rutter *et al.*, 1998), modulating the responses of neurons and hepatocytes, producing the sustained $[Ca^{2+}]_c$ necessary for T cell activation (Rutter *et al.*, 1998), and likely representing a common mode of Ca^{2+} modulation among a variety of cell types.

The location of mitochondria within cells is also critical. Conventional TEM (Sommer & Johnson, 1970; Shore & Tata, 1977) and high-resolution 3D reconstructions of GFP-tagged organelle-specific proteins in HeLa cells demonstrate that a significant amount (5-20% of the mitochondrial membrane) of ER and mitochondrial membranes are in close proximity, ~100 nm apart (Rizzuto *et al.*, 1998). In addition, IP_3R along the ER are often concentrated in these regions. Of course, $[Ca^{2+}]_c$ spikes elevate $[Ca^{2+}]_m$ as well. In polarized cells, mitochondria can prevent calcium elevations from reaching the wrong pole, as seen in pancreatic acinar cells (Tinel *et al.*, 1999).

Calcium and Cell Physiology

Microfilaments: Assembly, Kinetics, and Associated Proteins

Actin monomers contain a high-affinity divalent cation-binding site that modulates the dissociation of ATP and promotes F-actin formation (Gershman *et al.*, 1994). Although Mg^{2+} is generally associated with actin, shifts in the relative concentrations of Mg^{2+} and Ca^{2+} can lead to an increase in bound Ca^{2+}, which dissociates more slowly than Mg^{2+}, promoting filament formation for an extended period (Gershman *et al.*, 1994). The effect of Ca^{2+}'s direct binding to microfilaments is secondary to the

impact of Ca^{2+}-sensitive actin-binding proteins (ABPs), which are capable of producing rapid and radical changes in the actin cytoskeleton and of using F-actin as a basis for contraction and transport. For example, gelsolin, an F-actin severing protein, increases the dynamic turnover of actin filaments when activated by Ca^{2+} (Southwick, 2000). Fascin, an actin bundling protein, carries a PKC binding domain (Ono *et al.*, 1997), and pH-dependent phosphorylation of fascin by protein kinases has been demonstrated to reduce its actin-binding activity (Yamakita *et al.*, 1996). Fascin localizes to microvilli and to dynamic cellular processes (lamellopodia, filopodia, etc.), where microdomains of elevated Ca^{2+} have been shown to regulate morphological changes (Silver *et al.*, 1990). In addition, the activity of many members of the myosin superfamily is regulated by calmodulin light chain activity; myosins I, V, and VI are notable due to their role in vesicular transport (DePina & Langford, 1999), including nurse cell-oöcyte transport in *Drosophila* (Bohrmann & Biber, 1994; Bohrmann, 1997). Activation of myosin II, involved in contraction and cytokinesis, depends on phosphorylation of the regulatory light chain by Ca^{2+}/CaM-activated myosin light chain kinase (MLCK; Lodish *et al.*, 2000). Other components of the contractile machinery, such as troponin C from skeletal and cardiac muscle, may be regulated by calcium directly (Filatov *et al.*, 1999).

Microtubules: Assembly, Kinetics, and Associated Proteins

The stability of microtubules is influenced by a variety of factors, including post-translational modifications, microtubule-associated proteins, temperature, and calcium (Dustin, 1979). The assembly and turnover of purified microtubules in the absence of other proteins is not affected by increased $[Ca^{2+}]_c$ (Olmsted & Borisy,1975; Simon *et al.*,

1992). *In vivo*, however, microtubule-binding, Ca^{2+}/CaM-dependent kinases are responsible for Ca^{2+} sensitivity in microtubules (Larson *et al.*, 1985), and disassembly under elevated $[Ca^{2+}]_c$.

Microtubule motor proteins mediate transport of various cargo including vesicles and mitochondria, and RNA critical to pattern formation in *Drosophila* (Theurkauf, 1994) and *Notonecta* (Stebbings, 1997; Stephen *et al.*, 1999). They also coordinate the assembly of chromosomes along the metaphase plate and the segregation of chromosomes during anaphase (Lodish *et al.*, 2000). The (-)-end directed dynein motor has been implicated in nurse cell-oöcyte transport of mitochondria in the telotrophic ovarioles of *Notonecta* (Stebbings & Hunt, 1987; Stebbings, 1997) and *Rhodnius* (Harrison & Huebner, 1997), and of mRNA in *Notonecta* (Hurst *et al.*, 1999; Stephen *et al.*, 1999). Upon binding Ca^{2+}/CaM, cytoplasmic dynein purified from sea urchin egg homogenates increases its processivity 6-fold (Hisanaga & Sakai, 1983). Kinesin II has been shown to be dependent on Ca^{2+} (Cole, 1999) and CaM (Jaffe, 1999). As a result, Ca^{2+} may regulate transport of cytoplasmic constituents in telotrophic ovarioles.

Metabolic Activity

In addition to buffering $[Ca^{2+}]_c$ and mediating apoptosis, $[Ca^{2+}]_m$ exerts functional effects within mitochondria, including modulation of isocitrate, oxoglutarate, and pyruvate dehydrogenases, key limiting enzymes in the TCA cycle (Pozzan *et al.*, 2000). Elevated $[Ca^{2+}]_m$ stimulates mitochondrial metabolism. Mitochondrial calcium levels in some tissues are hormonally regulated (Bygrave, 1978a, 1978b), and this may be linked

to metabolic activity. Local increases in ATP production caused by elevated $[Ca^{2+}]_m$ may also influence ER dynamics and energize SERCA activity.

Regulation of Gap Junctions

Elevated $[Ca^{2+}]_c$ as well as Ca^{2+}/CaM activity regulates the activity of several gap junctional connexin and innexin proteins (Perrachia & Perrachia, 1980a; Van Eldik *et al.*, 1985). One reason for this regulation may be to block transmission of diffusible initiators of apoptosis, including elevated Ca^{2+}, among coupled cells. Elevated extracellular Ca^{2+} levels have also been shown to inhibit GJ communication in some systems (Bohrmann & Haas-Assenbaum, 1993; Quist *et al.*, 2000).

Interaction with Other Signalling Pathways

In addition to being the central player in its own signalling pathway, Ca^{2+} also modulates the cAMP pathway in all cells (Rasmussen, 1981). cAMP phosphodiesterase, an enzyme that reduces the cAMP pool, is activated by elevated Ca^{2+} levels (Tkachuk & Men'shikov, 1981), thereby attenuating the cellular response to a cAMP-mediated external signal. These two pathways often antagonize each other, for example in cellular glucose metabolism that is increased by insulin via Ca^{2+} pathways and decreased by glucagon through cAMP signalling (Voet & Voet, 1990). Crosstalk between Ca^{2+} and cAMP signalling pathways permits their coordinated activity.

Cell Division

Calcium's ability to control a broad range of cellular processes makes it an ideal agent to synchronize disparate events during early development. For example, cell

division involves precise control of intracellular organelle dispersion, including nuclear envelope breakdown, chromosomal migration, and cell cleavage. Failure to perform any one of these at the proper time could be disastrous for the cell. Not surprisingly, nuclear envelope breakdown, microtubule-mediated retrograde transport of chromosomes, and actomyosin-based cytokinesis are all Ca^{2+}-regulated events. Further consideration of Ca^{2+}'s roles during development is discussed below.

The timing of Ca^{2+} oscillations in a number of cell types, including embryos and a variety of cultured somatic cells, is synchronous with cell cycle progression through critical checkpoints. Meiotic events are regulated by calcium: upon fertilization in starfish oöcytes, a spike in nuclear Ca^{2+} levels and increased calmodulin activity are required for meiosis to resume and for GVBD (Santella, 1996). Similarly, there are a number of checkpoints during mitosis: Ca^{2+}/CaM–dependent kinase II (CaMKII) regulates G_1/S transition, G_2 to M progression, the metaphase/anaphase transition (MPF), and return from G_0 (reviewed by Santella, 1998). While most cyclins are degraded by Ca^{2+}-independent proteases, cyclin D_1 (essential for progression into S phase) is degraded by the Ca^{2+}-dependent protease calpain, which can promote mitosis and meiosis when injected into somatic cells or oöcytes (Santella, 1998). Furthermore, it has been shown that external Ca^{2+} is required for cells to enter the G_1 phase (Santella, 1998). During fertilization of sea urchin eggs, Ca^{2+} release from intracellular stores triggers nuclear envelope breakdown and chromatin condensation (Gilbert, 2000). In mouse zygotes, fertilization-induced spiking is temporally related to cell cycle events, although spiking appears to be started, but not stopped, by cell cycle events (Day *et al.*, 2000). Essentially,

Ca^{2+} spiking in some systems appears to be driven by the cell cycle, rather than being essential for cell cycle progression, and may be produced to carry out downstream events.

In addition to regulating nuclear events, Ca^{2+} also plays a role in cytokinesis, where the contractile actinomyosin ring is activated by a transient local calcium influx at the cell membrane (Fluck *et al.*, 1991; Miller *et al.*, 1993; Webb *et al.*, 1997). In this series of papers, Miller and coworkers described transient Ca^{2+} influx in *Xenopus* and *Medaka* eggs and *Danio* embryos using the Ca^{2+}-sensitive photoprotein aequorin, and demonstrated that abolishing the increase in $[Ca^{2+}]_i$ in the region of the future or forming cytoplasmic furrow through injection of the calcium buffer BAPTA blocked further constriction of the contractile ring in *Xenopus* eggs (Miller *et al.*, 1993).

Pattern Formation

Considering calcium's prominent role as regulator and the numerous mechanisms cells can employ to confine its effect to discrete microdomains (Pozzan *et al.*, 1999), it is hardly surprising that it is commonly employed by developing oöcytes and embryos for axis specification and the establishment of polarity in general. The following are a few examples of the diverse roles Ca^{2+} plays in regulating pattern formation.

Fucoid zygotes are initially apolar (Kropf, 1997), until the action of environmental cues, including polarized light, results in the formation of a rhizoid from one pole (Jaffe, 1956). Early embryonic polarity is established by driving Ca^{2+} flux through the cell (Robinson & Jaffe, 1975; Robinson, 1996), creating a zone of elevated $[Ca^{2+}]_c$ at the future rhizoid pole (Pu & Robinson, 1998). Abolishing the intracellular Ca^{2+} gradient using BAPTA buffers prevents rhizoid formation, without losing the

developmental potential of the embryo (Speksnijder *et al.*, 1989). Calcium is thought to direct its own polarization, possibly by local exocytosis of Ca^{2+}-bearing vesicles or cell wall softening proteins (see Jaffe, 1999 for review).

In ascidian development, the sperm entry site is the epicenter of an initial fertilization Ca^{2+} wave followed by a barrage of fast Ca^{2+} waves (Speksnijder *et al.*, 1990). These trigger a preformed microfilament basket at the 'contraction pole' to contract, establishing the polar lobe enriched in ER, mitochondria, and presumptive myoplasm. The polar lobe becomes the epicenter of a second volley of fast Ca^{2+} waves, and defines the site of gastrulation and the future dorsal side of the embryo.

During *Drosophila* embryogenesis, a weak elevation in ventral Ca^{2+} levels appears to destabilize the Cactus protein, releasing Toll protein to dephosphorylate Dorsal protein, allowing this transcription factor to enter ventral nuclei (Jaffe, 1986, 1999; Kubota & Gay, 1995). Later, elevated Ca^{2+} is observed along the dorsal surface, and has been implicated in modulating Decapentaplegic-mediated dorsal specification, possibly by affecting transcription or secretion (Creton *et al.*, 2000).

Calcium signalling is also involved in axis formation during oögenesis. In *Xenopus* and *Danio*, IP_3 levels are elevated along the future ventral surface (Ault *et al.*, 1996); blocking this elevation results in its dorsalization (Kume *et al.*, 1997). Depletion of IP_3 in response to Li^+ exposure also results in hyperdorsalization in *Xenopus* (Berridge *et al.*, 1989; Maslanski *et al.*, 1992; Ault *et al.*, 1996) and *Danio* (Stachel *et al.*, 1993), as does inhibition of signalling through injection of antibodies specific for IP_3R in *Xenopus* (Kume *et al.*, 1997). Similarly, zones of elevated Ca^{2+} essential for pattern formation

have also been described in the animal and vegetal poles of *Medaka* embryos (Fluck *et al.*, 1992, 1994).

In a number of insect meroistic ovaries, nurse cells and oöcytes maintain different levels of intracellular free Ca^{2+}. Insects studied to date include *Actias luna* (Cole & Woodruff, 1997), *Dysdercus intermedius* (Dittmann, 1996), *Hyalophora cecropia* (Woodruff & Telfer, 1994), and *Rhodnius prolixus* (Bjornsson *et al.*, submitted). For the most part, the role of these Ca^{2+} differences is unknown, although progress is being made. In the meroistic ovarioles of the silkworm moth, *Hyalophora cecropia*, a difference in $[Ca^{2+}]_i$ is established between nurse cells and oöcyte at the onset of vitellogenesis (Woodruff & Telfer, 1990, 1994). Experimental removal of this difference results in resumed transcriptional activity in the germinal vesicle, and this activity can also be induced by microinjection of nurse cell cytoplasm into the oöcyte (Woodruff *et al.*, 1998). Thus it appears that Ca^{2+} establishes a gradient between the syncytial compartments that inhibits transport of a nurse cell-synthesized factor to the oöcyte. It has been postulated that an extracellular calcium loop exists to balance and maintain this intracellular gradient, by pumping calcium out of the nurse cells and taking in calcium along the oöcyte surface (Woodruff & Telfer, 1994).

Calcium action potentials (APs), or 'ultrafast' Ca^{2+} waves (Jaffe & Creton, 1998), have been described in the eggs of mammals (Georgiou *et al.*, 1984) and a variety of marine invertebrates (reviewed by Stricker, 1999). In insects, Ca^{2+}-dependent, Na^{+}-independent action potentials can be elicited in vitellogenic oöcytes of *Rhodnius prolixus* upon membrane depolarization (O'Donnell, 1985). Previtellogenic follicles (< 400 μm in length) could also produce Ca^{2+} APs, albeit of shorter duration, as could oöcytes from

follicles where chorionation had been initiated. *Rhodnius* oöcytes also appear to have a significant resting Cl^- conductance, possibly due to a Cl^-/HCO_3^- exchanger (O'Donnell, 1986). cAMP reduced AP overshoot and duration, and introduced a transient hyperpolarization at the end of the AP, likely by increasing K^+ conductance (O'Donnell, 1988). APs in *Rhodnius* are generated by the oöcyte, not the follicle cells, as demonstrated by experiments on isolated epithelia, where conditions that could evoke APs in intact follicles did not reproduce APs (O'Donnell, 1985). While single or multiple follicle cells were impaled in different trials, no mention was made as to whether follicle cell-follicle cell coupling is retained once GJ coupling to the oöcyte is lost. Initial observations suggested *Drosophila* (Miyazaki & Hagiwara, 1976) and *Locusta* (Wollberg *et al.*, 1976) eggs do not generate APs; however under conditions in which voltage-dependent K^+ conductances were suppressed, Ca^{2+} APs could be unmasked in *Triatoma*, *Locusta*, and *Hyalophora columbiae*, none of which generated APs under normal conditions (O'Donnell, 1985b, 1988). O'Donnell has postulated that APs may play an important role following fertilization and during embryogenesis.

Bioelectric Currents in Insect Oögenesis

The steady Ca^{2+} gradient established during *Fucus* rhizoid formation is a classic reflection of the presence and role of bioelectric currents during development, which have been described in a wide range of systems and during oögenesis in a variety of organisms, including insects (Jaffe, 1986). Extracellular currents have been described

around the panoistic ovarioles of *Locusta* (Wollberg *et al.*, 1976; Verachtert & DeLoof, 1986), and in the cockroaches *Blattella* and *Periplaneta*, where they predict the future body axes (Bowdan & Kunkel, 1990, 1994; Kunkel & Faszewski, 1995). In every meroistic ovariole studied to date except *Ips perturbatus* (Huebner & Sigurdson, 1986), bioelectric currents take on a characteristic conformation: a net positive efflux is observed over developing follicles, while net influx occurs over the nurse cells. Other species studied include *Hyalophora cecropia* (Jaffe & Woodruff, 1979; Woodruff *et al.*, 1986b), *Drosophila melanogaster* (Overall & Jaffe, 1985; Bohrmann *et al.*, 1986; Sun & Wyman, 1989), *Sarcophaga bullata* (Verachtert & DeLoof, 1986), *Sialis velata* (Huebner & Sigurdson, 1986), *Dysdercus intermedius* (Dittmann *et al.*, 1981), and *Rhodnius prolixus* (Huebner & Sigurdson, 1986; Diehl-Jones & Huebner, 1989, 1991, 1992),

Bioelectric currents are established by polarized transmembrane ion fluxes, and consequently are influential in altering the distribution of ions within the cell(s) involved in transport. Polarized ion transport may result in the establishment of intracellular ion gradients, which in turn can establish microdomains suitable for the graded activity of cell processes. The $[Ca^{2+}]_i$ gradient established in *Fucus* is an ideal example, where local $[Ca^{2+}]_i$ elevation is thought to facilitate exocytosis of wall-softening expansions and membrane fusion of vesicles bearing Ca^{2+} channels (Jaffe, 1999). Ca^{2+} gradients spanning the nurse cell-oöcyte syncytium may regulate transport in insect models like *Hyalophora* (Woodruff & Telfer, 1994; Woodruff *et al.*, 1998) and *Actias* (Cole & Woodruff, 1997).

Intracellular ionic gradients established by bioelectric currents are typically accompanied by intracellular voltage gradients, which may exert unique effects of their own. Specifically, it has been postulated that voltage gradients may help direct the

distribution and migration of charged non-tethered cytoplasmic constituents. In support of this, microinjected charged proteins have been shown to distribute according to charge in *Hyalophora* (Woodruff & Telfer, 1973, 1980), *Drosophila* (Woodruff *et al.*, 1974; Woodruff *et al.*, 1988; Woodruff, 1989; Singleton & Woodruff, 1994; but see Bohrmann & Gutzeit, 1987; Sun & Wyman, 1987, 1989, 1993; Bohrmann & Schill, 1997), *Dysdercus* (Dittmann *et al.*, 1981; Munz & Dittmann, 1987), and *Rhodnius* (Huebner & Sigurdson, 1986; Diehl-Jones, 1991). Furthermore, the distribution of native charged proteins corresponds to nurse cell-oöcyte voltage differences in *Actias* (Cole & Woodruff, 1997) and *Drosophila* (Cole & Woodruff, 2000), and changes in follicles of both insects when the voltage difference is disrupted.

Extracellular ion currents are the external component of bioelectric currents, and are generated by active and passive plasma membrane-bound ion transport proteins. Except during events like APs in which membrane potential (E_m) changes, net ionic influx balances net ionic efflux, and in many instances these two processes are separated spatially and may be operating at opposite poles of the cell. Current loops are established between regions of influx and efflux. One of the consequences of this spatial asymmetry is that ionic gradients may be established between these regions. Local changes in ion concentration resulting from ion transport protein activity are antagonized in both intra- and extracellular compartments by diffusion, which is necessarily operating more slowly than transport in cases where extracellular ion flux can be detected. As long as polarized transport continues, the compartment will defy homogeneity and maintain an ionic gradient.

Plasma Membrane: Bridge Between Intra- and Extracellular Ion Dynamics

When considering the nature of extracellular ionic fluxes and their importance to developmental events, it is informative not only to consider the location and timing of the fluxes themselves, but also the distribution of the membrane ion transport proteins responsible for generating these fluxes. Such analysis can shed light on which specific transport proteins may be involved, and thus on the mechanisms involved in regulating regional differences in ion activity, particularly whether this regulation occurs at the level of protein expression, function, or substrate availability.

General Survey of Membrane Transport Proteins

Before considering the molecular basis of ion transport in *Rhodnius* ovarioles, a general survey of membrane transport proteins is useful. These fall into three broad categories and are further classified based on the biochemical nature and details of transport. As a general rule, ion transport proteins may be coded for by single or multiple genes that often produce several tissue-specific isoforms. Transport proteins are either electroneutral, if the distribution of charge is unaffected by their activity, or electrogenic.

Ion Pumps

Ion pumps use energy derived from ATP hydrolysis to transport ions across the membrane against the electrochemical gradient, and are typically electrogenic (Lodish *et al.*, 2000). Pumps are classified according to their interaction with ATP during the transport cycle; P-type pumps form a transient phosphorylated intermediate during

transport, while V- and F-type pumps do not (Pederson & Carafoli, 1987). P-type pumps include the Na^+/K^+-ATPase, H^+/K^+-ATPase, and the Ca^{2+}-ATPases of the plasma membrane and endoplasmic reticulum. V-type pumps have been identified in vacuoles, endosomes, lysosomes, and the plasma membrane, while F-type pumps are unique to the mitochondria; both of these pumps are strictly H+ transporters. While P-type pumps often consist of only one (PMCA) or two subunits (Na^+/K^+, H^+/K^+), both V- and F-types are considerably more complex, requiring precise assembly of seven to ten different subunits (Nelson, 1991). A fourth class of pump, the ABC (ATP binding cassette) superfamily, consists of a group of transport proteins, each one specific for a particular substrate. These transport a broad range of molecules including ions, sugars, and proteins (Lodish *et al.*, 2000).

Channels

Channels constitute the second category of ion transport proteins (Lodish *et al.*, 2000). This diverse group of proteins forms hydrophilic pores in the membrane, permitting ion translocation driven by the electrochemical gradient. The size and selectivity of the hydrophilic pore varies tremendously; as a result channels can permit movement of a single ion type or several types of anions, cations, or both. Channels are often gated to remain inactive until stimulated by specific ligands, changes in voltage, or lateral forces (stretch activation). Channels are like floodgates, allowing rapid transport on the order of 10^8 ions per second, depending on the strength of the electrochemical gradient as well as the maximum conductance of the channel (Lodish *et al.*, 2000).

Transporters

The third category of ion transport protein is the transporter (Lodish *et al.*, 2000). These rest until ions bind to specific sites, inducing a conformational change that carries them to the other membrane face, where they are released. Upon release, the protein's conformation changes once again, returning it to its original state. If the transporter returns to its original state empty-handed, it is called a uniporter (typical of glucose and amino acid porters); if it carries another ion back with it, it is classified as an antiporter (or exchanger). If instead the transporter carries a second ion type along with the first, it is considered a symporter. Both cotransporters (symporters and antiporters) harness energy derived from transporting one ion down its concentration gradient to drive another against its electrochemical gradient; in doing so they are considered secondary active transport mechanisms, since they make use of the electrochemical gradient established by primary transport mechanisms. Transporters are typically slower than channels, moving approximately 10^2-10^4 ions per second (Lodish *et al.*, 2000).

Plasma Membrane H^+ Transport Proteins

Several proteins have been characterized that transport protons across the plasma membrane. Two pumps are known, including the V-type ATPase and the H^+/K^+-ATPase. The discovery of particles along the cytoplasmic face of the cell membrane (Gupta & Berridge, 1966) led to the description of V-ATPases along the cell membranes of a number of invertebrate cells, as well as toad bladder epithelia, fish gills, osteoclasts, epididymis, and kidney tubule cells (Wieczorek *et al.*, 1999). In many insects, electrogenic H^+ pumps associated with the cell membrane contribute to the resting

membrane potential (E_m), as Na^+/K^+-ATPase does in most mammalian cells (Wieczorek *et al.*, 1999; Harvey & Wieczorek, 1997; Haley & O'Donnell, 1997; Dittmann, 1997). The H^+/K^+-ATPase was initially described in vertebrate tissues including gastric parietal cells (Wallmark *et al.*, 1990), colon (Binder *et al.*, 1999), and in kidney collecting ducts (Xia *et al.*, 1999). More recently, English & Cantley (1984) described a ouabain-insensitive, vanadate-inhibited (ergo P-type) H^+/K^+ exchange in an insect cell line. Some insect cells also express a K^+/H^+ exchanger and a Na^+/H^+ exchanger (NHE), both of which may act as secondary transport mechanisms following initial H^+ secretion (Harvey, 1992; Harvey & Wieczorek, 1997). Additionally, an electrogenic $2H^+/Na^+$-exchanger found in the oöcyte membrane of *Dysdercus intermedius* has been described (Dittmann & Muenz, 1999)

Although H^+ transport is not involved in the activity of the Cl^-/HCO_3^- exchanger, pH is affected on both sides of the membrane. HCO_3^- efflux buffers extracellular H^+ giving the appearance of H^+ influx, and lowers intracellular pH through expulsion of HCO_3^- (a product of CO_2 and OH^-). Another exchanger, the $Na^+HCO_3^-/Cl^-$ antiporter, imports bicarbonate to combine with H^+ to yield H_2O and CO_2. CO_2 diffuses passively across the cell membrane; upon reaching the extracellular space it may combine with water to form HCO_3^-, generating H^+ in the process (Harvey, 1992).

Plasma Membrane Ca^{2+} Transport Proteins

A large collection of calcium transport proteins have been identified, in part through numerous toxins that target these important proteins. Calcium efflux is managed by the plasma membrane calcium ATPase (PMCA) and to a lesser extent by the Na^+/Ca^{2+}

exchanger (NCX) (Lodish *et al.*, 2000). Four PMCA isoforms and 20 splice variants have been described in vertebrates, some of which are ubiquitous while others display tissue specificity (Guerini, 1998). A number of channels regulate Ca^{2+} entry along the steep chemical gradient, and are classified as voltage-operated (VOCCs), receptor-activated (RACCs) or store-operated channels (SOCs)(Barritt, 1999). VOCCs are further divided into 6 types (L-, N-, P-, Q-, R- and T-type), classified according to the threshold voltage at which they activate, their maximal transport rate, how long they remain open following stimulation, and their response to specific toxins (Moreno, 1999). In adult *Rhodnius* ovarioles, exposure to diltiazem and verapamil, selective inhibitors of L-type VOCCs, resulted in ion current alterations detected using the voltage-sensitive vibrating probe (Diehl-Jones & Huebner, 1992), suggesting that L-type channels are present and that they contribute to the overall current patterns.

Mechanisms of Establishing Polarized Transport

Examination of the diverse repertoire of ion transport proteins expressed by cells demonstrates that cells have a broad range of functional capability at their disposal. The potential for transcriptional and translational regulation as well as post-translational modification extends the cell's ability to tailor its transport capabilities (Harvey & Wieczorek, 1997). In addition, cells have devised a number of mechanisms to meet the added demands of establishing cell and tissue polarity during development. Some of these mechanisms will be considered below, since they may be related to the

establishment of extracellular ion fluxes during oögenesis in the telotrophic ovarioles of *Rhodnius prolixus*.

Polarized Trafficking and Formation of Membrane Domains

Complex tissues often develop a more elaborate strategy to placing ion transport proteins only where they are needed. Many of the best examples have been identified in polarized epithelia, where ions must often be transported unidirectionally across the tissue. These cells often establish discrete apical and basolateral domains separated by a barrier or 'fence' that prevents diffusion of proteins from one domain to the other. In vertebrate tissue, tight junctions exert a 'fence function' (van Meer & Simons, 1986, Severs, 2000), while invertebrate tissue achieves the same end using septate junctions (Tepass, 1997; Aschenbrenner & Walz, 1998; Severs, 2000). Membrane compartmentalization coupled with sorting of Golgi-derived vesicles as they are produced and targeting them to one of the two surface domains provides one simple solution to establishing cell polarity (Gottardi *et al.*, 1993). The details of intracellular trafficking can vary tremendously. In MDCK cells, proteins destined for the apical surface travel directly to the apical surface, while those fated for the basolateral membrane travel first to both domains, but are subsequently endocytosed at the apical surface and transcytosed to their proper location (Nelson & Veshnock, 1987). In other systems proteins are targeted to the proper domain at the outset (Mostov & Cardone, 1995).

Cytoskeletal Anchors

The actin cytoskeleton is often used to restrict the mobility of membrane proteins, by anchoring them in place once they get there by the action of polarized transport mechanisms. While numerous intermediate proteins have been identified that link actin to plasma membrane proteins, one in particular has been shown to bind a number of ion transport proteins. Ankyrin has been identified in MDCK cells, hepatocytes, neurons, and (sensory) hair cells, where it has affinity for several proteins including: Na^+/K^+-ATPase (Nelson & Veshnock, 1987); gastric H^+/K^+-ATPase (Festy *et al.*, 2001), Na^+/H^+-exchanger; calcium, sodium and potassium channels, and the erythrocyte Cl^-/HCO_3^- exchanger (Mohler *et al.*, 2002). One advantage of this restricted mobility is that it is highly dynamic; transport proteins can be anchored in regions where they are needed temporarily and quickly dispersed or disassembled. This type of dynamic organization is best exemplified at the leading edge of migrating fibroblasts, where Na^+/H^+-exchangers are anchored by actin and serve a number of roles including pH_i regulation at the leading edge, regulation of local signalling events, and simply helping to anchor the cytoskeleton (Denker & Barber, 2002; Putney *et al.*, 2002).

Intercellular Interactions

Interactions between cells are another means of establishing membrane polarity in addition to the intracellular mechanisms described so far. In honeybee photoreceptor cells, for example, Na^+/K^+-ATPase is localized to discrete regions of the membrane through interactions with neighboring glial cells. Normally, the ion pump is found on the photoreceptor cell only where the two cells establish contact. Elegant studies by

Baumann & Takeyasu (1993) have demonstrated that if the sensory cells and glia are dissociated, Na^+/K^+-ATPase is dispersed across the entire membrane. When glia are added back, polarized distribution of the pump is reestablished. Clearly, as interactions in multicellular systems become more complex, the potential for increasingly complex and highly regulated activity and polarization of ion transport proteins increases as well.

Measuring Extracellular Ionic Fluxes

Early voltage-sensitive vibrating probes were capable of rapidly detecting minute voltage differences between positions sampled close to the tissue, allowing 1-dimensional and later 2-D mapping of extracellular bioelectric currents for the first time (Jaffe & Nuccitelli, 1974; Nuccitelli, 1986). These probes could measure total ionic flux, and researchers using this technique in conjunction with ion substitution experiments and application of pharmacological agents were able to infer the contribution of individual ions to the total current (Diehl-Jones & Huebner, 1992). However, the potential for synergistic and pleiotropic effects introduced by these treatments made identification of an individual ion's contribution to the overall current uncertain.

The development of a Ca^{2+}-selective probe technique (Kuhtreiber & Jaffe, 1990) meant that the extracellular dynamics of individual ions could be directly measured without perturbation of the tissue. The ion-selective probe (ISP) utilizes a column of liquid ionophore exchanger (LIX) with high affinity for a single ion type at the tip of a glass microelectrode. A range of LIXs are available that are selective for a number of

different ions, including H^+ (Somiesky & Nagel, 2000). At the probe tip, the LIX chelates a number of ions depending on the ion concentration in the surrounding medium; within the electrode the other face of the LIX column is exposed to a fixed ion concentration in the backing solution. The difference between these two concentrations establishes a voltage difference across the LIX that can be amplified and recorded by conventional electrophysiological equipment. Like its voltage-sensitive counterparts the ISP is self-referencing, using a single probe to compare ion concentrations between different locations, thus minimizing drift between consecutive measurements. The ISP is also non-invasive, allowing measurement without impalement or injury to the tissue. With the ISP mounted to a stepper motor platform, movement and measurement in three dimensions can be performed. The only drawback to this technique is that the speed with which measurements can be taken is limited, as the LIX must equilibrate with the local medium when moved to a new position.

Calculation of the ion flux from ion-selective probe measurements invokes Fick's law of diffusion ($J = -D(\partial c/\partial x)$, where J is an ion flux in the x direction, D is the diffusion coefficient for the ion, and $\partial c/\partial x$ is the concentration gradient in the x direction) and yields a flux value that conveys the number of ions in moles travelling across a given area over a set period of time (Kuhtreiber & Jaffe, 1990). This differs only slightly from voltage-sensitive probes, where measured currents are an expression of charge (proportional to the number of ions, in moles) across a unit area. Essentially, flux is current per unit area. The application of Fick's law to ISP flux calculations takes into consideration bath ion concentration, temperature, the diffusion rate of the ion being measured, the distance between measured points, and the ion concentration at each point

measured (Kuhtreiber & Jaffe, 1990). Ideally, diffusion rate for each ion measured would be determined empirically, since the presence of other ions with different mobilities can influence diffusion rate; however, for most practical applications the diffusion rate in water with a single counterion (eg. Cl^- when measuring H^+ or Ca^{2+}) is sufficient (Kuhtreiber & Jaffe, 1990).

CHAPTER 1: EXTRACELLULAR HYDROGEN ION DYNAMICS DURING OÖGENESIS IN *RHODNIUS PROLIXUS*

INTRODUCTION

Throughout the life of most metazoan organisms, the germ cells are set apart to prepare for their roles in sexual reproduction. Both sperm and egg are highly specialized to perform their appointed tasks. The egg is a truly remarkable cell that not only stockpiles enough synthetic material to last the future embryo through early development, but also contains maternal determinants necessary to lay out the blueprint for the future organism, including determination of body axes and initial segmentation patterns. While it is astounding enough that these stores and determinants are localized in the polarized oöcyte during oögenesis, it is even more impressive that in insect meroistic ovarioles, most of these products are not synthesized by the oöcyte itself; rather mitochondria, ribosomes, various RNAs, and proteins are produced by nurse cells and transported to the oöcyte via cytoplasmic bridges (Vanderberg, 1963; Davenport, 1974; Hyams & Stebbings, 1977; Huebner, 1981a; Gutzeit, 1986). Yolk products, synthesized by the fat body and ovarian follicle cells (Telfer, 1965, 1975), are actively endocytosed by oöcytes undergoing vitellogenesis, a process that typically involves activation and differentiation of the oöcyte. Nurse cells and oöcytes originate from a common progenitor, retaining cytoplasmic continuity after undergoing incomplete cell divisions (Lutz & Huebner, 1980, 1981; King & Buning, 1985; Deng & Lin, 2001). How can cells, sharing a common

cytoplasm, establish and maintain such radical differences in structure and function? And what are the mechanisms regulating the oöcyte's entry into vitellogenesis?

One of the hallmarks of germ tissue in insect meroistic ovarioles is a high degree of polarity between nurse cells and oöcytes. This polarity is manifold, including differences in transcriptional and synthetic activity (Telfer, 1975), cytoskeletal dynamics (Huebner, 1984; Gutzeit & Huebner, 1986; Riparbelli & Callaini, 1995), and cell membrane activity and bioelectrical properties (Woodruff *et al.*, 1986a; Woodruff & Telfer, 1990; O'Donnell & Sharda, 1994). Research in each of these areas offers novel insights into the establishment and maintenance of cell polarity.

Among the physiological differences between nurse cell and oöcyte compartments, differences in intracellular ion activity possess the power to impact a broad spectrum of cellular functions relevant to oögenesis. Alterations in intracellular pH (pH_i) can simultaneously influence metabolic activity (reviewed by Busa & Nuccitelli, 1984), microtubule and F-actin assembly and dynamics (Tilney *et al.*, 1978; Tilney & Jaffe, 1980; Regula *et al.*, 1981; Schatten *et al.*, 1985; Southwick, 2000), gap junctional coupling (Perrachia and Perrachia, 1980; Bohrmann & Haas-Assenbaum, 1993; Anderson & Woodruff, 2001; Levin, 2002), and signalling through modulating calmodulin (Busa & Nuccitelli, 1984; Danylovych & Tuhai, 2001) and cyclic AMP stores (Reynolds & Haugaard, 1967; Yajima & Ui, 1975; Busa & Nuccitelli, 1984).

The regulatory capacity of H^+ during early development in a variety of organisms is also well established. In sea urchins, for example, fertilization causes the egg to release 'fertilization acid' from the cytoplasm into the extracellular space, elevating pHi from ~6.8 to 7.3 (Shen & Steinhardt, 1978). This event sets in motion a suite of changes

collectively referred to as the 'late events' of fertilization, including increased protein synthesis, increased metabolism, increased cell membrane K^+ conductance, and rearrangements in the cortical actin cytoskeleton (see Busa & Nuccitelli, 1984 for review). There are numerous examples of extra- and intracellular pH effects during insect oögenesis: vitellogenesis in *Drosophila* is impaired by low extracellular pH, presumably through dissociation of the vitellogenin-receptor complex (DiMario & Mahowald, 1986), and vesicular acidification is required for subsequent processing of the endosomal compartments in a number of species (Nordin *et al.*, 1990,1991). In polytrophic ovarioles of the silkworm moth, *Hyalophora cecropia*, a rise in intracellular pH is accompanied by a myriad of physiological changes at the onset of vitellogenesis (Woodruff & Telfer, 1990). Woodruff & Telfer (1990) have suggested that the pH change may increase metabolic activity in the oöcyte. In *Rhodnius* oöcytes, membrane potential and intracellular pH are affected by changes in pH of the medium (O'Donnell & Sharda, 1994).

In managing pH_i, cells typically exchange hydrogen ions with the extracellular environment. This is especially true of insect cells, which take advantage of the electrogenic nature of H^+ transport to assist in maintaining the membrane potential and to produce a H^+ chemical gradient across the cell membrane to drive secondary transport mechanisms (Harvey & Wieczorek, 1997; Haley & O'Donnell, 1997; Dittmann, 1997). The dependence of cellular H^+ regulation on the extracellular space makes the study of cellular H^+ regulation ideally suited to investigation of extracellular H^+ fluxes using a non-invasive, self-referencing extracellular ion-selective probe (ISP), an approach which permits selective measurement of a single ion type with minimal perturbation of the

tissue. Previous studies using extracellular voltage-sensitive vibrating probes have established that dynamic extracellular bioelectric currents are present around ovarioles of numerous insects including *Blattella* (Bowdan & Kunkel, 1990, 1994), *Locusta* (Verachtert & DeLoof, 1986), *Hyalophora* (Jaffe & Woodruff, 1979; Woodruff *et al.*, 1986b), *Drosophila* (Overall & Jaffe, 1985; Bohrmann *et al.*, 1986), *Sarcophaga* (Verachtert & DeLoof, 1986), *Dysdercus* (Dittmann *et al.*, 1981), *Ips, Sialis* (Huebner & Sigurdson, 1986), and *Rhodnius* (Sigurdson, 1984; Huebner & Sigurdson, 1986; Diehl-Jones & Huebner, 1989, 1992). Ion substitution studies along with pharmacological perturbations have established that Na^+, Cl^-, K^+, and Ca^{2+} contribute to these currents in *Rhodnius* (Diehl-Jones & Huebner, 1993). Although voltage-sensitive probes have offered some insight into the character of these ionic currents they are inherently limited, since current alterations due to secondary or synergistic effects of pharmacological perturbation are difficult to rule out. The ion-selective probe offers a considerable advantage as a direct measuring tool without pharmacological complications.

The regulation of developmental processes during oögenesis in *Rhodnius* is not fully understood. Despite the importance of pH_i in many cell processes, little is known about pH_i and H^+ flux during oögenesis in *Rhodnius*. O'Donnell & Sharda (1994) determined the pH_i of vitellogenic follicles 400-600 μm in length and carefully investigated the dependence of oöcyte membrane potential on both intra- and extracellular pH, but did not examine H^+ flux and pH_i changes within the follicle related to oöcyte growth over a complete oögenesis cycle. Determining the timing and magnitude of extracellular H^+ dynamics is the essential first step towards understanding the potential role(s) of pH_i changes during oögenesis. By non-invasively measuring

extracellular H^+ dynamics across a range of stages of oögenesis, we can gain insight into regional and stage-specific pH_i changes in the adult *Rhodnius* ovariole. The research presented here undertook to determine the spatial and temporal distribution of H^+ fluxes around the ovariole during a complete oögenesis cycle, and to relate these fluxes to cell differentiation and regulatory events of oögenesis.

MATERIALS AND METHODS

Ovariole Preparation

A colony of *Rhodnius prolixus* was maintained at 27°C and 65% relative humidity in controlled environment incubators, and fed every 3-4 weeks on rabbits or using an artificial membrane technique (Huebner *et al.*, 1994). Ovaries dissected from mated adult females 3-12 days post-feed (dpf) were transferred to Petri dishes containing modified O'Donnell's *Rhodnius* Ringers (O'Donnell, 1985), composed of 129 mM NaCl, 8.6 mM KCl, 0.02 mM $CaCl_2$, 10.48 mM $MgCl_2$, 48 mM dextrose, and 1mM HEPES, adjusted to 340 mOsm. Ovarioles were carefully isolated and desheathed, without stretching or damaging the ovariole. The Ringers used for these trials had reduced [HEPES] to minimize dampening of extracellular H^+ fluxes (Kunkel & Faszewski, 1995) and reduced calcium to improve the signal-to-noise ratio (Somiesky & Nagel, 2001). Ovarioles under these conditions behaved normally: follicle cells remained adherent to the oöcyte (an association that is lost in Ca^{2+}-free saline) and muscular contractions of the ovariole sheaths appeared to be unaffected over the time period needed to complete a scan.

Magnesium was added to compensate for the reduced [Ca^{2+}], and osmolarity was adjusted using glucose. Ovarioles were transferred to a specially designed recording chamber that facilitated rotation and positioning of the ovariole while minimizing deformation and stretching (Huebner & Bjornsson, 2002).

Ovarioles were staged based on the length of the T follicle, after Pratt & Davey (1972). Briefly, ovarioles between 300-1000 μm were grouped into stages (1-7) spanning 100 μm intervals. Stage 8 ovarioles include T follicles spanning 1000-1500 μm in length, and stage 9 ovarioles are from 1500-2000 μm in length (see table 1). Previtellogenesis typically spans stages 1-3 (300-500 μm), vitellogenesis begins around stage 3-4, and chorionation occurs during stage 9. T follicle length was measured to the nearest 5 μm with Northern Eclipse™ imaging software using an image taken during each scan. The software was calibrated using a micrometre image captured under identical conditions.

STAGE	T Oöcyte Length (μm)	Features
1	300-400	Late previtellogenesis
2	400-500	Onset of vitellogenesis
3	500-600	Early vitellogenesis
4	600-700	Midvitellogenesis
5	700-800	Midvitellogenesis
6	800-900	Mid-late vitellogenesis
7	900-1000	Late vitellogenesis
8	1000-1500	NC-oöcyte continuity lost (trophic cord closes)
9	1500-2000	Chorionation

Table 1: Ovariole stage descriptions for a complete oögenesis cycle in *Rhodnius*. Staging is based on T oöcyte length, and several stages are characterized by specific developmental events, as outlined here.

Ion-Selective Probe (ISP) Technique

Extracellular H^+ flux was measured with the automated scanning electrode technique (ASET) using a non-invasive ion-selective probe (ISP)(Applicable Electronics, Inc., Sandwich, MA; Science Wares, Inc., Falmouth, MA). Glass probes were fashioned from TW150-4 borosilicate capillary tubes (World Precision Instruments, Inc., Sarasota, FL) pulled to a 4 μm-diameter tip on a programmable Sutter P-97 Flaming/Brown pipette puller. H^+ probes were backfilled with 40 mM KH_2PO_4 and 100 mM KCl, pH 7.0, and then frontfilled with a 40-50 μm column of hydrogen liquid ion exchanger (LIX)(#85293, Fluka Chemie, Inc., Switzerland). The H^+ probe was placed in an electrode holder (#MEH2SW15, WPI, Inc.) having a chlorided silver wire. Chloriding was accomplished by placing the freshly sanded wire in a 0.1 M HCl solution while connected to the positive terminal of a 9V battery with a 1 kΩ resistor in series. The half-cell was completed by placing a coiled silver wire, connected to the negative battery terminal, into the acid. Chloriding was complete when the electrode-holder wire displayed a uniform brownish-black coat. A DRIREF2 reference electrode (WPI, Inc.) was chosen for its low ion leakage properties.

The ISP and reference electrodes were connected to a preamplifier mounted on a 3-D stepper motor-driven motion stage (Applicable Electronics, Inc.) operated by a PC computer using ASET software v.1.04 (Science Wares, Inc.). The signal from the preamplifier was passed to an amplifier (Applicable Electronics, Inc.) and then to the PC, where data were collected using ASET software. Transmitted images capturing the X-Y axes were taken with a Cohu 6500 video camera mounted on a Zeiss IM35 inverted

microscope using a Zeiss plan 2.5x objective. In addition, side view (Z-axis) images were captured using a Panasonic WV-CD50 video camera fitted with a long focal length Optem Zoom-70 lens. Both were displayed on a Sony Trinitron colour monitor from which the signal was conveyed to a PC via a Computer Eyes 1024 framegrabber that received the analogue inputs from both cameras. A Fostec fibre-optic lamp fitted with an infrared filter was used to illuminate the preparation. The microscope and probe assembly were isolated from vibration by a Melles Griot air table and electronically by a Faraday cage. The ISP signal was also independently monitored using a Tektronics 2205 oscilloscope to assess signal noise and fidelity. The oscilloscope signal provided the first indication if a probe was losing responsiveness. All ISP and peripheral equipment was powered by a dedicated AC wall outlet whose neutral line was connected through an isolation transformer directly to ground to eliminate noise from other equipment in the building; this arrangement was of paramount importance to achieve the low noise necessary to detect ion fluxes at the biological level.

Electrode calibrations were performed at the beginning and end of each ovariole scan, by measuring voltage offset in 0.1 M phosphate buffers with pH 8.0, 7.0, and 6.0, providing a measure of the probe's accuracy and its speed of response. H^+-selective probes were only used if the slope of a line derived by plotting the logarithm of $[H^+]$ vs. the electrode's voltage output equalled the expected Nernst value of $56.2 \pm 5\%$ mV per 10-fold change in concentration. If the calibration at the start or end of the scan deviated from expected Nernst values, or if the probe took longer than 10 seconds to settle on a voltage value during the calibration procedure, the reliability of the probe was questioned, and data from that scan were considered invalid and were excluded.

A 3D sampling routine was used that measured hydrogen ion concentration at an 'origin' position within 2 μm of the ovariole surface, and 10 μm away from this origin in a single direction in each of the X-, Y- and Z-axes, for a total of four measurements. After moving to a new point, the probe was paused for 1 second before taking a 1 second reading. Each measurement is an average of 200 samples per second. Five complete 3D measurements were taken at each position along the ovariole, and subsequently averaged during analysis. H^+ readings usually provided extremely stable measurements over extended periods of time (an example is shown in Figure 1a); however, the probe periodically required more time to equilibrate at a new position. If the signal at any position along the ovariole appeared to drift during measurement, further readings were taken until they stabilized for at least five measurements or until two minutes had elapsed, whichever happened first (see Figure 1b). If the probe eventually settled the last five values were averaged as usual. However if, in this time, the measurements did not reach an asymptote (an example is shown in Figure 1c), values for the entire reading were averaged and the resulting large standard deviation was accepted.

Each scan included background noise measurements taken at a point more than 500 μm away from the tissue before and after points along the ovariole were scanned. Twenty-five points were measured along all stage 2-9 ovarioles, and additional points were measured in later stage ovarioles. Additional points were added to acquire more information as the connective stalk anterior to the T follicle grew and the follicle cells began to differentiate during stages 2-3, and to measure specific areas associated with the development of regionally specialized areas of chorion production during stages 8-9. Figure 2 depicts the standard points measured including points added during later stages

of development. An image was captured at every point measured, recording the precise position of the probe. This allowed proper placement of a vector representing the H^+ flux at that point during data analysis (described below), and provided a means of assessing the ovariole's condition after the scan was complete.

Positions were measured at the midline of the ovariole, i.e., halfway up the ovariole in the vertical Z-axis. The midline was easily seen along most of the ovarioles using the side view camera and transmitted light, except for positions along opaque vitellogenic follicles. To overcome the opacity problem, the probe was moved to the interfollicular stalk separating T and T-1 follicles, which was defined as zero distance for the Z-axis. Next, the probe was moved to the pedicel, and the distance above or below Z-axis zero was noted. To calculate the height of positions 3/4, 1/2, and 1/4 along the T follicle, the difference in distance between pedicel and interfollicular stalk was multiplied by the fractional distance along the T follicle. For example, if the pedicel was 80 μm higher than the T connective in the Z-axis, then the 3/4, 1/2, and 1/4 positions were taken at 60, 40, and 20 μm, respectively. This procedure allowed proper positioning of the probe along the Z-axis midline despite the opacity of vitellogenic follicles.

Most features of the roughly cylindrical adult *Rhodnius* ovariole possess a high degree of radial symmetry, with only a few indications of polarity outside the anteroposterior axis. During previtellogenesis the oöcyte nucleus, or germinal vesicle, moves from its central position to the cell periphery, providing a landmark allowing consistent orientation of the ovariole relative to the probe. The oöcyte nucleus was used because it is an obvious marker of oöcyte polarity, and while it is unknown how this relates to the future body axes of the embryo in *Rhodnius*, work on *Drosophila* has

established that nuclear position defines both the anteroposterior and dorsoventral axes by restricted signalling to follicle cells in the immediate vicinity (Gonzales-Reyes *et al.*, 1995; Roth *et al.*, 1995). Ovarioles were oriented in one of four 'quadrants', each separated from neighboring quadrants by 90°, so that the offset germinal vesicle of the penultimate (T-1) follicle was held towards or away from the probe, or facing up or down in the chamber (see Figure 3). In a few cases the T-1 follicles of early stage (stage 2) ovarioles still possessed a central nucleus; in these cases the nucleus of the previtellogenic T oocyte was still visible and was used for orientation instead. In stage 9 ovarioles in which the T-1 follicle was vitellogenic and the T-1 nucleus obscured, the T-2 oöcyte nucleus was used instead. Initially, ovarioles were rotated through 360° and positions along all four quadrants were measured. Due to physical constraints of the ISP technique, these scans often lasted 6-7 hours, so subsequent scans were restricted to a single quadrant to collect data within the shortest physiological window possible. Only the first quadrant from early trials was used for subsequent data analysis, except for the analysis of rotational differences that compares differences observed in ovarioles with four quadrants measured to differences found among the first measured quadrant of all ovarioles.

Data Analysis

Data were exported in text file format and analyzed using Microsoft Excel™. Visual basic macros were developed (see Appendix II) in Excel to calculate proton flux based on the method of Kuhtreiber & Jaffe (1990), and to generate 2D and 3D resultant

vectors from the X- and Y-axis values and the X-, Y-, and Z-axis values, respectively. Z-axis data were excluded because upon further analysis it became clear that they confounded the data while not contributing any essential further information, since the trends seen in 2D vectors were merely confirmed in the 3D vectors. Z-axis flux corresponds to rotational flux that would be present if, for example, a source of efflux were present in one orientation and coupled to a source of influx in another orientation. Z-axis fluxes measured during these trials showed no consistent pattern or magnitude. Since no differences in H^+ flux were observed between different orientations in the X-Y plane either, the Z-axis flux was excluded from subsequent data analysis. Next, an image was generated using Adobe Illustrator 9™ that displayed H^+ flux at each position measured along the ovariole. To accomplish this, the first image taken during the trial was used as a backdrop. Next, the image corresponding to the vector being placed (showing the position of the probe in relation to the ovariole) was positioned over the original image and rendered partially transparent allowing the two ovariole images to be juxtaposed. If the second picture needed rotating to line up correctly, as sometimes happened when the ovariole moved slightly during a trial, it was adjusted to the nearest 0.5°, and the corresponding vector was similarly rotated before being placed. A line of arbitrary, consistent length was scaled according to the vector magnitude, so that H^+ flux at different positions and from different ovarioles could be directly compared. Each vector was positioned so that the origin was next to the ovariole at the location where the probe measurement was taken. Once positioned in this way, each vector was scored as a positive efflux if it travelled away from the ovariole, or as a negative influx if it travelled over the ovariole image. Examples of these images are shown in the results (Figure 4).

Once signs were assigned, data from each ovariole were grouped according to ovariole stage, and stage-specific averages and standard errors were calculated for each position measured along the ovariole. Using StatView software (SAS Institute Inc., Cary, NC), single-factor ANOVAs followed by pairwise comparisons of each position were calculated for each stage, using ovariole position as the categorical variable, to assess the significance of signal vs. background noise. Significant difference was assigned as $P < 0.05$. Pairwise comparisons were corrected using a Fishers' PLSD (Protected Least Significant Differences) post-test to reduce the likelihood of type I errors.

RESULTS

General Features of Extracellular H^+ Flux Around Adult *Rhodnius* Ovarioles

H^+ flux measured near the ovariole was an order of magnitude above the background noise. Noise measurements taken several hundred microns from the ovariole averaged 29 mV or 10 fmoles/cm^2/sec and never surpassed 68 mV (26 fmoles/cm^2/sec) in any single trial, while H^+ flux along the ovariole surface routinely measured several hundred mV (~200 fmoles/cm^2/sec) and reached 1473 mV or 561 fmoles/cm^2/sec.

A large body of data was collected for this study, from nearly 30 positions along each of 88 ovarioles (over 2600 measured points) representing 8 stages of oögenesis; ovarioles with atretic follicles, ovarioles in which the 30 positions were measured along each of four quadrants, and additional positions in regions of special interest are not included in this main body of data. In analyzing these data we were interested in

detecting both spatial differences in H^+ flux along the ovariole surface, as well as temporal differences occurring within an oögenesis cycle, as represented by ovarioles grouped according to stage (see Methods above). Consequently, there were several options for displaying the data, each with characteristic strengths in terms of highlighting different aspects of the data set. The inferences derived from three such modes of data presentation are discussed in turn below.

Before describing the data in detail, it is worth highlighting one of the most striking features of H^+ flux measured around adult *Rhodnius* ovarioles and averaged according to stage, namely that it was dominated by efflux. Influx was observed at a few points along the ovariole, including the anterior tropharium and the anterior T follicle surface. However, influx at the anterior tropharium was barely detectable and not significantly different from background noise, and influx along the anterior T follicle did not appear until later stages. Neither of these regions of influx is capable of balancing efflux during any stage. Possible explanations for this phenomenon are considered later, in the Discussion.

1. Prominent H^+ Fluxes Occur at Specific Ovariole Structures

Plotting average H^+ flux vs. ovariole position for each ovariole stage revealed that H^+ fluxes are localized to discrete regions of the ovariole, as depicted in the series of graphs in Figure 5. In all stages, H^+ flux at a few positions was especially prominent, including the three positions along the interfollicular stalk separating the T and T-1 follicles, and both positions along the pedicel. In addition, H^+ flux at several other

positions became significant during later stages, notably at the junction between T-1 and T-2 follicles during stages 7-9, and the position where the anterior and lateral surfaces of the T follicle meet during stage 9. Furthermore, H^+ flux along the anterior of the T follicle appeared to change with stage, although a comparison between stages was difficult using this series of graphs. Average H^+ flux along the tropharium, previtellogenic follicles and the lateral surfaces of T follicles were not significantly greater than background H^+ flux, as determined by two-way analysis of variance. Regions of significant H^+ flux along the ovariole are considered below for each individual stage.

Previtellogenesis

During the entire course of experimentation, using ovarioles from insects dissected 3-12 dpf, only one stage 1 ovariole was encountered. This ovariole appeared to be distressed, and was consequently removed from subsequent analysis.

During stage 2 (T follicle length 400-500 μm), H^+ efflux at the connective stalk separating T and T-1 follicles was significantly different from background noise; efflux at the posterior stalk averaged 145 ± 82 fmoles/cm^2/sec ($P = 0.0001$, $n = 2$), efflux at the mid stalk averaged 123 ± 26 fmoles/cm^2/sec ($P < 0.0001$, $n = 10$), and efflux at the anterior stalk averaged 48 ± 2 fmoles/cm^2/sec ($n = 2$) but was not significantly different from background ($P = 0.2675$). Efflux at the posterior pedicel stalk averaged 121 ± 33 fmoles/cm^2/sec ($P < 0.0001$, $n = 10$), while efflux at the mid-pedicel region averaged 176 ± 41 fmoles/cm^2/sec ($P < 0.0001$, $n = 9$). All other positions were not significantly different from background noise.

Early Vitellogenesis

During stage 3 (T follicle length 500-600 μm), H^+ efflux at the connective stalk separating T and T-1 follicles increased marginally; efflux at the posterior stalk measured 236 fmoles/cm^2/sec ($P < 0.0001$, $n = 1$), at the mid stalk averaged 202 ± 30 fmoles/cm^2/sec ($P < 0.0001$, $n = 10$), and at the anterior stalk measured 211 fmoles/cm^2/sec ($P < 0.0001$, $n = 1$). Interestingly, only one of 10 ovarioles measured at this stage had formed a connective stalk long enough to permit measurement at three positions. Efflux at the T-1 3/4 averaged 44 ± 8 fmoles/cm^2/sec ($P = 0.0374$, $n = 10$). Along the T follicle, efflux at the anterior T 1/3 position also increased, averaging 117 ± 21 fmoles/cm^2/sec ($P < 0.0001$, $n = 10$), and at the anterior T 2/3 position averaged 47 ± 10 fmoles/cm^2/sec ($P = 0.0239$, $n = 10$). Efflux at the pedicel increased; the posterior stalk averaged 274 ± 30 fmoles/cm^2/sec ($P < 0.0001$, $n = 9$), while the mid stalk region averaged 246 ± 23 fmoles/cm^2/sec ($P < 0.0001$, $n = 8$). All other positions were not significantly different from background noise.

During stage 4 (T follicle length 600-700 μm), H^+ efflux at the connective stalk separating T and T-1 follicles reached its maximal rate and its maximum variability; efflux at the posterior stalk averaged 316 ± 74 fmoles/cm^2/sec ($P < 0.0001$, $n = 5$), at the mid stalk averaged 237 ± 53 fmoles/cm^2/sec ($P < 0.0001$, $n = 9$), and at the anterior stalk averaged 174 ± 76 fmoles/cm^2/sec ($P < 0.0001$, $n = 5$). Efflux at the T-1 3/4 averaged 39 ± 7 fmoles/cm^2/sec ($n = 9$), diminishing slightly and no longer significantly different from background noise ($P = 0.3202$). Along the T follicle, the anterior T 1/3 position also increased, averaging 145 ± 44 fmoles/cm^2/sec ($P < 0.0001$, $n = 9$). Efflux at the pedicel

remained comparable to stage 3; efflux at the posterior stalk averaged 235 ± 48 fmoles/cm^2/sec ($P < 0.0001$, $n = 9$), while the mid stalk region averaged 223 ± 26 fmoles/cm^2/sec ($P < 0.0001$, $n = 9$). All other positions were not significantly different from background noise.

Midvitellogenesis

During stage 5 (T follicle length 700-800 μm), H^+ efflux at the connective stalk separating T and T-1 follicles declined slightly, resembling stage 3 levels; the posterior stalk averaged 291 ± 47 fmoles/cm^2/sec ($P < 0.0001$, $n = 9$), the mid stalk averaged 181 ± 29 fmoles/cm^2/sec ($P < 0.0001$, $n = 10$), and the anterior stalk averaged 116 ± 20 fmoles/cm^2/sec ($P < 0.0001$, $n = 9$). By this stage, all ovarioles sampled but one had well developed interfollicular stalks. Efflux at the T-1 3/4 averaged 41 ± 6 fmoles/cm^2/sec ($n = 10$), and was not significantly different from background noise during this stage ($P = 0.1475$). Along the T follicle, efflux at the anterior T 1/3 position continued to increase, averaging 153 ± 37 fmoles/cm^2/sec ($P < 0.0001$, $n = 10$), and efflux at the anterior T 2/3 averaged 74 ± 16 fmoles/cm^2/sec ($P < 0.0029$, $n = 10$). Efflux at the pedicel remained comparable to previous stages; efflux at the posterior stalk averaged 210 ± 27 fmoles/cm^2/sec ($P < 0.0001$, $n = 10$), while efflux at the mid stalk region averaged 190 ± 24 fmoles/cm^2/sec ($P < 0.0001$, $n = 7$). All other positions were not significantly different from background noise.

During stage 6 (T follicle length 800-900 μm), H^+ efflux at the connective stalk separating T and T-1 follicles diminished further; efflux at the posterior stalk averaged

146 ± 26 fmoles/cm^2/sec ($P < 0.0001$, $n = 12$), at the mid stalk averaged 101 ± 21 fmoles/cm^2/sec ($P < 0.0001$, $n = 12$), and at the anterior stalk averaged 60 ± 17 fmoles/cm^2/sec ($P < 0.0042$, $n = 12$). Efflux at the T-1 3/4 averaged 25 ± 6 fmoles/cm^2/sec ($n = 12$), and was not significantly different from noise ($P = 0.4450$). Along the T follicle, efflux at the anterior T 1/3 position also decreased, averaging 66 ± 23 fmoles/cm^2/sec ($P = 0.0016$, $n = 12$). Efflux at the pedicel remained comparable to previous levels; the posterior stalk averaged 198 ± 25 fmoles/cm^2/sec ($P < 0.0001$, $n = 11$), while the mid stalk region averaged 180 ± 19 fmoles/cm^2/sec ($P < 0.0001$, $n = 10$). All other positions were not significantly different from background noise.

Late Vitellogenesis

During stage 7 (T follicle length 900-1000 μm), H^+ efflux at the connective stalk separating T and T-1 follicles declined further; efflux at the posterior stalk averaged 136 ± 23 fmoles/cm^2/sec ($P < 0.0001$, $n = 10$), at the mid stalk averaged 74 ± 18 fmoles/cm^2/sec ($P = 0.0001$, $n = 10$), and at the anterior stalk averaged 45 ± 12 pmoles/cm^2/sec ($n = 10$). Efflux at the T-1 diminished further, averaging 21 ± 8 fmoles/cm^2/sec ($n = 10$). Along the T follicle, the anterior T 1/3 position dropped to a level insignificantly different from background noise, diminishing to an average of 16 ± 33 fmoles/cm^2/sec ($n = 10$). Efflux at the pedicel remained comparable to previous levels; the posterior stalk averaged 206 ± 14 fmoles/cm^2/sec ($P < 0.0001$, $n = 9$), while the mid stalk region averaged 202 ± 21 fmoles/cm^2/sec ($P < 0.0001$, $n = 9$). Beginning with stage 7 ovarioles, a small increase in H^+ efflux over the T-1 T-2 junction can be detected that is

higher than other positions nearby, averaging 41 ± 7 fmoles/cm^2/sec (n = 10). All other positions were not significantly different from background noise or from the positional average during previous stages.

During stage 8 (T follicle length 1000-1500 μm), H^+ efflux at the connective stalk separating T and T-1 follicles reached its minimum rate; efflux at the posterior stalk averaged 86 ± 10 fmoles/cm^2/sec ($P < 0.0001$, n = 16), at the mid-stalk averaged 47 ± 9 fmoles/cm^2/sec ($P = 0.0143$, n = 17), and the anterior stalk averaged 29 ± 7 fmoles/cm^2/sec ($P = 0.2254$, n = 15). By this stage, H^+ efflux over the posterior T-1 was no longer significantly different than noise, averaging 15 ± 6 fmoles/cm^2/sec ($P = 0.6977$, n = 17). Along the T follicle, the anterior T 1/3 and 2/3 positions actually reversed, and influx averaging 38 ± 18 fmoles/cm^2/sec ($P = 0.0021$, n = 17) and 23 ± 17 fmoles/cm^2/sec ($P = 0.0328$, n = 17), respectively, was observed. Efflux at the pedicel remained comparable to previous levels; efflux at the posterior stalk averaged 244 ± 35 fmoles/cm^2/sec ($P < 0.0001$, n = 12), and at the mid stalk region averaged 237 ± 27 fmoles/cm^2/sec ($P < 0.0001$, n = 10). H^+ efflux at the T-1 T-2 junction averaged 41 ± 12 fmoles/cm^2/sec ($P = 0.0370$, n = 17), and once again nearby positions were similar to previous stages. All other positions were not significantly different from background noise.

Chorionation

Stage 9 ovarioles (T follicle length 1500-2000 μm) developed two strong H^+ fluxes not seen in earlier stages. First, efflux averaging 116 ± 22 fmoles/cm^2/sec was

observed at the T-1 T-2 junction ($P < 0.0001$, $n = 10$), anterior to the newly activated T-1 follicle. Weaker efflux in this region was observed during stages 7 and 8, and by stage 9 many T-1 follicles had entered vitellogenesis and formed well-developed interfollicular stalks. The stage average is heavily weighted by trials with T-1 follicles in midvitellogenesis. H^+ efflux at the connective stalk separating T and T-1 follicles during stage 9 also increased; the posterior stalk averaged 212 ± 44 fmoles/cm^2/sec ($P < 0.0001$, $n = 8$), the mid stalk averaged 149 ± 24 fmoles/cm^2/sec ($P < 0.0001$, $n = 9$), and the anterior stalk averaged 48 ± 29 fmoles/cm^2/sec ($P = 0.2457$, $n = 6$). H^+ efflux at the T-1 3/4 resembled stage 8 levels, averaging 14 ± 11 fmoles/cm^2/sec ($n = 10$), again not significantly different than noise ($P = 0.9717$). Along the T follicle, influx along the anterior 2/3 position averaged 28 ± 20 fmoles/cm^2/sec ($P = 0.1129$, $n = 9$), while the anterior 1/3 position returned to an efflux averaging 32 ± 26 fmoles/cm^2/sec ($P = 0.4667$, $n = 10$). The second new H^+ flux is seen over the specialized rim and pseudomicropyle structures of the forming chorion. A strong, discretely localized efflux in this region was observed in two ovarioles and reached an average of 271 ± 10 fmoles/cm^2/sec ($P < 0.0001$, $n = 3$). While the graphs presented here show only a single point, this efflux was characterized further, and is considered below along with other special regions of interest. Efflux at the pedicel remained comparable to previous levels; the posterior stalk averaged 230 ± 32 fmoles/cm^2/sec ($P < 0.0001$, $n = 6$), while the mid stalk region averaged 208 ± 13 fmoles/cm^2/sec ($P < 0.0001$, $n = 6$). All other positions were not significantly different from background noise.

2. Localized H^+ Fluxes Change Over an Oögenesis Cycle

While the graphs in Figure 5 convey a sense of the spatial patterns of extracellular H^+ flux during individual stages, a broad view of the dynamic nature of H^+ fluxes over an entire oögenesis cycle is difficult to extract from them. These temporal differences are best conveyed in a complementary set of plots displaying extracellular H^+ flux vs. stage for each position along the ovariole, shown in Figure 6. This series of graphs more clearly represents the stage-specific variation in magnitude and direction of flux at many positions along the ovariole. H^+ flux at many regions along the ovariole did not change significantly, including (from anterior to posterior) the tropharium, previtellogenic follicles, and the lateral surface of the T follicle. Even the prominent efflux at the interfollicular stalk at the posterior pole of the T follicle was steady, averaging 216 fmol/cm^2/sec across all stages. Some regions displayed considerable change, as indicated by two-way analysis of variance, which confirmed that several positions exhibited significant changes in H^+ flux during oögenesis.

3. Spatiotemporal Pattern of Extracellular H^+ Flux during an Oögenesis Cycle

Once the discrete spatial and temporal patterns of H^+ flux have been considered independently, their interrelationships can be more conveniently combined to display the spatiotemporal 'landscape' of extracellular H^+ flux measured along the entire ovariole surface over a complete oögenesis cycle. In Figure 7, data from Figures 5 and 6 are collectively presented in a contour plot. The advantage of this plot is that one can survey

the overall pattern of both positional and stage-specific trends more easily, although detailed information on each point (as shown in Figures 5 & 6) is not readily extracted.

Detailed Analysis of H^+ Flux Along Specific Regions of the Ovariole

The spatiotemporal patterns of extracellular H^+ flux, derived from the average flux at each position along ovarioles grouped according to stage, constitute the major focus of this work. During the course of experimentation a few special cases, which for a variety of reasons were not evident in the graphs above, were encountered that merit discussion. These are considered next.

During scans of stage 9 ovarioles, in order to resolve more accurately the source of the prominent H+ efflux near the forming chorion rim, an increased number of positions were measured. H^+ efflux was confined to a narrow region along the horizontal (anteroposterior) XY-plane (Figure 8), and continued circumferentially around the ovariole along the Z-axis (not shown). In addition, H^+ efflux in this region could be detected along stage 9 T follicles held in different orientations, suggesting it formed a complete ring encircling the rim. Fine mapping of the region to identify individual cells responsible for generating H^+ efflux was not possible due to probe tip size, the limited optics of the side-mounted camera, and difficulties in visualizing specific groups of cells using the XY-plane camera due to the curvature of the ovariole. Still, the resolution was such that we could resolve a distinct and narrow zone (likely 3-4 cells wide at most) that composed part of the rim close to the junction between the cap and the neck region of the main body (Figure 8). Remarkably, H^+ efflux in this area continued even after ovulation,

when the associated chorionated oöcyte had been released into the oviduct (Figure 9). No H^+ flux was detected around the corresponding region of recently ovulated eggs (Figure 10).

The tropharium and early previtellogenic follicles displayed H^+ fluxes only marginally greater than background noise levels, but stronger fluxes were detected over the prefollicular region in a few ovarioles. In these cases, irregularly shaped cells that are not part of the ovariole proper had been retained on the outer surface of the basal lamina during desheathing (Figure 11).

H^+ efflux begins at the junction between T-1 and T-2, in the region of the newly forming connective, by stage 7 (Figure 6). Finer mapping, obtained by increasing the number of positions sampled in the region, reveals that H^+ efflux in this region also extends posteriorly, presumably associated with the columnar follicle cells at the anterior pole of the oöcyte (Figure 12, asterisk).

During the course of experimentation a few ovarioles with atretic follicles were encountered, and these were scanned out of interest although they were not included in the compiled data. A comparison of these ovarioles to ovarioles from the corresponding stages is shown in Figure 15 (Figures 13 and 14 are referred to later, in the Discussion). H^+ flux around atretic follicles did not differ considerably from healthy follicles of similar stage.

H^+ Fluxes Did Not Show Rotational Differences Relative to T-1 Orientation

An original goal of these experiments was to determine whether radial asymmetries exist in H^+ flux relative to the orientation of the follicle. Previous studies of *Rhodnius* ovarioles using non-invasive voltage-sensitive vibrating probe technology revealed radial asymmetries when the ovariole was positioned according to the trophic cord (Diehl-Jones & Huebner, 1992). In the present study, the orientation of the T-1 nucleus was used as a marker in an effort to detect differences in H^+ flux associated with one of the early signs of oöcyte dorsoventral polarity. During initial trials, measurements were made at each position along all four quadrants of every ovariole. While most positions remained relatively consistent and showed no differences among the four quadrants measured, significant radial differences in H^+ flux magnitude were observed at a few positions, most notably the interfollicular stalk joining T and T-1 follicles. However, H^+ flux changed regardless of which radial quadrant was measured first, and in a manner independent of the quadrant measured. Additionally, in trials where the original quadrant was measured a second time at the end of the trial, the results generally differed from initial values. As a further test, several ovarioles were measured either at the same position along the interfollicular stalk anterior to the T follicle over several hours or along the same quadrant four consecutive times. This allowed determination of the general stability of these steady-state fluxes over time, and of the consistency of the overall trend. H^+ efflux at the T connective during these trials declined over the first three readings and held steady for the final reading.

Clearly to do a comprehensive 4-quadrant scan over many positions along a complex structure requires a significantly long time. As a result, the observed variation could be due to physiological changes as the ovariole adjusts to *in vitro* conditions in the saline, or to unknown, potentially deleterious effects of extended periods *in vitro*, rather than being attributable solely to rotational differences. Still, the extensive initial experiments measuring all 4 quadrants instill confidence in the positional specificity of H^+ events overall, and provide support for the comparison of single-quadrant scans, all taken within a similar timeframe, to determine H^+ patterns during oögenesis.

For these reasons later scans were restricted to measuring a single quadrant, and only the first quadrant measured from earlier scans of all 4 sides was used for analysis. The orientation of each trial was recorded so that data from single-sided trials could be grouped according to T-1 orientation in a further attempt to determine whether radial differences in H^+ flux exist around adult *Rhodnius* ovarioles. Data from stages 3-5 and from 6-8 were combined to increase the sample size; these groups were chosen since the H^+ fluxes among them were relatively similar. Comparison of H^+ flux along different sides of the ovariole based on orientation of the T-1 oöcyte nucleus from each group of data reveals that no significant radial asymmetries exist (see Figure 16), as determined by two-way analysis of variance using ovariole position and quadrant as categorical variables.

DISCUSSION

The foundation and blueprint for development is established during oögenesis, a process that requires a complex orchestration of numerous cellular events involving coordination between the germ cells and various intra- and extraovarian somatic cell types, each with their own important contributions. Determining the mechanisms involved in regulating the location and timing of these events is fundamental to understanding oögenesis. The discovery of dynamic, localized transmembrane H^+ fluxes in *Rhodnius* ovarioles raises new potential roles for H^+ and pH changes in regional cell differentiation and regulatory events during oögenesis in the telotrophic ovariole. Below, I will consider some general aspects of the observed H^+ flux before addressing specific localized and stage-related events, and finally the possible importance of these fluxes to changes occurring during oögenesis.

General Features of Extracellular H^+ Flux during Oögenesis in *Rhodnius prolixus*

One of the most striking features of H^+ flux around adult *Rhodnius* ovarioles is that the large, sustained fluxes at the interfollicular stalk separating T and T-1 follicle and at the pedicel are effluxes. While average influxes were observed, they were small and stage-specific, and by no means balanced overall efflux. Influxes were also observed during individual trials, especially over the lateral T follicle, although they were not always present and in many cases were not observed at all; therefore they did not show up when stage averages were calculated. As a result, it appears that H^+ flux across the cell

membranes of the ovariole did not add up to zero, raising questions regarding the source of the extruded H^+.

Rhodnius ovarioles are dynamic, syncytial systems in which volume and content are subject to change. Therefore, we can only expect that total ion flux and accompanying changes in concentration (resulting from unequal influx and efflux) must balance across all membranes and between all compartments over any given period of time. Growing follicles accumulate proteins, RNA, mitochondria, and yolk precursors; as a result their volume increases considerably. If materials synthesized in the nurse cells act as a H^+ buffer, source or sink, then presumably conditions within both compartments will change as these materials are transported to growing oöcytes. Without determining the change in $[H^+]$ in the extracellular space and between various intracellular compartments over an entire oögenesis cycle, there is no reason to assume that H^+ influx and efflux measured extracellularly must be balanced within individual trials or within each ovariole stage.

Having said this, there must clearly be a spatially or temporally unaccounted fo H^+ source to account for the H^+ efflux observed in these trials (H^+ *source* to account for the observed H^+ efflux that is either spatially or temporally unaccounted for by these trials), i.e., an extracellular source that was tapped earlier than stage 2, or an intracellular source accumulated either previously or during the stages studied. While influx is observed during ovariole development in the 5^{th} instar (see Chapter 4, this thesis), it is unlikely this modest accumulation could account for the large, sustained efflux observed during later oögenesis. Thus it seems more likely that an intracellular source provides H^+ for efflux. Potential sources of H+ will be considered below, under the heading of metabolism.

As mentioned above, the lateral surfaces of the T follicle did produce substantial H^+ fluxes; however, both influxes and effluxes were observed, and in averaging these fluxes according to stage, the balance of influx and efflux in these regions resulted in a mean that was not significantly different from noise. There are two possible explanations for these differences: first, it is possible that the differences reflected the future embryonic axis, as shown for bioelectric currents around ovarian follicles in *Blattella germanica* (Bowdan & Kunkel, 1994) and that we were incapable of discriminating between the different T follicle orientations on the basis of T-1 rotation. A second possibility arises from the morphology of the lateral follicular epithelium, which forms large intercellular spaces during vitellogenesis. When the ion-selective probe was positioned over the lateral T follicle, it may have been placed over the basal surface of a follicle cell, or over the intercellular space. If differences in H^+ flux existed between these two regions, as might occur if small local current loops were established, one might expect the measurements we obtained.

In assessing the biological significance of H^+ fluxes observed during oögenesis, it is necessary to ensure they are of sufficient magnitude to affect the underlying tissue. Although the complexity and syncytial nature of the telotrophic ovariole does not permit simple calculations based on membrane area or cell volume, comparing the magnitude of H^+ fluxes observed in *Rhodnius* to other systems can offer insight into the relative strength of these phenomena. Large H^+ fluxes around adult *Rhodnius* ovarioles were on the order of 200-250 fmoles/cm^2/sec, relatively small when compared to those of other ions like calcium, typically 2-10 pmoles/cm^2/sec (Kuhtreiber & Jaffe, 1990). Similarly, H^+ fluxes generated by a diversity of biological systems are often quite large, ranging

from 8-100 pmol/cm^2/sec in amphibian skin and turtle bladder, and up to 200-300 pmol/cm^2/sec in rat collecting duct (Somiesky & Nagel, 2001). Regions of the midgut in mosquito larvae produce H^+ efflux around 65 nmol/cm^2/sec (Boudko *et al.*, 2001). H^+ flux around growing hyphal tips has been reported in the fmol/cm^2/sec range (Lew, 1999). It is important to remember that in *Rhodnius* as in most biological systems, intracellular and extracellular concentrations of H^+ are both relatively low compared to other ions, so large H^+ fluxes may not be required to bring about significant changes in pH. Furthermore, a complete oögenesis cycle in *Rhodnius* lasts approximately 4 days (Huebner, 1981b; Davey, 1965, 1967), and since H^+ efflux at the connective stalk separating T and T-1 follicles appears to continue over this entire period, the cumulative transport of H^+ becomes quite large.

Regional Extracellular H^+ Fluxes Observed during Oögenesis

As outlined in the results, prominent extracellular H^+ fluxes measured using the ion-selective probe were mapped to discrete regions of the ovariole, suggesting they are important to the physiology of cells in the region. At many locations, the pattern of H^+ flux also changed over an oögenesis cycle, suggesting these temporal changes are linked to dynamic events during oögenesis. Thus it is important to consider the location and temporal dynamics of these fluxes relative to the germ and somatic cell events contributing to the development of a viable mature oöcyte.

H^+ Efflux at the Junctions Separating Follicles

Locations like the interfollicular stalk are ideally situated to regulate interfollicular communication. They may isolate follicles, allowing only a single follicle to enter vitellogenesis at once, or they may produce or relay the intraovariolar physiological feedback that keeps previtellogenic follicles from entering vitellogenesis until the terminal oöcyte is nearly ready to leave the ovariole. They may also generate anteroposterior polarity in both adjoining follicles. Therefore, the prominent H^+ efflux observed at the interfollicular stalk separating T and T-1 follicles is of great interest. The stage-related variation in the strength of this H^+ efflux is particularly interesting, since it suggests a relationship to the development of the terminal follicle. Oögenesis in insect ovarioles involves a progression of stages: an oöcyte in the penultimate (T-1) position becomes the terminal oöcyte once the current chorionated T follicle passes into the oviduct. The H^+ efflux at the anterior end of the T follicle can be traced back to follicles in the T-1 position as early as stage 7, where efflux begins before the connective stalk starts to constrict (see Figure 12 and Results).

Analysis of transmembrane bioelectric currents during oögenesis in *Rhodnius* ovarioles also indicates that the interfollicular junction is the source of the largest efflux along the ovariole (Sigurdson, 1984; Sigurdson & Huebner, 1986; Diehl-Jones & Huebner, 1989, 1992; Diehl-Jones, 1994). Stage-related differences were also detected in these studies, although the peak current was identified at stage 7 (Diehl-Jones & Huebner, 1992), rather than at stage 4 (present study). Since voltage-sensitive techniques measure total current carried by all ions, it is possible that current at the interfollicular

stalk is carried by other ions in addition to H^+, and that these exhibit different stage-related dynamics. Indeed, pharmacological studies suggest that Na^+ is a major component of the efflux in this region (Diehl-Jones & Huebner, 1992). Highly selective Na^+ LIXs that did not respond to K^+ were not available when this work began; recently a more Na^+-selective LIX has been developed (Carden *et al.*, 2001). Characterization of the transmembrane Na^+ flux at the interfollicular stalk could help resolve this issue.

Which Cells are Responsible for H^+ Efflux at the Interfollicular Stalk?

Identification of the cell group(s) that generates H^+ efflux is essential to identify which cells might be affected by possible changes in pH_i. This in turn will permit a more refined assessment of potential downstream effects of H^+ efflux, helping to define and direct future avenues of research. Several groups of cells are present at the junction separating T and T-1 follicles that could be wholly or partly responsible for generating the H^+ efflux observed. While the cells responsible for H^+ efflux in this region cannot be absolutely identified, a list of the possible contributors and their associations will permit an appreciation of the potential outcomes of H^+ flux and which compartments may be affected.

The somatic cells of the connective stalk appear to be functionally isolated from the adjacent follicles, since fluorescent dyes (Lucifer yellow, Procion yellow, fluorescein) injected into either follicle do not diffuse into the cells of the stalk, suggesting stalk cells are not coupled to adjacent follicles via gap junctions (Huebner, 1981, unpublished results; Telfer *et al.*, 1984). While restriction of relatively large fluorescent compounds

injected into the adjacent follicles does not rule out ionic coupling absolutely, it suggests that other, more favourable routes of ion transport likely exist.

Comparing the magnitude of H^+ efflux along the stalk reveals whether the source of H^+ efflux is localized to a small region, or spread across the entire stalk. Results presented here clearly demonstrate that of the three connective positions measured, the strongest H^+ efflux was associated with the posterior position during all stages, while the weakest H^+ efflux was consistently associated with the anterior position. Furthermore, a comparison of H^+ efflux at the three stalk positions (see Figure 5) indicates that efflux changes more dramatically at the posterior connective over an oögenesis cycle.

In addition, H^+ flux vectors at more anterior stalk positions (and positions along the anterior T follicle as well) are also regularly directed away from the posterior stalk region. The interfollicular stalks are relatively small, typically no more than 100μm in length. Although the H^+-selective probe was positioned next to somatic cells of the stalk, the close proximity of H^+ fluxes from adjacent follicles could have unavoidably influenced probe readings along the stalk. In studies involving artificial point sources, H^+ flux is often observed up to 100μm away from the source, depending on the strength of the gradient and buffer concentration. On the other hand, in cases where H^+ efflux at the posterior stalk is not as strong (during stage 8 for example), the vector orientations of H^+ fluxes at anterior connective positions do not travel away from the posterior stalk region, but still exhibit a strong component perpendicular to the surface of the ovariole. Thus, even if cells at the posterior end of the stalk produce a significant component of the H^+ flux in this region, it appears that somatic stalk cells over the entire length of the stalk contribute at least partially.

Which Cells Are Affected by H^+ Efflux at the Stalk?

Because H^+ efflux is spatially associated with the interfollicular stalk and appears as the adjacent follicles begin to separate, it is tempting to conclude that H^+ efflux affects the somatic stalk cells, and no more. However, this does not take into account that H^+ flux is closely related to the size of the T follicle. Could H^+ efflux at the interfollicular stalk regulate oöcyte pH_i? To do so it must involve movement of H^+ out of the oöcyte, which could occur either through active H^+ efflux from the oöcyte and either active or passive transport across the follicular epithelium, or through H^+ from the oöcyte entering follicle cells via gap junctions followed by efflux at the follicle cell membrane.

Consider the first scenario, H^+ efflux from the oöcyte followed by transport across the follicular epithelium. If the somatic cells of the interfollicular stalk are actively responsible for H^+ efflux, and since they do not appear to be electrically coupled to the adjoining follicles, then they must take up H^+ from the apical extracellular space at the centre of the stalk. This apical space contains the trophic cord (until it closes in early stage 8 follicles and is gradually resorbed by the tropharium), and is continuous with the intercellular space formed between the oöcyte and follicle cells, in both neighboring follicles. The intercellular space between vitellogenic oöcytes and the associated lateral follicle cells is only separated from the extraovariolar space by the porous basal lamina (tunica propria), since the lateral follicle cells of the posterior vitellogenic (T) follicle develop large extracellular spaces to facilitate yolk uptake. It would seem, therefore, that H^+ extruded from the oöcyte would simply leak out locally instead of moving to the stalk.

A second scenario may offer a simpler explanation in which there are cells next to the connective that are electrically coupled to the T oöcyte and actively engaged in H^+

export (see Figure 14). The presence of such cells would explain the greater efflux observed at the posterior stalk as well as the stage-specific differences in H^+ efflux in this region. Their activity would draw protons out of the anterior pole of the oöcyte, altering oöcyte pH, and establishing a pH gradient in the oöplasm that could play a role in establishing anteroposterior polarity or influencing the stability of the trophic cord. In order to verify the feasibility of this scenario, it must be determined whether H^+ export by the follicle cells would in fact draw H^+ from the oöcyte. A similar mechanism has been postulated for ion transport generally in *Dysdercus* (Munz, 1988). Microinjecting H^+ buffer into the oöcyte to look for reduced H^+ efflux in the interfollicular stalk region may provide an answer to this question.

As previously mentioned, there seems to be a component of the H^+ efflux around the interfollicular stalk that is produced by the stalk cells in addition to stage-related H^+ efflux potentially produced by the posterior follicle. It could be possible that the somatic cells forming the stalk and the putative group of cells coupled to the oöcyte and actively transporting H^+ arise from a common progenitor during early follicle cell differentiation. In *Drosophila* ovarioles, two polar cells are present between the interfollicular stalk and the oöcyte at each pole of the follicle. These cells differentiate from a stalk/polar cell precursor that is set aside in the germarium, and diverge from stalk cells in stage 1 follicles (see Spradling, 1993 for a description of *Drosophila* oögenesis). If a similar group of cells exist in *Rhodnius*, it is possible that they contribute to H^+ efflux at the interfollicular stalk and that they are coupled to the oöcyte. Interestingly, as follicle cells degenerate following ovulation in *Rhodnius*, a thicker region of the connective can be seen in which the cells maintain a strong H^+ efflux (Figure 13). This group of cells may

also be present at the anterior pole of developing follicles, where their situation could allow gap junctional coupling to the oöcyte as well as H^+ efflux.

H^+ Influx Along the Anterior T Follicle: The Influence of Vitellogenesis

A significant feature of stage 8 ovarioles is the onset of H^+ influx across the cap region of the T follicle. While H^+ influx is observed in some T follicles during earlier stages, it appears in the majority of follicles during stage 8 and early stage 9. Both the reduction in H^+ efflux at the connective stalk and the influx across the T follicle cap could serve to lower pH_i.

Vitellogenesis is also occurring at a rapid pace during this time, both in terms of the rate of yolk uptake and the rate of yolk endosomal processing and membrane recycling. Fusion of smaller yolk vesicles into larger, more membrane-efficient spheres requires acidification of the vesicle interior to release vitellogenin from its receptor, so that excess membrane can then return to the oöcyte surface (DiMario & Mahowald, 1986). This process appears to involve H^+-pump activity, likely a V-ATPase (DiMario & Mahowald, 1986; O'Donnell & Sharda, 1994), to move H^+ from the oöplasm into the yolk spheres, or a Na^+/H^+-antiporter (Dittmann, 1997). In some insects, yolk vesicle acidification is delayed until degradation and utilization begin during embryogenesis, while in others, acidification occurs as vitellogenin deposition is diminishing, and chorionation begins (Nordin *et al.*, 1990, 1991).

Therefore, while it is possible that H^+ influx along the T follicle cap and reduction of H^+ efflux along the interfollicular stalk are induced to regulate changes in the follicle

cells or the oöcyte, an alternative explanation is that yolk vesicle acidification becomes strong enough that it secondarily drains the H^+ pool available for efflux. If the total H^+ entering both vesicular and extracellular compartments is equivalent to the total H^+ exiting the cytoplasm during earlier stages, it is possible that oöplasmic pH and associated pH-regulated events (cytoskeletal changes, general metabolism, gap junctional coupling, etc.) could remain relatively constant throughout much of vitellogenesis. This may be testable by using intracellular pH-sensitive microelectrodes or pH-sensitive fluorescence-ratio techniques (dextran-conjugted BCECF, SNARF, etc.) to measure oöplasmic pH in early and late vitellogenic follicles.

Strong H^+ Efflux from Follicle Cells Forming Specialized Chorion Structures

The clearest example of H^+ flux generated by follicle cells is the H^+ efflux that develops during stage 9 near the cap rim, where the micropyle and pseudomicropyle cells form. H^+ efflux begins during chorionation (Figure 8), when most follicle cells are no longer coupled to the oöcyte and are separated from it by the chorion. After the fully developed egg passes into the oviduct, H^+ efflux even continues for a short period along the follicle cells (Figure 9) but not the egg (Figure 10), indicating the follicle cells generate this H^+ flux. H^+ efflux in this region occurs within a narrow zone and attenuates a short distance away in either direction along the anteroposterior axis. While it is difficult to identify the exact group(s) of follicle cells responsible for generating this efflux, fine mapping of the region narrowed the field to a band of cells anterior to the neck, over the cells forming the rim.

Could H^+ efflux near the forming rim affect oöcyte pH? Only one group of cells remains in contact with the oöcyte during choriogenesis, although it is unknown whether the cells are electrically coupled. These are the cells responsible for forming the micropyle, a channel in the shell through which the sperm travels to reach the oöcyte. Typically, no more than 16 of these micropyle cells are present, with single cells or doublets spaced relatively evenly around the circumference of the rim (Beament, 1947). Pseudomicropyle cells are similar to the micropyle cells in morphology but the channels they form in the chorion do not fully reach the oölemma; approximately 200 of these cells circle the rim, which is about 250 μm in radius (Beament, 1947). This means that the micropyle cells are spaced roughly 11-12 cells, or 100 μm, apart. H^+ flux can be measured for several tens of microns above and below the plane of measurement, and does not attenuate as it does along the anteroposterior axis, even though the distance between cells is great enough that it should; thus it appears that H^+ efflux in this region occurs around the entire rim and is not a product of the micropyle cells alone (if at all). Since micropyle cells are the only ones potentially coupled to the oöcyte, it would appear that H^+ efflux in this region does not affect the oöcyte.

H^+ Flux Around Atretic Follicles

During the course of experimentation a few atretic follicles were scanned out of interest, although they were not included in the compiled data. No observable differences were detected when H^+ flux from these ovarioles was compared to that around other ovarioles from the same stage (Figure 15). These results underscore the importance of

observed H^+ fluxes, since the mechanisms involved in H^+ flux are not impeded during atresia. Although it is unknown how long these oöcytes were in an atretic state, it may be possible to draw a comparison between these follicles and follicles in which the egg has recently moved into the oviduct, where H^+ flux near the micropyle region persists for some time after the follicle begins to degenerate. H^+ efflux along the stalk posterior to the T follicle may also fall into this category, since the somatic cells continue transporting H^+, while stage-related differences disappear in the absence of an associated oöcyte.

H^+ Fluxes Do Not Exhibit Rotational Differences Relative to T-1 Orientation

In *Rhodnius*, the oöcyte nucleus migrates from the centre of the cell to the cortex during early previtellogenesis, creating an early marker of oöcyte polarity. The significance of this event may compare to the *Drosophila* system, where nuclear migration from the posterior pole of the oöcyte to the anterior margin plays an essential role in establishing dorsoventral polarity (Gonzales-Reyes *et al.*, 1995; Roth *et al.*, 1995). By orienting the ovariole relative to the T-1 nucleus, we attempted to detect rotational differences during the earliest stages of oöcyte polarity. H^+ efflux has previously been described along the anterior surface of vitellogenic follicles in *Periplaneta*, where it is postulated to play a role in establishing future embryonic polarity (Kunkel & Faszewski, 1995). In *Rhodnius*, no rotational differences were observed (Figure 16). Considering that the extracellular H+ fluxes observed during oögenesis were strongly correlated to the state of T follicle differentiation, and not to that of the T-1 follicle, it seems sensible that no rotational differences were detected.

Potential Roles of Transmembrane H^+ Fluxes during Oögenesis

1. Regulation of Metabolism

Throughout the remainder of the Discussion, the potential of transmembrane H^+ flux for generating changes in pH_i and establishing changes in cellular structure and function will be considered. One additional possibility is that H^+ efflux occurs simply to maintain a constant pH_i by removing H^+ generated by ATP hydrolysis or balancing respiratory secretion of CO_2 produced by the ovariole. Aerobic metabolism is not an acidifying process, and anaerobic metabolism alone does not generate H^+ without the downstream hydrolysis of ATP (see Busa & Nuccitelli, 1984 for an excellent review). The *in vitro* conditions used for these studies are essentially anaerobic, and metabolism under these conditions would conceivably generate H^+. Most H^+ fluxes appear to be associated with the T follicle, which is certainly very active during vitellogenesis; H^+ efflux at the interfollicular stalk is greatest during stage 4, and declines during later stages. However, if anything oöcyte activity is greater during later stages, as the rate and sheer quantity of yolk uptake increases over larger oöcytes. In addition, the nurse cells are highly active during all stages of oögenesis, and so it seems more reasonable to expect that H^+ efflux should increase during later stages, rather than decrease. Given this, it appears that the observed H^+ efflux at the interfollicular stalk cannot be explained strictly as a mechanism to maintain pH_i during ATP hydrolysis.

H^+ efflux may also accompany respiratory CO_2 secretion and could be expected to manifest itself as an efflux along the entire ovariole surface (Kunkel & Faszewski, 1995).

Indeed, low-level H^+ flux matching this description was observed over the tropharium and early previtellogenic follicles during all stages of oögenesis. Nurse cells in the telotrophic ovariole are highly and constitutively active, providing a steady supply of newly synthesized material to previtellogenic and early vitellogenic oöcytes. If the prominent H^+ fluxes observed were entirely attributable to respiration, one would expect that the tropharium would generate considerable H^+ efflux during all stages of oögenesis as well. A direct, quantitative comparison of respiratory rates between the tropharium and follicles could be made using non-invasive O_2-sensitive probes. If the amount of H^+ efflux observed around the tropharium can be considered the baseline due to respiration, then it truly did not exceed background noise to a significant degree, and prominent H^+ fluxes observed along the vitellarium likely do more than simply accompany respiration.

If H^+ export instead elevates pH_i, it raises the possibility that metabolic enzyme activity is affected. In sea urchin eggs, cytoplasmic alkalinization activates key rate-limiting enzymes including glucose-6-phosphate dehydrogenase (Aune & Epel, 1978), phosphoglycerate mutase (Setlow & Setlow, 1980; but see also Swerdlow *et al.*, 1981) and glycogen catabolism generally (Baginsky, 1981), as well as increasing the rate of translation (Winkler & Steinhardt, 1981; Winkler, 1982; Brandis & Raff, 1979). Assuming the oöcyte must increase ATP production to support cell mechanisms involved with vitellogenesis (endocytosis, vesicle fusion, or membrane recycling), a rise in pH due to steady H^+ efflux may enhance this process.

2. Regulation of Membrane Potential

H^+ fluxes observed during *Rhodnius* oögenesis could affect membrane potential in the ovariole. In many insects, electrogenic H^+ pumps associated with the cell membrane contribute to the resting membrane potential (E_m) (Harvey & Wieczorek, 1997; Dittmann, 1997), as Na^+/K^+-ATPase does in most mammalian cells. In *Rhodnius*, an H^+ pump contributes to E_m and regulates pH_i in vitellogenic follicles (O'Donnell & Sharda, 1994), as does Na^+/K^+-ATPase activity (O'Donnell, 1985). Prior to visible accumulation of yolk spheres in *Hyalophora* ovarian follicles, oöcyte pH rises from 6.7 to 7.4, gap junctional coupling is established between follicle cells and the germ syncytium, and the membrane of both nurse cells and oöcytes hyperpolarizes, among other events (Stynen *et al.*, 1988; Woodruff & Telfer, 1990). Cell membranes in nurse cells hyperpolarized more than in oöcytes, creating a ~5 mV difference between the compartments and resulting in the charge-dependent restriction of protein transport (Woodruff & Telfer, 1990). In *Hyalophora*, azide-treated ovarioles lose gap junctional coupling and membrane hyperpolarization, presumably due to an H^+-extrusion mechanism (Stynen *et al.*, 1988). In *Rhodnius* ovarioles, changes in membrane potential may indicate a shift in the way the traffic of other ions is conducted during vitellogenesis.

3. Cytoskeletal Regulation

Each of the prominent extracellular H^+ fluxes observed around *Rhodnius* ovarioles coincides spatially and temporally with morphological changes and cytoskeletal

reorganization in nearby cells, making a role for H^+ flux and associated pH changes in regulating cytoskeletal events particularly appealing. Both oöcyte and follicle cells undergo substantial reorganization of microtubules and microfilaments concomitant with vitellogenesis. In vitellogenic oöcytes, the organization of F-actin and microtubules in the cortex is clearly different in the anterior and lateral regions (McPherson & Huebner, 1993). Anteriorly, columnar follicle cells also establish different F-actin and microtubule distributions than their lateral counterparts during yolk uptake (Watson & Huebner, 1986). As chorionation begins, follicle cells take on a secretory role (Huebner & Anderson, 1972a). While chorion secretion is uniform over much of the oöcyte surface, specialized structures essential for fertilization and hatching are formed where the anterior cap meets the main body of the chorion (Beament, 1946, 1947). One of the follicle cell populations involved in sculpting the specialized features of the cap edge and rim of the main body undergoes considerable rearrangement of its actin cytoskeleton, becoming very long and narrow, with a slender process rich in F-actin filaments (Huebner & Bjornsson, 2002) that occupy channels in the forming chorion (Beament, 1947; Huebner & Bjornsson. 2002). These cells form the pseudomicropyles in a single row completely encircling the rim, and the true micropyles interspersed between them.

Formation of the interfollicular stalk is an essential step in the functional isolation of vitellogenic follicles. H^+ efflux at the interfollicular junctions between follicles was observed anterior to T-1 follicles in stage 7 ovarioles, before the formation of a discrete stalk, suggesting H^+ efflux may play a role in stalk formation. This would entail changes in cell shape and cytoskeleton to produce the flattened cells of the stalk. The rise in intracellular pH resulting from H^+ efflux may alter actin dynamics within follicle cells

through activation of pH-sensitive ABPs like ADF/cofilin (Southwick, 2000) and profilin (Machesky, 1998), increasing microfilament turnover and enhancing motility, similar to migrating cells (Svitkina & Borisy, 1999). Furthermore, when the stalk is only a pinched constriction, before assuming its final uniform cylindrical structure, H^+ efflux extends posterior to the stalk, along the anterior surface of the oöcyte (Figure 12). Active shape changes in the anterior follicle cells, accompanied by H^+ efflux, may help form the connective as it elongates. Alternatively, H^+ efflux observed at the interfollicular junction and especially along the follicle cells posterior to the forming stalk may indicate the early differentiation of these cells. H^+ efflux in this region may be an integral part of the early differentiation of the anterior follicle cells as they undergo morphological and cytoskeletal changes to assume their columnar form.

The persistence of H^+ efflux throughout subsequent stages of oögenesis may be indicative of additional roles beyond stalk formation. Once the interfollicular stalk is formed, it does not undergo further (overt) change until stage 8 when the trophic cord supplying the T follicle closes and retracts anteriorly towards the tropharium, vacating the centre of the stalk. Increased H^+ efflux at the posterior region of the stalk strongly suggests a correlation with T follicle growth. H+ extrusion from the anterior pole of the oöcyte may alkalinize and affect the cytosol much as it does during fertilization in some marine invertebrate eggs, stabilizing microtubules (Schatten *et al.*, 1985; Suprenant, 1991; Hamaguchi & Hamaguchi, 2001) and enhancing formation of microvilli by promoting F-actin bundling (Bryan & Kane, 1978; Begg & Rebhun, 1979; Tilney & Jaffe, 1980; Begg *et al.*, 1982; Carron & Longo, 1982), possibly involving regulation of fascin activity (Yamakita *et al.*, 1996).

Reduced H^+ efflux at the interfollicular stalk and influx along the cap region may acidify the anterior pole of the oöcyte and could considerably influence microtubule dynamics in the trophic cord. Disassembly of microtubules as the trophic cord closes and begins to retract during late vitellogenesis (stage 8) may be enhanced by acidification of the cytoplasm. While trophic cord microtubules are cold-, Ca^{2+}-, and colchicine-resistant in *Notonecta* (Hyams & Stebbings, 1979), and cold-resistant in *Rhodnius* (Huebner, 1981b), the effects of pH on microtubules in these systems are unknown. In addition, intercellular transport during *Rhodnius* oögenesis depends in part on microtubule-based dynein transport (Harrison & Huebner, 1997), which presumably stops before the trophic cord closes. Dynein activity is inhibited at lower pH in a number of systems (Schatten *et al.*, 1985, 1986; Parton *et al.*, 1991), and H^+ accumulation in the cord cytoplasm due to H^+ influx may have the same effect in *Rhodnius* ovarioles. The effects of pH on *Rhodnius* cytoplasmic dynein are presently unknown.

H^+ extrusion in the micropyle region may be instrumental in regulating follicle cell cytoskeletal changes during chorion formation, specifically the formation of actin-rich cytoplasmic processes unique to the pseudomicropyle and micropyle cells. In addition to the spatial correlation between the two events, the timing of H^+ efflux in this region provides a clue as to its role. H^+ efflux in the rim region of the forming chorion does not coincide with early deposition of the eggshell; rather it emerges during the later stages of chorionation, when the processes of the pseudomicropyle cells form, narrow, and ultimately retract (Beament, 1947). Activation of ADF/cofilin could promote pH-dependent reorganization of the actin cytoskeleton in these cells.

4. Regulation of Gap Junctions

Interactions between the oöcyte and follicle cells and follicle cell-follicle cell interactions via gap junctions (GJs) have been shown to be an inherent feature of oögenesis, essential to the coordination of these different cell types. GJ activity is regulated by pH in a range of vertebrate and invertebrate tissue (Giaume *et al.*, 1980; Perrachia & Perrachia, 1980; Bohrmann & Haas-Assenbaum, 1993; Rozental *et al.*, 2001; Levin, 2002), despite differences in protein structure (reviewed by Levin, 2002). In vertebrates, subtle modulation of GJ coupling by pH_i can be achieved by mixing different connexin isoforms to form heteromeric proteins (Francis *et al.*, 1999). Alkalinization as a consequence of H^+ efflux, regardless of whether oöcytes or associated follicle cells are affected, should increase gap junctional (GJ) coupling between these cells.

In *Rhodnius*, gap junctions can be detected through freeze fracture techniques by late previtellogenesis (400 μm, stage 2)(Huebner & Injeyan, 1981); however, dye coupling can be demonstrated between follicle cells and oöcytes around 200 μm in diameter (Huebner, unpublished results). Thus while H^+ efflux may stimulate formation of larger GJ plaques, strengthening this avenue of communication, 'baseline' pH_i' seems adequate to establish dye-coupling initially. Nevertheless, it would be interesting to know whether lowering pH_i in the oöcyte or follicle cells does in fact affect dye-coupling in *Rhodnius*, as demonstrated in other insect ovarioles (*Drosophila*: Bohrmann & Haas-Assenbaum, 1993; *Oncopeltus*: Anderson & Woodruff, 2001). Considering the relative timing of GJ coupling and H^+ efflux at the interfollicular stalk, there is a strong possibility that H^+ extrusion may be initiated by follicle cells to regulate oöcyte pH_i, at

least in part. All else (GJ proteins, number and size of GJ plaques, etc.) being equal, if H^+ efflux at the interfollicular stalk does in fact affect GJ coupling, by modifying either follicle cell or oöcyte pH, one would expect greater GJ coupling between the oöcyte and anterior follicle cells relative to lateral follicle cells. Intracellular recording electrodes could be used to test this hypothesis.

5. Coordination of Developmental Events during Oögenesis

The temporal and spatial pattern of transmembrane H+ flux underscores the importance of pH change in a number of cell differentiation and developmental events during oögenesis. It is apparent that a number of developmental events during oögenesis in *Rhodnius* are potentially regulated by changes in pH, including gap junctional coupling, actin and microtubule rearrangements in both oöcyte and follicle cells, and increased metabolic activity in the oöcyte. One of the more compelling reasons to consider ΔpH as a regulator of many if not all of these events is that it possesses the ability to influence all of these events in synchrony. Changes in pH_i do in fact regulate a number of concurrent cellular events during sea urchin fertilization (Busa & Nuccitelli, 1984). In *Hyalophora*, the suite of changes that occur at the onset of vitellogenesis appears to be the result of a singular initiation of a cascade of downstream events (Woodruff & Telfer, 1990), and H^+ efflux similarly begins near the onset of vitellogenesis in *Rhodnius*. Future studies have the potential to shed light on the importance and extent of pH regulation during *Rhodnius* oögenesis.

SUMMARY

This is the first study to demonstrate the presence of H^+ fluxes along an insect ovariole over an oögenesis cycle. H^+ fluxes were observed at several discrete positions along the ovariole, and several fluxes changed considerably according to ovariole stage. While the location of H^+ fluxes to the interfollicular stalks make it difficult to determine which cells are responsible for these fluxes and which cells are affected by them, the stage-related change in H^+ flux at the interfollicular stalk connecting T and T-1 follicle coincide with a number of specific events during oögenesis that have been shown to be pH-regulated in other systems. Future experiments may clarify whether a clear link exists between any of these events and extracellular H^+ flux. Other regions where H^+ flux was observed seem to be more straightforward; for example, efflux near the micropyle region of stage 9 follicles appears to be generated by the follicle cells, and may be involved in the differentiation and cytoskeletal specialization of follicle cells in the region. This study raises a number of interesting questions worthy of further consideration.

PLATE 1

Figure 1. Representative traces of non-invasive H^+-selective probe measurements. (a) The majority of measurements were stable for extended periods of time. (b) Periodically, the probe took some time to equilibrate at a new position after moving. This effect was observed for noise at the beginning of each trial and after rotation, and was a normal part of each scan. Equilibration typically took under 2 minutes to occur, so if the probe settled within this time the average of the last five measurements was used for data analysis. (c) In rare cases probe measurements fluctuated considerably, and did not settle within a two-minute time window. Here, the average of the entire measurement was taken and the correspondingly larger standard deviation was included in subsequent analysis.

Figure 2. An image depicting the positions measured along adult *Rhodnius* ovarioles. The ovariole used as an example here is stage 8.

Figure 3. An illustration depicting the quadrants measured during each scan. Ovarioles were rotated so the T-1 nucleus was oriented towards or away from the probe, or up or down in the recording chamber.

Figure 4. Examples of H^+ influx and efflux. When the vector calculated from X- and Y-axis measurements was superimposed over an image of the ovariole, it was considered an influx if the vector travelled over the ovariole image (left), and was scored as an efflux of the vector travelled away from the ovariole (right).

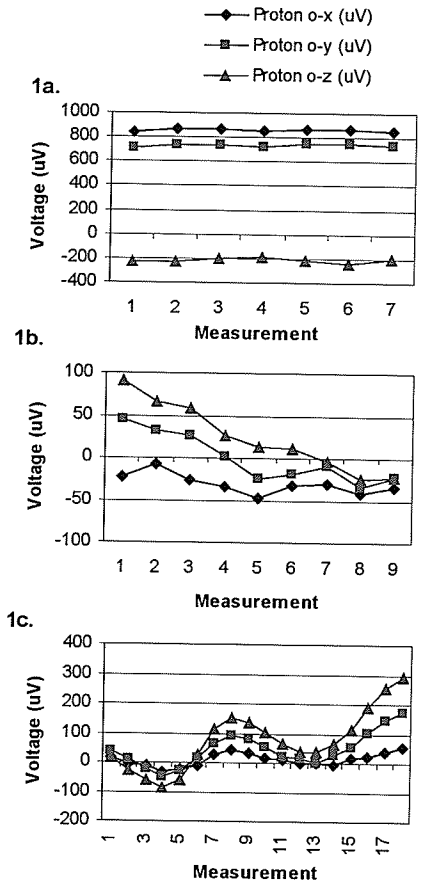
Proton o-x (uV)
Proton o-y (uV)
Proton o-z (uV)
1a.
Voltage (uV)
Measurement
1b.
Voltage (uV)
Measurement
1c.
Voltage (uV)
Measurement

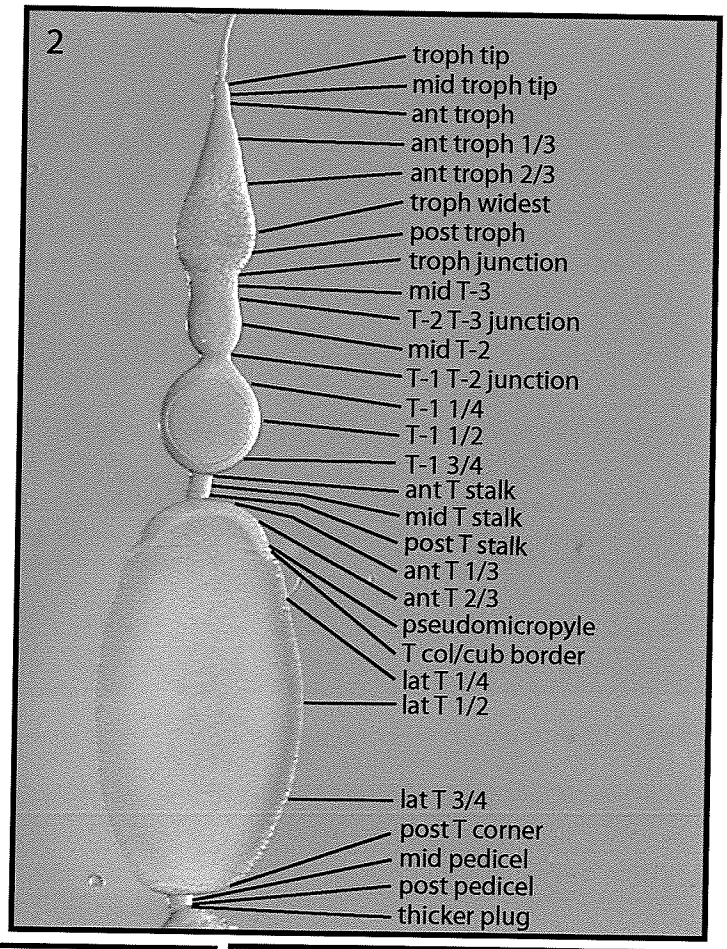
2
troph tip
mid troph tip
ant troph
ant troph 1/3
ant troph 2/3
troph widest
post troph
troph junction
mid T-3
T-2 T-3 junction
mid T-2
T-1 T-2 junction
T-1 1/4
T-1 1/2
T-1 3/4
ant T stalk
mid T stalk
post T stalk
ant T 1/3
ant T 2/3
pseudomicropyle
T col/cub border
lat T 1/4
lat T 1/2
lat T 3/4
post T corner
mid pedicel
post pedicel
thicker plug

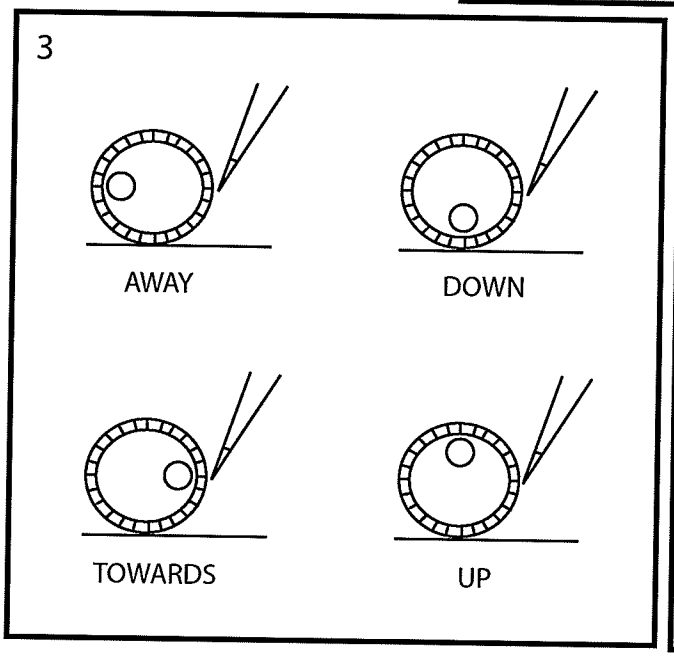
3
AWAY
DOWN
TOWARDS
UP

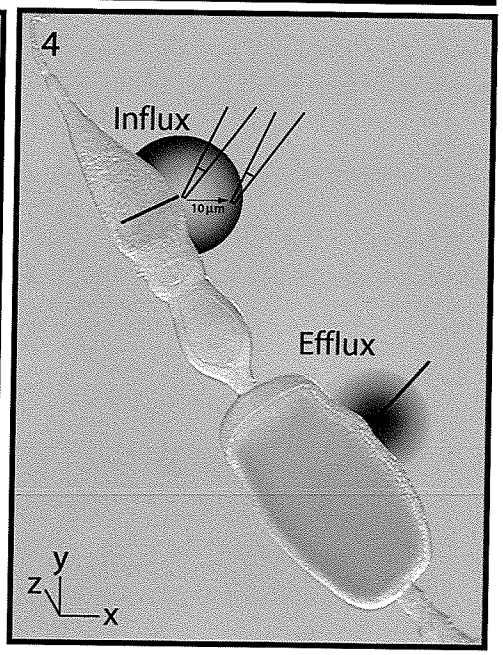
4
Influx
10µm
Efflux
y
z
x

PLATES 2-4

Figure 5. H^+ flux at all measured positions along the adult *Rhodnius* ovariole, grouped according to stage. Bars represent average H^+ flux; error bars indicate standard error. Grouped in this way, large differences in H^+ flux between positions can be clearly identified.

Figure 5.

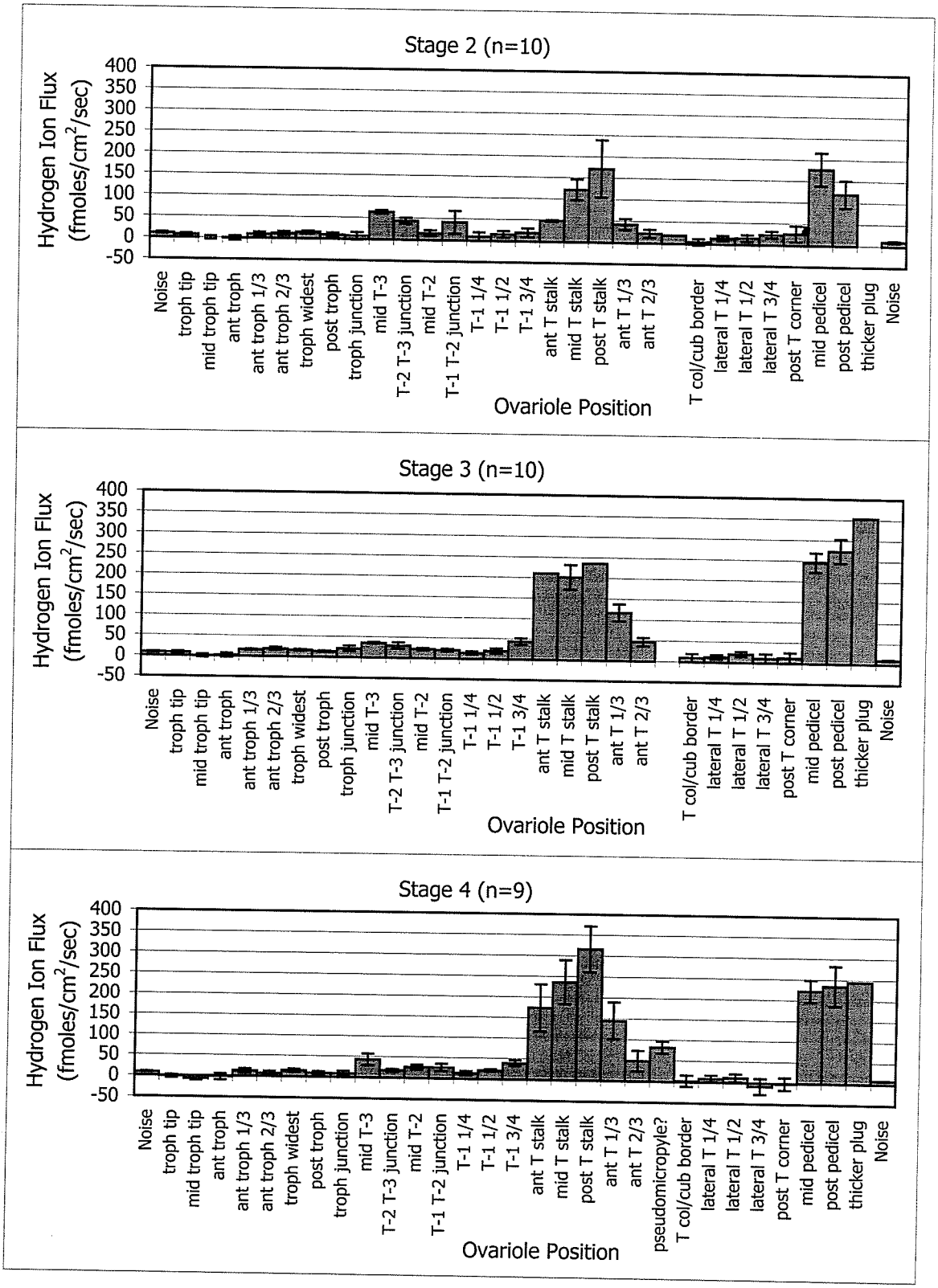
Stage 2 (n=10)
Hydrogen Ion Flux (fmoles/cm²/sec)
400
350
300
250
200
150
100
50
0
-50
Noise
troph tip
mid troph tip
ant troph
ant troph 1/3
ant troph 2/3
troph widest
post troph
troph junction
mid T-3
T-2 T-3 junction
mid T-2
T-1 T-2 junction
T-1 1/4
T-1 1/2
T-1 3/4
ant T stalk
mid T stalk
post T stalk
ant T 1/3
ant T 2/3
T col/cub border
lateral T 1/4
lateral T 1/2
lateral T 3/4
post T corner
mid pedicel
post pedicel
thicker plug
Noise
Ovariole Position
Stage 3 (n=10)
Hydrogen Ion Flux (fmoles/cm²/sec)
400
350
300
250
200
150
100
50
0
-50
Noise
troph tip
mid troph tip
ant troph
ant troph 1/3
ant troph 2/3
troph widest
post troph
troph junction
mid T-3
T-2 T-3 junction
mid T-2
T-1 T-2 junction
T-1 1/4
T-1 1/2
T-1 3/4
ant T stalk
mid T stalk
post T stalk
ant T 1/3
ant T 2/3
T col/cub border
lateral T 1/4
lateral T 1/2
lateral T 3/4
post T corner
mid pedicel
post pedicel
thicker plug
Noise
Ovariole Position
Stage 4 (n=9)
Hydrogen Ion Flux (fmoles/cm²/sec)
400
350
300
250
200
150
100
50
0
-50
Noise
troph tip
mid troph tip
ant troph
ant troph 1/3
ant troph 2/3
troph widest
post troph
troph junction
mid T-3
T-2 T-3 junction
mid T-2
T-1 T-2 junction
T-1 1/4
T-1 1/2
T-1 3/4
ant T stalk
mid T stalk
post T stalk
ant T 1/3
ant T 2/3
pseudomicropyle?
T col/cub border
lateral T 1/4
lateral T 1/2
lateral T 3/4
post T corner
mid pedicel
post pedicel
thicker plug
Noise
Ovariole Position

Figure 5. (continued)

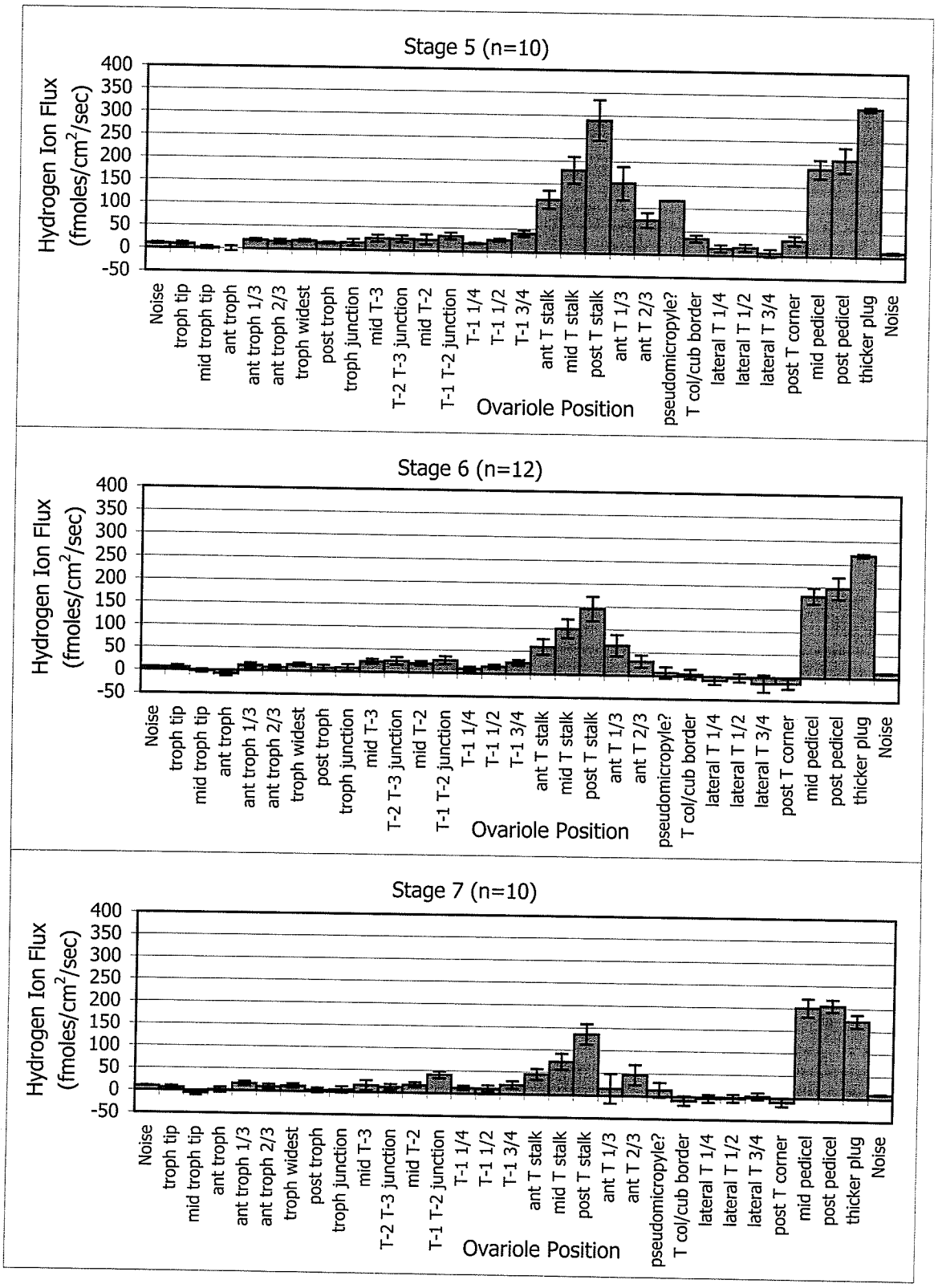

Figure 5. (continued)

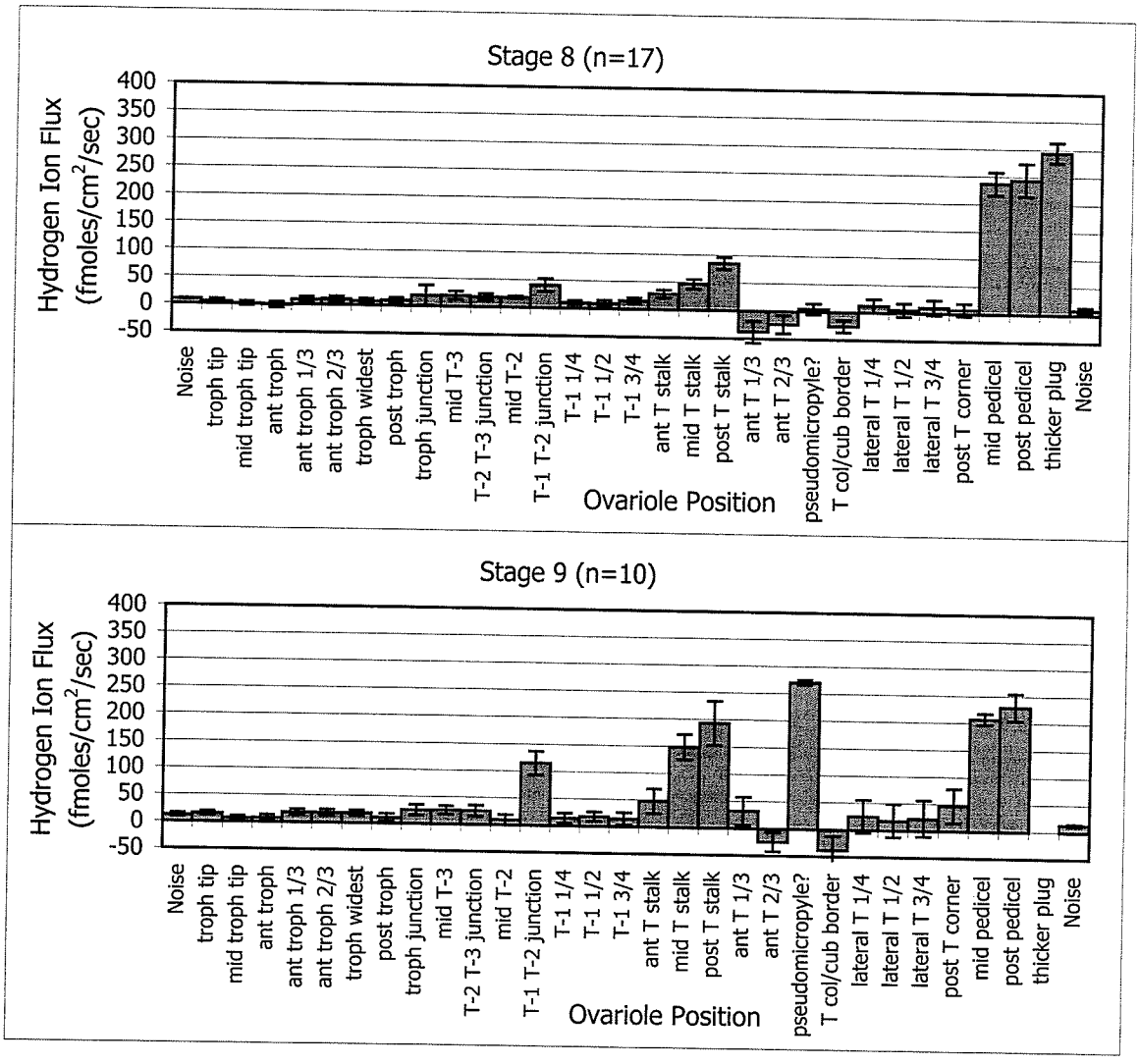

PLATES 5-7

Figure 6. Extracellular H^+ flux at each position along the adult *Rhodnius* ovariole throughout an oögenesis cycle, grouped according to position. Bars represent average H^+ flux; error bars indicate standard error. When grouped in this way, significant stage-specific differences can be observed at a number of positions along the ovariole. H+ flux for each graph is in nmoles/cm^2/sec.

Figure 6.

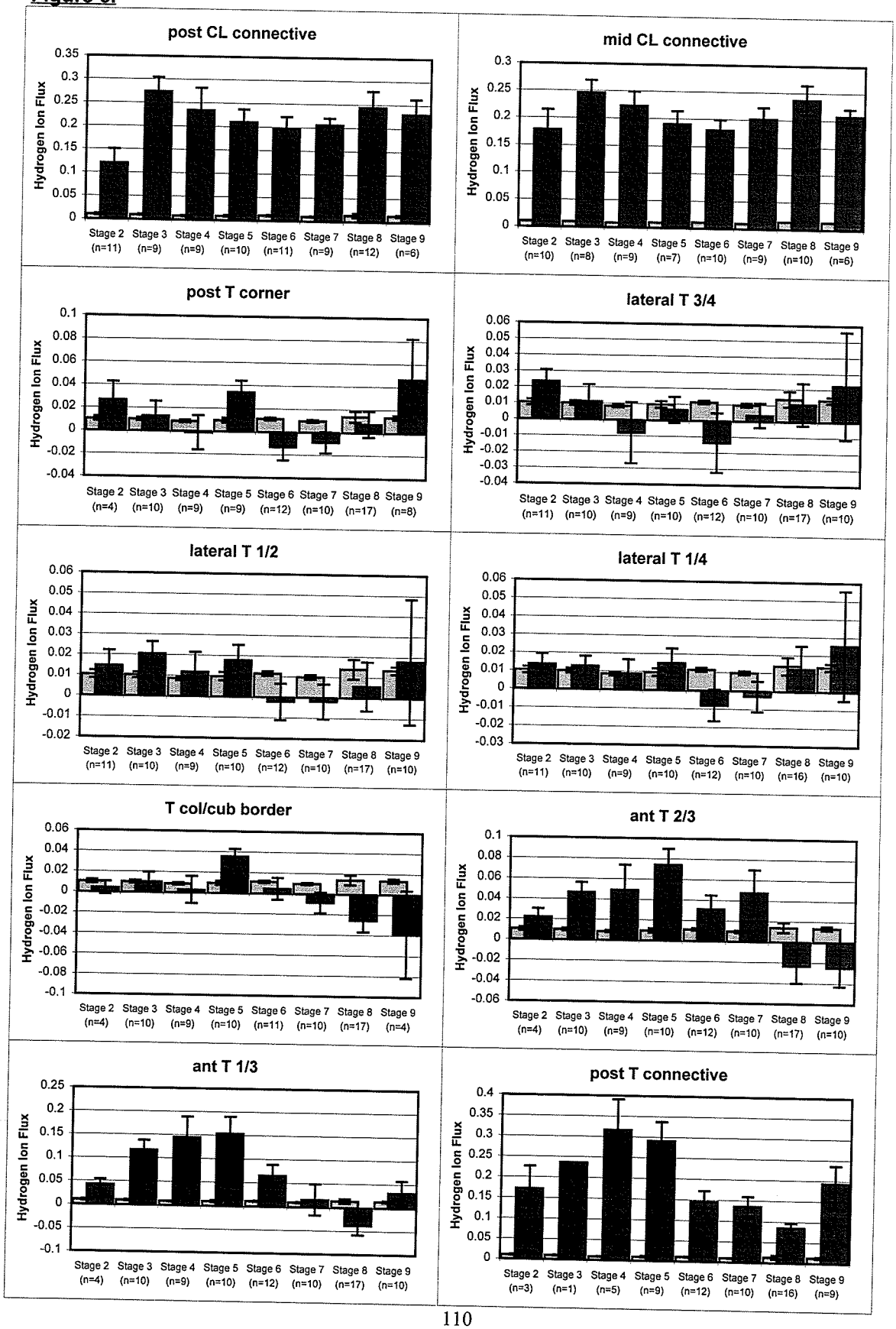
post CL connective
Hydrogen Ion Flux
0.35
0.3
0.25
0.2
0.15
0.1
0.05
0
Stage 2 (n=11)
Stage 3 (n=9)
Stage 4 (n=9)
Stage 5 (n=10)
Stage 6 (n=11)
Stage 7 (n=9)
Stage 8 (n=12)
Stage 9 (n=6)
mid CL connective
Hydrogen Ion Flux
0.3
0.25
0.2
0.15
0.1
0.05
0
Stage 2 (n=10)
Stage 3 (n=8)
Stage 4 (n=9)
Stage 5 (n=7)
Stage 6 (n=10)
Stage 7 (n=9)
Stage 8 (n=10)
Stage 9 (n=6)
post T corner
Hydrogen Ion Flux
0.1
0.08
0.06
0.04
0.02
0
-0.02
-0.04
Stage 2 (n=4)
Stage 3 (n=10)
Stage 4 (n=9)
Stage 5 (n=9)
Stage 6 (n=12)
Stage 7 (n=10)
Stage 8 (n=17)
Stage 9 (n=8)
lateral T 3/4
Hydrogen Ion Flux
0.06
0.05
0.04
0.03
0.02
0.01
0
-0.01
-0.02
-0.03
-0.04
Stage 2 (n=11)
Stage 3 (n=10)
Stage 4 (n=9)
Stage 5 (n=10)
Stage 6 (n=12)
Stage 7 (n=10)
Stage 8 (n=17)
Stage 9 (n=10)
lateral T 1/2
Hydrogen Ion Flux
0.06
0.05
0.04
0.03
0.02
0.01
0
-0.01
-0.02
Stage 2 (n=11)
Stage 3 (n=10)
Stage 4 (n=9)
Stage 5 (n=10)
Stage 6 (n=12)
Stage 7 (n=10)
Stage 8 (n=17)
Stage 9 (n=10)
lateral T 1/4
Hydrogen Ion Flux
0.06
0.05
0.04
0.03
0.02
0.01
0
-0.01
-0.02
-0.03
Stage 2 (n=11)
Stage 3 (n=10)
Stage 4 (n=9)
Stage 5 (n=10)
Stage 6 (n=12)
Stage 7 (n=10)
Stage 8 (n=16)
Stage 9 (n=10)
T col/cub border
Hydrogen Ion Flux
0.06
0.04
0.02
0
-0.02
-0.04
-0.06
-0.08
-0.1
Stage 2 (n=4)
Stage 3 (n=10)
Stage 4 (n=9)
Stage 5 (n=10)
Stage 6 (n=11)
Stage 7 (n=10)
Stage 8 (n=17)
Stage 9 (n=4)
ant T 2/3
Hydrogen Ion Flux
0.1
0.08
0.06
0.04
0.02
0
-0.02
-0.04
-0.06
Stage 2 (n=4)
Stage 3 (n=10)
Stage 4 (n=9)
Stage 5 (n=10)
Stage 6 (n=12)
Stage 7 (n=10)
Stage 8 (n=17)
Stage 9 (n=10)
ant T 1/3
Hydrogen Ion Flux
0.25
0.2
0.15
0.1
0.05
0
-0.05
-0.1
Stage 2 (n=4)
Stage 3 (n=10)
Stage 4 (n=9)
Stage 5 (n=10)
Stage 6 (n=12)
Stage 7 (n=10)
Stage 8 (n=17)
Stage 9 (n=10)
post T connective
Hydrogen Ion Flux
0.4
0.35
0.3
0.25
0.2
0.15
0.1
0.05
0
Stage 2 (n=3)
Stage 3 (n=1)
Stage 4 (n=5)
Stage 5 (n=9)
Stage 6 (n=12)
Stage 7 (n=10)
Stage 8 (n=16)
Stage 9 (n=9)

Figure 6. (continued)

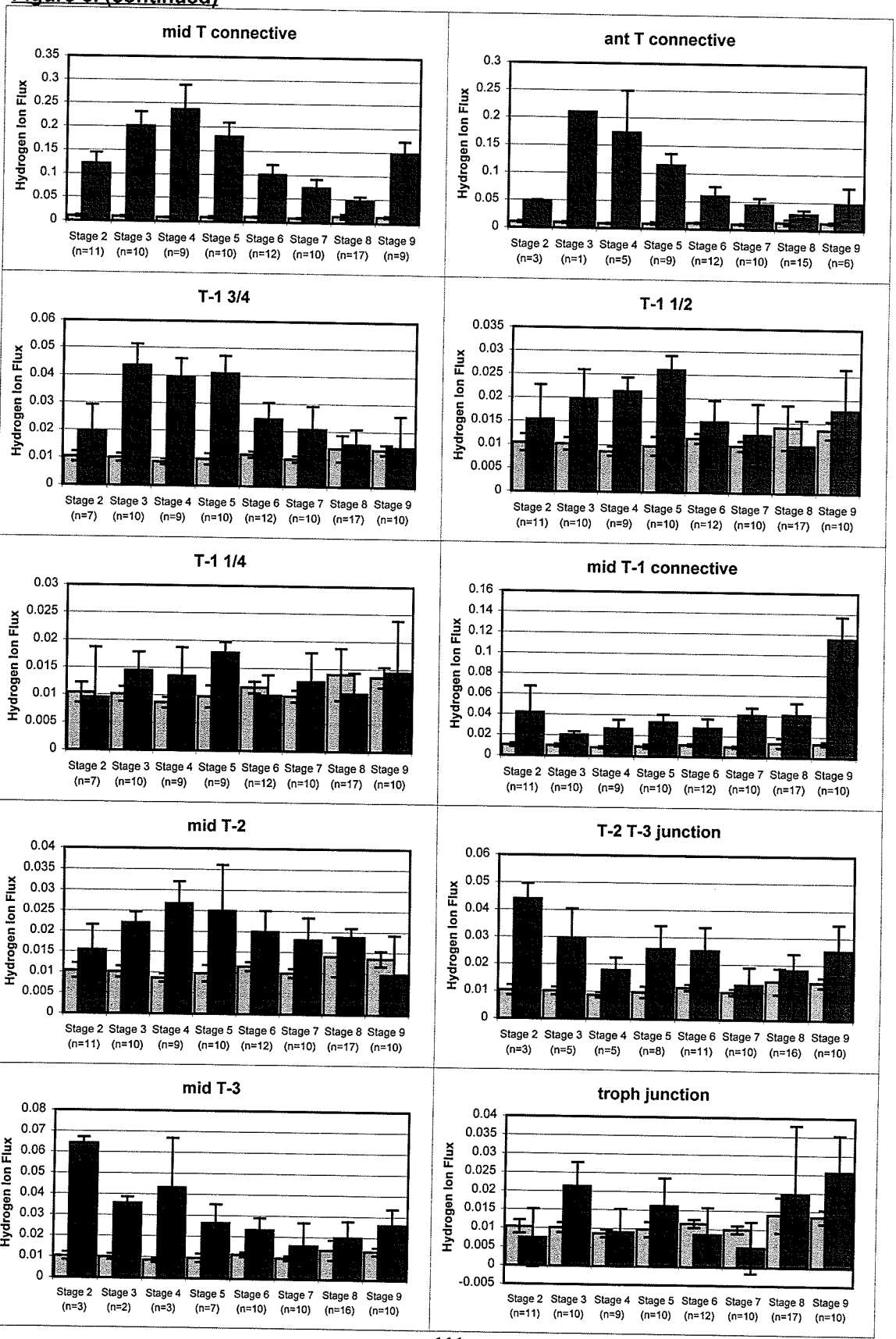

Figure 6 (continued)

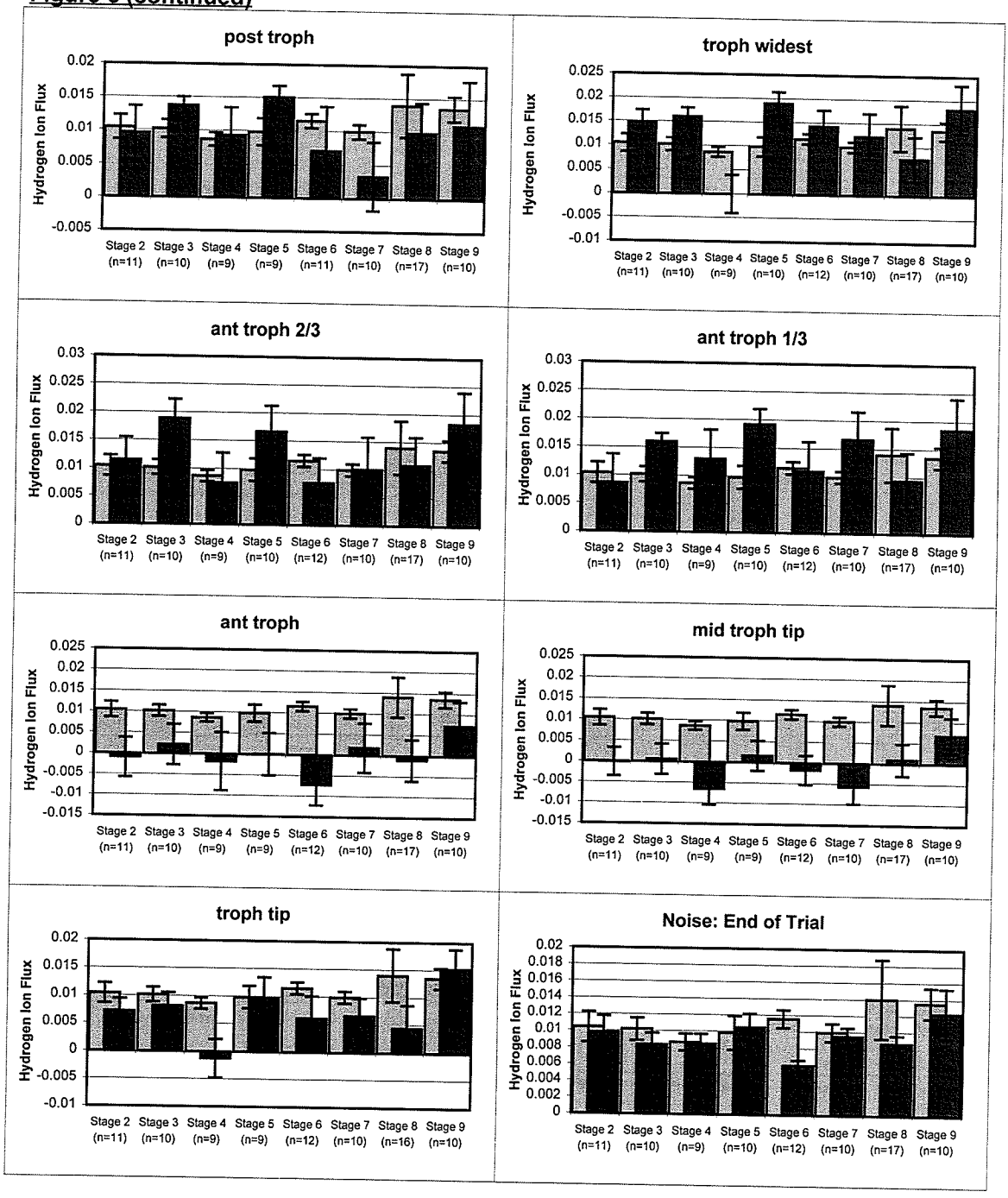

PLATE 8

Figure 7. Contour plot representation of extracellular H^+ fluxes along adult *Rhodnius* ovarioles. The bottom graph depicts H^+ flux magnitude and direction (influx/efflux) relative to position along ovariole and ovariole stage. The vertical lines correspond to specific points along the ovariole. The data for each ovariole stage, represented by fluctuating black lines running through the coloured region of the plot, are superimposed on each other making it difficult to show stage differences. However these are clearly discerned in a top view of the contours as seen in the top plot. The colour coding indicates H^+ flux magnitude and direction, which is calibrated in the bottom plot. Each vertical column on the surface plot corresponds to a specific point along the ovariole as indicated by the ovariole images. The leftmost and rightmost columns display background noise. Horizontal rows display the average H^+ flux for each ovariole stage (see Methods). Prominent efflux occurs near the interfollicular stalks on either side of the T follicle. The H^+ efflux at the anterior stalk is greatest around stage 4 (previtellogenesis) and declines gradually until stage 8 (late vitellogenesis) when it is significantly diminished. Stage 8 ovarioles are also characterized by the appearance of H^+ influx along the anterior columnar epithelium of the T follicle.

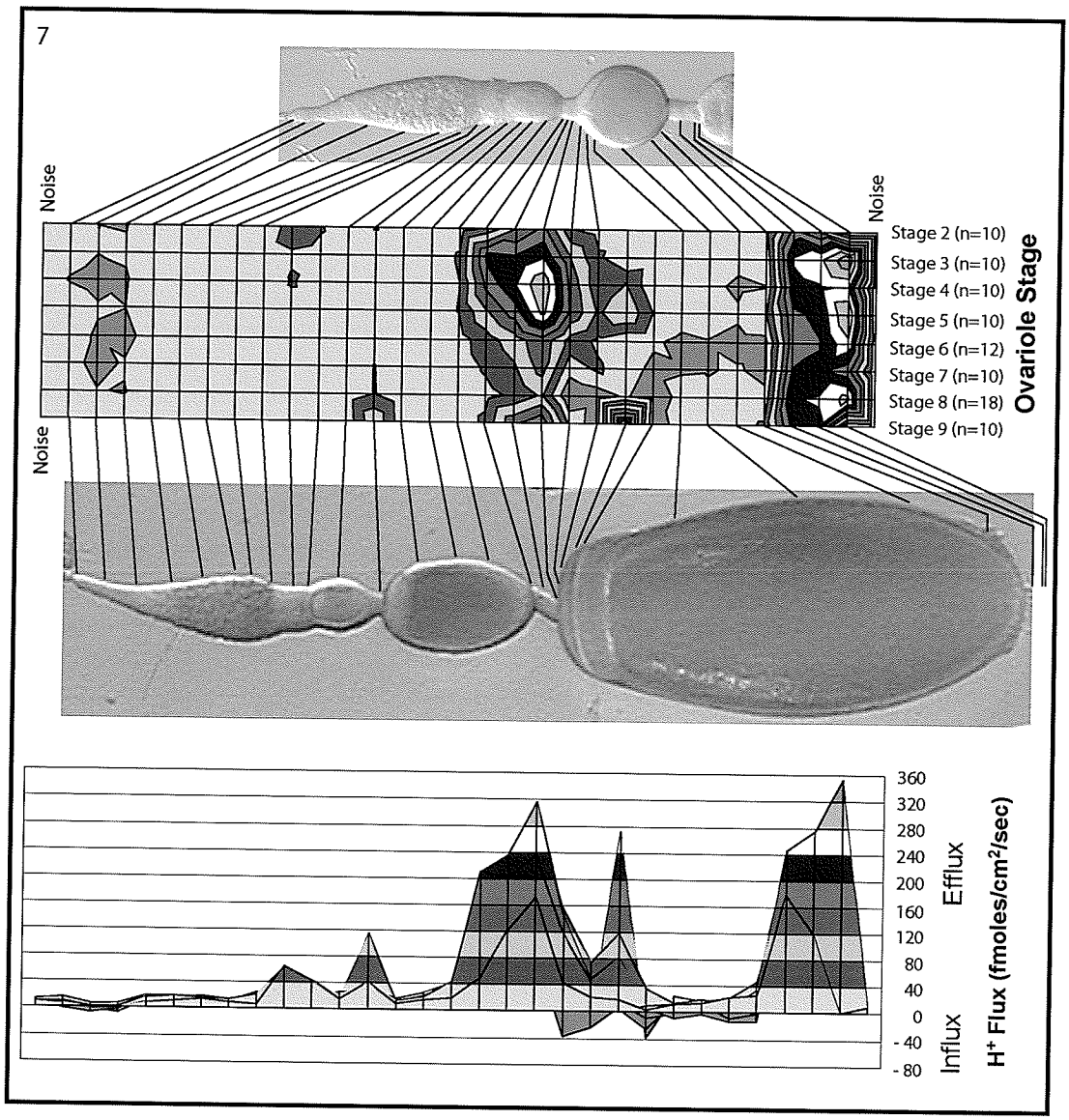
7
Noise
Noise
Noise
Stage 2 (n=10)
Stage 3 (n=10)
Stage 4 (n=10)
Stage 5 (n=10)
Stage 6 (n=12)
Stage 7 (n=10)
Stage 8 (n=18)
Stage 9 (n=10)
Ovariole Stage
360
320
280
240
200
160
120
80
40
0
- 40
- 80
Efflux
Influx
H+ Flux (fmoles/cm2/sec)

PLATE 9

Figure 8. H^+ flux around a stage 9 ovariole. H^+ flux is indicated by red vectors, with length proportional to the flux magnitude. Vectors travelling away from the oöcyte surface represent H^+ efflux; vectors travelling over the ovariole are influx. Of interest is the H^+ efflux near the forming chorion rim in late vitellogenic oöcytes (asterisk), which remains throughout choriogenesis.

Figure 9. H^+ flux around a recently ovulated follicle. The chorionated oöcyte in this ovariole was unattached to and loosely contained by the follicular epithelium, and fell away from the ovariole during dissection. H^+ efflux in the region of the rim is still present during ovulation, suggesting the follicle cells generate this H^+ flux.

Figure 10. H^+ flux around the chorion rim of a recently ovulated egg. No significant efflux was detected. This suggests that the oöcyte does not contribute to the H^+ efflux seen in this region during oögenesis.

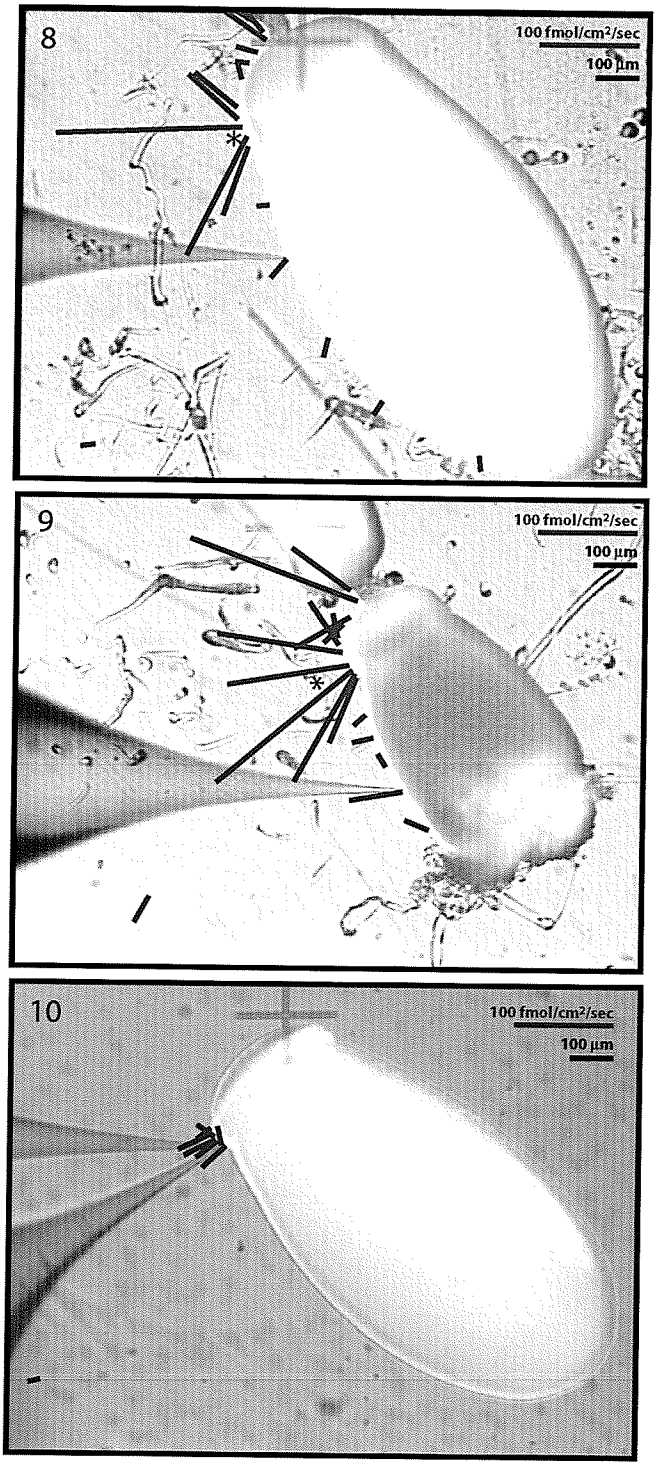
8
100 fmol/cm²/sec
100 µm
9
100 fmol/cm²/sec
100 µm
10
100 fmol/cm²/sec
100 µm

PLATE 10

Figure 11. H^+ flux around a stage 5 ovariole. Strong efflux around the smallest follicles is observed where cells reside on the outer surface of the basal lamina.

Figure 12. H^+ flux along the anterior portion of a stage 9 ovariole. Additional measurements near the junction between T-1 and T-2 follicles reveal that H^+ efflux extends to the anterior pole of the T-1 follicle (asterisk). These follicle cells presumably are also involved in interfollicular stalk morphogenesis, and will ultimately form the columnar cells at the anterior pole of the follicle.

Figure 13. An example of the thicker group of cells at the posterior end of the pedicel visible as the follicular epithelium begins to degenerate (arrow). If these cells are present throughout vitellogenesis, they may contribute to extracellular H^+ efflux in the area. Scale bar represents 100 μm.

Figure 14. Longitudinal section of the interfollicular stalk separating T-1 (top) and T follicle (bottom). The ovariole sheath is still intact. The three positions measured along the stalk are shown as red dots, from anterior (top) to posterior (bottom). Two groups of cells are present near the posterior stalk position: the stalk cells which are not dye-coupled to either adjacent follicle (a), and follicle cells which are coupled to the T oöcyte. One micron section stained with 1% toluidine blue in 1% Borax. Scale bar represents 20 μm.

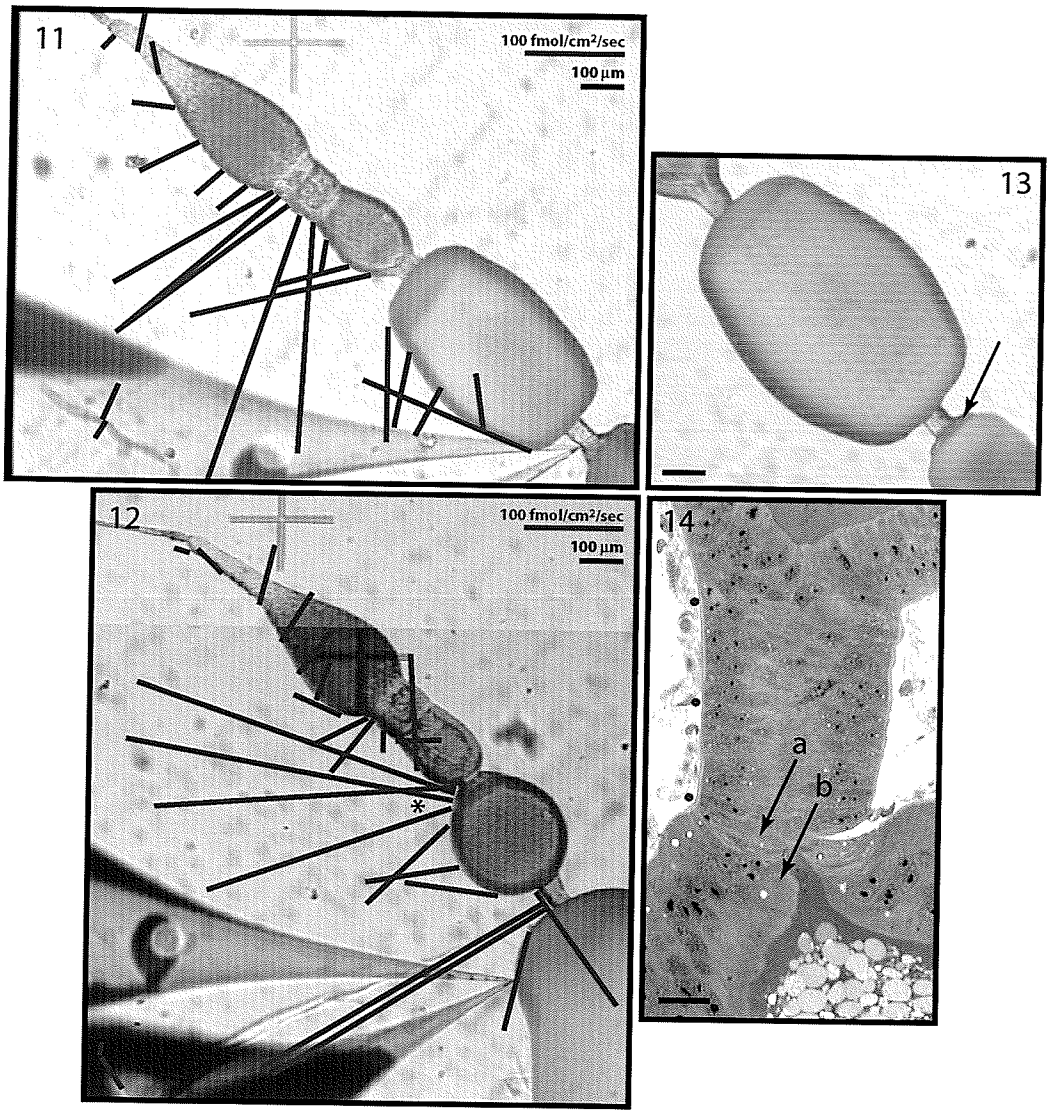
11
100 fmol/cm²/sec
100 µm
13
12
100 fmol/cm²/sec
100 µm
*
14
a
b

PLATE 11

Figure 15. H^+ flux around atretic follicles. The two line graphs plot H^+ flux vs. ovariole position, highlighting ovarioles with atretic T follicles (open circles and rectangles) and compare them to other individual ovarioles of similar stage (stages 7 and 8), with atretic follicles included so that they can be easily distinguished.

Figure 15.

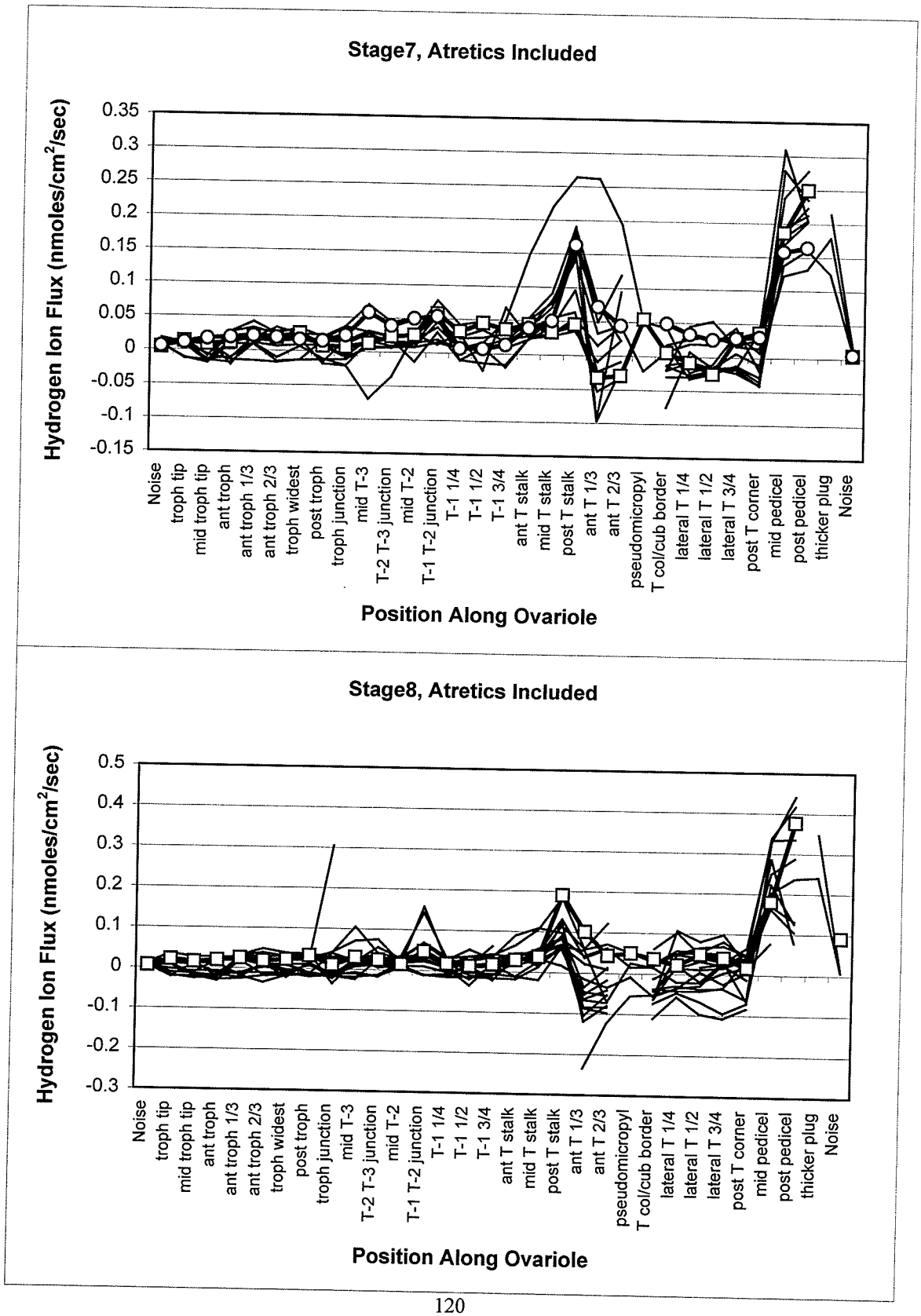
Stage7, Atretics Included
Hydrogen Ion Flux (nmoles/cm²/sec)
0.35
0.3
0.25
0.2
0.15
0.1
0.05
0
-0.05
-0.1
-0.15
Noise
troph tip
mid troph tip
ant troph
ant troph 1/3
ant troph 2/3
troph widest
post troph
troph junction
mid T-3
T-2 T-3 junction
mid T-2
T-1 T-2 junction
T-1 1/4
T-1 1/2
T-1 3/4
ant T stalk
mid T stalk
post T stalk
ant T 1/3
ant T 2/3
pseudomicropyl
T col/cub border
lateral T 1/4
lateral T 1/2
lateral T 3/4
post T corner
mid pedicel
post pedicel
thicker plug
Noise
Position Along Ovariole
Stage8, Atretics Included
Hydrogen Ion Flux (nmoles/cm²/sec)
0.5
0.4
0.3
0.2
0.1
0
-0.1
-0.2
-0.3
Noise
troph tip
mid troph tip
ant troph
ant troph 1/3
ant troph 2/3
troph widest
post troph
troph junction
mid T-3
T-2 T-3 junction
mid T-2
T-1 T-2 junction
T-1 1/4
T-1 1/2
T-1 3/4
ant T stalk
mid T stalk
post T stalk
ant T 1/3
ant T 2/3
pseudomicropyl
T col/cub border
lateral T 1/4
lateral T 1/2
lateral T 3/4
post T corner
mid pedicel
post pedicel
thicker plug
Noise
Position Along Ovariole

PLATE 12

Figure 16. Radial differences in H+ flux relative to orientation of the T-1 nucleus. Pooled data from stages 3-5 and stages 6-8 were grouped according to T-1 orientation. No significant differences between groups were observed, especially over the T-1 follicle where early indicators of oöcyte polarity may have developed.

Figure 16.

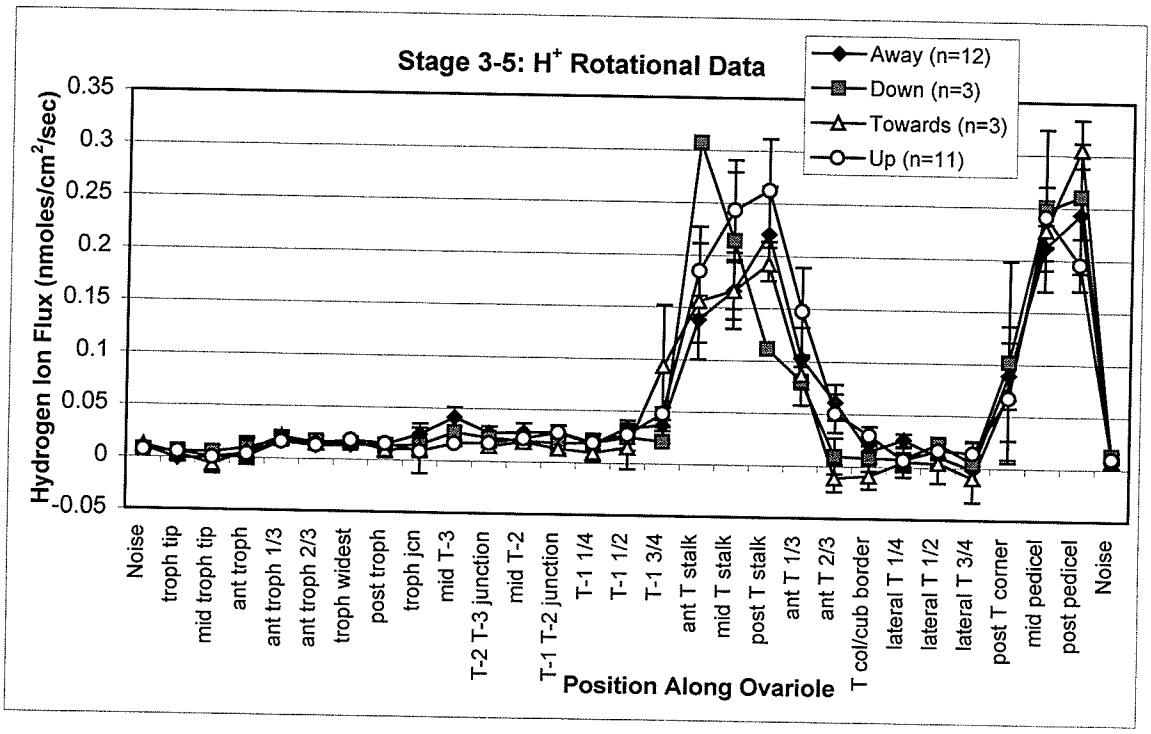
Stage 3-5: H+ Rotational Data
Away (n=12)
Down (n=3)
Towards (n=3)
Up (n=11)
Hydrogen Ion Flux (nmoles/cm2/sec)
0.35
0.3
0.25
0.2
0.15
0.1
0.05
0
-0.05
Noise
troph tip
mid troph tip
ant troph
ant troph 1/3
ant troph 2/3
troph widest
post troph
troph jcn
mid T-3
T-2 T-3 junction
mid T-2
T-1 T-2 junction
T-1 1/4
T-1 1/2
T-1 3/4
ant T stalk
mid T stalk
post T stalk
ant T 1/3
ant T 2/3
T col/cub border
lateral T 1/4
lateral T 1/2
lateral T 3/4
post T corner
mid pedicel
post pedicel
Noise
Position Along Ovariole

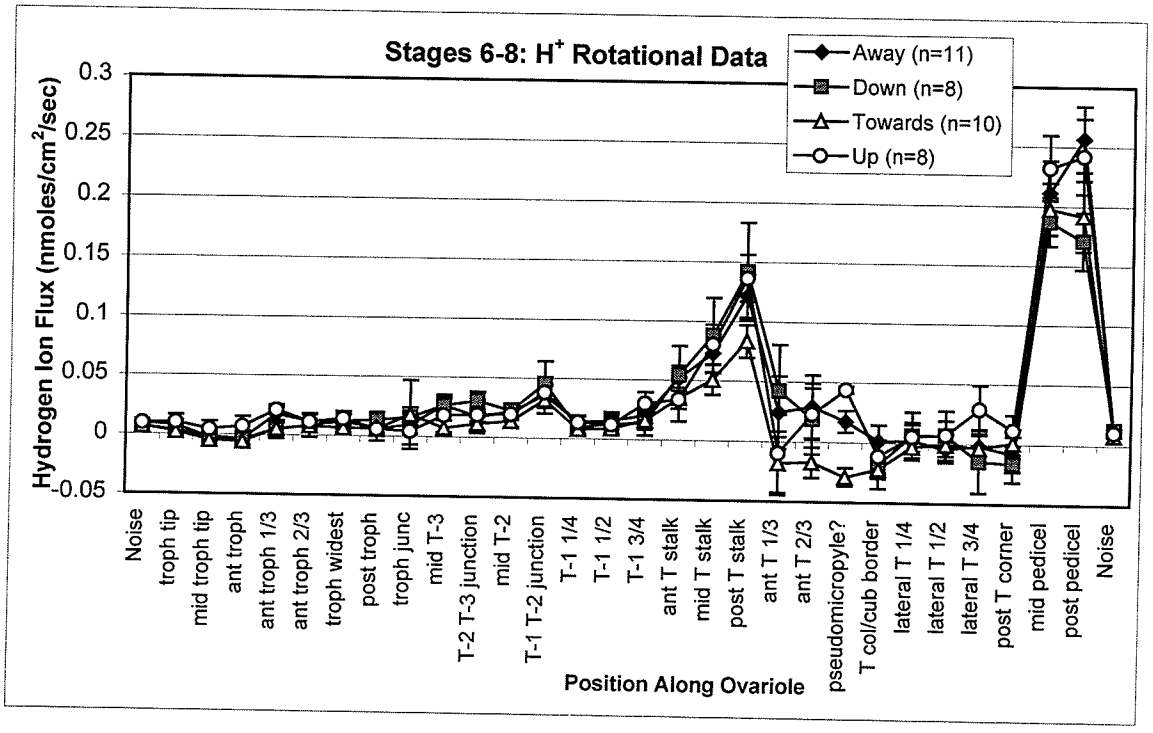
Stages 6-8: H+ Rotational Data
Away (n=11)
Down (n=8)
Towards (n=10)
Up (n=8)
Hydrogen Ion Flux (nmoles/cm2/sec)
0.3
0.25
0.2
0.15
0.1
0.05
0
-0.05
Noise
troph tip
mid troph tip
ant troph
ant troph 1/3
ant troph 2/3
troph widest
post troph
troph junc
mid T-3
T-2 T-3 junction
mid T-2
T-1 T-2 junction
T-1 1/4
T-1 1/2
T-1 3/4
ant T stalk
mid T stalk
post T stalk
ant T 1/3
ant T 2/3
pseudomicropyle?
T col/cub border
lateral T 1/4
lateral T 1/2
lateral T 3/4
post T corner
mid pedicel
post pedicel
Noise
Position Along Ovariole

CHAPTER 2: EXTRACELLULAR CALCIUM DYNAMICS DURING OÖGENESIS IN *RHODNIUS PROLIXUS*

INTRODUCTION

One of the hallmarks of germ tissue in insect meroistic ovarioles is a high degree of polarity between nurse cells and oöcytes. Morphological differences between nurse cells and oöcytes attest to functional differences between these cells despite their syncytial association. In the telotrophic ovarioles of *Rhodnius prolixus*, nurse cells synthesize protein, various RNAs, ribosomes, and mitochondria, which are transported to developing oöcytes through elongate intercellular bridges, the trophic cords (Vanderberg, 1963; Telfer, 1975; Huebner, 1981a). In the prefollicular zone of the ovariole, follicles are established with the proliferation of follicle cells that form a simple epithelium surrounding the developing oöcyte. During previtellogenesis, follicle cells express gap junctions that couple them to the oöcyte and each other (Huebner, 1981b; Huebner & Injeyan, 1981). Follicle cells also play an important role in regulating vitellogenesis by forming intercellular spaces to allow vitellogenin access to the oölemma, where it is taken up via receptor-mediated endocytosis (Telfer *et al.*, 1982). In *Rhodnius*, columnar follicle cells at the anterior pole of the follicle form a layer that is relatively impermeable to larger molecules including vitellogenin, and yolk uptake occurs across the lateral and posterior surfaces of the follicle where large spaces develop between cuboidal follicle cells (Huebner & Anderson, 1972a; Telfer *et al.*, 1982). Once vitellogenesis is complete

the lateral follicle cells restructure, becoming closely apposed, and initiate synthesis and secretion of the chorion. Oögenesis within each ovariole is highly coordinated in *Rhodnius*, where other oöcytes remain arrested in previtellogenesis until the terminal (T) oöcyte completes vitellogenesis and begins chorionation (Huebner & Anderson, 1972; Pratt & Davey, 1972).

The regulation of developmental processes during oögenesis in *Rhodnius* is not fully understood. Among the physiological differences between nurse cell and oöcyte compartments, regional ion fluxes and differences in intracellular ion activity are remarkable in that they can impact a broad spectrum of cellular functions relevant to oögenesis, including metabolic activity, membrane and cytoskeletal dynamics, and intercellular communication and signalling.

Intracellular calcium ($[Ca^{2+}]_i$) is especially well known for its role as a second messenger regulating a spectrum of events that extend to nearly every cellular activity. Calcium also modulates metabolic activity, by regulating a number of key regulatory enzymes, including isocitrate, oxoglutarate, and pyruvate dehydrogenases, key rate-limiting enzymes in the TCA pathway (reviewed by Pozzan *et al.*, 2000). Elevated extracellular calcium or intracellular calcium can inhibit gap junctional coupling (Perrachia & Perrachia, 1980a; Van Eldik *et al.*, 1985), a critical step in controlling the spread of apoptosis and the resulting rise in $[Ca^{2+}]_c$. Differences in connexon sensitivity to Ca^{2+} clearly exist, since intercellular calcium waves are often propagated among cells to coordinate contraction, ciliary beating, etc. Microfilament dynamics are also regulated by Ca^{2+}, which acts by modulating F-actin formation outright and by activating several actin-binding proteins, including gelsolin (Southwick, 2001), fascin (Ono *et al.*, 1997),

and most of the myosin superfamily of motor proteins (Mooseker & Cheney, 1995; Lodish *et al.*, 2000). Microtubule assembly is hindered in the presence of elevated $[Ca^{2+}]_i$, and several Ca^{2+}-dependent microtubule-associated proteins (MAPs), including dynein and kinesin motor proteins, have been identified (Hisanagi & Sakai, 1983; Cole, 1999). Nuclear activity is regulated by changes in nuclear calcium levels, and transcription of certain genes is activated by changes in nuclear $[Ca^{2+}]$ (Hardingham *et al.*, 1997, 1998; Hardingham & Bading, 1998, 1999).

How cells take a change in $[Ca^{2+}]_i$ and interpret it to select specific downstream responses is the subject of intense research. Calcium signals are often transient and repetitive, and the amplitude, frequency, and duration of these transients are used to tune signals to target specific cellular receptors. In addition and in response to extracellular Ca^{2+} signals induced by activation of receptor-activated calcium channels (RACCs), stretch-operated channels, and voltage-operated channels (VOCCs), calcium signals can be initiated, attenuated, amplified, and relayed by intracellular stores and sinks including mitochondria and smooth endoplasmic reticulum (SER)(Berridge *et al.*, 1998; Rutter *et al.*, 1998). Location of these components is critical to the dynamics of intracellular signalling, and intracellular Ca^{2+} stores are often aligned to facilitate propagation of Ca^{2+} signals to specific regions of the cell and between cells (Peterson *et al.*, 1999).

The role of calcium during development is similarly widespread. In early embryos from every species examined to date, one or more cytoplasmic calcium spikes are necessary for completion of meiosis (Stricker, 1999). In addition to transient Ca^{2+} spikes, slower waves may be generated and these are often associated with developmental events, where the roles of calcium are similarly widespread. Calcium waves have recently

been classified according to speed of the wavefront (Jaffe & Creton, 1998; Jaffe, 1999), and each type of wave appears to modulate a different set of events.

Furthermore, standing calcium gradients may be established that help break symmetry and establish zones of differential activity in unpolarized organisms. For example, photoactivation of the symmetric *Fucus* zygote defines the pole where a focused calcium efflux forms to direct pollen tube outgrowth (reviewed by Jaffe, 1999). In the meroistic ovarioles of the silkworm moth, *Hyalophora cecropia*, a difference in $[Ca^{2+}]_i$ is established between nurse cells and oöcyte at the onset of vitellogenesis (Woodruff & Telfer, 1994). Experimental removal of this difference results in resumed transcriptional activity in the germinal vesicle, and this activity can also be induced by microinjection of nurse cell cytoplasm into the oöcyte; thus it appears that Ca^{2+} establishes a gradient between the syncytial compartments that inhibits transport of a nurse cell-synthesized activating factor to the oöcyte (Woodruff & Telfer, 1998). It has been postulated that an extracellular calcium loop exists to balance and maintain this intracellular gradient, by pumping calcium out of the nurse cells and taking in calcium along the oöcyte surface (Woodruff & Telfer, 1994).

A difference in nurse cell and oöcyte Ca^{2+} levels, similar to that observed in *Hyalophora*, has recently been detected in the telotrophic ovarioles of *Rhodnius prolixus* (Bjornsson *et al.*, submitted); however its function remains unclear. Many events that are central to oögenesis are potentially regulated by changes in $[Ca^{2+}]_i$, including follicle cell shape changes (Sevala & Davey, 1989, 1993), cytoskeletal changes (Southwick, 2000; Ono *et al.*, 1997), intercellular transport (Bohrmann & Biber, 1994; Bohrmann, 1997), and establishing differences in nuclear activity between nurse cells and oöcytes

(Woodruff & Telfer, 1998). Calcium signalling may also be a part of the intraovariolar feedback mechanism involved in allowing only the posterior follicle to enter vitellogenesis, while others are held in a previtellogenic state until yolk uptake ceases in the terminal follicle. Therefore I was interested in examining Ca^{2+} dynamics during oögenesis in *Rhodnius*.

One approach to investigating the extracellular component of Ca^{2+} dynamics is by using a non-invasive Ca^{2+}-sensitive self-referencing probe (Kuhtreiber & Jaffe, 1990), which permits selective measurement of Ca^{2+} flux without injury to the tissue. Using this approach, it is possible to observe extracellular Ca^{2+} fluxes that are an external reflection of intracellular signalling events (due to SOCC or PMCA activity), or that are independent of signalling events (through RACC, VOCC, or PMCA activity, for example). Exploration of the location, timing and magnitude of extracellular Ca^{2+} flux is the first step towards understanding the potential roles of $[Ca^{2+}]_i$ during oögenesis. By using the extracellular Ca^{2+}-selective probe I hoped to observe position- and stage-specific calcium fluxes during oögenesis in *Rhodnius prolixus*, and to confirm the existence of a calcium efflux along the tropharium and an influx along the oöcyte surface as part of the current loop expected to balance and maintain the intracellular calcium gradient.

MATERIALS AND METHODS

Ovariole Preparation

A colony of *Rhodnius prolixus* was maintained at 27°C and 65% relative humidity in controlled environment incubators, and fed every 3-4 weeks on live rabbits or using an artificial membrane technique (Huebner *et al.*, 1994). Ovaries dissected from mated adult females 3-12 days post-feed (dpf) were transferred to Petri dishes containing modified O'Donnell's *Rhodnius* Ringers (O'Donnell, 1985), composed of 129mM NaCl, 8.6mM KCl, 0.02mM $CaCl_2$, 10.48mM $MgCl_2$, 48mM dextrose, and 1mM HEPES. Ovarioles were carefully isolated and desheathed. The Ringers used for these trials had reduced [HEPES] to minimize dampening of extracellular H+ fluxes (Kunkel & Faszewski, 1995) and reduced calcium to improve the signal-to-noise ratio. Ovarioles under these conditions behaved normally; follicle cells remained adherent to the oöcyte (an association that is lost in calcium-free saline) and muscular contractions of the ovariole sheaths appeared to be unaffected over the time period needed to complete a scan. Magnesium was added to compensate for the reduced [Ca^{2+}], and osmolarity was adjusted with glucose. Ovarioles were transferred to a specially designed recording chamber that facilitated rotation and positioning of the ovariole while minimizing deformation and stretching (Bjornsson & Huebner, 2002). Ovarioles were staged based on T follicle length, according to the method of Pratt & Davey (1972), as outlined in chapter 2.

Ion-Selective Probe (ISP) Technique

Extracellular Ca^{2+} flux was measured with the automated scanning electrode technique (ASET) using an ion-selective probe (ISP)(Applicable Electronics, Inc., Sandwich, MA; Science Wares, Inc., Falmouth, MA), as described in Chapter 2, with the following exceptions. Ca^{2+} probes were backfilled with 100 mM $CaCl_2$, and then frontfilled with a 20-30 μm column of calcium liquid ion exchanger (LIX; #IE 200, WPI, Inc., Sarasota, FL). The reference electrode consisted of a Ag/AgCl wire inserted into an open capillary tube (TW150-4, WPI, Inc.) filled with 3 M KCl and 3% agar.

Electrode calibrations were performed before and after each ovariole scan by measurement of potential in 0.1 mM, 1.0 mM, and 10.0 mM $CaCl_2$ solutions; this provided a measure of the probe's accuracy and its speed of response. Calcium probes were only used if the slope of a line derived by plotting $[Ca^{2+}]$ vs. potential equalled the expected Nernst value of 28.1 ± 7.5% mV per 10-fold change in concentration. If the calibration at the start or end of the scan deviated from expected Nernst values, or if the probe took longer than 10 seconds to settle on a potential during the calibration procedure, the reliability of the probe was brought into question, and data from that scan were considered invalid and excluded.

Data Analysis

Data were exported in text file format and analyzed using Microsoft Excel™. Visual basic macros were developed (see Appendix II) in Excel to calculate proton flux

based on the method of Kuhtreiber & Jaffe (1990), and to generate 2D and 3D resultant vectors from the X- and Y-axis values and the X-, Y-, and Z-axis values, respectively. Z-axis data were excluded because upon further analysis it became clear that they confounded the data while not contributing any essential further information, since the trends seen in 2D vectors were merely confirmed in the 3D vectors (see Chapter 1). Next, an image was generated using Adobe Illustrator 9™ or KineMage that displayed Ca^{2+} flux at each position measured along the ovariole. To accomplish this, the first image taken during the trial was used as a backdrop. The image corresponding to the vector being placed (showing the position of the probe in relation to the ovariole) was positioned over the original image and rendered partially transparent allowing the two ovariole images to be juxtaposed. If the second picture needed rotating to line up correctly, as sometimes happened when the ovariole moved slightly during a trial, it was adjusted to the nearest 0.5°, and the corresponding vector was similarly rotated before being placed. A line of arbitrary, consistent length was scaled according to the vector magnitude, so that Ca^{2+} flux at different positions and from different ovarioles could be directly compared. Each vector was positioned so that the origin was next to the ovariole at the location where the probe measurement was taken. Once positioned in this way, each vector was scored as a positive efflux if it travelled away from the ovariole, or as a negative influx if it travelled over the ovariole image. For KineMage images, an outline of the ovariole was traced using the ISP software after each scan was completed, and the position information for the ovariole and the ion flux at each position were added to a text file that could be read by the KineMage program. Kinemage images were analyzed in the same way as the Adobe images.

Once signs were assigned, data from each ovariole were grouped according to ovariole stage, and stage-specific averages and standard errors were calculated for each position measured along the ovariole. Using StatView software (SAS Institute Inc., Cary, NC), single-factor ANOVAs were performed to assess the significance of the signal in relation to background noise. Significant difference was defined as <0.05. In addition, a Levine's test for heterogeneity was conducted to determine whether the variability at different locations along the ovariole was significantly different from background noise.

RESULTS

General Features of Extracellular Ca^{2+} Flux Around Adult *Rhodnius* Ovarioles

The average Ca^{2+} flux at each ovariole position is shown for each stage in Figure 1, and a contour graph of the same data depicting the relationship between Ca^{2+} flux at each ovariole position over an oogenesis cycle is shown in Figure 2. Except for a few positions, average Ca^{2+} flux calculated at each position along the ovariole for each stage was not appreciably different than the average background noise. Single-factor ANOVAs, corrected using a Fishers' PLSD (Protected Least Significant Differences) post-test to reduce the likelihood of type I errors, comparing ovariole positions for each stage identified the Ca^{2+} flux at the connective posterior to the T follicle as being significantly different from noise during stage 5, 7, and 8. During stage 3, Ca^{2+} efflux at the midpoint of the interfollicular stalk between T and T-1 follicles was also significantly higher than noise; during stage 5, Ca^{2+} flux at the posterior end of the interfollicular stalk

separating T and T-1 follicles, and at the medial position along the anterior cap of the T follicle, was significantly different than background noise as well. While the Ca^{2+} flux at other positions along the ovariole showed significant differences between them, none of these were significantly different from background noise; therefore a comparison between these points is of little value.

Previtellogenesis

During the entire course of experimentation using adult ovarioles dissected 3-12 dpf, only one stage 1 ovariole was encountered. This ovariole was unhealthy, and was consequently excluded from subsequent analysis.

For stage 2 (T follicle length 400-500 μm) ovarioles, none of the extracellular Ca^{2+} flux measurements taken at positions along the ovariole were significantly different from Ca^{2+} flux measured as background noise.

Early Vitellogenesis

During stage 3 (T follicle length 500-600 μm), Ca^{2+} efflux at the midpoint of the interfollicular stalk between T and T-1 follicles was significantly higher than Ca^{2+} flux at both start and end background positions. In addition, Ca^{2+} flux at the lateral T 3/4 position and the posterior region of the pedicel was significantly different from Ca^{2+} flux measured as background noise at the end of the trial (end noise). Ca^{2+} flux at all other positions was not significantly different from that measured as background noise (either start or end noise).

For stage 4 (T follicle length 600-700 μm) ovarioles, none of the Ca^{2+} flux measurements taken at positions along the ovariole were significantly different from Ca^{2+} flux measured as background noise.

Midvitellogenesis

For stage 5 (T follicle length 700-800 μm) ovarioles, average Ca^{2+} efflux at the posterior region of the interfollicular stalk separating T and T-1 follicles, the anterior 1/3 region of the T follicle cap, and the posterior region of the pedicel were all significantly greater than Ca^{2+} flux measured as both start and end noise. In addition, average Ca^{2+} efflux at the T-1 1/4 position was significantly greater than Ca^{2+} measured as end noise. Ca^{2+} flux at all other positions was not significantly different from Ca^{2+} measured as background noise.

For stage 6 (T follicle length 800-900 μm) ovarioles, none of the Ca^{2+} flux measurements taken at positions along the ovariole were significantly different from Ca^{2+} flux measured as background noise.

Late Vitellogenesis

During stage 7 (T follicle length 900-1000 μm), Ca^{2+} flux at the mid and posterior regions of the pedicel was significantly different from Ca^{2+} flux measured as both start and end noise measurements. Ca^{2+} flux measured at all other positions was not significantly different from Ca^{2+} flux measured as background noise.

During stage 8 (T follicle length 1000-1500 μm), Ca^{2+} flux at the mid and posterior regions of the pedicel was significantly different from Ca^{2+} flux measured as

both start and end noise measurements. Ca^{2+} flux measured at all other positions was not significantly different from Ca^{2+} flux measured as background noise.

Chorionation

For stage 9 ovarioles (T follicle length 1500-2000 μm), none of the Ca^{2+} fluxes measured at positions along the ovariole were significantly different from the Ca^{2+} flux measured as background noise.

Significant Ca^{2+} Flux Around Individual *Rhodnius* Ovarioles

Although averaging Ca^{2+} flux for each ovariole stage did not reveal stage- or position-specific Ca^{2+} fluxes, there were several instances where Ca^{2+} flux was measured at discrete positions during scans of individual trials. An example of one such scan is shown in Figure 5, where Ca^{2+} influx over the T-1 and T-2 follicles of this stage 7 ovariole was measured. While Ca^{2+} influx was significantly different from noise within the scope of this trial, this information is lost when the average of Ca^{2+} influxes and effluxes is grouped according to stage.

The presence of position-specific Ca^{2+} fluxes in the absence of stage-specific Ca^{2+} flux suggests that Ca^{2+} flux observed during individual trials may be transient in nature. To determine whether this was the case, several positions were scanned repeatedly to look for changes in Ca^{2+} flux. The results of one such trial are shown in Figure 4, where a transient influx was observed over the anterior surface of the T follicle in a stage 8 ovariole. Ca^{2+} influx gradually increased over time, and eventually reversed. These

results support the idea that the Ca^{2+} fluxes observed during oogenesis in *Rhodnius* are transient in nature.

Heteroscedasticity of Ca^{2+} Flux Around Adult *Rhodnius* Ovarioles

Once the presence of transient, localized Ca^{2+} fluxes during oogenesis in *Rhodnius* seemed evident, I was interested in determining whether specific regions of the ovariole generated more transient Ca^{2+} flux than others. Increased variability (heteroscedasticity) at some positions may reveal the presence of increased transient Ca^{2+} flux. As shown in Figure 3, simply graphing the standard error of average Ca^{2+} flux at each position grouped according to stage revealed that some positions, notably at the interfollicular stalks at both ends of the T follicle and over the T-1 follicle, appear to be more variable than others. To determine whether these regions were significantly more variable than others, a Levine's test for heterogeneity of variances was performed. Variability at each position during each stage was compared to the variability of background noise measurements for that stage. If the variability at any position proved to be significantly different than that of background noise the position would have been compared to other ovariole positions during that stage and to the same position during different stages. The Levine's test revealed that none of the positions measured along the ovariole had significantly greater variance than either start or end noise measurements. Therefore, while transient Ca^{2+} fluxes could be detected over discrete regions of adult Rhodnius ovarioles of different stages, no position or stage had a greater or reduced tendency to produce transient Ca^{2+} fluxes.

DISCUSSION

The role of calcium in establishing developmental polarity during early embryogenesis and oögenesis in a number of organisms is well established. Single repetitive calcium spikes, slower propagating waves, and stable cytosolic gradients have all been described (Stricker, 1999; Jaffe, 1999). In meroistic insect ovarioles where syncytial nurse cells and oöcytes maintain a difference in cytosolic Ca^{2+} levels, it has been postulated that maintenance of this gradient is achieved by steady efflux over the nurse cells and influx along the oöcyte surface (Woodruff & Telfer, 1994; Dittmann, 1996).

A significant finding of this study is that there do not appear to be consistent stage or position-specific calcium fluxes during oögenesis above background noise levels. On one hand, this result is unexpected, since a difference in $[Ca^{2+}]_i$ between nurse cells and oöcytes, where oöcytes possess higher $[Ca^{2+}]_i$, has been observed in *Rhodnius* ovarioles (Bjornsson *et al.*, submitted). This difference between the syncytial germ cells suggests that a $[Ca^{2+}]_i$ gradient is established between the two compartments, which could be maintained by an extracellular Ca^{2+} loop consisting of efflux at the tropharium and influx at the oöcyte. A similar mechanism has been postulated for other insect ovarioles exhibiting a similar calcium distribution (Woodruff & Telfer, 1994; Dittmann, 1997), and has been demonstrated in other developing systems, including *Fucus* (Jaffe, 1999). Based

on the extracellular Ca^{2+} data presented here, it would appear that a similar mechanism does not maintain the nurse cell-oöcyte $[Ca^{2+}]_i$ gradient in *Rhodnius* ovarioles.

On the other hand, given the dynamic nature of calcium transport across biological membranes, and the prevalence of calcium transients in development (O'Donnell, 1985; Jaffe, 1999; Stricker, 1999), it is perhaps not surprising that steady calcium fluxes were not detected. In *Rhodnius*, oöcytes are connected to nurse cells via slender, elongate trophic cords that can reach up to a millimetre in length (Huebner, 1981a). Considering the limited diffusibility of Ca^{2+} through the cytoplasm due to the abundance of buffering molecules (Allbritton & Meyer, 1993; van den Brink *et al.*, 1999), it seems likely that nurse cell and oöcyte compartments simply regulate their own Ca^{2+} levels, aided perhaps by coupled follicle cells.

It is worth emphasizing that these trials were performed using modified *Rhodnius* Ringers containing $1/100^{th}$ the normal concentration of Ca^{2+}. While the activity of Ca^{2+} channels may have been affected by the lower transmembrane concentration gradient, this compromise was necessary to be able to see biologically relevant Ca^{2+} fluxes at all. Kuhtreiber & Jaffe (1990) stated that biologically relevant extracellular Ca^{2+} fluxes around developing systems including *Drosophila* follicles are on the order of 1-10 pmoles/cm^2/sec. The Ca^{2+}-selective probes used in the present study routinely exhibited noise levels of 20 μV, which in regular (2 mM) Ca^{2+} Ringers equates to ~26.2 pmoles/cm^2/sec, but in the 0.02 mM Ca^{2+} Ringers used here equates to ~0.262 pmoles/cm^2/sec. Unlike 0.002 mM Ca^{2+} Ringers, where sheath contractions stopped almost immediately, the ovariole sheath maintained regular muscular contractions during

the period of each ovariole scan in 0.02 mM Ca^{2+} Ringers, suggesting that the saline was not incompatable with normal cell function or survival.

With regard to the nurse cell-oöcyte $[Ca^{2+}]_i$ gradient, the lack of a steady efflux over the tropharium coupled with an influx along the oöcyte may be because the calcium gradient is managed by intracellular sinks and stores, although one would expect these would require occasional replenishment through either store-operated Ca^{2+} entry (Barritt, 1999) or by traffic between nurse cells and oocyte compartments of vesicles or cytosolic macromolecules carrying Ca^{2+}. It is also entirely possible that sustained extracellular Ca^{2+} flux occurs below the limits of detection of the ISP. A third explanation could be provided by the fact that the nurse cell-oöcyte voltage difference in *Rhodnius* ovarioles increases upon exposure to juvenile hormone (Telfer *et al.*, 1981); it is possible that extracellular Ca^{2+} fluxes may begin or increase upon application of juvenile hormone.

Alternatively, Ca^{2+} efflux along the tropharium and influx along the oöcyte could take the form of transient bursts of activity instead of a constant flux; if this were the case, one might expect the variability of extracellular Ca^{2+} flux detected in this region to be greater than at other positions along the ovariole. To address this possibility, a Levine's test for heterogeneity of variance was conducted. This analysis indicated no significant increase in variability at any position along the ovariole relative to that observed for background noise measurements.

An alternative approach to detection of extracellular Ca^{2+} transients is to repeatedly measure positions along a single ovariole. Although individual trials have the potential to turn up empty-handed and lack the strength of larger sample sizes, the duration and spatial dynamics of Ca^{2+} waves and spikes may sometimes be captured. An

example of one such event is shown in Figure 4, where transient Ca^{2+} influx was observed over the anterior pole of a 1050 μm T follicle (stage 8 ovariole). Influx initiated around the columnar population of follicle cells continued to increase over several minutes, and was followed a short time later by moderate efflux over the region. During this period, background noise and extracellular Ca^{2+} flux over the lateral T follicle remained more consistent. At the end of the trial, morphological changes were observed near the edge of the columnar cells, corresponding to the region where distinct groups of follicle cells would ultimately form the specialized structures of the chorion, including the micropyle and pseudomicropyle structures. In addition, the timing of this influx corresponded to the point in oögenesis when the T follicle loses its association with nurse cells in the tropharium, through closure of the trophic cord. Unfortunately, the state of the cord during this trial was not recorded. Elevated $[Ca^{2+}]_i$ levels may increase dynamic turnover of microfilaments and microtubules by altering polymer stability and activity of associated proteins (ABPs and MAPs)(Olmsted & Borisy, 1979). Microtubules in the trophic cords of *Notonecta* are known to be calcium-insensitive (Hyams & Stebbings, 1969); however the effects of calcium on trophic cord microtubules are not known. Although Ca^{2+} influx was not observed in the compiled data set for stage 8 ovarioles, this is perhaps not surprising, since only two of the ten ovarioles from stage 8 had T follicles of similar length. The T follicles from the other eight ovarioles had already lost their connection to the tropharium, suggesting that Ca^{2+} influx may have already taken place.

Although consistent extracellular Ca^{2+} influx and efflux were not detected, localized transient Ca^{2+} fluxes were observed, and these offer a foundation on which future investigation may be based. Fluorescence ratioing techniques may yield new

insight into the dynamics of intracellular calcium regulation in oöcytes and follicle cells, especially within T-1 follicles, the interfollicular stalks, and the anterior pole of the T follicle.

SUMMARY

This is the first study to demonstrate the presence of Ca^{2+} fluxes along an insect ovariole over an oögenesis cycle. Although steady, stage-specific Ca^{2+} fluxes significantly greater than background noise were not measured, significant fluxes were observed during individual trials that appear to represent transient transmembrane Ca^{2+} flux. These transient fluxes were associated with specific regions of the ovariole during individual trials but did not appear to be spatially restricted in general; rather they were observed in nearly every position along the ovariole. These results suggest that extracellular Ca^{2+} fluxes likely do not operate to maintain an intracellular nurse cell-oocyte Ca^{2+} gradient, although they may operate in conjunction with signalling pathways to lower cytosolic Ca^{2+} levels during signalling or replenish intracellular Ca^{2+} stores once signalling has subsided.

PLATES 1-3

Figure 1. Extracellular Ca^{2+} flux at all measured positions along the adult *Rhodnius* ovariole, grouped according to stage. Bars represent average Ca^{2+} flux; error bars indicate standard error.

Figure 1.

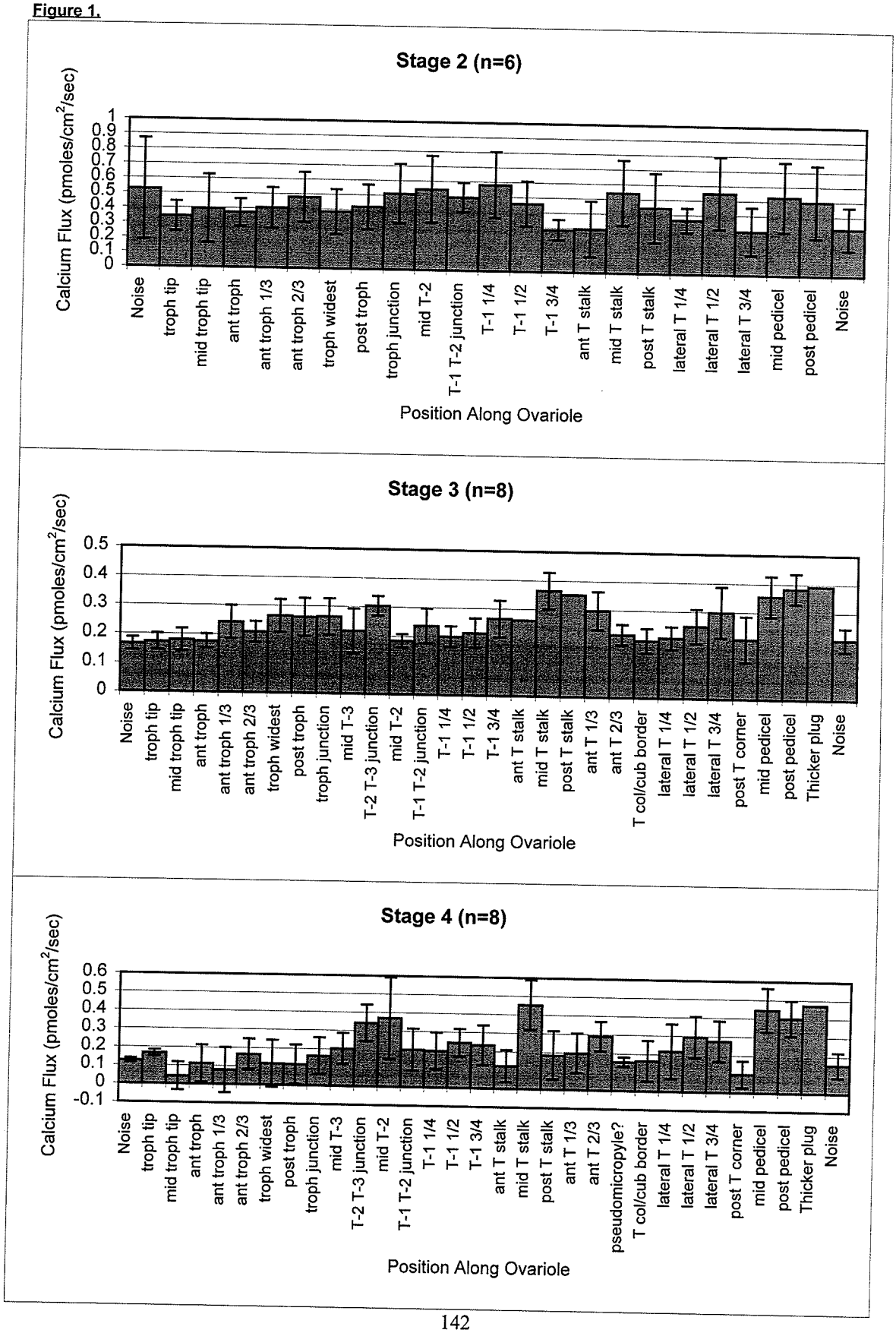
Stage 2 (n=6)
Calcium Flux (pmoles/cm2/sec)
1
0.9
0.8
0.7
0.6
0.5
0.4
0.3
0.2
0.1
0
Noise
troph tip
mid troph tip
ant troph
ant troph 1/3
ant troph 2/3
troph widest
post troph
troph junction
mid T-2
T-1 T-2 junction
T-1 1/4
T-1 1/2
T-1 3/4
ant T stalk
mid T stalk
post T stalk
lateral T 1/4
lateral T 1/2
lateral T 3/4
mid pedicel
post pedicel
Noise
Position Along Ovariole
Stage 3 (n=8)
Calcium Flux (pmoles/cm2/sec)
0.5
0.4
0.3
0.2
0.1
0
Noise
troph tip
mid troph tip
ant troph
ant troph 1/3
ant troph 2/3
troph widest
post troph
troph junction
mid T-3
T-2 T-3 junction
mid T-2
T-1 T-2 junction
T-1 1/4
T-1 1/2
T-1 3/4
ant T stalk
mid T stalk
post T stalk
ant T 1/3
ant T 2/3
T col/cub border
lateral T 1/4
lateral T 1/2
lateral T 3/4
post T corner
mid pedicel
post pedicel
Thicker plug
Noise
Position Along Ovariole
Stage 4 (n=8)
Calcium Flux (pmoles/cm2/sec)
0.6
0.5
0.4
0.3
0.2
0.1
0
-0.1
Noise
troph tip
mid troph tip
ant troph
ant troph 1/3
ant troph 2/3
troph widest
post troph
troph junction
mid T-3
T-2 T-3 junction
mid T-2
T-1 T-2 junction
T-1 1/4
T-1 1/2
T-1 3/4
ant T stalk
mid T stalk
post T stalk
ant T 1/3
ant T 2/3
pseudomicropyle?
T col/cub border
lateral T 1/4
lateral T 1/2
lateral T 3/4
post T corner
mid pedicel
post pedicel
Thicker plug
Noise
Position Along Ovariole

Figure 1. (continued)

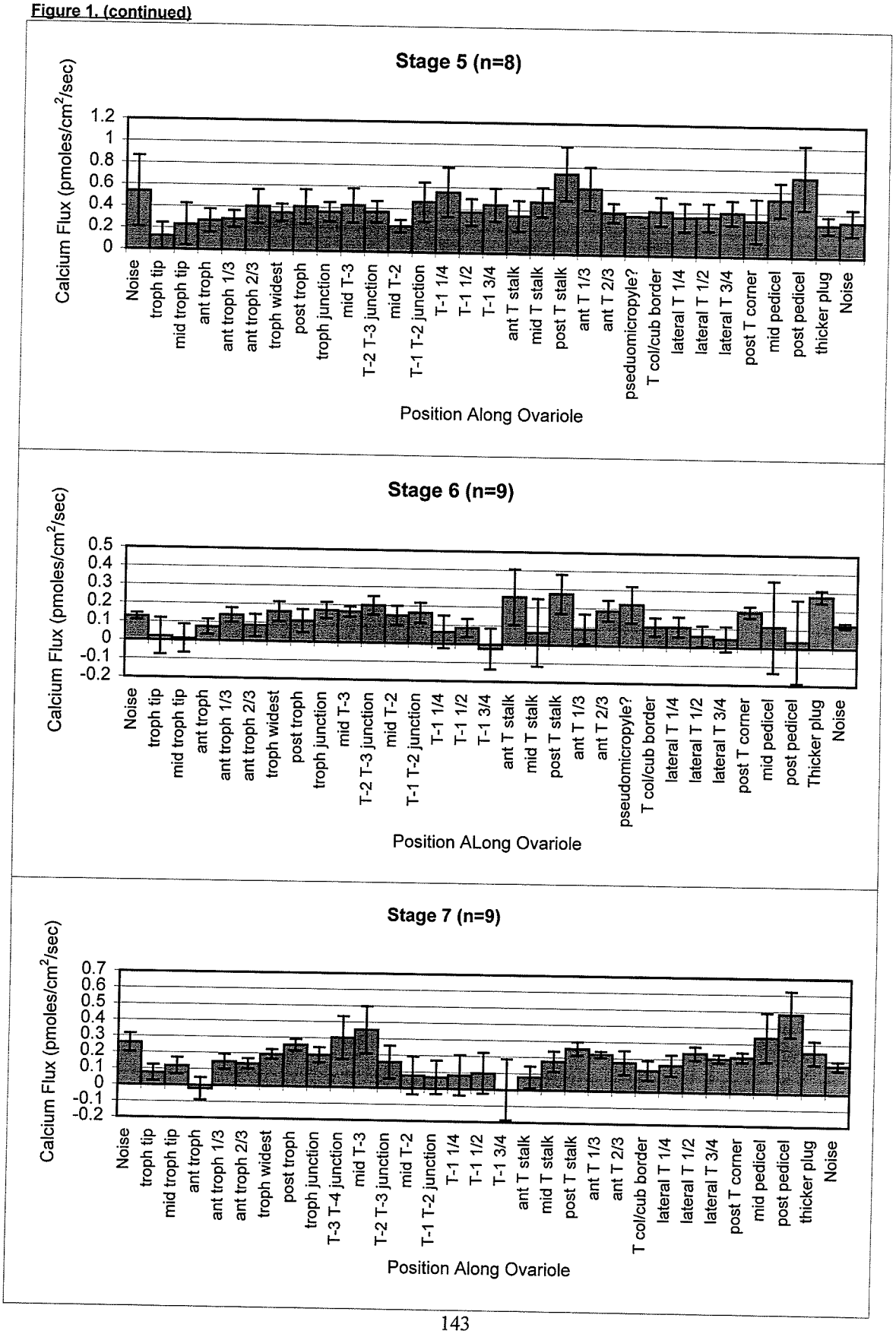

Figure 1. (continued)

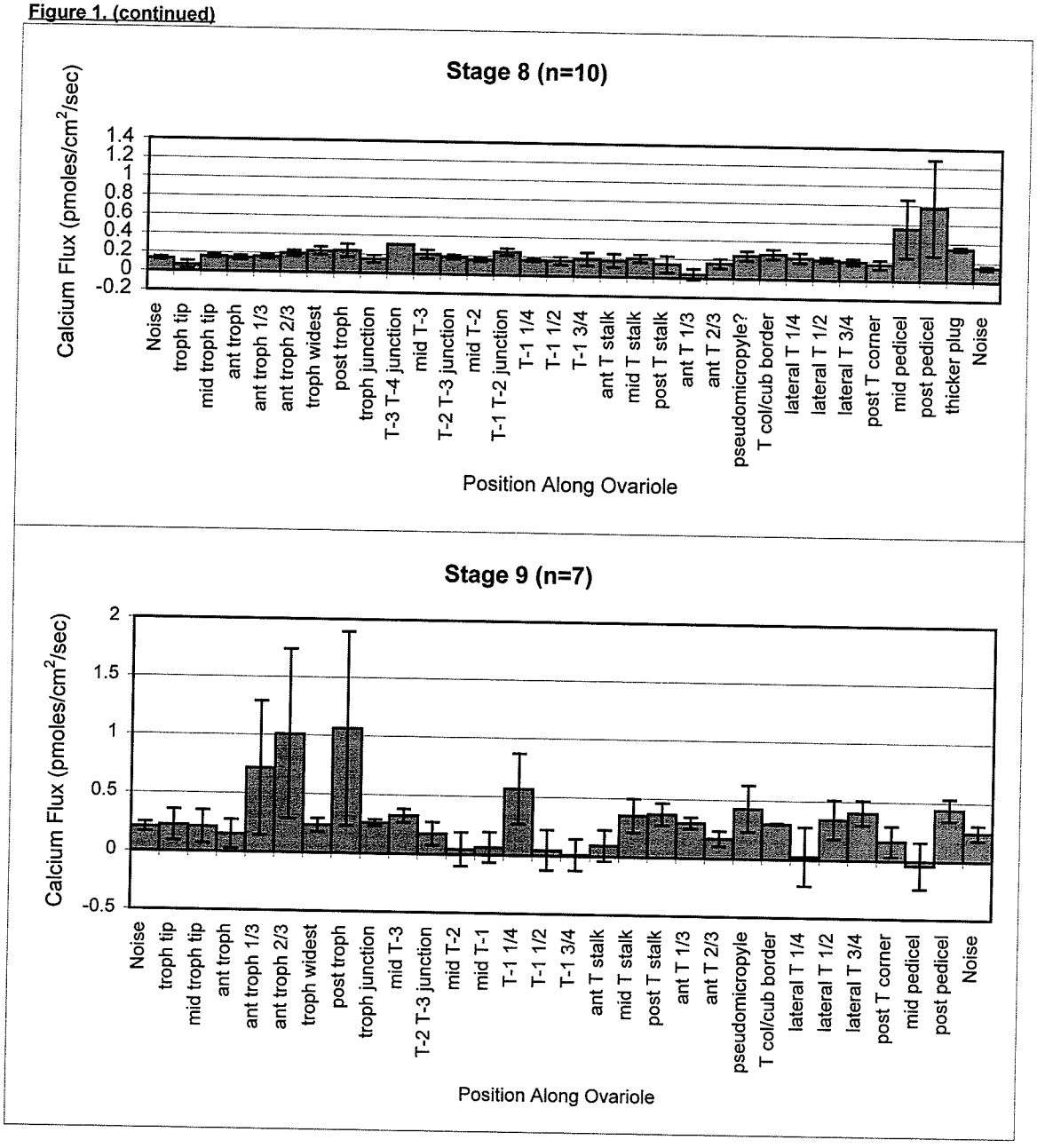

PLATE 4

Figure 2. Contour plot representing average extracellular Ca^{2+} fluxes along adult *Rhodnius* ovarioles. The bottom graph depicts Ca^{2+} flux magnitude and direction (influx/efflux) relative to position along ovariole and ovariole stage. The vertical lines correspond to specific points along the ovariole. The data for each ovariole stage, represented by bent black lines running through the coloured region of the plot, are superimposed on each other making it difficult to show stage differences. However these are clearly discerned in a top view as seen in the top plot. The colour coding indicates Ca^{2+} flux magnitude and direction, which is calibrated in the bottom plot. Each vertical column on the surface plot corresponds to a specific point along the ovariole as indicated by the ovariole images. The leftmost and rightmost columns display background noise. Horizontal rows display the average Ca^{2+} flux for each ovariole stage (see Methods).

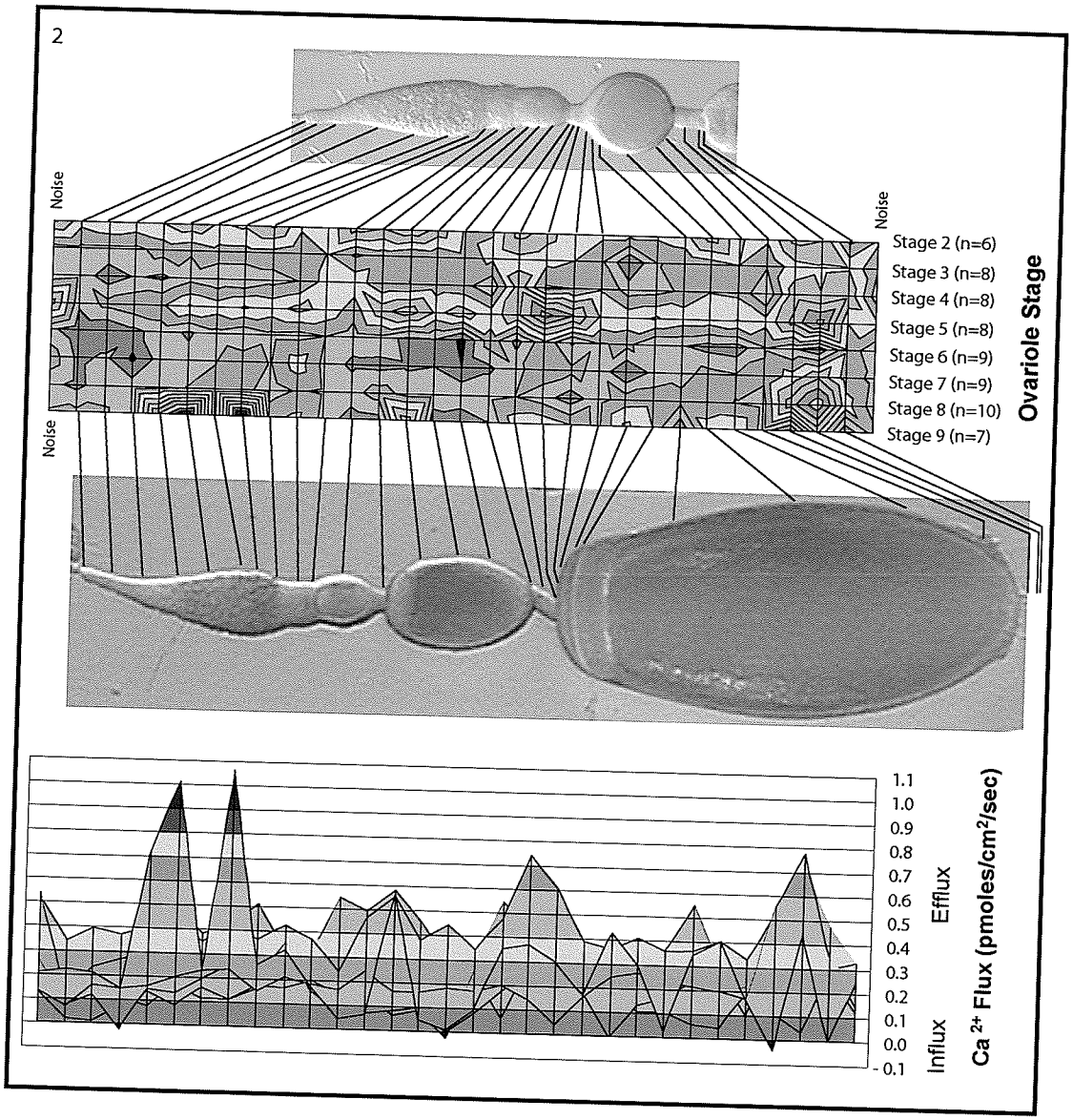
2
Noise
Noise
Noise
Stage 2 (n=6)
Stage 3 (n=8)
Stage 4 (n=8)
Stage 5 (n=8)
Stage 6 (n=9)
Stage 7 (n=9)
Stage 8 (n=10)
Stage 9 (n=7)
Ovariole Stage
1.1
1.0
0.9
0.8
0.7
0.6
0.5
0.4
0.3
0.2
0.1
0.0
-0.1
Efflux
Influx
Ca 2+ Flux (pmoles/cm2/sec)

PLATE 5

Figure 3. Contour plot displaying standard error of extracellular Ca^{2+} fluxes along adult *Rhodnius* ovarioles. The bottom graph depicts the standard deviation of Ca^{2+} fluxes relative to position along the ovariole and ovariole stage. The plots for ovariole stage are superimposed on each other making it difficult to show stage differences. However these are clearly discerned in a top view as seen in the top plot. Colour coding retains an indication of the magnitude of Ca^{2+} flux variability, and is calibrated on the bottom plot. Each vertical column on the top surface plot corresponds to a specific point along the ovariole as indicated by the ovariole images. The left- and rightmost columns display background noise. Horizontal rows display the standard error of average Ca^{2+} flux for each ovariole stage (see Methods). While some regions appeared to be more variable, notably the pedicel, the interfollicular stalk between T and T-1 follicle and along the T-1 follicle, a Levine's test did not reveal any regions where increased variability was significant.

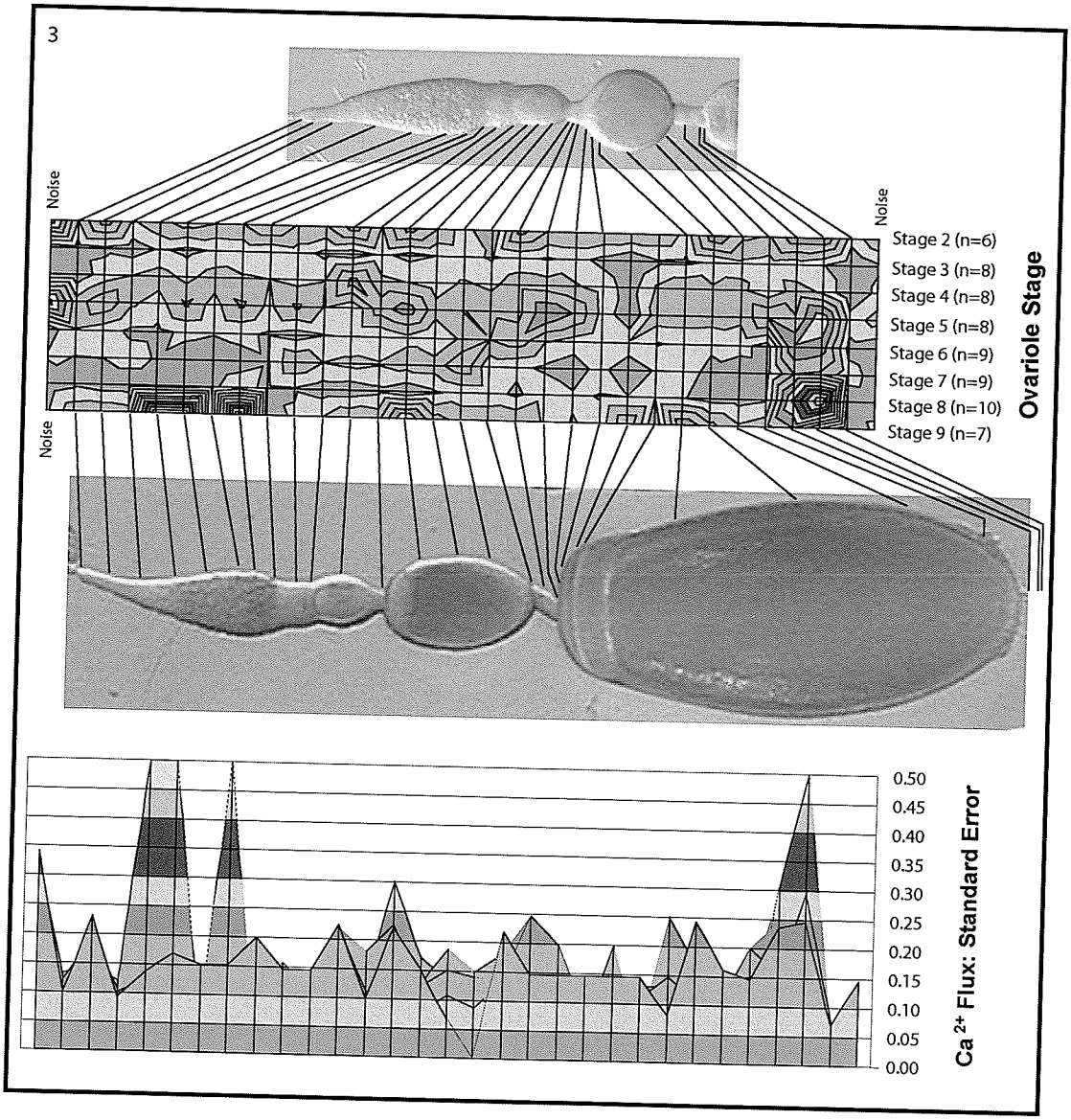
3
Noise
Noise
Noise
Stage 2 (n=6)
Stage 3 (n=8)
Stage 4 (n=8)
Stage 5 (n=8)
Stage 6 (n=9)
Stage 7 (n=9)
Stage 8 (n=10)
Stage 9 (n=7)
Ovariole Stage
0.50
0.45
0.40
0.35
0.30
0.25
0.20
0.15
0.10
0.05
0.00
Ca 2+ Flux: Standard Error

PLATE 6

Figure 4. Kinemage rendition of calcium fluxes around a 1000 μm T oöcyte (stage 8). The amount of time elapsed since the start of the trial is indicated above each image (hours: minutes). Dark blue lines represent the ovariole outline; red lines indicate direction (with the origin at the follicle surface) and magnitude (relative length) of calcium fluxes. Calcium influx exists where the lines appear to enter the ovariole, while with calcium efflux the lines appear to travel away from the follicle. Apical fluxes at t = 0:00 range from 19.5 -110.4 pmoles/cm^2/sec, and gradually increase in magnitude until t = 0:51 (51 minutes from the start of the scan), at which point they range from 22.4 - 355 pmoles/cm^2/sec. Not to scale.

Figure 5. Calcium flux around a stage 7 ovariole. Extracellular Ca^{2+} fluxes of greater magnitude than background levels were often observed along ovarioles during individual trials, as shown here with Ca^{2+} influx over the T-1 and T-2 follicles. However Ca^{2+} fluxes did not occur frequently enough to register when included in stage averages.

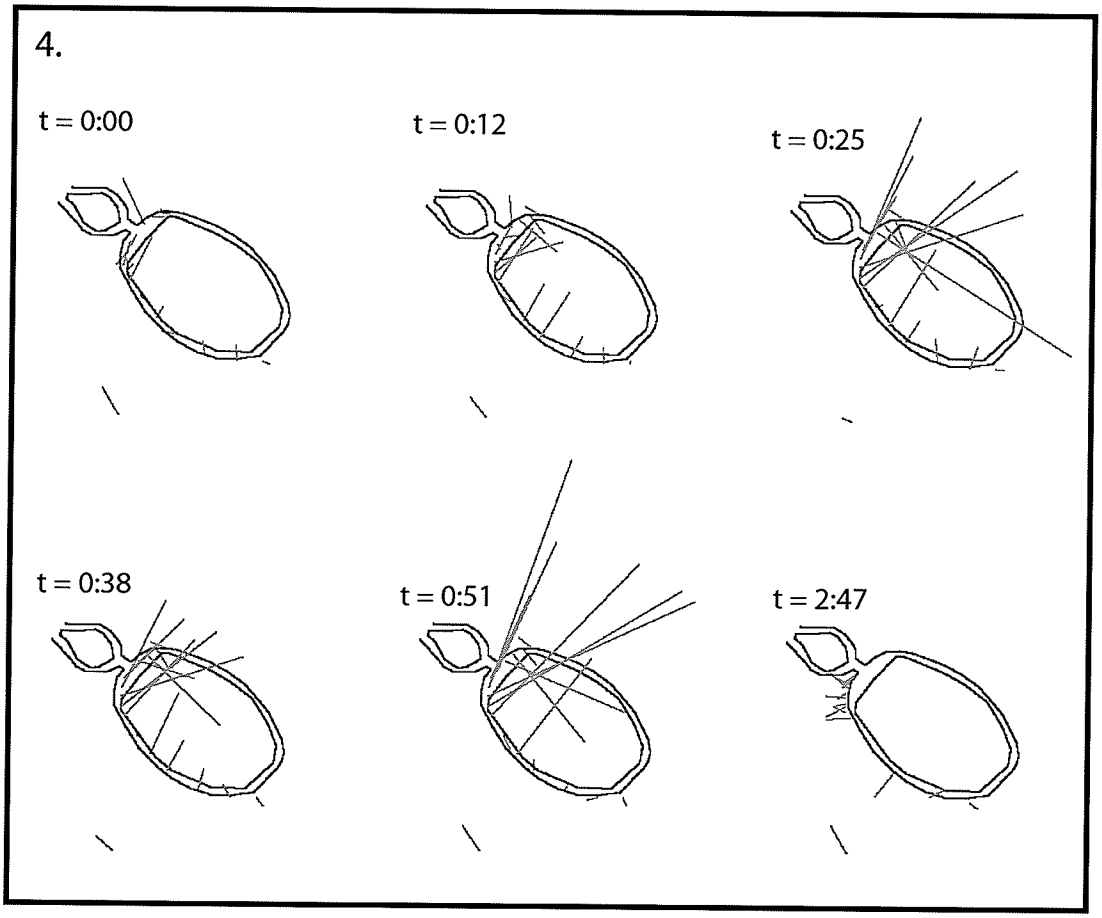
4.
t = 0:00
t = 0:12
t = 0:25
t = 0:38
t = 0:51
t = 2:47

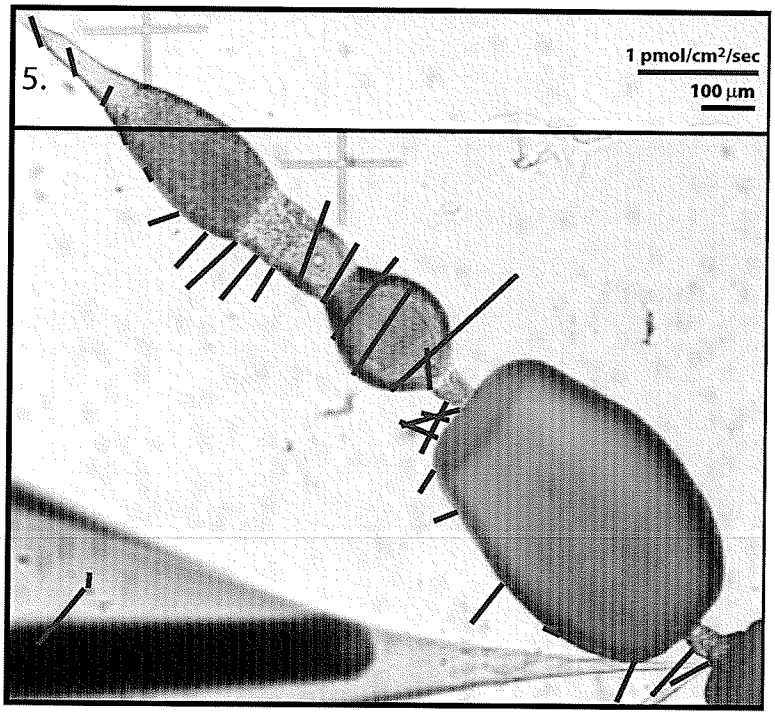
5.
1 pmol/cm²/sec
100 μm

CHAPTER 3: BIOELECTRIC CURRENTS DURING GERM CELL DIFFERENTIATION IN *RHODNIUS PROLIXUS*

INTRODUCTION

Oögenesis is a complex process involving precise orchestration of physiological and endocrinological activity of a number of cells. In insect meroistic ovarioles, the oöcyte interacts not only with somatic cells but also with sister germ cells, the nurse cells. Differences in structure and function between nurse cells and oöcytes affect nearly every aspect of cell activity during oögenesis, including differences in nuclear structure and activity (Telfer, 1975; Woodruff & Telfer, 1998), cytoskeletal architecture and dynamics (Huebner & Gutzeit, 1986; McPherson & Huebner, 1993; Riparbelli & Callaini, 1995), and cell membrane activity and bioelectrical properties (Woodruff *et al.*, 1986; Woodruff & Telfer, 1990, 1994; O'Donnell & Sharda, 1994), despite the fact that these cells share a common cytoplasm. In polytrophic meroistic ovaries, early signs of this polarity develop in the adult, within each germ cell cluster through coordinated divisions and somatic cell interactions after they have formed from a progenitor germline stem cell (reviewed by Deng & Lin, 2001). In the telotrophic meroistic ovaries characteristic of hemiptera, megaloptera and some coleoptera (Buning, 1994), differences between nurse cells and oöcytes occur even earlier. In the hemipteran *Rhodnius prolixus*, oöcyte determination occurs during the last (5^{th}) larval instar (Lutz & Huebner, 1980), establishing a population of oöcytes and nurse cells all sharing a common cytoplasm. It is in the 5^{th} instar that the

larval to adult transformation takes place. *Rhodnius* is an ideal system to study the timing of germ cell differentiation, since ovarian development is triggered by a single blood meal that sustains the insect until the final moult. In addition, a wealth of background morphological, physiological and endocrinological information is available (Wigglesworth, 1936; Huebner & Anderson, 1972a; Pratt & Davey, 1972; Lutz & Huebner, 1980, 1981).

Following ingestion of a blood meal, undifferentiated germ cells increase their numbers through mitosis during the proliferative stage, which occurs over the period of 1-8 days post-feed (dpf; Lutz & Huebner, 1980). Differences in nuclear structure appear between nurse cells and oöcytes during the early differentiation stage (9-15 dpf), when a basal zone of cells can be identified since they lack a prominent nucleolus and possess lighter cytoplasmic staining than the apical (nurse) cells. By the end of the early differentiation phase, three zones of nurse cells can be distinguished (apical, mid-, and basal regions), and some degree of nurse cell-oöcyte transport has begun (Lutz & Huebner 1980). During the late differentiation stage (16-21 dpf), basal nurse cell cytoplasm becomes increasingly basophilic, and nurse cell fusion occurs (Lutz & Huebner, 1981). Prefollicular cells begin to invade the oöcyte region, and some early follicles form with several initiating previtellogenic growth. Formation of the trophic core and nutritive cords also occurs during this period (Lutz & Huebner, 1980), a process involving elaboration of the ring canals to form an F-actin mesh (Yeow, 1994), as well as reorganization of microtubule arrays (Valdimarsson, 1987). Once the 5^{th} instar is ready to moult at 21 dpf, ovarioles resemble adult ovarioles, and await the first adult blood meal and hormonal factors to stimulate oögenesis (Wigglesworth, 1936). The initial

differentiation of the syncytial germ tissue into nurse cells and oöcytes is central to *Rhodnius* oögenesis, and highlights the need to understand how nurse cell-oöcyte differences are established and regulated.

In addition to establishing nuclear and cytoskeletal asymmetries (Telfer, 1975; Huebner & Gutzeit, 1986; Deng & Lin, 2001), differentiating nurse cells and oöcytes often undergo changes in membrane structure and function. This is apparent not only in the polarized E-cadherin distribution essential for oöcyte determination in *Drosophila* (Deng & Lin, 2001), but also in the bioelectric properties of developing telotrophic ovarioles in a hemipteran, *Dysdercus intermedius*, where a calcium gradient between syncytial nurse cells and oöcytes appears to be established before oöcyte determination (Dittmann, 1998). Steady intracellular Ca^{2+} gradients and pH changes in the cytosol are often established by asymmetric activity or distribution of plasma membrane pumps and channels creating regions of influx and efflux (Jaffe, 1999). The extracellular component of this membrane activity can be measured non-invasively using ion-selective probes, which can detect regions of ion influx and efflux outside complex tissues.

Differences in cytoplasmic ion activity, particularly global regulatory ions like H^+ and Ca^{2+}, can have profound effects. Intracellular pH has been shown to affect numerous metabolic events including core metabolic pathways and protein synthesis (Busa & Nuccitelli, 1984). Both Ca^{2+} and H^+ play prominent roles in cytoskeletal regulation, modulating the activity of numerous actin- and microtubule-based molecular motors, bundling proteins, and capping and severing proteins. Regulation of the cell cycle, mitosis, meiosis, and nuclear activity are all achieved by changes in nuclear and cytoplasmic Ca^{2+} activity (Hardingham *et al.*, 1997, 1998; Hardingham & Bading, 1998,

1999; Santella, 1996, 1998; Santella & Carafoli, 1997; Stricker, 1999). Key checkpoints, including the metaphase-anaphase and G_1-S transition, are regularly accompanied by a transient rise in $[Ca^{2+}]_c$ during mitosis, and these rises are necessary to perpetuate the cell cycle (Santella, 1998). Similarly, Ca^{2+} spikes following fertilization are required to arouse starfish oöcytes from meiotic arrest (Santella, 1996; Santella & Kyozuka, 1994, 1997).

The importance of both Ca^{2+} and H^+ to events that are central to nurse cell-oöcyte polarity raises the possibility that these ions may be employed by germ cells to establish differences between the two compartments. We are interested in determining whether extracellular ion fluxes are present during ovarian development in *Rhodnius prolixus*, and whether these fluxes accompany intracellular ionic gradients and coincide with specific differentiation events. This information could provide a foundation towards understanding the physiological control of these events. Extracellular H^+ and Ca^{2+} fluxes have been detected around adult *Rhodnius* ovarioles during oögenesis, appearing where significant physiological changes occur during oögenesis (this thesis). Here, I describe the pattern of extracellular Ca^{2+} and H^+ fluxes around 5^{th} instar ovarioles over the course of ovarian maturation and nurse cell-oöcyte differentiation, and explore whether or not patterns of H+ and Ca^{2+} flux correlate with the onset of germ cell differentiation and other events of the larval to adult transformation.

MATERIALS AND METHODS

Ovariole Preparation

A colony of *Rhodnius prolixus* was maintained at 27°C and 65% relative humidity in controlled environment incubators, and fed every 3-4 weeks on live rabbits or using an artificial membrane technique (Huebner *et al.*, 1994). Ovaries dissected from 5th instar females 4-21 days post-feed (dpf) were transferred to Petri dishes containing modified O'Donnell's *Rhodnius* Ringers (O'Donnell, 1985), composed of 129 mM NaCl, 8.6 mM KCl, 2.0 mM $CaCl_2$, 8.5 mM $MgCl_2$, 48 mM dextrose, and 1 mM HEPES, adjusted to 340 mOsm. Ovarioles were isolated and desheathed, carefully avoiding stretching or damaging the ovariole. The Ringers used for H^+ trials had reduced [HEPES] to minimize dampening of extracellular H^+ fluxes (Kunkel & Faszewski, 1995). H+ flux was measured at up to nine positions along the ovariole, while Ca^{2+} flux was measured at six of these ovariole positions (Figure 1).

Ion-Selective Probe (ISP) Technique and Data Analysis

Extracellular H^+ and Ca^{2+} fluxes were measured with the automated scanning electrode technique (ASET) using non-invasive H^+- and Ca^{2+}-selective probes (ISP; Applicable Electronics, Inc., Sandwich, MA; Science Wares, Inc., Falmouth, MA), as described in Chapters 1 and 2.

Data Analysis

Data were exported in text file format and analyzed using Microsoft Excel™. Visual basic macros were developed (see Appendix II) in Excel to calculate ion flux based on the method of Kuhtreiber & Jaffe (1990), and to generate 2D and 3D resultant vectors from the X- and Y-axis values and the X-, Y-, and Z-axis values, respectively. Z-axis data were excluded because upon further analysis it became clear that they confounded the data while not contributing any essential further information, since the trends seen in 2D vectors were merely confirmed in the 3D vectors. Next, an image was generated using Adobe Illustrator 9™ or KineMage that displayed ion flux at each position measured along the ovariole. For Adobe images, the first image taken during the trial was used as a backdrop. Next, the image corresponding to the vector being placed (showing the position of the probe in relation to the ovariole) was positioned over the original image and rendered partially transparent allowing the two ovariole images to be juxtaposed. If the second picture needed rotating to line up correctly, as sometimes happened when the ovariole moved slightly during a trial, it was adjusted to the nearest 0.5°, and the corresponding vector was similarly rotated before being placed. A line of arbitrary, consistent length was scaled according to the vector magnitude, so that ion flux at different positions and from different ovarioles could be directly compared. Each vector was positioned so that the origin was next to the ovariole at the location where the probe measurement was taken. Once positioned in this way, each vector was scored as a positive efflux if it travelled away from the ovariole, or as a negative influx if it travelled over the ovariole image. For KineMage images, an outline of the ovariole was traced

using the ISP software after each scan was completed, and the position information for the ovariole and the ion flux at each position were added to a text file that could be read by the KineMage program. KineMage images were analyzed in the same way as the Adobe images.

Once signs were assigned, data from each ovariole were grouped according to ovariole stage, and stage-specific averages and standard errors were calculated for each position measured along the ovariole. Using StatView software (SAS Institute Inc., Cary, NC), single-factor ANOVAs were performed to assess the significance of signal vs. background noise. Significant difference was defined as $P<0.05$.

RESULTS

Extracellular H^+ Flux

Extracellular H^+ fluxes were measured around 5th instar ovarioles, much smaller in magnitude than those around adult tissue, but significant nevertheless. Averages for H^+ flux at each position are shown in a series of graphs in Figure 2 grouped according to days post-feed, and the same data is shown in a contour plot in Figure 4 to better represent the spatiotemporal features of H^+ flux around 5th instar ovarioles. The results of single-factor ANOVAs for ovarioles grouped according to days post-feed revealed the following trends.

Proliferative Stage

Among ovarioles from 6 dpf 5th instars, H^+ efflux at the mid somatic tissue region averaged 9 ± 5 fmoles/cm^2/sec and was significantly different from H^+ flux measured as background noise. H^+ flux at this position was only different from H^+ measured as noise at the end of the trial (end noise), which averaged 5 ± 2 fmoles/cm^2/sec (P = 0.0195), but not H^+ flux measured as start noise, which averaged 10 ± 5 fmoles/cm^2/sec (P = 0.1493). The mid-somatic region was also significantly different from several positions along the ovariole, including the anterior germ tissue (P = 0.0377), mid-anterior germ tissue (P = 0.0010), mid-germ tissue (P = 0.0143), the germ/somatic junction (P = 0.0350), and the somatic constriction (P = 0.0027). H^+ flux measured at all other positions was not significantly different from H^+ flux measured as background noise.

Early Differentiation

Among ovarioles from 9 dpf 5th instar ovarioles, several regions of H^+ influx appeared that were significantly different from H^+ flux measured as background noise. Influx over the mid somatic tissue region, averaging –18 ± 7 fmoles/cm^2/sec, was significantly different than H^+ flux measured as both start (P = 0,0004) and end noise (P = 0.0008), which averaged 9 ± 1 fmoles/cm^2/sec and 7 ± 1 fmoles/cm^2/sec, respectively. H^+ flux at the germ/somatic junction, averaging –10 ± 4 fmoles/cm^2/sec, was also significantly different than H^+ flux measured as both start (P = 0.0119) and end noise (P = 0.0200). In addition, H^+ flux at the mid-anterior germ tissue region, averaging –7 ± 5

fmoles/cm^2/sec, differed significantly from H^+ flux measured as start (P = 0.0290) and end noise (P = 0.0462). H^+ flux at two other regions, the mid somatic cap and the mid-posterior region of the germ tissue, was different from H^+ flux measured as start but not end noise (P = 0.0397 and 0.346, respectively). H^+ flux measured at all other positions was not significantly different from H^+ flux measured as background noise.

Among ovarioles from 12 dpf 5th instar ovarioles, influx over the germ tissue increased substantially. H^+ flux measured as start and end noise averaged 8 ± 2 fmoles/cm^2/sec and 8 ± 1 fmoles/cm^2/sec, respectively. The most dramatic difference was observed over the mid-region of the germ tissue, including the mid-anterior germ tissue, where H^+ flux averaged –23 ± 4 fmoles/cm^2/sec (P = <0.0001 for both); mid germ tissue, where H^+ flux averaged 24 ± 5 fmoles/cm^2/sec (P = 0.0001 for both); and mid-posterior germ tissue, where H^+ flux averaged 21 ± 7 fmoles/cm^2/sec, in all cases the difference relative to H^+ flux measured as both start and end noise was highly significant (P < 0.0001). H^+ flux at several other positions were also significantly different than H^+ flux measured as both start and end noise, including the anterior germ tissue, where H^+ flux averaged –12 ± 9 fmoles/cm^2/sec (P = 0.0060 and 0.0057 for start and end noise, respectively); the posterior germ tissue, where H^+ flux averaged 15 ± 6 fmoles/cm^2/sec (P = 0.0035 and 0.0034); the germ somatic junction, where H^+ flux averaged 13 ± 4 fmoles/cm^2/sec (P = 0.0041 and 0.0040); the somatic constriction, where H^+ flux averaged 7 ± 3 fmoles/cm^2/sec (P = 0.0394 and 0.0381); and the mid somatic region, where H^+ flux averaged 11 ± 6 fmoles/cm^2/sec (P = 0.0088 and 0.0085).

Among ovarioles from 15 dpf 5th instar ovarioles, H^+ influx over the germ tissue decreased, and none of the positions measured along the ovariole had H^+ flux significantly different from H^+ flux measured as background noise. H^+ flux measured as start and end noise averaged 8 ± 2 fmoles/cm^2/sec and 4 ± 1 fmoles/cm^2/sec, respectively. H^+ flux averaged –1 ± 7 fmoles/cm^2/sec along the anterior germ tissue, H^+ flux averaged –4 ± 8 fmoles/cm^2/sec at the mid-anterior germ tissue, -5 ± 4 fmoles/cm^2/sec at the mid germ tissue, -3 ± 4 fmoles/cm^2/sec at the mid-posterior germ tissue, -1 ± 4 fmoles/cm^2/sec at the posterior germ tissue, -3 ± 7 fmoles/cm^2/sec at the germ somatic junction, 6 ± 5 fmoles/cm^2/sec at the mid somatic cap, 6 ± 5 fmoles/cm^2/sec at the somatic constriction, and 9 ± 31 fmoles/cm^2/sec at the mid somatic region.

Late Differentiation

Among ovarioles from 21 dpf 5th instar ovarioles, influx persisting over the mid-anterior germ tissue region, averaging –18 ± 6 fmoles/cm^2/sec, remained significantly different from both start ($P = 0.0011$) and end background H^+ flux measurements ($P = 0.0042$), which averaged 9 ± 1 fmoles/cm^2/sec and 6 ± 1 fmoles/cm^2/sec, respectively. In addition, efflux over the mid somatic region, averaging 26 ± 11 fmoles/cm^2/sec, was significantly greater than H^+ flux measured as start ($P = 0.0418$) and end noise ($P = 0.0145$). Among this group of ovarioles, a considerable range of development was observed; some ovarioles had already produced a small (~200 μm) previtellogenic oöcyte (Figure 5). These ovarioles were also remarkable in that they had developed a considerable H^+ efflux over the posterior stalk, averaging 63 ± 14 fmoles/cm^2/sec, which

was significantly different from H^+ flux measured as both start and end noise ($P < 0.0001$). H^+ flux measured at all other positions was not significantly different from H^+ flux measured as background noise.

Extracellular Ca^{2+} Flux

Average extracellular Ca^{2+} flux at each position is tabulated in Table 2 below, shown in a series of graphs in Figure 3 grouped according to days post-feed, and shown in a contour plot in Figure 5 to better represent the spatiotemporal features of Ca^{2+} flux during ovariole differentiation in the 5th instar. Single-factor ANOVAs comparing Ca^{2+} flux at all ovariole positions for ovarioles grouped according to days post-feed indicated that none of the Ca^{2+} fluxes measured at any position during any day post-feed was significantly different from Ca^{2+} flux measured as background noise. A Levine's test for homogeneity of variances performed in the same manner indicated that none of the differences in variability in Ca^{2+} flux measured at different positions along the ovariole were significantly different from the variability of Ca^{2+} flux measured as background noise for the corresponding day post-feed.

	Anterior Germ Tissue	Midant Germ Tissue	Midpost Germ Tissue	Junction	Somatic Constriction	Mid Somatic Tissue	Noise
4 dpf	–38.3 ± 19.9	–24.9 ± 25.0	–30.2 ± 24.8	–32.9 ± 25.7	–44.4 ± 17.3	–40.2 ± 19.6	36.3 ± 19.0
5 dpf	22.0 ± 11.1	13.2 ± 11.3	–2.3 ± 6.3	1.7 ± 6.0	3.0 ± 6.4	3.4 ± 6.4	14.6 ± 2.7
6 dpf	–19.3 ± 16.5	–6.8 ± 15.1	–17.8 ± 13.3	–13.5 ± 15.9	–22.2 ± 12.9	–20.1 ± 22.3	26.8 ± 9.9
7 dpf	–15.8 ± 11.4	–2.0 ± 14.1	8.5 ± 27.0	–13.1 ± 11.8	–17.7 ± 11.3	–24.9 ± 10.7	24.2 ± 7.9
8 dpf	–18.0 ± 7.8	–24.4 ± 7.0	–14.8 ± 8.2	–24.0 ± 11.1	–16.4 ± 7.4	–16.8 ± 6.8	23.2 ± 4.3
9 dpf	–6.7 ± 12.6	1.3 ± 10.9	–3.8 ± 9.9	–1.6 ± 17.2	–4.8 ± 14.7	–1.1 ± 13.5	23.6 ± 5.4
10 dpf	–0.1 ± 6.0	–3.3 ± 5.4	8.8 ± 2.9	–3.0 ± 8.3	–3.8 ± 9.9	–8.9 ± 9.4	7.4 ± 2.6
11 dpf	–22.6 ± 26.3	–14.5 ± 15.7	–19.0 ± 19.1	–29.2 ± 16.3	–11.2 ± 35.9	–28.9 ± 23.8	34.9 ± 9.1
12 dpf	–44.0 ± 28.3	–23.5 ± 19.1	–21.1 ± 21.4	–27.9 ± 26.3	–24.2 ± 21.0	–22.0 ± 28.8	54.0 ± 17.5
15 dpf	–4.5 ± 6.2	–1.7 ± 5.9	–4.1 ± 4.7	–8.4 ± 6.5	–20.4 ± 26.5	–3.3 ± 5.5	17.5 ± 2.7
18 dpf	–9.5 ± 32.3	–21.6 ± 23.9	–14.8 ± 24.3	15.3 ± 22.6	–11.2 ± 31.1	3.8 ± 31.1	42.1 ± 10.8

Table 2: Average Ca^{2+} flux around 5th instar ovarioles. Positive values represent efflux; negative values represent influx. Data are presented as the mean ± standard error in pmoles/cm^2/sec.

DISCUSSION

Extracellular H^+ Fluxes during Germ Cell Differentiation

The non-invasive H^+-selective probe has previously been successful in measuring extracellular H^+ fluxes around adult ovarioles with minimal background noise (Chapter 1, this thesis). Strong H^+ fluxes were associated with developing follicles, and were not prominent around the tropharium. The success of this technique and the polarity of H^+ flux in adult tissue made the prospect of measuring H^+ fluxes around 5th instar ovarioles feasible, and provided a way to investigate potential membrane and cytoplasmic changes that may be instrumental in the establishment of nurse cell-oöcyte polarity within the syncytial germ tissue. A number of the changes occurring during the larval-adult transformation involve elements that are potentially regulated by changes in intracellular pH, including cytoskeletal reorganization, changes in nuclear structure and function, and cytoplasmic activity. Extracellular H^+ fluxes associated with specific periods of ovariole differentiation and localized to discrete regions of the ovariole were detected around 5th instar ovarioles. These fluxes were associated with both germ and somatic tissues at different points in development. This is the first study to establish the existence of extracellular H^+ fluxes around 5th instar ovarioles, during the period when nurse cell and oöcyte populations are established. Two fluxes observed during this period are particularly noteworthy, and will be considered in more depth below.

H^+ Influx Around the Germarium

The prevalence of H^+ influx across the 5th instar ovariole is especially intriguing. At 12 dpf, H^+ influx in the 5th instar occurs over the entire central region of the germ tissue, in the region where three zones of presumptive nurse cells are being formed through the establishment of nuclear differences as well as differences in synthetic activity (Lutz & Huebner, 1980). Considering the relative timing of these events in relation to the influx of H^+ observed here, it is possible that changes in intracellular H^+ activity may affect these early differentiation events. If H^+ influx does in fact result in cytosol acidification, one might expect a reduction in protein synthesis and metabolic pathways (Busa & Nuccitelli, 1984), depending on the initial pH_i. Still, the situation may be more complex, and the effects of pH_i on other events during this period including establishment of ploidy in nurse cells, the introduction of mitotic block, and a myriad of cell membrane and cytoplasmic events are presently unknown.

In addition, a dramatic transformation in the cytoskeleton occurs as the mature *Rhodnius* ovariole is formed, involving the formation and elaboration of ring canals to create an F-actin mesh lining the trophic core. Ring canals form from cleavage furrows that are arrested during incomplete cytokinesis as germ cells proliferate and later serve as nucleation sites for a more extensive branching network of microfilaments separating nurse cell lobes from the central, nuclei-free trophic core (Yeow, 1994). Ovarian ring canal structure has been well characterized in *Drosophila*, due to the ease with which female sterile mutants can be produced and analyzed. Ring canals begin as an electron dense thickening of the plasma membrane containing mucin glycoproteins (Kramerova & Kramerov, 1999) and phosphotyrosine protein (Robinson *et al.*, 1994) formed along the

rims of arrested cleavage furrows (Mahowald, 1971). Next, circumferentially oriented F-actin (Warn *et al.*, 1985; Gutzeit, 1986b) of mixed polarity (Tilney *et al.*, 1996) and a ring canal-specific form of the hu-li tai shao (Hts) gene product (Lin & Spradling, 1994; Robinson *et al.*, 1994) are added to form an inner rim. This step requires the Cheerio protein, a *Drosophila* filamin, which becomes associated with both inner and outer rims (Robinson *et al.*, 1997; Sokol & Cooley, 1999). Before the cyst leaves the germarium the last characterized component, a product of the kelch gene, lines the inner rim (Robinson & Cooley, 1997). Both Hts and Kelch are needed for normal actin regulation in the ring canal. Hts^- mutants lack F-actin in the ring canals, suggesting a role for Hts in actin recruitment or maintenance. Kelch may prevent F-actin disassembly by stabilizing adjacent actin subunits, or it may link two adjacent filaments, preventing bundle fraying (Tilney *et al.*, 1996b). Additionally, immunofluorescent staining has revealed the presence of non-muscle myosin II regulatory light chain (Spaghetti Squash; Edwards & Kiehart, 1996; Jordan & Karess, 1997) and 95F (class VI myosin; Bohrmann, 1997), though their function is unknown. Ring canals continue to grow in thickness and diameter during oögenesis; the increase in ring canal diameter may occur through a sliding filament mechanism (Tilney *et al.*, 1996b) and may involve Kelch, since ring canals in $kelch^-$ mutants begin to fray as their diameter starts to increase (Robinson & Cooley, 1997). As ring canals grow, actin bundles become organized into several discrete bundles visible in cross-sectional views.

In *Rhodnius*, ring canals act as nucleation sites for the formation of F-actin struts that fuse to form a meshwork surrounding the trophic core. Actin filaments begin to extend from the ring canals by 13-15 dpf, becoming thicker and branching as

development proceeds (Yeow, 1994). During this period extensive membrane fusion and restructuring is also occurring, and the membrane association of ring canals is lost. Before the moult, these branching structures form an interconnected mesh encircling the central trophic core. Strut formation may involve a mechanism similar to that involved in *Drosophila* bristle formation (Yeow, 1994), where actin filaments are held together loosely by the protein Forked until they are more extensively crosslinked by the protein Singed, the *Drosophila* fascin (Tilney *et al.*, 1996a, b). The timing of H^+ influx over the germarium suggests that it precedes the initial formation of F-actin projections from the ring canals. However, if a drop in pH results from this influx, it is unclear what effect this may have on the actin cytoskeleton, since the pH-sensitive ABP, fascin, would be increasingly prone to inactivation under more acidic conditions. Still, the timing of these two events supports the possibility that extracellular H^+ fluxes and cytoskeletal events may be related. Apart from myosin, the pH-dependence of other ABPs involved in ring canal formation and maturation is currently unknown.

Ovariole restructuring during the larval-adult transformation in *Rhodnius* also involves the establishment of a microtubule-rich trophic core, which begins to form 6 days before the moult in conjunction with the initiation of previtellogenic growth by some oöcytes (Valdimarsson, 1987). The adult structure does not appear until after the moult, possibly in response to feeding. The timing of microtubule growth in the core relative to the earlier H^+ influx (roughly 9 days before moult) suggest that H^+ influx is probably not involved in this process.

H^+ Efflux Around Somatic Tissue during Late Differentiation

The appearance of H^+ efflux along the posterior stalk by day 21 in the more mature ovarioles is significant in that it foreshadows the development of the adult pattern as the transformation from larva to adult nears completion. Efflux observed over the mid somatic tissue region of 5th instar ovarioles is significantly greater than background noise, though the average efflux is quite low (26 ± 11 fmoles/cm^2/sec), presumably since not all ovarioles had reached the point where efflux is initiated. Flux measurements from individual ovarioles in this region did in fact reach as much as 96 fmoles/cm^2/sec, a value comparable to and even exceeding H^+ efflux seen in several stages of adult ovarioles (see Chapter 1, this thesis).

Extracellular Ca^{2+} Fluxes during Germ Cell Differentiation

Many insect ovarioles develop a calcium gradient between nurse cell and oöcyte compartments in the adult. In the polytrophic ovarioles of *Hyalophora cecropia*, this gradient is established at the onset of vitellogenesis (Woodruff & Telfer, 1994), while in the telotrophic ovarioles of the hemipteran, *Dysdercus intermedius*, a nurse cell-oöcyte Ca^{2+} gradient in the adult is established earlier, as germ cells differentiate during the last larval instar, (Dittmann, 1998). In some systems, such gradients have been shown to be vanadate-sensitive, and therefore reliant on the activity of a P-type pump such as the PMCA (Woodruff & Telfer, 1994; Dittmann, 1996), and so should be accompanied by extracellular Ca^{2+} efflux. Since a similar Ca^{2+} gradient was recently observed in adult *Rhodnius* ovarioles (Bjornsson *et al.*, submitted), I was interested in determining whether

extracellular calcium fluxes occurred around 5th instar ovarioles, suggesting the presence of a Ca^{2+} gradient there as well.

The flux values obtained during the 5th instar trials, both for background noise and for positions measured along the ovariole, are noticeably and consistently higher than those reported for adult ovarioles. This difference can be attributed primarily to the difference in bath [Ca^{2+}]: 2 mM for the present study and 20 μM for the adult trials. One inherent characteristic of ion-selective probes is that they are significantly affected by the background ion concentration. Future experiments performed using lower bath calcium concentrations may unmask calcium fluxes around 5th instar ovarioles; however, lowering the bath Ca^{2+} concentration during scans around adult ovarioles did not yield dramatically improved results.

Extracellular calcium fluxes above background levels were not observed at any point during germ cell differentiation in 5th instar *Rhodnius* ovarioles. Furthermore, noise measurements made during individual trials were comparable to measurements taken along the ovariole, and departures that may correspond to transient calcium fluxes, similar to those seen in individual adult trials, were not observed. While intracellular Ca^{2+} levels are different between nurse cell and oöcyte compartments in adult *Rhodnius* ovarioles, the presence of a similar gradient in the larval ovariole, similar to that observed in *Dysdercus* (Dittmann, 1996), has not been confirmed. If a Ca^{2+} difference is established as germ cells differentiate to form nurse cells and oöcytes, it may make use of other, intracellular, Ca^{2+} stores.

SUMMARY

This is the first study to measure extracellular H^+ and Ca^{2+} fluxes around 5th instar ovarioles in *Rhodnius*. While the H+ fluxes measured did not precede differentiation they appeared during the period when nurse cells and oocytes become morphologically distinct, and may be involved in the process of germ cell differentiation or in the elaboration of ring canals to form the F-actin mesh. Extracellular Ca^{2+} fluxes were not detected around 5th instar ovarioles, complimenting the findings in adult *Rhodnius* ovarioles that extracellular Ca^{2+} fluxes do not accompany intercellular Ca^{2+} gradients that may be established as the germ cells differentiate.

PLATE 1

Figure 1. Positions measured along 5th instar ovarioles. Six of these positions were measured for the earlier Ca^{2+} trials; additional positions were sampled in later H^{+} trials to improve the spatial resolution of the technique, especially over larger ovarioles from older instars.

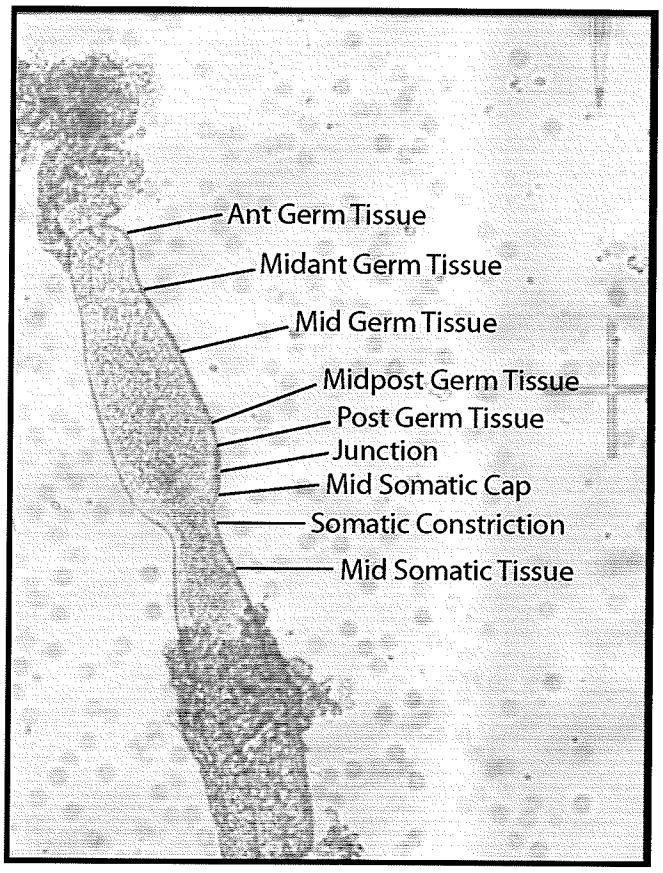
Ant Germ Tissue
Midant Germ Tissue
Mid Germ Tissue
Midpost Germ Tissue
Post Germ Tissue
Junction
Mid Somatic Cap
Somatic Constriction
Mid Somatic Tissue

PLATE 2

Figure 2. Extracellular H^+ flux at each position along 5th instar *Rhodnius* ovarioles over the course of ovarian maturation, grouped according to position. Positive values represent efflux, while negative values represent influx. Bars represent average H^+ flux; error bars indicate standard error.

Figure 2.

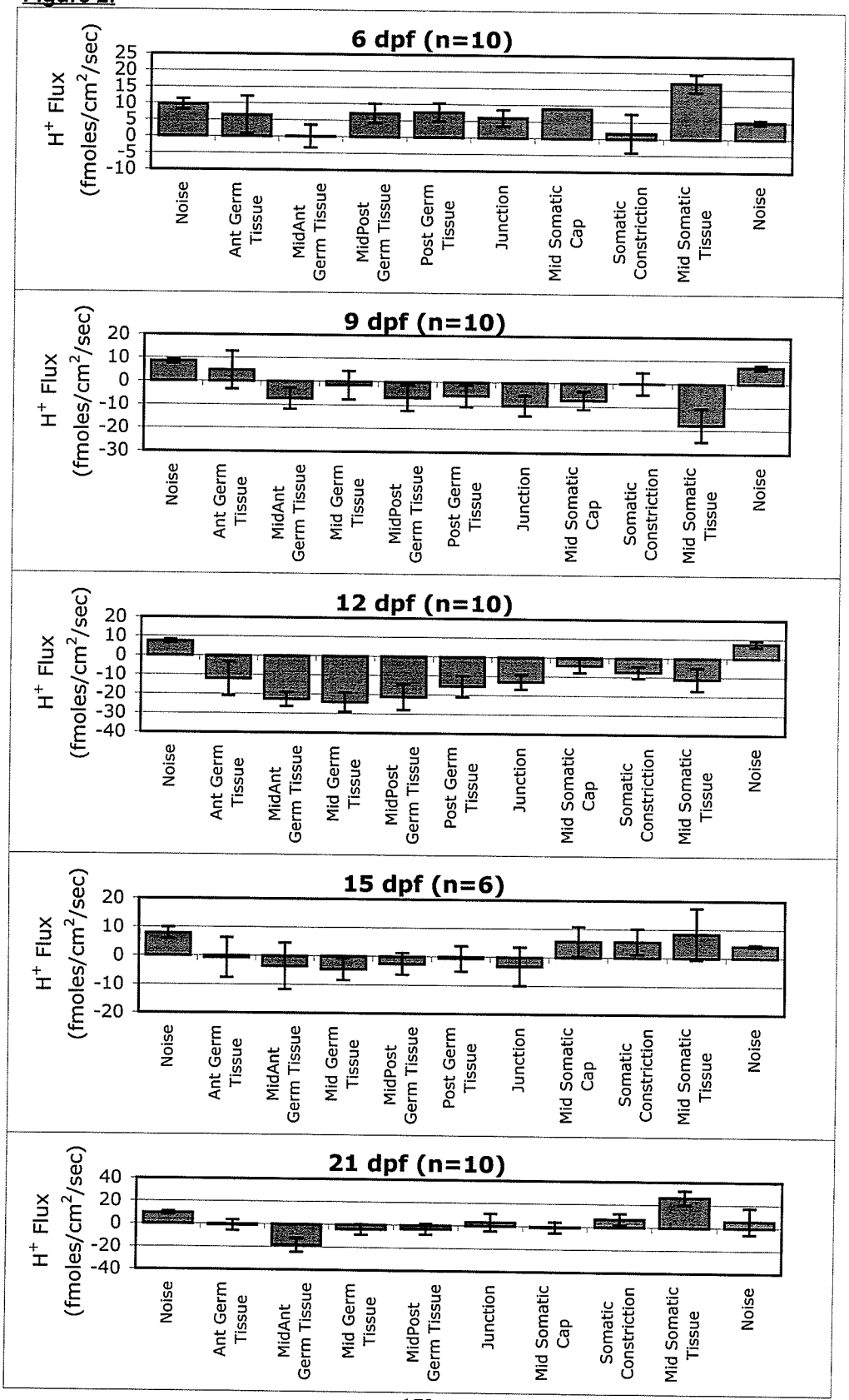
6 dpf (n=10)
9 dpf (n=10)
12 dpf (n=10)
15 dpf (n=6)
21 dpf (n=10)
H+ Flux (fmoles/cm2/sec)
Noise
Ant Germ Tissue
MidAnt Germ Tissue
Mid Germ Tissue
MidPost Germ Tissue
Post Germ Tissue
Junction
Mid Somatic Cap
Somatic Constriction
Mid Somatic Tissue
Noise

PLATES 3-4

Figure 3. Extracellular Ca^{2+} flux at each position along 5th instar *Rhodnius* ovarioles over the course of ovarian maturation, grouped according to position. Positive values represent efflux, while negative values represent influx. Bars represent average Ca^{2+} flux; error bars indicate standard error.

Figure 3.

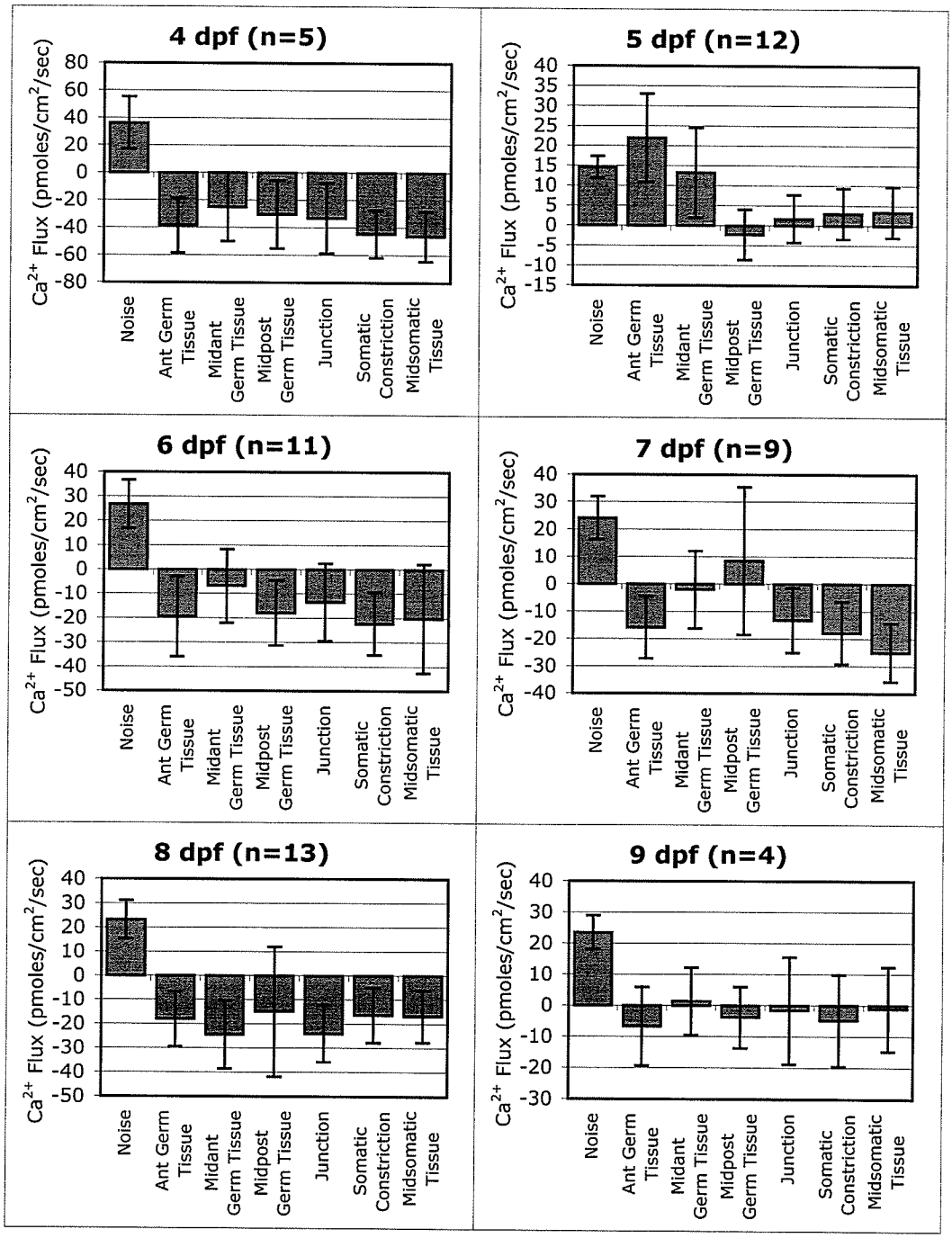
4 dpf (n=5)
5 dpf (n=12)
6 dpf (n=11)
7 dpf (n=9)
8 dpf (n=13)
9 dpf (n=4)
Ca2+ Flux (pmoles/cm2/sec)
Noise
Ant Germ Tissue
Midant Germ Tissue
Midpost Germ Tissue
Junction
Somatic Constriction
Midsomatic Tissue

Figure 3. (continued)

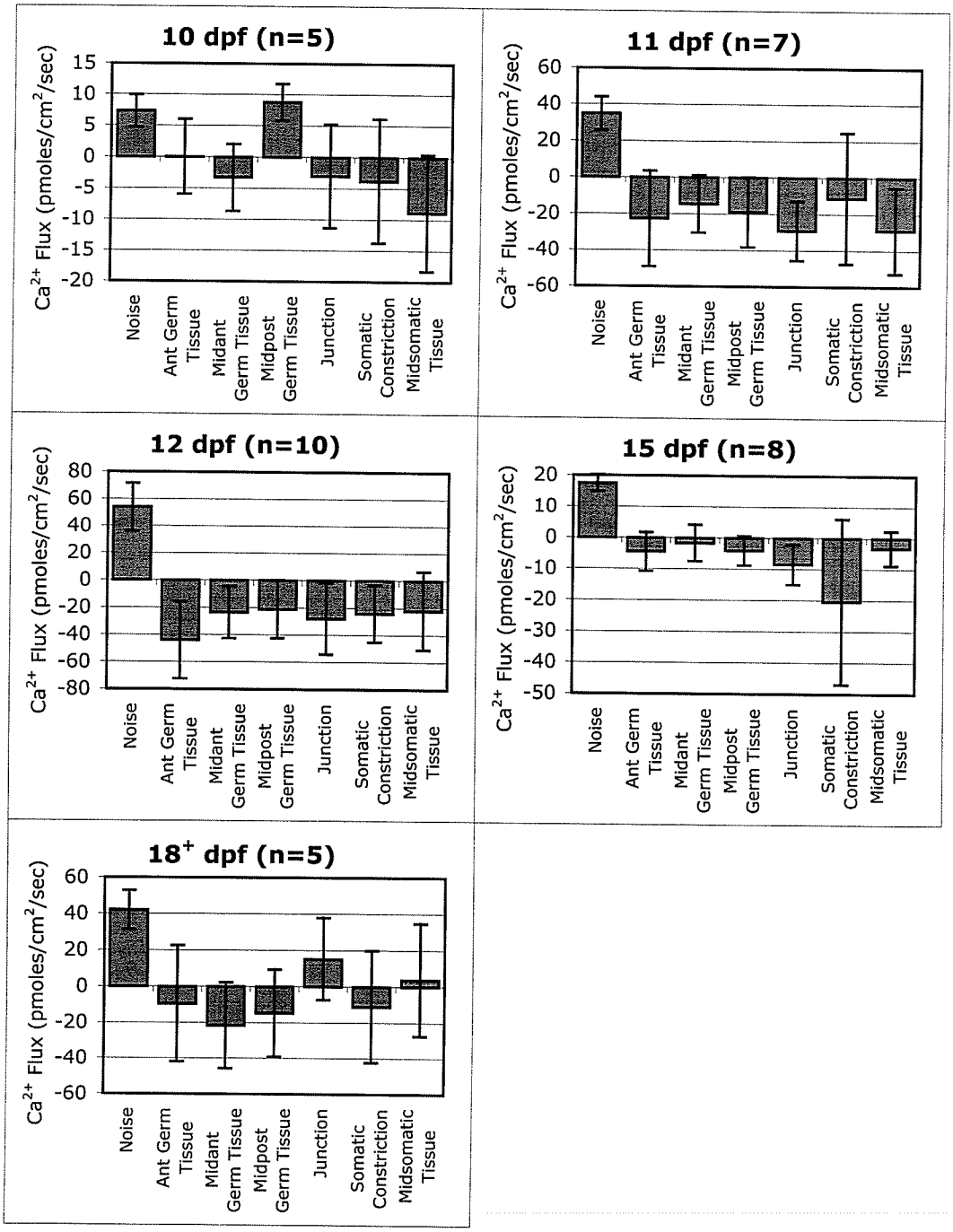

PLATE 5

Figure 4. Contour plot representation of extracellular H^+ fluxes along 5th instar *Rhodnius* ovarioles. The bottom graph depicts H^+ flux magnitude and direction (influx/efflux) relative to position along ovariole and ovariole stage. The plots for ovariole stage are superimposed on each other making it difficult to show stage differences. However these are clearly discerned in a top view as seen in the top plot. The colour coding indicates H^+ flux magnitude and direction. Each vertical column on the surface plot corresponds to a specific point along the ovariole as indicated by the ovariole images. The left- and rightmost column displays background noise. Horizontal rows display the average H^+ flux for each ovariole stage (see Methods).

4

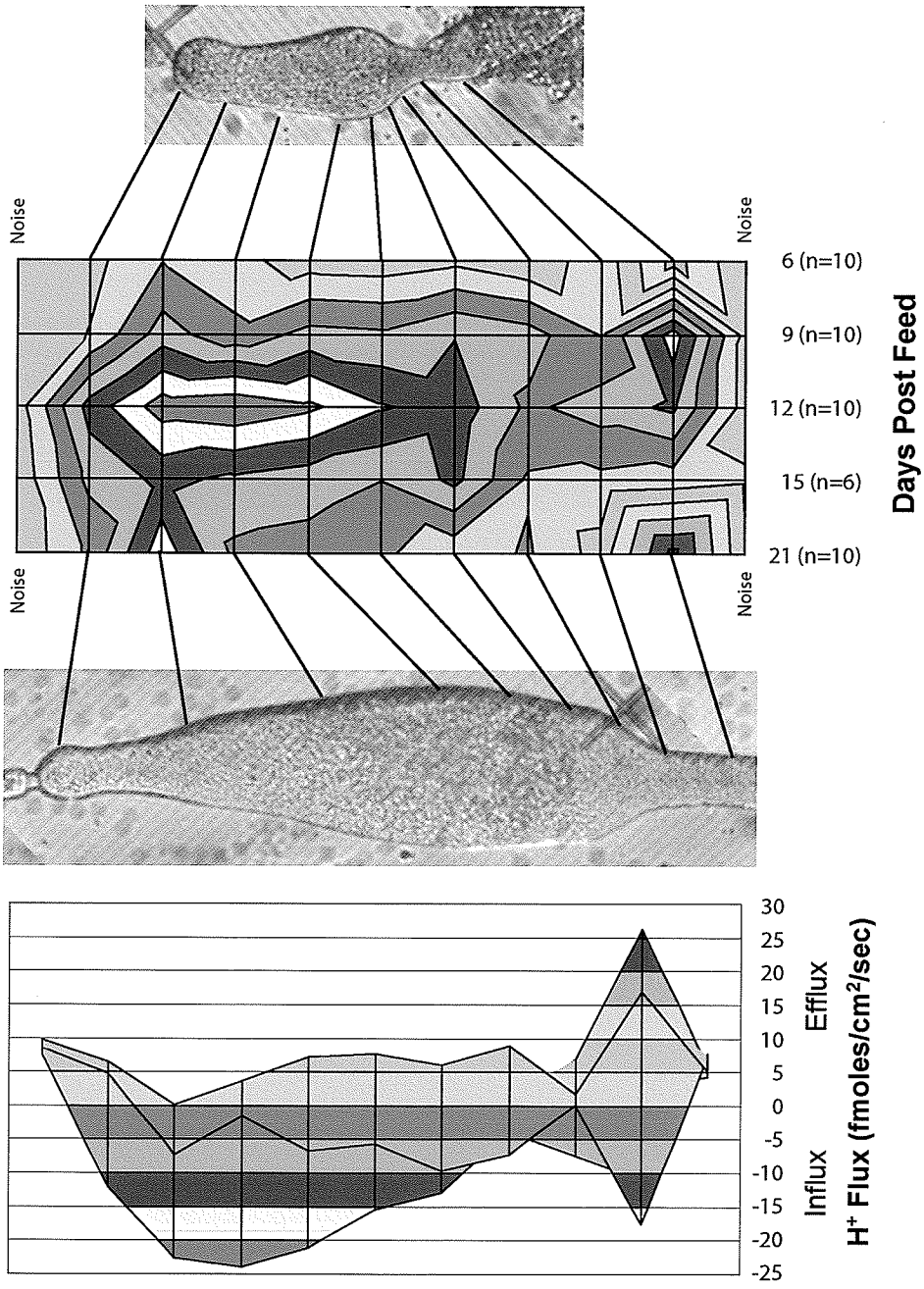
Noise
Noise
6 (n=10)
9 (n=10)
12 (n=10)
15 (n=6)
21 (n=10)
Days Post Feed
Noise
Noise
30
25
20
15
10
5
0
-5
-10
-15
-20
-25
Efflux
Influx
H+ Flux (fmoles/cm2/sec)

PLATE 6

Figure 5. Contour plot representation of extracellular Ca^{2+} fluxes along 5th instar *Rhodnius* ovarioles. The bottom graph depicts Ca^{2+} flux magnitude and direction (influx/efflux) relative to position along ovariole and ovariole stage. The plots for ovariole stage are superimposed on each other making it difficult to show stage differences. However these are clearly discerned in a top view as seen in the top plot. The colour coding indicates Ca^{2+} flux magnitude and direction. Each vertical column on the surface plot corresponds to a specific point along the ovariole as indicated by the ovariole images. The left- and rightmost column displays background noise. Horizontal rows display the average Ca^{2+} flux for each ovariole stage (see Methods).

5

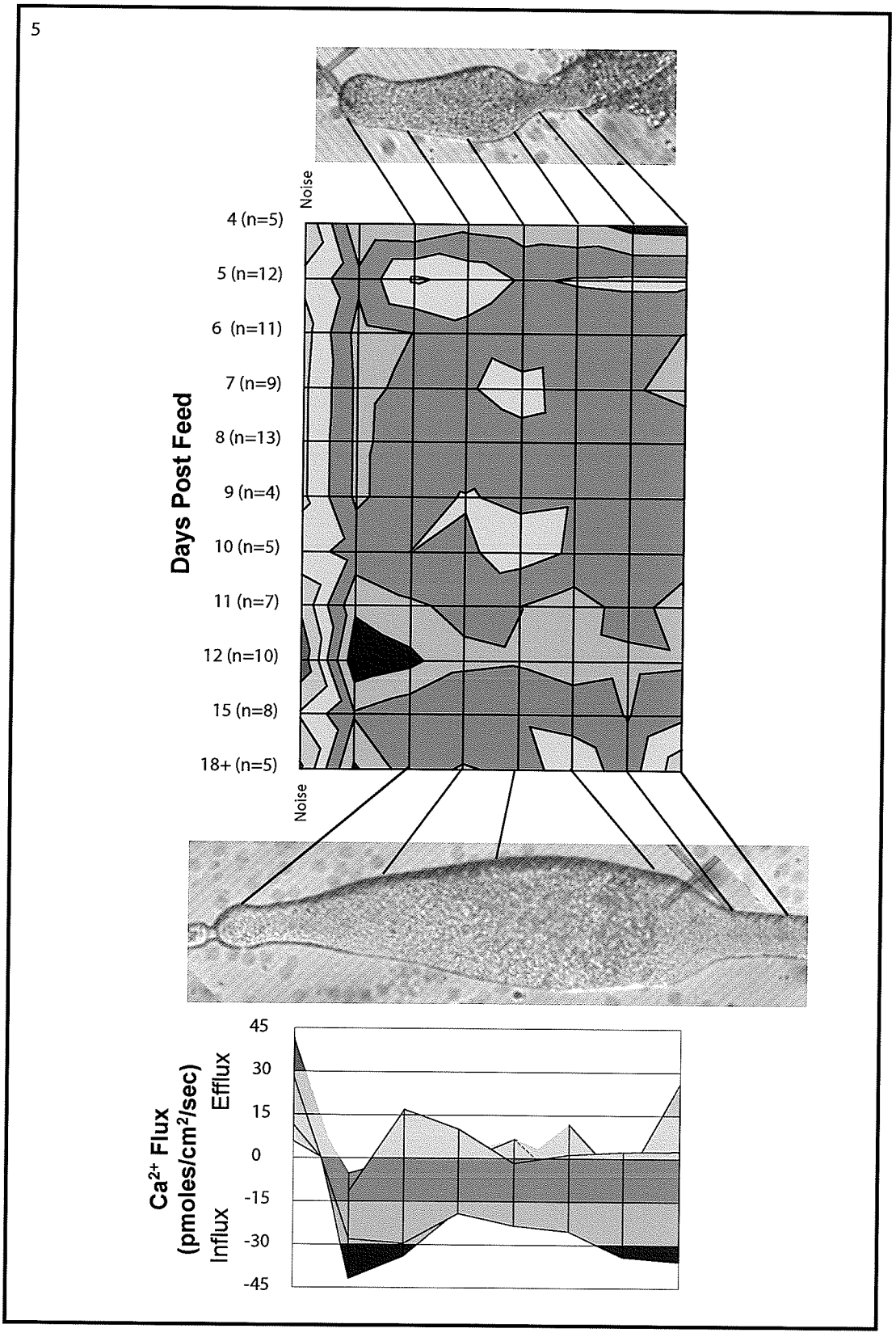
Noise
4 (n=5)
5 (n=12)
6 (n=11)
7 (n=9)
8 (n=13)
9 (n=4)
10 (n=5)
11 (n=7)
12 (n=10)
15 (n=8)
18+ (n=5)
Days Post Feed
Noise
45
30
15
0
-15
-30
-45
Efflux
Influx
Ca2+ Flux
(pmoles/cm2/sec)

PLATE 7

Figure 6. Extracellular H+ flux around two ovarioles from 21 dpf 5th instars. As the ovariole takes on a more adult appearance, as shown in Figure 5b, H^+ efflux along the posterior stalk increases dramatically, and begins to resemble the efflux seen around adult ovarioles.


6a
100 fmol/cm²/sec
100 µm

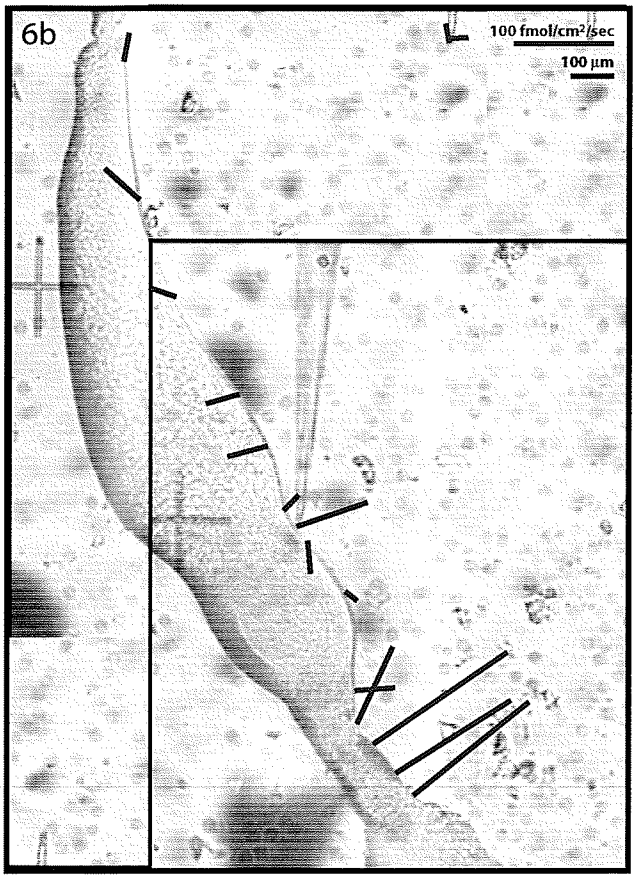
6b
100 fmol/cm²/sec
100 µm

CHAPTER 4: MOLECULAR BASIS OF EXTRACELLULAR HYDROGEN AND CALCIUM DYNAMICS DURING OÖGENESIS IN *RHODNIUS PROLIXUS*

INTRODUCTION

Oögenesis in insect meroistic ovarioles involves a complex choreography between germ and somatic tissue. The specific roles of each cell type are reflective of considerable differences in their physiological activity: protein synthesis and expression, transport, cell shape and volume, and membrane activity are all coordinated to ensure the assembly of a viable gamete. Bioelectrical currents are one manifestation of these cellular differences. The generation of localized and stage-specific extracellular ion fluxes during an oögenesis cycle can influence a myriad of cellular events including those listed above. Oöcytes, nurse cells, and follicle cells are all intrinsically polarized cells; the germ cells take on divergent paths with substantial differences in cell structure and function, and follicle cells establish the apicolateral and basal membrane domains characteristic of invertebrate simple epithelia. During the course of oögenesis, follicle cells associated with distinct regions of the ovariole undergo further differentiation into populations ultimately responsible for regulating the uptake of yolk from the haemolymph and the synthesis of proteins including yolk (Telfer, 1965; Huebner *et al.*, 1975; Isaac & Bownes, 1982; Melo *et al.*, 2000) and later lipoproteins and other components of the chorion (Beament, 1946, 1947). Consequently, there are many potential mechanisms to generate regionalized and stage-specific ion fluxes.

When considering the nature of extracellular ionic fluxes and their importance to developmental events, it is informative not only to consider the location and timing of the fluxes themselves, but also the distribution of the membrane ion transport proteins responsible for generating these fluxes. Molecular analysis can shed light on which specific transport proteins may be involved, allowing us to take advantage of a wealth of background biochemical and physiological data including how transport proteins are regulated, whether through transcriptional or translational regulation, at the level of protein function or localization, or through regulation of substrate availability.

Cells rely on a number of mechanisms to generate polarized ion traffic. In theory, one of the simplest is to establish a uniform distribution of ion transport proteins and activate them only when and where they are needed. One benefit of this approach is that the cell is globally prepared to respond to signals. For example, the fucoid egg is initially unpolarized (Kropf, 1997; Jaffe, 1999), and receptive to light stimulation from any side (Jaffe, 1967, 1969). However, once the initial signal has been received, the embryo rearranges the distribution of membrane transport proteins to allow the establishment of polarity and subsequent asymmetric growth of the embryo (Jaffe, 1999).

Complex tissues often develop a more elaborate strategy to placing ion transport proteins only where they are needed. Many of the best examples have been identified in polarized epithelia, where ions must often be transported unidirectionally across the tissue (kidney & Malphigian tubules, ependymal cells, glands, lungs, gastrointestinal tract). These cells often establish discrete apical and basolateral domains separated by a barrier or 'fence' that prevents diffusion of proteins from one domain to the other. In vertebrate tissue, tight junctions exert a 'fence function' (van Meer & Simons, 1986,

Severs, 2000), while invertebrate tissues achieve the same end using septate junctions (Tepass, 1997; Aschenbrenner & Walz, 1998; Severs, 2000). Membrane compartmentalization coupled with sorting of Golgi-derived vesicles as they are produced and targeting them to one of the two surface domains provides one simple solution to establishing cell polarity (Gottardi *et al.*, 1993). The details of intracellular trafficking can vary tremendously. In MDCK cells, proteins destined for the apical surface travel directly to the apical surface, while those fated for the basolateral membrane travel first to both domains, but are subsequently endocytosed at the apical surface and transcytosed to their proper location (Nelson & Veshnock, 1987). In other systems proteins are targeted to the proper domain at the outset (Mostov & Cardone, 1995).

The actin cytoskeleton is also used to restrict lateral diffusion of membrane proteins by anchoring them in place, often working in concert with polarized transport mechanisms. While numerous intermediate proteins have been identified that link actin to the plasma membrane, one in particular has been shown to bind a number of ion transport proteins. Ankyrin has been identified in MDCK cells, hepatocytes, neurons, and hair cells, where it has affinity for several proteins including: Na^+/K^+-ATPase (Nelson & Veshnock, 1987); gastric H^+/K^+-ATPase (Festy *et al.*, 2001), an NHE; calcium, sodium and potassium channels, and band 3, the erythrocyte Cl^-/HCO_3^- exchanger (Mohler *et al.*, 2002). One advantage of this mode of polarization is that it is highly dynamic; transport proteins can be anchored in regions where they are needed temporarily and quickly dispersed or disassembled. This type of dynamic organization is best exemplified at the leading edge of migrating fibroblasts, where Na^+/H^+-exchangers are anchored by actin

and serve a number of roles including pH regulation, regulation of signalling events, and simply to help anchor the cytoskeleton (Putney *et al.*, 2002). The intimate association of ion transport proteins, ankyrin, and the cytoskeleton may do more than simply anchor the membrane and restrict the diffusion of membrane proteins, allowing these different proteins to coordinate their activity within discrete microdomains of the cell (Denker & Barber, 2002).

As cellular interactions within tissues become more complex, additional possibilities for establishing membrane domains emerge. For example, Na^+/K^+-ATPase is localized to discrete regions of the membrane in honeybee photoreceptor cells through interactions with neighboring glial cells. Normally, the ion pump is found on the photoreceptor cell only where the two cells establish contact. Elegant studies by Baumann & Takeyasu (1993) have demonstrated that if the sensory cells and glia are dissociated, Na^+/K^+-ATPase is disperses across the entire membrane. When glia are added back, polarized distribution of the pump is reestablished. Clearly as interactions in cellular systems become more complex, involving gap junctions established between diverse cell types, the potential for increasingly complex and highly regulated activity and polarization of ion transport proteins becomes tremendous.

Extracellular H^+ and Ca^{2+} fluxes have been measured during oögenesis in the insect, *Rhodnius prolixus* that are localized to discrete regions of the ovarioles and change during the course of oögenesis (this thesis). To further characterize these extracellular ionic fluxes, we are interested in identifying the specific transport proteins responsible for generating them. This information will provide insight into which cells are involved in generating extracellular currents, and whether these currents are localized

through regulated activity, targeting to specific membrane domains, cytoskeletal anchoring, or differences in expression between different groups of cells.

Before initiating an investigation into the molecular basis of ion transport in *Rhodnius* ovarioles, a survey of proteins potentially involved in transport is useful so a selection of possible candidates for localization can be made. Several proteins have been characterized that transport protons across the plasma membrane. Two pumps have been identified, the V-type ATPase and the P-type H^+/K^+-ATPase. While V-type ATPases are primarily located in vesicles in vertebrate cells, they have also been detected in the plasma membrane of invertebrates (Wieczorek *et al.*, 1999), where they play a major role in ion homeostasis and maintaining membrane potential (Harvey, 1992). The H^+/K^+-ATPase was initially described in vertebrate tissues including gastric parietal cells (Wallmark *et al.*, 1990), colon (Binder *et al.*, 1999), and in kidney collecting ducts (Xia *et al.*, 1999); additionally, English & Cantley (1984) described an ouabain-insensitive, vanadate-inhibited (P-type) H^+/K^+ exchange in an insect cell line. Many insect cells also express a K^+/H^+ exchanger, as well as a Na^+/H^+ exchanger, both of which act as secondary transport mechanisms (Harvey, 1992; Harvey & Wieczorek, 1997). In *Rhodnius* ovarioles, O'Donnell & Sharda (1994) have demonstrated that electroneutral exchangers do not appear to be involved in the follicle's response to acidification/alkalinization, although their presence and role in other processes cannot be inferred of course. Although proton transport across the membrane is not involved in the activity of the chloride-carbonate exchanger, pH is affected on both sides of the membrane when the exchanger is active. Carbonate (CO_3^-) efflux buffers extracellular

H^+, giving the appearance of a proton influx when using extracellular H^+-sensitive probes.

Far more calcium transport proteins have been identified, in part because of the number of toxins that target them, reflective of the multitude of Ca^{2+} regulatory pathways. Calcium efflux is affected by the plasma membrane calcium ATPase (PMCA) and to a lesser extent by the Na/Ca exchanger (Lodish *et al.*, 2000). Four PMCA isoforms and 20 splice variants have been described in vertebrates, some of which are ubiquitous while others display tissue specificity (Guerini, 1998). A number of channels regulate Ca^{2+} entry along the steep chemical gradient, and are classified as voltage-operated (VOCCs), receptor-activated (RACCs) or store-operated channels (SOCs; Barritt, 1999). VOCCs are further divided into 5 types (T-, P-, Q-, N-, and L-type), classified according to the threshold voltage at which they activate, their maximal transport rate, the duration they remain open following stimulation, and their response to specific toxins (Moreno, 1999). In adult *Rhodnius* ovarioles, exposure to diltiazem and verapamil, selective inhibitors of L-type VOCCs, alters ion currents detected by the voltage-sensitive vibrating probe (Diehl-Jones & Huebner, 1992), suggesting L-type channels are present in *Rhodnius* ovarioles and that they contribute to the overall current patterns.

The purpose of this investigation was to visualize the distribution of selected plasma membrane calcium and proton transport proteins in an effort to understand the molecular basis for extracellular Ca^{2+} and H^+ flux around *Rhodnius* ovarioles during oögenesis. A full screen of all potential transport protein candidates was not feasible, so the following were selected on the basis of commercial availability of monoclonal antibodies (mAbs) specific for them: the P-type proton pump (H/K-ATPase), the plasma

membrane Ca^{2+} pump (PMCA), and the L-type calcium channel (dihydropyridine receptor, or DHPR, a VOCC). These proteins were labelled immunofluorescently in whole-mounted ovarioles, which were then viewed by means of epifluorescent and laser scanning confocal microscopy.

MATERIALS AND METHODS

Western Blotting

Tissue Preparation

Ovaries from ten adult *Rhodnius*, containing 140 ovarioles of various stages, with sheaths intact, were dissected and placed in 10x their volume of homogenization buffer (50mM Tris-Cl pH=7.50, ±1% Nonidet P-40 (NP-40), with a Bohringer Mannheim protease inhibitor tablet added immediately before extraction) and given 15-20 passes in a Radnoti homogenizer on ice. After a 30 second spin at 600 xg to sediment tracheoles and similar material, the supernatant was centrifuged for 10 minutes at 600 xg, 4°C. The pellet (enriched in nuclei) was resuspended in100µl extraction buffer +1% NP-40. The supernatant was centrifuged for 10 minutes at 15,000 xg, 4°C. The pellet (enriched in mitochondria) was resuspended in 100µl +1% NP-40; these fractions and the final supernatant (enriched in cytosol and microsomal fractions) were stored at –20°C. Later, a final centrifugation for 30 minutes at 100,000 xg, 4°C was performed to separate microsomal and cytosolic fractions.

Crude ovariole preparations were also used. For these, four whole ovaries were dissected into 10x volume extraction buffer (as above) and given 15 passes in a Radnoti homogenizer. After a 30 second spin at 600 xg to sediment tracheoles and similar material, the supernatant was removed, added directly to SDS-PAGE loading buffer, and prepared for gel electrophoresis.

Mouse tissues were used as positive controls for anti-DHPR and anti-H/K-ATPase since they were available to the lab and were listed in the Affinity Antibody product pages as having been successfully detected by other researchers using these primary antibodies. A single mouse brain (for DHPR) and two kidneys (for H/K-ATPase) were prepared by homogenization into 10x volume of extraction buffer (100 mM PIPES pH 6.90, 1 mM $MgSO_4$, 1 mM Pefabloc, 2 mM DTT, 1μg/ml leupeptin, 1 μg/ml pepstatin, 1 mM EGTA) with 15-20 passes in a Dounce homogenizer on ice. The homogenate was centrifuged for 10 minutes at 1,600 xg, 4°C in a PM180R refrigerated centrifuge using an A-H-11 rotor. The pellet (enriched in nuclei) was resuspended in 100μl extraction buffer. The supernatant was centrifuged for 20 minutes at 13,000 xg, 4°C. The pellet (enriched in mitochondria) was resuspended in 100μl extraction buffer. Each fraction, including the supernatant, enriched in microsomal and cytosolic fractions, was stored at –20°C until used.

Rabbit erythrocytes were also prepared as a positive control for anti-PMCA. Three ml of whole blood (+0.02% heparin, +0.15% anticoagulant citrate dextrose) were suspended in 10ml isotonic buffer (0.9% NaCl, 5 mM sodium phosphate, pH 8.0) by trituration, and centrifuged at 600 xg (2400 rpm) for 10 minutes at 4°C in a PM180R refrigerated centrifuge using an A-H11 rotor. The pellet was resuspended in 10 ml

isotonic buffer and re-centrifuged. The pellet was then resuspended in 10 ml hypotonic buffer (5 mM sodium phosphate, pH 8.0) and centrifuged at 12,000 xg (10,500 rpm). Pellet resuspension in 10ml hypotonic buffer and centrifugation at 12,000 xg was repeated twice more. The pellet was finally resuspended by agitation and stored at –20°C.

SDS-PAGE

25-50 µg of protein was added to a microcentrifuge tube containing sample buffer (0.5 M Tris pH 6.8, 30% glycerol, 10% SDS, 2 mg bromophenol blue, 0.6 ml ß-mercaptoethanol) and heated to 99°C for 5 minutes. Samples were centrifuged briefly (< 30 seconds) at 12,800 rpm in an Eppendorf centrifuge prior to loading. Standards were prepared by adding sample buffer to Amersham RPN 756 (high range) standards and centrifuging briefly prior to loading. Samples and standards were loaded onto NuPage Bis-Tris 4-12% polyacrylamide gradient gels (Invitrogen) in a Novex XCell SureLock gel box to which chilled NuPage MES SDS running buffer (50 mM MES, 50 mM Tris base, 3.465 mM SDS, 1.025 mM EDTA) was already added. Gels ran at 110V for 3 hours, powered by a BioRad Power Pac 200.

Western Blotting

Western blotting was performed using a Hoefer miniVE vertical electrophoresis system (Pharmacia). A BioRad Immuno-blot 0.2 µm PVDF membrane for protein blotting (Cat. #162-0177) was prepared by equilibrating first for 30 seconds in 100% methanol, followed by 10 minutes in distilled deionized H_2O on a shaking tray, and finally immersed in Towbin buffer (25 mM Tris, 192 mM glycine, 0.1% SDS, 5% v/v methanol) for 15 minutes. The gel and extra thick criterion-size blotting paper (BioRad)

were also equilibrated in Towbin buffer for 15 minutes. Transfers lasted 2 hours at 25 V. Transfer efficiency was assessed by comparing the gel after rinsing in ddH2O for 1 hour and staining with GelCode Blue reagent Stain (Pierce) for 1 hour, followed by an overnight wash in ddH_2O, to a duplicate gel that was run simultaneously but not transferred, identically stained. Both gels were dried side by side between two Novex cellulose sheets tightly clamped on all sides.

Immunodetection

PVDF membranes were transferred to blocking buffer (PBS +5% skim milk) overnight at 4°C to reduce non-specific binding. Primary antibody incubation (PMCA MA3-914 diluted 1:2000, DHPR MA3-921 1:500, H/K-ATPase MA3-923 1:4000) diluted in blocking buffer was performed for 90 minutes after initially warming the primary antibody (Ab) mix to 37°C. All subsequent steps were performed at room temperature. The primary Ab incubation was followed by three ten-minute washes in PBS +5% skim milk +0.01% Tween-20. Secondary Ab incubation used Amersham's peroxidase-labelled anti-mouse mAb (NIF 825, diluted 1:20,000) in PBS +5% skim milk +0.01% Tween-20 for 1 hour; this was followed by two 10 minute washes in PBS +5% skim milk +0.01% Tween-20 and a final wash in PBS +0.3% Tween-20 for two hours to reduce background signal. Pierce's Super-Signal West Fempto Maximum Sensitivity Substrate was used for detection, using the prescribed one-minute reaction. Kodak BioMax film was exposed for 5 seconds up to 1 minute and processed on a Feline 14 automatic quick-cleaning X-ray film processor (Fisher Industries, Inc.). To calculate the molecular weight of labelled proteins, the distances travelled by protein standards were

measured and used to plot a standard curve displaying distance vs. log(molecular weight), and the equation for the line of best fit was used to estimate the molecular weight of proteins from other lanes based on the distance they migrated.

Immunofluorescence of Whole-Mounted Ovarioles

Ovarioles dissected from adult females were transferred to Petri dishes containing modified O'Donnell's Rhodnius Ringers where they were isolated and desheathed using jeweler's tweezers and tungsten needles. Ovarioles were prepared for immunofluorescence by fixing in 3% paraformaldehyde in PBS (8.0 g NaCl, 0.2 g KCl, 1.44 g Na_2HPO_4, 0.24 g KH_2PO_4, in 1l ddH_2O pH 7.2) for 15 minutes, washed twice in PBS for 5 minutes, permeabilized 15 minutes in PBST (PBS +0.1% Tween-20), and washed three times in PBST, all at room temperature on a KS 125 shaking tray (IKA Labortechnik, Inc.). The primary antibody incubation was carried out in PBST for 1 hour or overnight (PMCA 1:200, DHPR 1:100, HK-ATPase 1:200), followed by three 10 minutes washes in PBST. A one-hour secondary antibody incubation using $Alexa_{568}$ (epifluorescence) or $Alexa_{488}$ (confocal) conjugated goat anti-mouse IgG (Molecular Probes, Inc., Eugene, OR) diluted 1:200 in PBST ended with the addition of 5 μg/ml Hoechst 33258 (Sigma) to the solution for the final 15 minutes of secondary Ab incubation to stain nuclei. Ovarioles were washed three times in PBS for 10 minutes, and mounted on slides in PBS with or without antifade agents, either 5mg/ml n-propyl gallate or ProLong mounting media (Molecular Probes, Inc., Eugene OR). Controls were treated identically except that in place of the primary Ab incubation, they were incubated for 1 hour in PBST without primary Ab. The Alexa fluorophores were intense enough that

results were identical under all three mounting conditions, and photobleaching during image acquisition was negligible. Ovarioles were viewed on a Zeiss Photo II epifluorescence microscope, illuminated by a 50W mercury bulb or an EFOS X-Cite halogen lamp. Images were acquired using a Sony DXC-950 3CCD camera and captured by a Matrox framegrabber in a PC computer using Northern Eclipse imaging software (Empix Imaging, Missisauga, ON).

Ovarioles were also prepared for confocal microscopy at the St. Boniface Research Centre, which was conducted with the assistance of Mike Czubryt. Three-dimensional images of fluorescently labelled, whole mounted ovarioles were obtained using a BioRad MRC600UV confocal system connected to a Nikon Diaphot 300 epifluorescence microscope and using a Nikon Fluor 40X/1.3 N.A. oil immersion objective lens. A BioRad argon ion UV-Vis laser was employed, using the 488 nm laser line at 1% power in conjunction with a VHS (violet, high selectivity) or UBHS (ultraviolet-blue, high selectivity) filter block to visualize $Alexa_{488}$-labelled samples. Hoechst 33258-labelled samples were visualized on the same system, using the 351 nm laser line at 100% power with the UBHS filter block in position one and the IN2 filter block in position two. Three images of each field were collected and Kalman filtered to reduce random noise from the photomultiplier. For three-dimensional Z-axis series images, the photomultiplier aperture was set to five, and the focal plane stepped by 2 μm for each image. The black level was typically 4.9-5.0 for all images, and the gain was set to 7.0 for $Alexa_{488}$ samples and 8.8 for Hoechst 33258 samples. Images were analyzed using Molecular Dynamics ImageSpace 3.2.1 or Confocal Assistant 4.02 software.

RESULTS

H^+/K^+-ATPase

The H^+/K^+-ATPase is composed of a large transmembrane catalytic α-subunit, and a smaller glycoprotein, the ß-subunit. MA3-923 detects an epitope between amino acid residues 1-13 or 15-28 on the cytoplasmic face of the ß-subunit of H^+/K^+-ATPase from bovine, canine, porcine, rabbit, mouse, ferret, and rat tissues. The antibody was raised against microsomes purified from hog stomach containing 34 kDa deglycosylated H^+/K^+-ATPase (Affinity Antibodies, Inc.). While the H^+/K^+-ATPase shares many features with the Na^+/K^+-ATPase, sequence comparisons between the β–subunits in a number of species archived in the Entrez protein database show that the MA3-923 epitope is not conserved in any Na^+/K^+-ATPase subunits. Recently, Okamura *et al.* (2003) reported on the similarities between the two pumps in *Drosophila*, with similar findings: the antigenic region is not conserved between H^+/K^+-ATPase and Na^+/K^+-ATPase.

Western Blotting

Under denaturing conditions three bands were expected, a glycosylated protein around 60-80 kDa, a 52 kDa beta subunit precursor, and the 34 kDa core peptide (Affinity Antibodies, Inc.). Two strong bands were seen in the mouse kidney lane run as a positive control: one at ~71 kDa and one at ~59 kDa. In the lane containing crude protein extracts from *Rhodnius* ovarioles, a faint single band was detected at around 101 kDa (Figure 1).

Immunofluorescence

In adult ovarioles, staining was primarily observed along the lateral surfaces of the follicle cells. Staining was not detected in the nurse cells or inner sheath cells of the tropharium (Plate 2, Figure 1; henceforth Figure 2-1). In early previtellogenic follicles a faint punctate staining pattern was observed along the lateral surfaces of the follicular epithelium (Figures 2-2,3,5). Staining intensity increased over larger follicles (Figure 2-6), and by late vitellogenesis intense punctate staining was observed over the lateral follicle cell surfaces (Figures 3-2 to 3-6). Interestingly, no qualitative differences in staining intensity were detected among groups of differentiated follicle cells where the rim and micropyles would later be formed, even though different cell populations could be identified based on morphology (Figure 3-1). No appreciable staining was observed among cells in the interfollicular stalk (Figure 2-4).

Plasma Membrane Calcium ATPase

The plasma membrane Ca^{2+}-ATPase (PMCA) is a P-type pump with a α-subunit that shares little gene or protein sequence homology with other P-type pumps (Okamura *et al.*, 2003). Consequently, selection of a primary antibody was based primarily on its ability to recognize an epitope common to as many known PMCA isoforms as possible. MA3-914 is a mouse monoclonal antibody raised against the human erythrocyte PMCA, a transport protein consisting of a single polypeptide. The antibody recognizes an epitope between amino acids 724-783, part of a highly conserved cytoplasmic hinge region found

in all four known PMCA isoforms. MA3-914 was previously known to detect PMCA from human, primate, canine, feline, rabbit, chicken, rabbit, hamster, and eel.

Western Blotting

Three bands were expected on the western blot: the primary product at 140 kDa, an aggregation product at 180 kDa, and a breakdown product at 95 kDa (Affinity Antibodies, Inc.). Immunodetection of protein isolated from mouse brain run as a positive control detected three bands: one at around 133 kDa, a second at around 83 kDa, and a third at around 40 kDa. Immunodetection of total protein isolated from *Rhodnius* ovaries detected a band at around 146 kDa, another at 110 kDa, a third at around 54 kDa, and a fourth protein at around 49 kDa (Figure 1-1).

Immunofluorescence

As with H^+/K^+-ATPase, PMCA was primarily localized to the somatic tissue of the ovariole. In the tropharium, some of the inner sheath cells express detectable levels of PMCA (Figure 4-1,3), but not all cells, as seen when images of Hoechst-labelled DNA and Alexa568-labelled PMCA are overlaid (Figure 4-4). PMCA staining assumes a stellate pattern around some, but not all, of the small ISC nuclei. Interestingly, the membrane over ISC nuclei does not label for PMCA.

Follicle cells around previtellogenic follicles are labelled on their basal surface (Figures 4-5,6,8), and staining is more intense among follicle cells at the junctions between follicles prior to interfollicular stalk formation (Figures 4-5,6). Also, where trophic cords pass through the follicular epithelium, the basal surfaces of follicle cells adjacent to the cord appear to express a more mosaic pattern of PMCA (Figure 4-7).

Otherwise, follicle cells surrounding previtellogenic oöcytes express relatively uniform levels of PMCA. In contrast, early vitellogenic follicles contain three populations of follicle cells clearly identifiable on the basis of PMCA staining Figure 5-1,3,4). Follicle cells surrounding the lateral and posterior aspects of the oöcyte express relatively uniform levels of PMCA. Anterior to these cells is a dark band roughly 5 cells wide, indicating lower PMCA expression among this group of cells. Follicle cells at the anterior pole of the oöcyte exhibit mosaic expression of PMCA. Comparison to corresponding brightfield images reveals that both the mosaic apical cells and the dark band of cells correspond to the columnar cells, and the more uniformly staining posterior cells are cuboidal in morphology. By late vitellogenesis, the number of follicle cell groups that can be identified on the basis of PMCA staining has increased to five, mostly located in the region where the chorion rim, micropyles, and pseudomicropyles will be formed (Plate 6). Cells at the anterior end of the follicle still express mosaic levels of PMCA; immediately posterior to these a single row of large, dark cells can be identified, followed more posteriorly by a ring 3-4 cells wide of mosaic staining cells, then a group of darker cells 3-4 cells wide, and finally the more uniform lateral follicle cells where the body of the chorion will be formed. Lateral follicle cells of later stages of vitellogenic follicles do exhibit PMCA staining along their lateral surfaces (Figures 6-5,6), similar to the staining pattern seen with H^+/K^+-ATPase. No detectable staining was observed among cells forming the interfollicular stalk (Figure 5-5).

L-type Voltage-Operated Calcium Channel (DHPR)

DHPR consists of four subunits, α_1 and α_2-δ, β, and γ, all of which are present in every organism examined to date, including *Drosophila*. Mammals possess numerous isoforms of α_1 and β, but typically only a single α_2 subunit, therefore the likelihood of recognizing these channels in *Rhodnius* ovarioles should be greater using an antibody raised against the α_2-subunit. MA3-921 recognizes the α_2-subunit of the DHPR in rat, mouse, rabbit, and guinea pig tissues and was originally raised against purified rabbit DHPR.

Western Blotting

For western blots in which rabbit DHPR was labelled, a single band of 143 kDa is expected under reducing conditions (Affinity Antibodies, Inc.). Two bands were seen in the lane containing protein from mouse brain run as a positive control: one at around151 kDa, and another at around 72 kDa. In the lane containing protein from crude *Rhodnius* ovariole extracts, a single band, around 116 kDa, was detected (Figure 1-1).

Immunofluorescence

DHPR staining in most respects was very similar to PMCA staining in adult ovarioles. Staining in the tropharium was restricted to a few of the inner sheath cells (Figure 7-1,2); again, staining was absent in the membrane over ISC nuclei. Nurse cells did not express detectable levels of L-type channel. Labelling appeared uniform across the basal surfaces of follicle cells associated with previtellogenic oöcytes, except at interfollicular junctions prior to stalk formation (Figures 7-3,4), and over trophic cords

where a mosaic expression pattern was observed (Figure 7-5). No detectable staining was observed among cells forming the interfollicular stalk. Two separate groups of follicle cells surrounding early vitellogenic follicles could be identified on the basis of L-type channel staining, an anterior group expressing mosaic levels of calcium channel and a posterior group expressing uniform levels of channel (Figure 7-8). No dark band of cells, as seen with PMCA, was detected between these two groups. By late vitellogenesis, an increased number of follicle cell groups could be identified, again focused mainly where specialized chorion structures would later appear (Plate 8). A single band of follicle cells, larger in size than others in the region, which expressed far lower levels of the L-type channel was especially prominent.

DISCUSSION

During oögenesis in many insect polytrophic ovarioles, extracellular ionic currents are generated around discrete regions and correspond temporally to specific developmental events. Identification of the proteins involved in ion transport across the plasma membrane is a valuable step towards understanding the basis of extracellular ion fluxes. If ion transport proteins are exclusively expressed by cells that generate extracellular fluxes, future exploration of the mechanisms leading to the differentiation of those cells may yield exciting new insights. If, on the other hand, ion transport proteins are ubiquitously expressed, exploration of regulatory mechanisms potentially responsible for transporter activation in one group of cells and not others may prove more valuable.

In interpreting the distribution of ion transport proteins revealed by immunofluorescence labelling, the focus will be twofold: both the relationship to ionic fluxes during oögenesis and to cellular changes during oögenesis will be considered below. First, the western blot results will be considered.

Western Blots

The monoclonal antibodies used in this study were carefully chosen to target epitopes common to as many isoforms of a given ion transport protein as possible while avoiding cross-reactivity with other ion transport proteins. If polyclonal antibodies had been used they could have cross-reacted with other ion transport proteins, especially in the case of H^+/K^+-ATPase, where the β-subunit bears some resemblance to its Na^+/K^+-ATPase counterpart (Okamura *et al.*, 2003). Still, without knowing the sequence of these proteins in *Rhodnius*, it is not possible to account for the variations in protein size detected using western blot techniques. As a further complication, the abundance of yolk in the *Rhodnius* samples may have shifted the migration of proteins in these lanes. Unfortunately, the yolk protein did not separate well during cell fractionation, and was present in nuclear, mitochondrial, cytosolic, and microsomal fractions. While the proteins identified in *Rhodnius* lanes migrated differently than in controls, the strength of this technique is that western blots confirmed that specific proteins were targeted using these antibodies. Careful selection of antibodies, coupled with the detection of specific proteins using western blot techniques and the specific labelling of proteins associated with the plasma membranes of the ovariole using immunofluorescence labelling each support the premise that the antibodies are targeting the proper ion transport proteins.

Immunofluorescence

It is noteworthy that certain cells within individual ovarioles labelled more intensely, supporting the idea that differences in expression develop between cells during follicle morphogenesis. Specifically, it is evident that somatic tissue expresses significantly more PMCA, L-type Ca^{2+} channel, and H^+/K^+-ATPase than both nurse cells and oöcytes. This does not imply that germ tissue does not express ion transport proteins, only that the follicle cells express considerably more. Comparison may be made between germ and somatic tissue, since the germ tissue appeared to be adequately permeabilized and the antibody incubations were of sufficient duration. The lack of appreciable staining in the oölemma of vitellogenic oöcytes, where the surrounding patent follicle cells do not interfere with antibody access to the oöcyte membrane suggests the permeabilization step was sufficient. Furthermore, overnight incubations in primary antibody gave similar results to hour-long incubations. Previous studies on *Rhodnius* have inferred the presence of ion transport proteins along the oölemma. For example, verapamil blocks action potentials generated by the oöcyte (O'Donnell, 1985), suggesting that L-type Ca^{2+} channels are present along the oölemma. Therefore, the apparent 'restriction' of DHPR expression to the follicle cell membranes observed here is likely due to differences in the number of channels present as detected by the immunofluorescence methods used. More generally, Diehl-Jones (1991) found that denuded follicles, in which patches of follicle cells had been stripped away from the follicle, still produced bioelectric currents over the oölemma, although these currents were reduced. Similar results have been reported in cockroach (Anderson *et al.*, 1994), while in *Hyalophora* follicles no detectable currents

were observed over the denuded oocyte membranes (Woodruff *et al.*, 1986). In most cases, ion transport proteins are typically present along the oölemma.

The relative levels of ion transport protein expression by follicle cells compared to the germ cells suggests that follicle cells possess the capability to regulate ionic events in the ovariole. Throughout much of oögenesis, the oöcyte is actively engaged in endocytosis, and subject to considerable dynamic membrane cycling (Telfer *et al.*, 1984). Given this, and considering the widespread involvement of epithelia in ion transport and homeostasis, it seems reasonable that the follicular epithelium might play a significant role in regulating ionic events in the ovariole, especially since follicle cells are coupled to the germ tissue via gap junctions, providing an energetically favourable route to facilitate ion exchange with germ cells.

Adult Ovarioles - Hydrogen Transport Proteins

H^+/K^+-ATPase was predominantly localized to follicle cell membranes, present at lower levels in previtellogenic follicles and increasing in level during oögenesis. Staining was negligible over the tropharium, suggesting that follicle cells of the vitellarium have more capacity to regulate pH using this transport protein. This result is supported by the extracellular H^+-selective probe data (see Chapter 2), where prominent H^+ fluxes were measured around the follicles, not the tropharium. While different follicle cell populations could be identified based on morphology on later vitellogenic follicles, staining intensity did not appear qualitatively different between these different cell groups. Specifically, cells near the forming specialized cap structures (rim, pseudomicropyles and micropyles) where significant H^+ efflux occurs during stage 9, do

not express higher levels of the proton pump. This suggests that if this H^+ pump is responsible for localized H^+, its spatial constraints are achieved through local activation rather than through restricted protein expression.

If the H^+/K^+-ATPase is responsible for H^+ efflux at the connective, the immunofluorescence data presented here suggest that the stalk cells are not as well equipped to produce H^+ fluxes as the adjacent follicle cells. It follows that of several scenarios presented in Chapter 2, it is more likely that strong, stage-specific H^+ efflux is due to the activity of follicle cells immediately adjacent to the interfollicular stalk rather than from stalk cells. Furthermore, H^+ efflux may be linked to events in the oöcyte, including entry into vitellogenesis, changes in the oöcyte cortex and cytoskeletal changes. Before definite conclusions can be drawn, the distribution of plasma membrane V-ATPase and the role of both pumps in H^+ transport must be determined. V-ATPase is expressed in a number of insect tissues; in ovarian follicles of *Drosophila* it is localized along cytoplasmic vesicles in all cells and in yolk spheres, and later along the oölemma and apical follicle cell membranes (Bohrmann & Braun, 1999). In *Manduca*, the basal surfaces of follicle cells express V-ATPase throughout oögenesis (Bohrmann & Braun, 1999). Furthermore, the presence of V-ATPase has been inferred in *Rhodnius* (O'Donnell, 1994). Determining the distribution of this second pump may provide added information regarding the source of extracellular H^+ fluxes.

Calcium Transport Proteins

Since DHPR staining for the most part parallels the staining pattern observed for PMCA, both will be treated under a single heading with exceptions noted.

The expression of transport proteins over the tropharium by a few of the inner sheath cells (ISCs) shows that these cells are ideally suited to regulate calcium levels in this region. ISCs extend slender processes between nurse cells lobes (Huebner & Anderson, 1972c) and it is suspected that ISCs are coupled to nurse cells via gap junctions (Huebner, pers. comm.), which would provide a means for these cells to regulate nurse cell calcium. This role is further supported by previous studies of Ca^{2+} distribution in the ovariole using energy loss spectroscopy (Huebner & Rheidiger, unpublished data), which revealed ISCs possessing a calcium-rich cytoplasm. These cells may operate as a Ca^{2+} sink to buffer nurse cell Ca^{2+} levels.

For the most part, follicle cells surrounding previtellogenic oöcytes express uniform levels of PMCA and DHPR along their basal surface. Staining appears to intensify at interfollicular junctions prior to stalk formation; however, transport protein expression is not necessarily upregulated in this area. This is because there are more follicle cells in this region, each tapering towards the basal lamina and consequently occupying a smaller surface area along the extracellular matrix. Thus it is possible that each cell contains just as many transport proteins as cells over the lateral oöcyte surface, but they are concentrated in a smaller area. Of course, concentration of transport proteins in these cells may result in sufficiently different calcium dynamics to send these cells off

on a different differentiation pathway; perhaps these cells are fated to form the interfollicular stalk.

The mosaic expression of PMCA and DHPR among cells next to the trophic cord is interesting. It is possible that increased expression of PMCA and DHPR in the region corresponds to an increased capacity for calcium signalling, and follicle cells adjacent to the cord are prepared to relay information regarding the functional state of the trophic cord to lateral follicle cells. Specifically, trophic cord closure may trigger these cells to propagate a signal to initiate the entry into the patent state necessary for vitellogenesis to begin. Further exploration into the activation and regulation of Ca^{2+} signalling pathways among follicle cells in previtellogenic follicles is required before a role in initiating patency can be confirmed.

The appearance of distinct populations of follicle cells identifiable by Ca^{2+} transport protein expression during early vitellogenesis is especially intriguing. While differences in cell height over the anterior and lateral-posterior regions of the follicle are already apparent, regional differences in expression of PMCA and DHPR suggest a means by which differentiation may be maintained and further differentiation achieved. The PMCA-poor band of cells populates the region where specialized chorion structures including the rim, neck, pseudomicropyle, and micropyle structures will later be deposited (Beament, 1946, 1947). Reduced PMCA expression may mark an early stage of their differentiation.

The presence of a band of PMCA-poor cells at the boundary between columnar and cuboidal cell groups raises the possibility that this group of cells may modulate or prevent communication between anterior and posterior follicle cell populations, possibly

by establishing a communication barrier allowing divergence along different developmental pathways. In a number of systems, PMCA is activated by Ca^{2+}/calmodulin, and in pancreatic acinar cells PMCA activation during prolonged signalling bouts helps to clear Ca^{2+} from the cytosol (Peterson *et al.*, 1999). Lower expression levels of PMCA might reflect a lower capacity for Ca^{2+} transport throughout these cells, so that signals passing to them from neighbouring compartments are rapidly attenuated. In light of this, determining the distribution of IP_3 and cADPr receptors, both mediators of intracellular signalling, could reveal more specifically the signalling capacity of different follicle cell populations. If the dark band of cells does in fact form a barrier to signalling, lower expression of these transport proteins might be expected.

While it has been established that follicle cells are coupled to their neighbors via gap junctions (Huebner, 1981b), it is not known whether coupling is limited to specific groups or clusters of cells. It would be extremely valuable to know whether dye or Ca^{2+} ions (using fluorescence ratioing of Fura-2) introduced into one population of follicle cells is capable of entering another population directly; however, the technical challenges of this experiment are considerable since follicle cells are also coupled to the oöcyte. Follicle cell - oöcyte junctions cannot be selectively closed without compromising the health of the follicle (by puncturing and evacuating the oöcyte, for example), possibly inducing closure of gap junctions between follicle cells due to initiation of atresis or apoptosis. Still, simply exposing the entire ovariole to a selective gap junctional uncoupler may provide valuable information as to the origin of follicle cells in different groups. Several different uncouplers have been tested on insect ovarioles (Adler &

Woodruff, 2000; Anderson & Woodruff, 2001), and these may prove useful for *Rhodnius* ovarioles.

At the very least, the existence of follicle cell groups expressing different levels of Ca^{2+} transport proteins establishes that each of these groups possesses a different capacity to regulate calcium. Although studies characterizing the extracellular calcium flux using the Ca^{2+}-selective probe did not reveal differences in magnitude or variability between different areas of early vitellogenic follicles (Chapter 3, this thesis), the temporal resolution of this technique may not have been sufficient to capture dynamic Ca^{2+} events. Analysis of Ca^{2+} flux variability indicated that the T-1 oöcyte and the interfollicular stalk show more variability than other regions during stages 5-7. This activity precedes a developmentally significant period of oögenesis, when the trophic cord is about to close and the T-1 oöcyte is about to enter vitellogenesis, and also occurs over a period when the follicle cells have not yet differentiated into columnar and cuboidal populations. Future work using fluorescence ratioing to monitor intracellular calcium may provide additional insight into the importance to follicle growth of follicle cell groups expressing different levels of PMCA and DHPR.

The appearance of additional follicle cell groups during the late vitellogenesis phase is of special interest, since these emerge where specialized chorion structures will be produced. While it is difficult to directly match individual groups of cells to Beament's early classification scheme (Beament, 1947), the dark band of cells (3-4 cells wide) likely corresponds to the cells that will synthesize the rim or the neck. Furthermore, the group of cells that appears thinner in the anteroposterior axis may be the single ring of cells that will produce the pseudomicropyle structures. These are immediately posterior

to a single row of larger polygonal cells slightly longer in the anteroposterior axis, whose identity is unknown.

SUMMARY

This study provides the first analysis of ion transport protein distribution in an insect telotrophic ovariole. The distribution of ion transport proteins in this study suggested that the follicle cells are primarly responsible for generating transmembrane H^+ and Ca^{2+} flux. The distribution of a H^+ pump, H^+/K^+-ATPase, agreed with H^+ ISP studies by showing that H^+ pump distribution was limited to the follicles, but offered little insight as to the source of H^+ efflux at the interfollicular stalks. The distribution of PMCA and an L-type Ca^{2+} channel were particularly interesting, and revealed differences in expression among follicle cell populations that may influence their ability to communicate with each other. While the work presented here provides an initial foundation towards understanding the molecular basis for transmembrane H^+ and Ca^{2+}fluxes, there is much more to do. As more antibodies become available, a more complete description of the distribution of H^+ and Ca^{2+} transport proteins, as well as other ion transport proteins, may be developed that will provide greater insight into how extracellular ion currents are generated and regulated, as well as the interplay between germ and somatic cells within the *Rhodnius* ovariole.

PLATE 1

Figure 1. Immunolabelling of PMCA on western blot. Lanes 1 and 5 contain protein standards, lane 2 contains protein from rabbit erythrocytes, lane 3 contains protein from nuclear and mitochondrial protein fractions isolated from *Rhodnius* ovaries, and lane 4 contains whole protein from *Rhodnius* ovaries. A smear of protein was seen in the erythrocyte lane. In both *Rhodnius* lanes, a band at 146 kDa was detected, along with three fainter bands: one at 110 kDa, one at 54 kDa, and one at 49 kDa.

Figure 2. Immunolabelling of PMCA on western blot. Lane 1 contains protein standards, lane 2 contains rabbit erythrocyte protein, and lane 3 contains protein from mouse brain, and lanes 2 and 3 both contain whole protein isolated from *Rhodnius* ovaries. Four bands labelled in the mouse brain lane at 133, 80, 71, and 40 kDa.

Figure 3. Immunolabelling of L-type Ca^{2+} channel on western blot. Lanes 1 and 5 contain protein standards, lane 2 contains protein isolated from mouse brain, lane 3 contains protein from nuclear and mitochondrial protein fractions isolated from *Rhodnius* ovaries, and lane 4 contains whole protein from *Rhodnius* ovaries. Two bands were strongly labelled in the mouse brain lane: one at 151 kDa and one at 72 kDa. In addition, a band at 38 kDa and another at 24 kDa were less evident. In the lane containing whole protein from *Rhodnius* ovary, a single 116 kDa band was detected.

Figure 4. Immunolabelling of H^+/K^+-ATPase on western blot. Lanes 1 and 5 contain protein standards, lane 2 contains mouse kidney proteins, lane 3 contains protein from nuclear and mitochondrial fractions of *Rhodnius* ovaries, and lane 4 contains whole protein from *Rhodnius* ovaries. Two bands are labelled in the mouse kidney lane at 71 kDa and 59 kDa. A 101 kDa band was detected in lane 4 containing whole ovary protein.

Figure 1. PMCA (a)

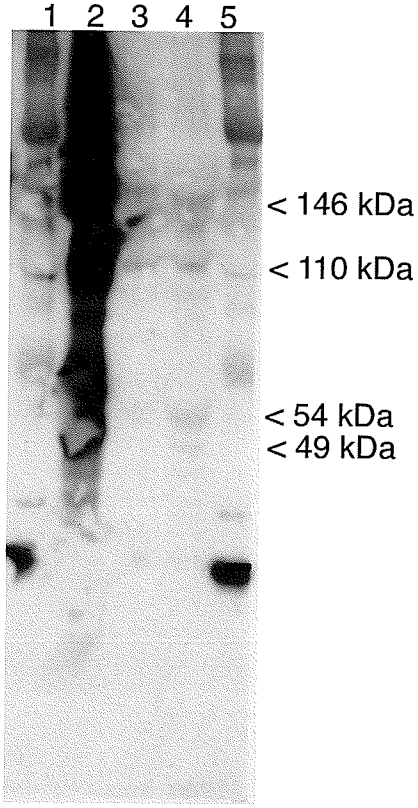

Figure 2. PMCA (b)

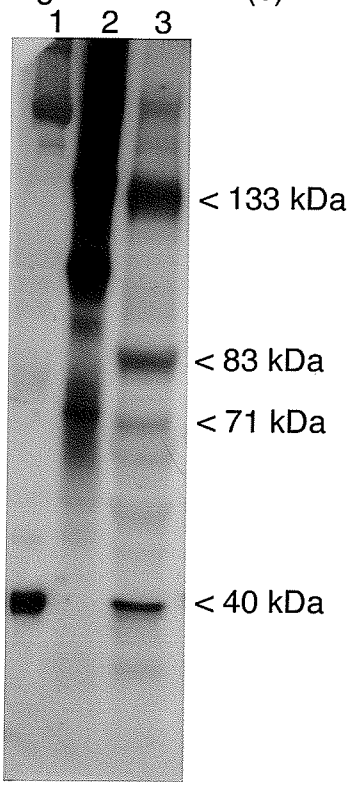

Figure 3. H/K-ATPase

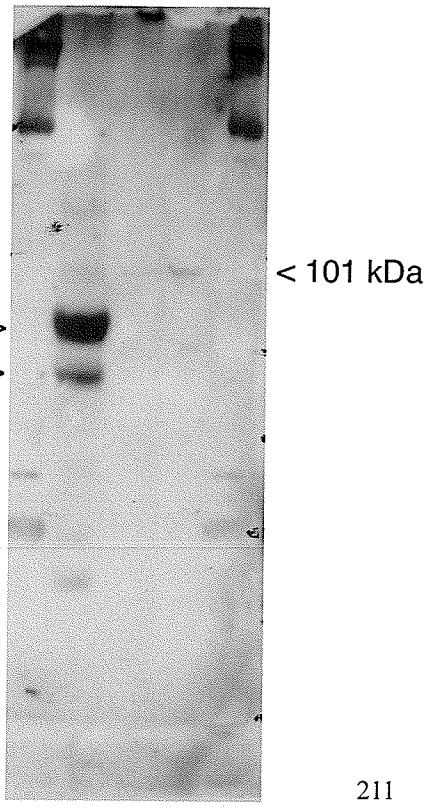

Figure 4. DHPR

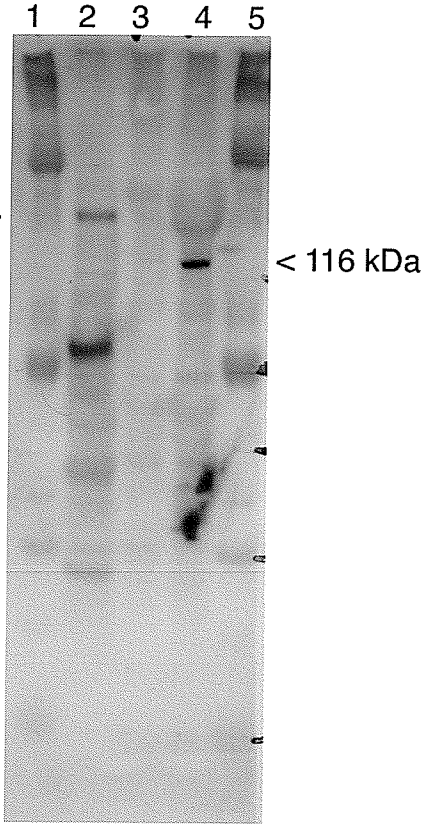

PLATE 2

Immunofluorescence labelling of H^+/K^+-ATPase in adult *Rhodnius* ovarioles. (1) Labelling is restricted to the follicles and is virtually absent over the tropharium (upper left). Strong labelling highlights individual migratory cells that are not a part of the ovariole proper, over the smallest previtellogenic follicles. Scale bar is 50 μm. (2) H^+/K^+-ATPase labelling is more intense at the junctions between previtellogenic follicles. Scale bar is 50 μm. (3) Higher magnification of the junction between previtellogenic follicles, displaying increased labelling along the lateral membranes of follicle cells at the junction. Scale bar is 10 μm. (4) No appreciable labelling was observed among cells in the interfollicular stalk separating T and T-1 follicles. Scale bar is 50 μm. (5) Follicle cells of the T-1 oöcyte express low levels of H^+/K^+-ATPase, localized to the lateral membrane in a punctate staining pattern. Scale bar is 10 μm. (6) H^+/K^+-ATPase labelling among follicle cells at the anterior pole of a late vitellogenic follicle. The anterior groups of follicle cells remain closely apposed and staining is restricted to the lateral membrane (upper left). A narrow band of micropyle and pseudomicropyle cells can be identified based on their unique cell shape. Posterior to these, a band of follicle cells 4 to 5 cells wide can be identified that remain closely apposed, followed posteriorly by the lateral follicle cells which develop large intercellular spaces. Expression levels of the pump appear to be roughly similar between these different groups of cells. Scale bar is 25 μm.

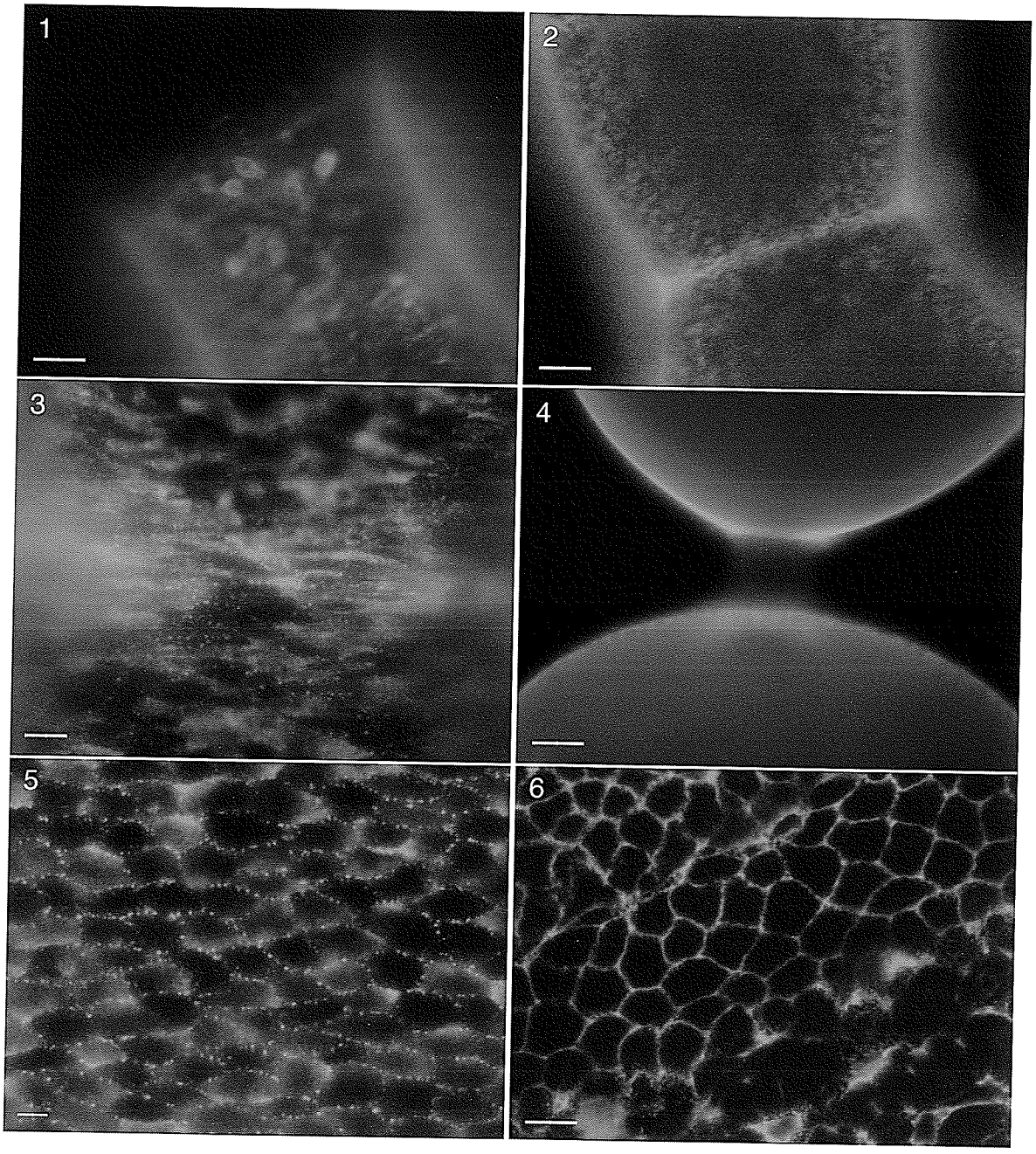
1
2
3
4
5
6

PLATE 3

Immunofluorescence staining of H^+/K^+-ATPase in late vitellogenic follicles of adult *Rhodnius* ovarioles. Higher magnification views of the follicle shown in the last image of the previous plate. (1) Staining intensity appeared to be roughly equivalent between different follicle cell groups over the anterior pole of late vitellogenic follicles, and was observed along the lateral follicle cell surfaces. Scale bar is 10 μm. (2) A punctate staining pattern was observed among the follicle cells along the lateral surface of the follicle, again restricted to the lateral cell membranes, including the cytoplasmic struts formed between neighboring cells. Scale bar is 10 μm. (3-6) Images taken at several different focal planes through a group of follicle cells along the lateral surface of the follicle, from the basal surface (Figure 3) to the apical pole (Figure 6). Immunofluorescence staining of H^+/K^+-ATPase was observed along the lateral follicle cell membranes, not at the apical or basal poles. Scale bar is 10 μm.

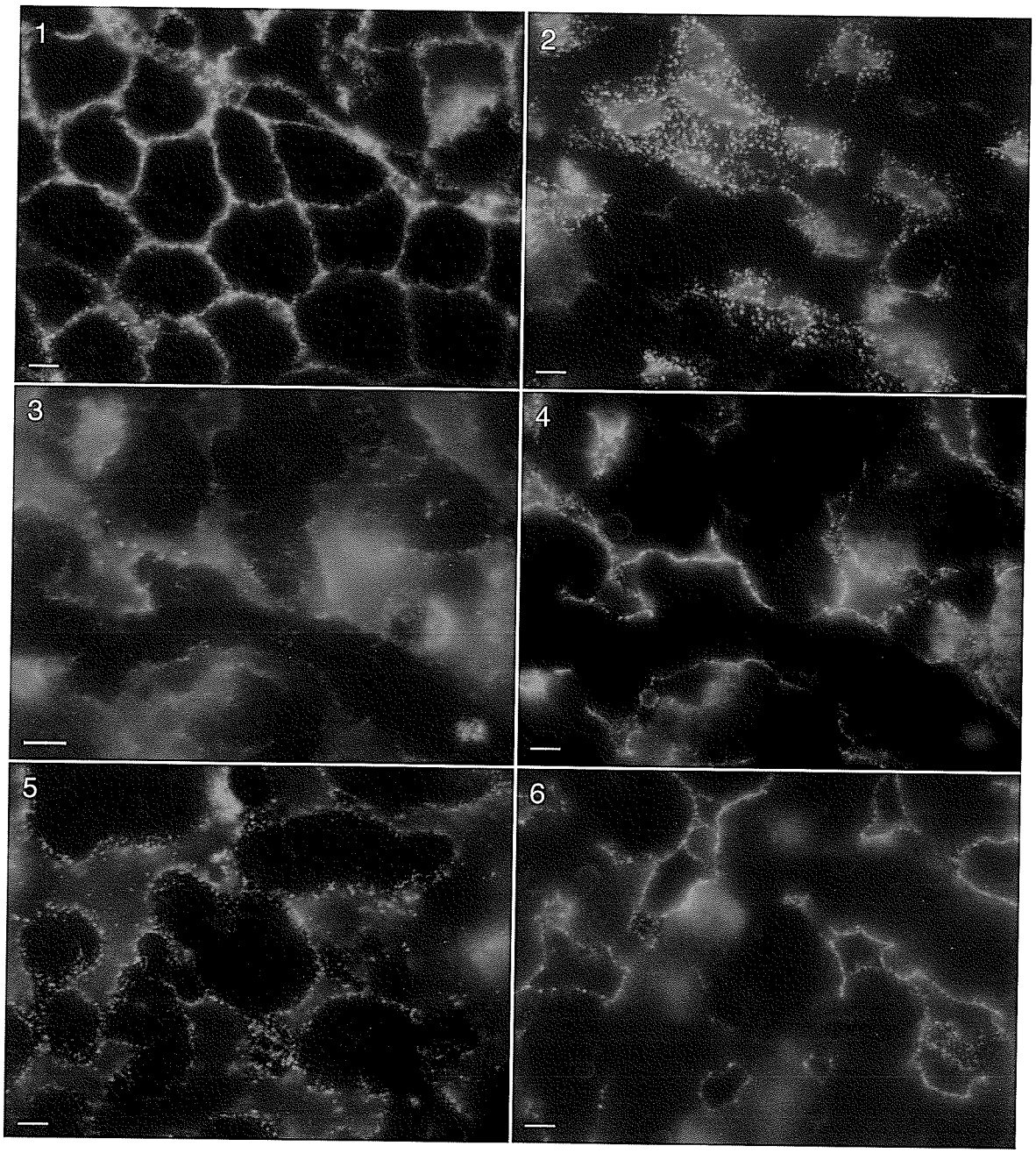
1
2
3
4
5
6

PLATE 4

PMCA distribution in the tropharium and previtellogenic follicles in adult *Rhodnius* ovarioles. (1) Staining in the tropharium is restricted to a meshlike pattern across the surface of the ovariole. Scale bar is 50 μm. (2) This pseudocoloured confocal image demonstrates minimal staining of central nurse cells (bottom half of image) relative to the overlying inner sheath cells (shown in red indicating intense labelling). (3) Higher magnification of the tropharium surface. PMCA staining appears as a branching network. Scale bar is 10 μm. (4) Closer inspection of the same region with an overlay of ISC nuclei stained with Hoechst 33258 shows that it is the somatic ISCs expressing PMCA. Notice that not all of the follicle cells express similar levels of Ca^{2+} pumps. Scale bar is 10 μm. (5) PMCA staining is relatively uniform across smaller previtellogenic oöcytes, except for an intense band at the junctions between follicles. Scale bar is 50 μm. (6) Pseudocoloured image of the junction between two previtellogenic oöcytes demonstrates staining restricted to the basal follicle cell surfaces. PMCA labelling is more intense at the junction between follicles. (7) Follicle cells at the forming junction appear to present a smaller basal surface area, raising the possibility that PMCA expression levels in these cells may be equivalent to those of neighboring cells, with the difference being that they are incorporated into a smaller area. One micron plastic section, stained with 1% toluidine blue in 1% Borax. (8) Pseudocoloured confocal image of a later previtellogenic follicle demonstrating PMCA localized to the basal surfaces of follicle cells. The oöcyte occupies the left half of this image, and the apical follicle cell surfaces are faintly visible (light blue). (9) Pseudocoloured confocal image of the same region in a control ovariole. No labelling was observed in control ovarioles.

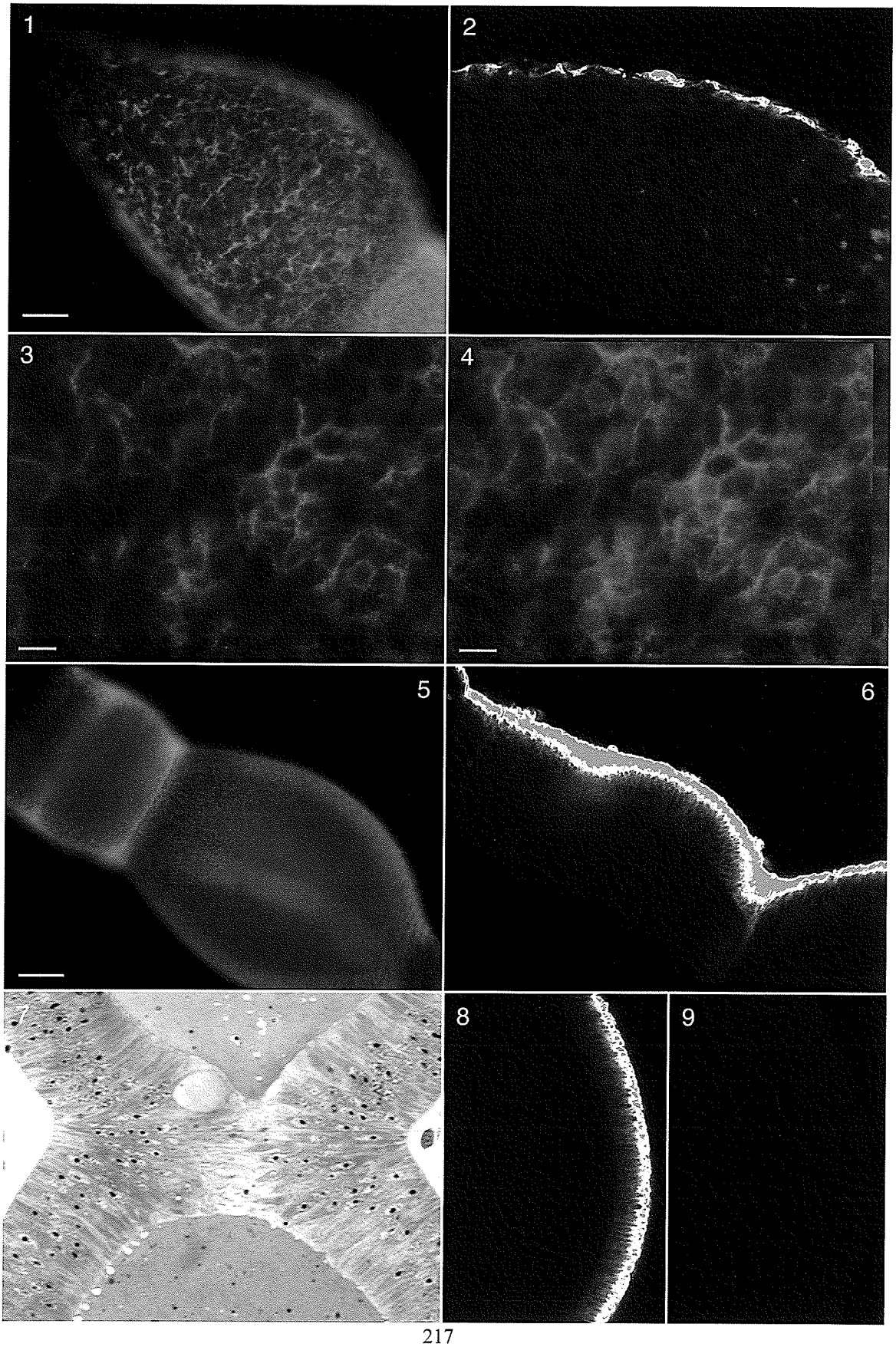
1
2
3
4
5
6
7
8
9

PLATE 5

PMCA distribution in early to mid-vitellogenic follicles of adult *Rhodnius* ovarioles. (1) During early vitellogenesis (c.450 μm), three distinct follicle cell populations can be identified on the basis of PMCA staining. The majority of follicle cells, over the lateral and posterior surface of the oöcyte (on the right), display a relatively homogenous staining pattern. Closer to the anterior end, a darker band of cells is observed, indicating lower expression of Ca^{2+} pumps. At the anterior end of the oöcyte (upper left) there is a mosaic group of follicle cells whose expression appears equal or greater than the lateral follicle cells. Scale bar is 50 μm. (2) Mosaic and darker follicle cells appear to correspond to the anterior columnar cells visible using brightfield microscopy. Scale bar is 50 μm. (3) Higher magnification of the anterior pole of the follicle in (1). The darker band of cells is on average around five cells wide. Scale bar is 10 μm. (4) Higher magnification of the homogenous population of lateral follicle cells along an early vitellogenic follicle. Scale bar is 10 μm. (5) Somatic cells of the interfollicular stalk do not express detectable levels of PMCA. Scale bar is 25 μm. (6). Follicle cells extend basally to cover the outer aspect of the trophic cord, as shown in this cross section though a previtellogenic follicle. One micron section stained with 1% toluidine blue in 1% Borax. Scale bar is 20 μm. (7) Follicle cell projections express mosaic levels of PMCA compared to the surrounding lateral follicle cells, with some cells labelling more or less intensely. Scale bar is 10 μm. (8) An image of the same region stained with Hoechst 33258 to label nuclei, showing the location of the trophic cord where follicle cell nuclei are absent. Scale bar is 10 μm.

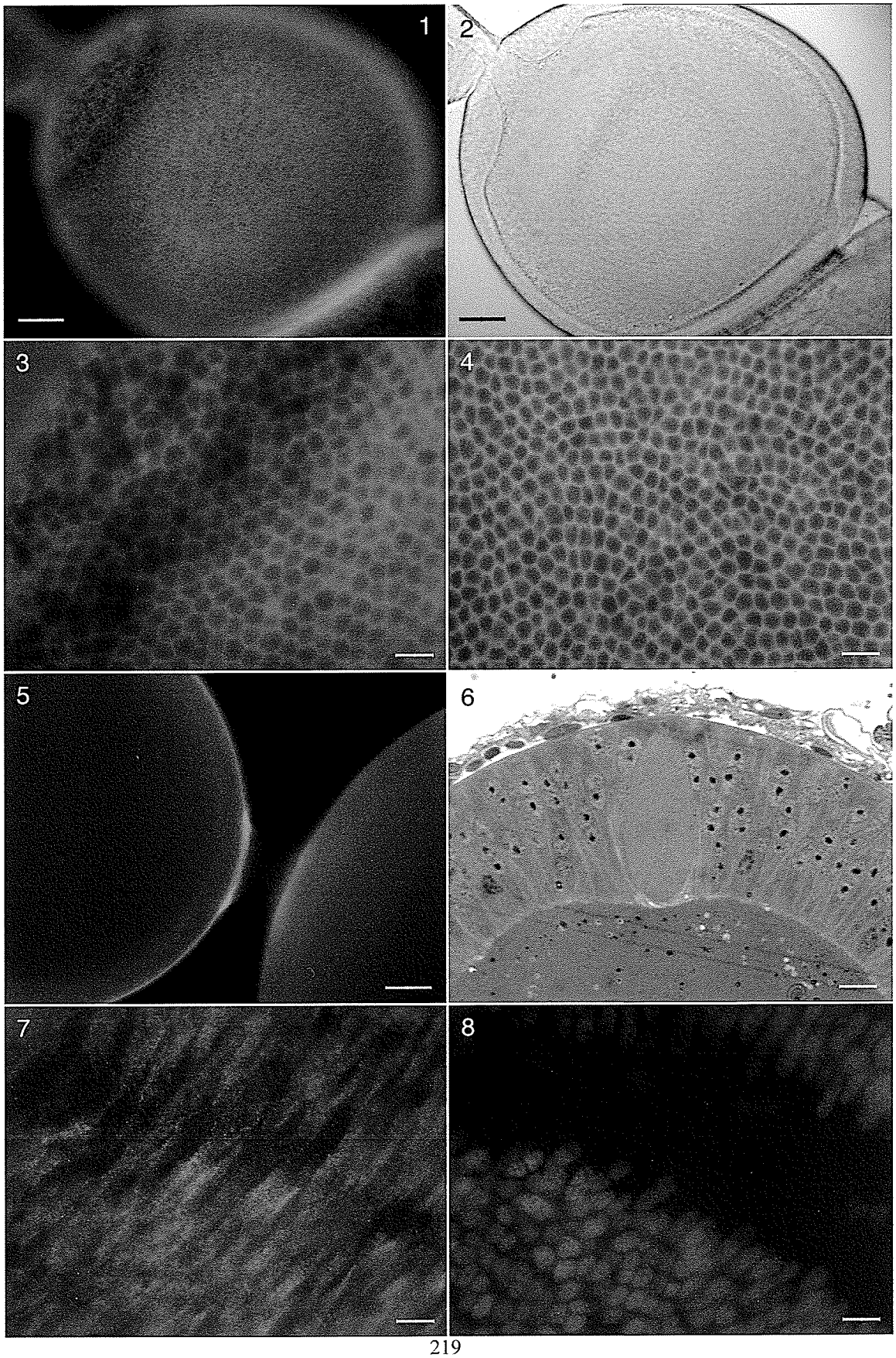
1
2
3
4
5
6
7
8

PLATE 6

PMCA distribution in late vitellogenic follicles of adult *Rhodnius* ovarioles. (1) Over larger vitellogenic follicles, five distinct populations can be distinguished. Anteriorly (on the left) is the mosaic group of cells, followed by a single row of dark cells, then a more intensely labelled band of cells, similar to the anterior group, a darker band of cells, and finally the homogenous group of lateral follicle cells. Scale bar is 50 μm. (2) Higher magnification of the anterior pole of the follicle, highlighting the different groups of cells in this region. Scale bar is 25 μm. (3) Pseudocoloured confocal image centered on the two darker groups of cells. (4) In follicles at later stages of vitellogenesis, the anterior pole labels more intensely and more groups of follicle cells can be identified on a morphological basis. Scale bar is 50 μm. (5) The anterior follicle cells in later vitellogenic follicles retain the basal localization of PMCA (upper half of image), while PMCA appears to become restricted to the lateral cell membrane domain of follicle cells along the lateral surface of the follicle. PCMA redistribution may be an indication of the morphological changes these cells undergo to prepare for chorionation. Scale bar is 50 μm. (6) Higher magnification of follicle cells along the lateral surface of the follicle, highlighting PMCA labelling along the lateral cell membrane surfaces. Scale bar is 10 μm.

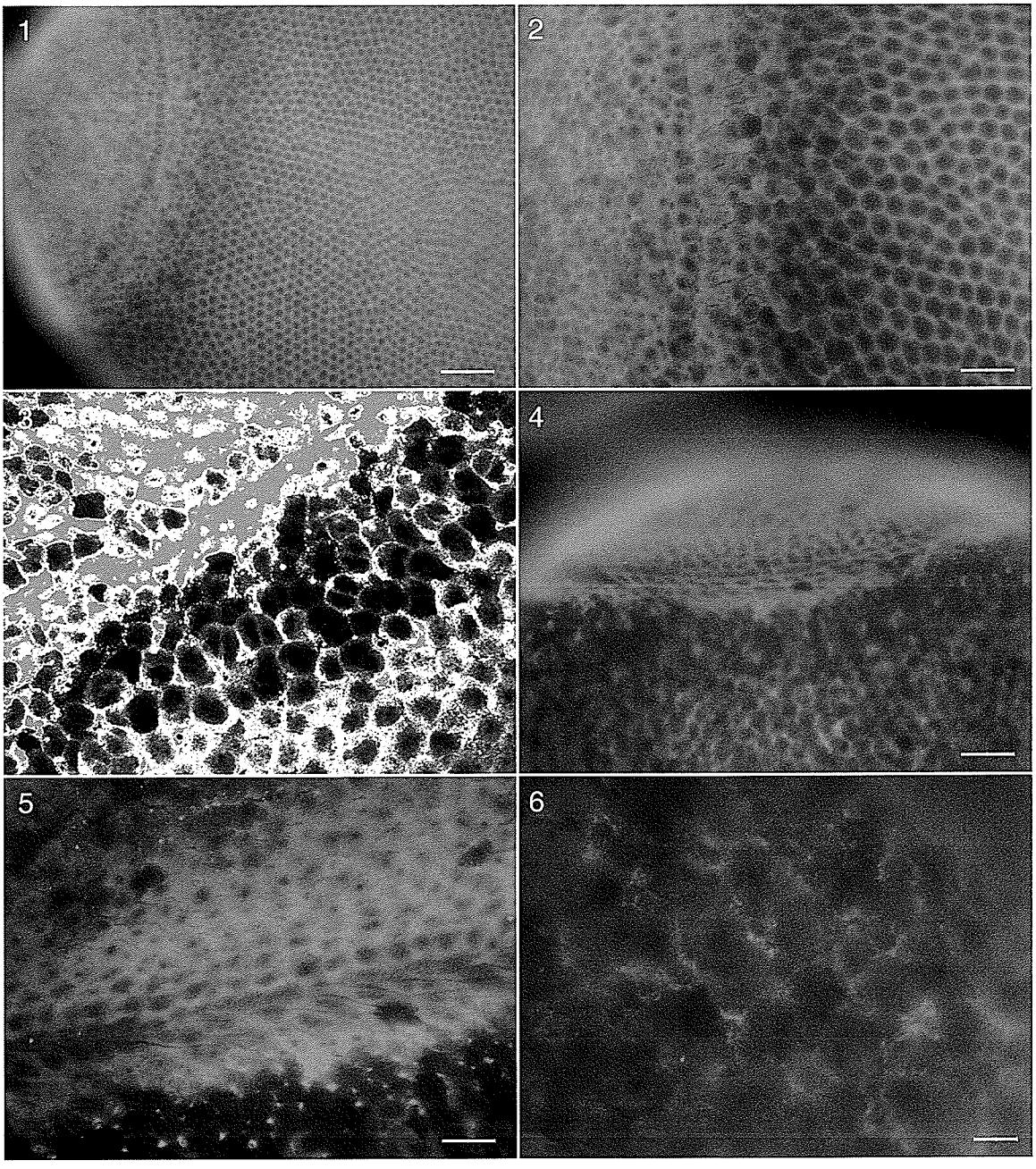
1
2
3
4
5
6

PLATE 7

L-type V-gated calcium channel distribution in the tropharium, previtellogenic follicles and early vitellogenic follicles of adult *Rhodnius* ovarioles. (1) Along the tropharium, labelling of Ca^{2+} channels was not detected in the nurse cells; staining was apparent in the inner sheath cells. Scale bar is 50 μm. (2) Channel expression by inner sheath cells around the tropharium resembles the branching network pattern observed with PMCA. Scale bar is 10 μm. (3) Expression of channels by the follicle cells of smaller previtellogenic follicles appears relatively homogenous except at the junction between follicles where an intensely labelled group of cells is present. Scale bar is 50 μm. (4) Increased labelling at the junction is also visible midway through the ovariole. Scale bar is 50 μm. (5) Follicle cells adjacent to the cord cover its outer aspect with projections that display a mosaic expression of channels. Scale bar is 10 μm. (6) An image of the same region stained with Hoechst 33258 to label nuclei showing the location of the trophic cord where follicle cells nuclei are absent. Scale bar is 10 μm. (7) Immunofluorescence labelling along the basal surfaces of follicle cells from an early vitellogenic follicle. Labelling of calcium channels is greatest along the basal surfaces of follicle cells. Scale bar is 25 μm. (8) In early vitellogenic follicles the anterior, columnar follicle cells appear to label more intensely, as shown in this image taken midway through the follicle. Scale bar is 50 μm.

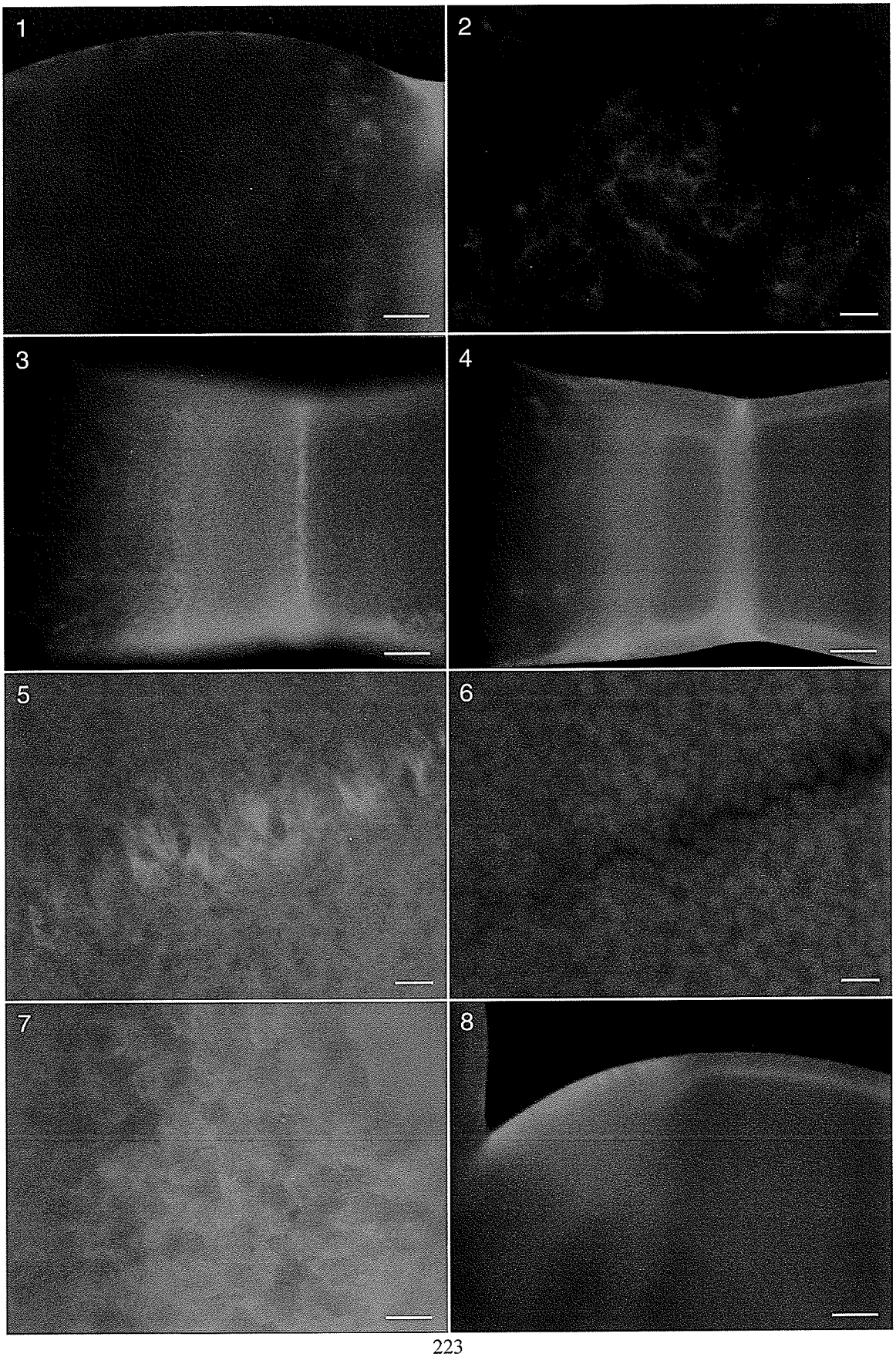
1
2
3
4
5
6
7
8

PLATE 8

L-type V-gated calcium channel distribution across vitellogenic follicles of adult *Rhodnius* ovarioles. (1) Differences in Ca^{2+} channel distribution among follicle cells can be observed once columnar and cuboidal follicle cells can be distinguished. Columnar follicle cells are labelled with slightly greater intensity, and like PMCA staining this pattern is mosaic in comparison to the follicle cells over the lateral follicle, which express uniform levels of the Ca^{2+} channel. Scale bar is 25 μm. (2) Higher magnification of the junction between columnar and cuboidal follicle cells highlights the presence of a single row of larger cells that label slightly less intensely. Scale bar is 10 μm. (3) The single dark row of follicle cells becomes more prominent as vitellogenesis proceeds. Scale bar is 25 μm. (4) By mid-late vitellogenesis (follicles 800-1200 μm in length) additional follicle cell groups can be identified on the basis of Ca^{2+} channel staining. Here, six different groups of cells can be identified. (5) Differences in the morphology of these different cell groups can also be identified on the basis of nuclei stained with Hoecsht 33258. Scale bar is 50 μm. (6) Higher magnification of the anterior pole of a similar follicle showing the six follicle cells groups: mosaic apical cells on the far left are bordered by a single ring of darker cells, then a lighter ring, a relatively intense ring, another darker ring, and finally the lateral follicle cells. Scale bar is 25 μm.

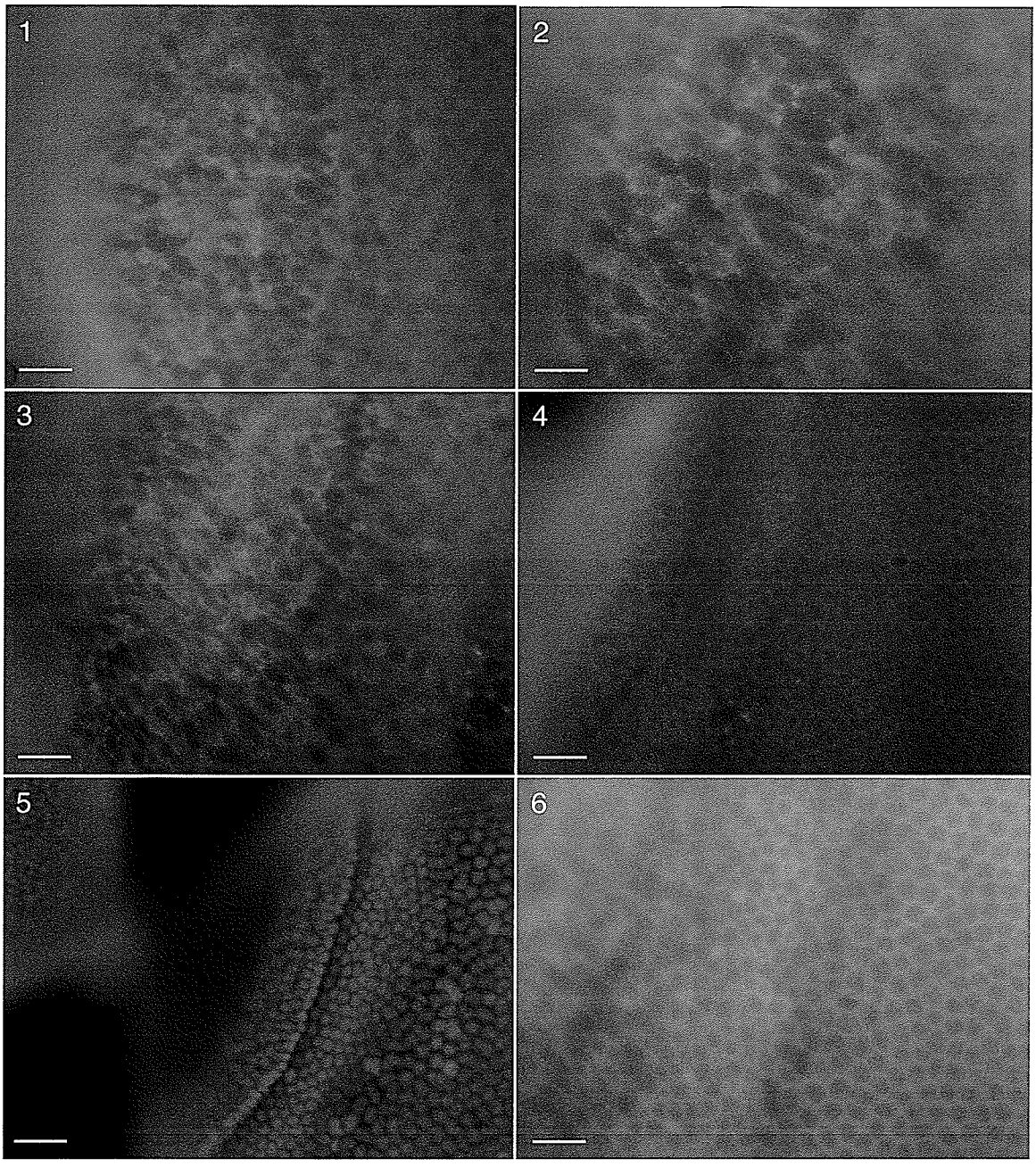
1
2
3
4
5
6

GENERAL CONCLUSIONS

The non-invasive self-referencing ion-selective probe has proven to be a valuable tool for measuring extracellular ionic fluxes around an insect telotrophic ovariole, and has allowed us for the first time to explore the ionic basis of the extracellular currents known to exist around insect telotrophic ovarioles. H^+ and Ca^{2+} fluxes were analyzed around the telotrophic ovarioles of *Rhodnius prolixus*, both during germ cell differentiation in the 5th instar, and throughout an entire oögenesis cycle in the adult. In the 5th instar, H^+ fluxes were detected at specific locations during development corresponding to early stages of nurse cell-oöcyte differentiation and to the development of the somatic tissue. H^+ fluxes around adult ovarioles were primarily associated with specific structures within the vitellarium, and changed throughout the course of an oögenesis cycle. These fluxes appeared to correlate with many of the events linked to vitellogenesis and chorionation, allowing us to develop more refined strategies to investigate the potential physiological roles of H^+ during these events. Investigation of extracellular Ca^{2+} fluxes was successful in detecting small transient fluxes around adult *Rhodnius* ovarioles. While an extracellular Ca^{2+} loop involving a steady efflux of Ca^{2+} over the tropharium coupled with influx over growing follicles was not observed, transient Ca^{2+} fluxes observed over several regions of the adult ovariole suggest that Ca^{2+} may play a subtler role in regulating events in during oögenesis.

Immunofluorescent studies of adult *Rhodnius* ovarioles revealed clear differences in the distribution of plasma membrane H^+ and Ca^{2+} transport proteins between nurse cell

and oöcyte compartments, and suggested that the follicle cells in particular are well equipped to contribute to the extracellular H^+ and Ca^{2+} fluxes observed around adult *Rhodnius* ovarioles. Restriction of Ca^{2+} transport protein expression to specific groups of follicle cells occurs early in the differentiation of specialized groups of cells from a single uniform population. The differential expression of Ca^{2+} pumps along early vitellogenic follicles suggests there may be interesting differences in how these cells communicate with each other that may not be detected using extracellular measurements. In contrast a proton pump, H^+/K^+-ATPase, appears to be expressed in equal amounts by different groups of follicle cells. If this pump is in fact responsible for the localized and stage-specific extracellular H^+ fluxes observed during vitellogenesis, a critical question is how these pumps are regulated to give rise to regional activity. Hopefully, further immunofluorescent descriptions of the distribution of ion transport proteins will assist in design of future experiments on the role of ion currents during oögenesis. Examination of extracellular ionic fluxes using the ion-selective probe coupled with immunofluorescent techniques to discover the underlying molecular basis of these fluxes will potentially lead to a greater understanding of the nature and role of extracellular ion fluxes during oögenesis.

LITERATURE CITED

Abu-Hakima, R., Davey, K.G. (1977)a. The action of juvenile hormone on the follicle cells of *Rhodnius prolixus*: the importance of volume changes. *J. Exp. Biol.* **69**, 33-44.

Abu-Hakima, R., Davey, K.G. (1977)b. The action of juvenile hormone on follicle cells of *Rhodnius prolixus* in vitro: the effects of colchicine and cytochalasin B. *Gen. Compar. Endocrin.* **32**, 360-370.

Abu-Hakima, R., Davey, K.G. (1979). A possible relationship between ouabain-sensitive (Na^+-K^+) dependent ATPase and the effect of juvenile hormone on the follicle cells of *Rhodnius prolixus*. *Insect Biochem.* **9**, 195-198.

Adler, E.L., Woodruff, R.I. (2000). Varied effects of 1-octanol on gap junctional communication between ovarian epithelial cells and oocytes of *Oncopeltus fasciatus*, *Hyalophora cecropia*, and *Drosophila melanogaster*. *Arch. Insect Biochem. Physiol.* **43**, 22-32.

Al-Mohanna, F.A., Caddy, K.W.T., Bolsover, S.R. (1994). The nucleus is insulated from large cytosolic calcium ion changes. *Nature* **367**, 745-750.

Allbritton, N.L., Meyer, T. (1993). Localized calcium spikes and propagating calcium waves. *Cell Calcium* **14**, 691-697.

Allbritton, N.L., Oancea, E., Kuhn, M.A., Meyer, T. (1994). Source of nuclear calcium signals. *Proc. Natl. Acad. Sci.* **91**, 12458-12462.

Anderson, K.L., Woodruff, R.I. (2001). A gap junctionally transmitted epithelial cell signal regulates endocytic yolk uptake in *Oncopeltus fasciatus*. *Dev. Biol.* **239,** 68-78.

Anderson, M.E., Bowdan, E., Kunkel, J.G. (1994). Comparison of defolliculated oocytes and intact follicles of the cockroach using the vibrating probe to record steady currents. *Dev. Biol.* **162**, 111-122.

Ault, K.T., Durmowicz, G., Galione, A., Harger, P.L., Busa, W.B. (1996). Modulation of *Xenopus* embryo mesoderm-specific gene expression and dorsoanterior patterning by receptors that activate the phosphatidylinositol cycle signal transduction pathway. *Development* **122**, 2033-2041.

Aune, T.M., Epel, D. (1978). Increased intracellular pH shifts the subcellular localization of G6PDH (abstract). *J. Cell Biol.* **79,** 164a.

Baginsky, R.M. (1981). On the timing and activation of glycogen catabolism in fertilized sea urchin eggs. *J. Exp. Zool.* **216,** 201-203.

Barritt, G.J. (1999). Receptor-activated Ca^{2+} inflow in animal cells: a variety of pathways tailored to meet different intracellular signalling requirements. *Biochem. J.* **337**, 153-169.

Barton, J.K., den Hollander, J.A., Lee, T.M., MacLaughlin, A., Shulman, R.G. (1980). Measurement of the internal pH of yeast spores by ^{32}P nuclear magnetic resonance. *Proc. Natl. Acad. Sci. USA* 77, 2470-2473.

Barton, J.S., Vandivort, D.L., Heacock, D.H., Coffman, J.A., Trygg, K.A (1987). Microtubule assembly kinetics. Changes with solution conditions. *Biochem. J.* **247**, 505-511.

Baumann, O., Takeyasu, K. (1993). Polarized distribution of Na,K-ATPase in honeybee photoreceptors is maintained by interaction with glial cells. *J. Cell Sci.* **105**, 287-301.

Beament, J.W.L. (1946). The formation and structure of the chorion of the egg in an hemipteran, *Rhodnius prolixus*. *Quart. J. Micr. Sci.* **87,** 393-437.

Beament, J.W.L. (1947). The formation and structure of the micropylar complex in the egg-shell of *Rhodnius prolixus* Stahl (Heteroptera Reduviidae). *J. Exp. Biol.* **23,** 213-233.

Begg, D.A., Rebhun, L.I. (1979). pH regulates the polymerization of actin in the sea urchin egg cortex. *J. Cell Biol.* **83,** 241-248.

Begg, D.A., Rebhun, L.I., Hyatt, H. (1982). Structural organization of actin in the sea urchin egg cortex: microvillar elongation in the absence of microfilament bundle formation. *J. Cell Biol.* **93,** 24-32.

Berridge, M.J. (1993). Inositol trisphosphate and calcium signaling. *Nature* **361**, 315-325.

Berridge, M.J. (1995). Calcium signaling and cell proliferation. *Bioessays* **17**, 491-500.

Berridge, M.J. (1997)a. The AM and FM of calcium signalling. *Nature*, **386**, 759-760.

Berridge, M.J. (1997)b. Elementary and global aspects of calcium signalling. *J. Physiol.* **499**, 291-306.

Berridge, M.J., Downes, C.P., Hanley, M.R. (1989). Neural and developmental actions of lithium: a unifying hypothesis. *Cell* **59**, 411-419.

Berridge, M.J., Bootman, M.D., Lipp, P. (1998). Calcium – a life and death signal. *Nature* **395**, 645-648.

Binder, H.J., Sangan, P., Rajendran, V.M. (1999). Physiological and molecular studies of colonic H^+,K^+-ATPase. *Semin. Nephrol.* **19**, 405-414.

Bjornsson, C.S., Huebner, E. (2002). Tissue rotation chamber for electrophysiology, microinjection, and microdissection. *Biotechniques* **33,** 38-42.

Bohrmann, J. (1993). Antisera against a channel-forming 16 kDa protein inhibit dye-coupling and bind to cell membranes in *Drosophila* ovarian follicles. *J. Cell Sci.* **105**, 513-518.

Bohrmann, J. (1997). *Drosophila* unconventional myosin VI is involved in intra- and intercellular transport during oogenesis. *Cell Mol. Life Sci.* **53**, 652-662.

Bohrmann, J., Biber, K. (1994). Cytoskeleton-dependent transport of cytoplasmic particles in previtellogenic to mid-vitellogenic ovarian follicles of *Drosophila*: time-lapse analysis using video-enhanced contrast microscopy. *J. Cell Sci.* **107**, 849-858.

Bohrmann, J., Bonafede, A. (2000). Tissue-specific distribution and variation of the channel-forming protein ductin during development of *Drosophila melanogaster*. *Int. J. Dev. Biol.* **44**, 883-890.

Bohrmann, J., Braun, B. (1999). Na,K-ATPase and V-ATPase in ovarian follicles of *Drosophila melanogaster*. *Biol. Cell* **91**, 85-98.

Bohrmann, J., Dorn, A., Sander, K., Gutzeit, H. (1986). The extracellular electrical current pattern and its variability in vitellogenic *Drosophila* follicles. *J. Cell. Sci.* **81,** 189-206.

Bohrmann, J., Gutzeit, H. (1987). Evidence against electrophoresis as the principal mode of protein transport in the vitellogenic ovarian follicles of *Drosophila*. *Development* **101**, 279-288.

Bohrmann, J., Haas-Assenbaum, A. (1993). Gap junctions in ovarian follicles of *Drosophila melanogaster*: inhibition and promotion of dye-coupling between oocyte and follicle cells. *Cell Tissue Res.* **273,** 163-173.

Bohrmann, J., Schill, S. (1997). Cytoplasmic transport in *Drosophila* ovarian follicles: the migration of microinjected fluorescent probes through intercellular bridges depends neither on electrical charge nor on external osmolarity. *Int. J. Dev. Biol.* **41**, 499-507.

Bootman, M.D., Berridge, M.J., Lipp, P. (1997). Cooking with calcium: the recipes for composing global signals from elementary events. *Cell* **91**, 367-373.

Bootman, M.D., Thomas, D., Tovey, S.C., Berridge, M.J., Lipp, P. (2000). Nuclear calcium signaling. *Cell Mol. Life Sci.* **57**, 371-378.

Bowdan, E., Kunkel, J.G. (1990). Patterns of ionic currents around the developing oocyte of the German cockroach, *Blattella germanica*. *Dev. Biol.* **137,** 266-275.

Bowdan, E., Kunkel, J.G. (1994). Ionic components of dorsal and ventral currents in vitellogenic follicles of the cockroach, *Blattella germanica*. *J. Insect Physiol.* **40,** 323-331.

Brandis, J.W., Raff, R.A. (1979). Elevation of protein synthesis is a complex response to fertilization. *Nature London* **278,** 467-469.

Bray, D., Thomas, C. (1976). Unpolymerized actin in fibroblasts and brain. *J. Mol. Biol.* **105**, 527-544.

Brini, M., Murgia, M., Pasti, L., Picard, D., Pozzan, T., Rizzuto, R. (1993). Nuclear Ca^{2+} concentration measured with specifically targeted recombinant aequorin. *EMBO J.* **12**, 4813-4819.

Bryan, J., Kane, R.E. (1978). Separation and interaction of the major components of sea urchin actin gel. *J. Mol. Biol.* **125,** 207-224.

Buning, J., (1994). "The Insect Ovary". Chapman & Hill, London.

Burton, P.R., Himes, R.H. (1978). Electron microscope studies of pH effects on assembly of tubulin free of associated proteins. Delineation of substructure by tannic acid staining. *J. Cell Biol.* **77**, 120-133.

Busa, W.B. (1982). Cellular dormancy and the scope of pH_i-mediated metabolic regulation. In "Intracellular pH: Its Measurement, Regulation, and Utilization in Cellular Functions". (R. Nuccitelli and D.W. Deamer, Eds.). New York: Liss, 1982, p. 417-426.

Busa, W.B., Nuccitelli, R. (1984). Metabolic regulation via intracellular pH. *Am. J. Physiol.* **246,** R409-R438.

Bygrave, F.L. (1978)a. Calcium movements in cells. *Trends Biochem. Sci.* **3**, 175-178.

Bygrave, F.L. (1978)b. Mitochondria and the control of intracellular calcium. *Biol. Rev. Camb. Philos. Soc.* **53**, 43-79.

Carafoli, E. (1987). Intracellular calcium homeostasis. *Annu. Rev. Biochem.* **56**, 395-433.

Carden, D.E., Diamond, D., Miller, A.J. (2001). An improved Na^+-selective microelectrode for intracellular measurements in plant cells. *J. Exp. Bot.* **52,** 1353-1359.

Carr, D.W., Acott, T.S. (1990). The phosphorylation of a putative sperm microtubule-associated protein 2 (MAP2) is uniquely sensitive to regulation. *Biol. Reprod.* **43**, 795-805.

Carron, C.P., Longo, F.J. (1982). Relation of cytoplasmic alkalinization to microvillar elongation and microfilament formation in the sea urchin egg. *Dev. Biol.* **89,** 128-137.

Clapham, D.E. (1995). Calcium signaling. *Cell* **80**, 259-268.

Claret-Berthon, B., Claret, M., Mazet, J.L. (1977). Fluxes and distribution of calcium in rat liver cells: kinetic analysis and identification of pools. *J. Physiol.* **272**, 529-552.

Clegg, J.S., Conte, F.P. (1980). A review of the cellular and developmental biology of *Artemia*. In "The Brine Shrimp *Artemia*". (G. Persoone, P. Sorgeloos, O. Roels, E. Jaspers *Eds.*). Wetteren, Belgium: Universa, 1980, p. 11-54.

Chen, J., Godt, D., Gunsalis, K., Kiss, I., Goldberg, M., Laski, F.A. (2001). Cofilin/ADF is required for cell motility during *Drosophila* ovary development and oogenesis. *Nat. Cell Biol.* **3,** 204-9.

Cole, D.G. (1999). Kinesin-II, the heteromeric kinesin. *Cell Mol. Life Sci.* **56**, 217-226.

Cole, R.W., Woodruff, R.I. (1997). Charge-dependent distribution of endogenous proteins within vitellogenic ovarian follicles of *Actias luna*. *J. Insect Physiol.* **43**, 275-287.

Cole, R.W., Woodruff, R.I. (2000). Vitellogenic ovarian follicles of *Drosophila* exhibit a charge-dependent distribution of endogenous soluble proteins. *J. Insect Physiol.* **46**, 1239-1248.

Colegrove, S.L., Albrecht, M.A., Friel, D.D. (2000). Quantitative analysis of mitochondrial Ca^{2+} uptake and release pathways in sympathetic neurons. Reconstruction of the recovery after depolarization-evoked $[Ca^{2+}]_i$ elevations. *J. Gen. Physiol.* **115**, 371-388.

Cornell-Bell, A.H., Finkbeiner, S.M., Cooper, M.S., Smith, S.J. (1990). Glutamate induces calcium waves in cultured astrocytes: long-range glial signaling. *Science* **247**, 470-473.

Cornell-Bell, A.H., Finkbeiner, S.M. (1991). Ca^{2+} waves in astrocytes. *Cell Calcium* **12**, 185-204.

Creton, R., Kreiling, J.A., Jaffe, L.F. (2000). Presence and roles of calcium gradients along the dorsal-ventral axis in *Drosophila* embryos. *Dev. Biol.* **217**, 375-385.

Dani, J.W., Chernjavsky, A., Smith, S.J. (1992). Neuronal activity triggers calcium waves in hippocampal astrocyte networks. *Neuron* **8**, 429-440.

Danylovych, V., Tuhai, V.A. (2001). Estimation of pH-dependence of calcium binding with calmodulin. *Ukr. Biokhim. Zh.* **73,** 33-37.

Davenport, R. (1974). Synthesis and intercellular transport of ribosomal RNA in the ovary of the milkweed bug, *Oncopeltus fasciatus*. *J. Insect Physiol.* **20,** 1949-1956.

Davey, K.G. (1997). Hormonal controls on reproduction in female Heteroptera. *Arch. Insect Biochem. Physiol.* **35**, 443-453.

Day, M.L., McGuiness, O.M., Berridge, M.J., Johnson, M.H. (2000). Regulation of fertilization-induced Ca^{2+} spiking in the mouse zygote. *Cell Calcium* **28**, 205-212.

De Koninck, P., Schulman, H. (1998). Sensitivity of CaM kinase II to the frequency of Ca^{2+} oscillations. *Science* **279**, 227-230.

Deng, W., Lin, H. (2001). Asymmetric germ cell division and oocyte determination during *Drosophila* oogenesis. *Int. Rev. Cytol.* **203,** 93-138.

Denker, S.P., Barber, D.L. (2002). Ion transport proteins anchor and regulate the cytoskeleton. *Curr. Opin. Cell Biol.* **14**, 214-220.

DePina, A.S., Langford, G.M. (1999) Vesicle transport: the role of actin filaments and myosin motors. *Micr. Res. Tech.* **47**, 93-106.

Diehl-Jones, W.L. (1991). Bioelectric current during oogenesis in *Rhodnius prolixus*. Ph.D. Thesis, Department of Zoology, University of Manitoba, Winnipeg, Canada.

Diehl-Jones, W.L., Huebner, E. (1989). Pattern and composition of ionic currents around ovarioles of the hemipteran, *Rhodnius prolixus* (Stahl). *Biol. Bull.* **176(S),** 86-90.

Diehl-Jones, W.L., Huebner, E. (1992). Spatial and temporal transcellular current patterns during oogenesis. *Dev. Biol.* **153,** 302-311.

Diehl-Jones, W.L., Huebner, E. (1993). Ionic basis of bioelectric currents during oogenesis in an insect. *Dev. Biol.* **158,** 301-316.

DiMario, P.J., Mahowald, A.P. (1986). The effects of pH and weak bases on the in vitro endocytosis of vitellogenin by oocytes of *Drosophila melanogaster*. *Cell Tissue Res*. **246,** 103-108.

Dittmann, F. (1996). Developmental aspects of calcium distribution in the trophocyte-oocyte syncytium of the telotrophic-meroistic ovariole (*Dysdercus intermedius*). *Invert. Reprod. Dev.* **29**, 157-165.

Dittmann, F. (1997). The effect of ooplasmic pH regulation on the formation of yolk spheres in the telotrophic ovariole of *Dysdercus intermedius*. *J. Insect Physiol.* **43,** 189-195.

Dittmann, F. (1998). Activation of a Ca^{2+} current coincides with the onset of oocyte differentiation in the larval telotrophic trophocyte-oocyte syncytium of D*ysdercus intermedius*. *Inv. Reprod. Dev.* **34**, 91-96.

Dittmann, F., Bizcowski, M. (1995). Induction and formation in hemipteran previtellogenic oocytes (*Dysdercus intermedius*). *Invert. Reprod. Dev.* **28**, 63-70.

Dittmann, F., Ehni, R., Engels, W. (1981). Bioelectric aspects of the hemipteran telotrophic ovariole (*Dysdercus intermedius*). *Roux's Arch. Dev. Biol.* **190,** 221-225.

Dittmann, F., Muenz, A. (1999). The proton/sodium antiporter (exchanger) in the oocyte membrane of *Dysdercus intermedius* is electrogenic ($2H^+/Na^+$) and causes perioocytic proton accumulation. *J. Insect Physiol.* **45**, 727-734.

Dolmetch, R.E., Lewis, R.S., Goodnow, C.C., Healy, J.I (1997). Differential activators of transcription factors induced by Ca^{2+} response amplitude and duration. *Nature* **386**, 855-858.

Duesbery, N.S., Masui, Y. (1996). The role of Ca^{2+} in progesterone-induced germinal vesicle breakdown of *Xenopus laevis* oocytes. *Dev. Genes Evol.* **206**, 110-124.

Duhe, R.J., Wang, L.H., Farrar, W.L. (2001). Negative regulation of Janus kinases. *Cell Biochem. Biophys.* **34**, 17-59.

Edwards, K.A., Kiehart, D.P. (1996). *Drosophila* nonmuscle myosin II has multiple essential roles in imaginal disc and egg chamber morphogenesis. *Development* **122**, 1499-1511.

Elliot, A.C., (2001). Recent developments in non-excitable cell calcium entry. *Cell Calcium* **30**, 73-93.

Feiguin, F., Ferreira, A., Kosik, K.S., Caceres, A. (1994). Kinesin-mediated organelle translocation revealed by specific cellular manipulations. *J. Cell Biol.* **127,** 1021-1039.

Festy, F., Robert, J.C., Brasseur, R., Thomas, A. (2001). Interaction between the N-terminal domain of gastric H,K-ATPase and the spectrin binding domain of ankyrin III. *J. Biol. Chem.* **276**, 7721-7726.

Fidelman, M.L., Seeholzer, K.B., Walsh, K.B., Moore, R.D. (1982). Intracellular pH mediates action of insulin on glycolysis in frog skeletal muscle. *Am. J. Physiol.* **242,** C87-C93.

Filatov, V.L., Katrukha, A.G., Bulargina, T.V., Gusev, N.B. (1999). Troponin: structure, properties, and mechanism of functioning. *Biochemistry (Moscow)* **64**, 969-985.

Finbow, M.E., Buultjens, T.E., John, S., Kam, E., Meagher, L., Pitts, J.D. (1987). Molecular structure of the gap junction channel. *CIBA Found. Symp.***125**, 92-107.

Finbow, M.E., Goodwin, S.F., Meagher, L., Lane, N.J., Keen, J., Findlay, J.B., Kaiser, K. (1994). Evidence that the 16 kDa proteolipid (subunit c) of the vacuolar H(+)-ATPase and ductin from gap junctions are the same polypeptide in *Drosophila* and *Manduca*: molecular cloning of the Vha 16k gene from *Drosophila*. *J. Cell. Sci.* **107**, 1817-1824.

Finbow, M.E., Harrison, M., Jones, P. (1995). Ductin—a proton pump component, a gap junction channel and a neurotransmitter release channel. *Bioessays* **17**, 247-255.

Finbow, M.E., Pitts, J.D. (1993). Is the gap junction channel—the connexon—made of connexin or ductin? *J. Cell Sci.* **106**, 463-471.

Fluck, R.A., Miller, A.L., Abraham, V.C., Jaffe, L.F. (1994). Calcium buffer injections inhibit ooplasmic segregation in medaka eggs. *Biol. Bull. Woods Hole* **186**, 254-262.

Fluck, R.A., Miller, A.L., Jaffe, L.F. (1991). Slow calcium waves accompany cytokinesis in medaka fish eggs. *J. Cell Biol.* **115**, 1259-1265.

Fluck, R.A., Miller, A.L., Jaffe, L.F. (1992). High calcium zones at the poles of developing medaka eggs. *Biol. Bull.* **186**, 254-262.

Ford, J.H., Roberts, C.G. (1983). Chromosome displacement and spindle tubule polymerization: 1. The effects of alterations in pH on displacement frequency. *Cytobios* **37**, 163-169.

Francis, D., Stergiopoulos, K., Ek-Vitorin, J.F., Cao, F.L., Taffet, S.M., Delmar, M. (1999). Connexin diversity and gap junction regulation by pH_i. *Dev. Genet.* **24,** 123-136.

Galella, G., Smith, D.B. (1979). Stability of microtubule protein over the pH range: 6.9 – 9.5. *Can. J. Biochem.* **57**, 1368-1375.

Ganong, W.F. (1991). Review of medical physiology (15^{th} Ed.). Appleton & Lange. Norwalk, CN.

Georgiou, P., Bountra, C., Bland, K.P., House, C.R. (1984). Calcium action potentials in unfertilized eggs of mice and hamsters. *Q. J. Exp. Physiol.* **69**, 365-380.

Gershman, L.C., Selden, L.A., Kinosian, H.J., Estes, J.E. (1994). Actin-bound nucleotide/divalent cation interactions. *Adv. Exp. Med. Biol.* **358**, 35-49.

Giaume, C., Spira, M.E., Korn, H. (1980). Uncoupling of invertebrate electrotonic synapses by carbon dioxide. *Neurosci. Lett.* **17,** 197-202.

Gilbert, S.F. (2000). Developmental Biology (6^{th} Ed.). Sinauer Associates. Sunderland, MA.

Gottardi, C.J., Pietrini, G., Roush, D.L., Caplan, M.J. (1993). Sorting of ion transport proteins in polarized cells. *J. Cell Sci. (Suppl.)* **17**, 13-20.

Greber, U.F., Gerace, L. (1995). Depletion of calcium from the lumen of endoplasmic reticulum reversibly inhibits passive diffusion and signal-mediated transport into the nucleus. *J. Cell Biol.* **128**, 5-14.

Gu, X., Spitzer, N.C. (1995). Distinct aspects of neuronal differentiation encoded by frequency of spontaneous Ca^{2+} transients. *Nature London* **375**, 784-787.

Guerini, D. (1988). The significance of the isoforms of plasma membrane calcium ATPase. *Cell Tissue Res.* **292**, 191-197.

Gunter, T.E., Buntinas, L., Sparagna, G., Eliseev, R., Gunter, K. (2000). Mitochondrial calcium transport: mechanisms and functions. *Cell Calcium* **28**, 285-296.

Gunter, T.E., Gunter, K.K. (2001). Uptake of calcium by mitochondria: transport and possible function. *IUBMB Life* **52**, 197-204.

Gupta, B.L., Berridge, M.J. (1966). A coat of repeating subunits on the cytoplasmic surface of the plasma membrane of the rectal papillae of the blowfly, *Calliphora erythrocephala*, (Meig.), studied in situ by electron microscopy. *J. Cell Biol.* **29**, 376-382.

Gutzeit, H.O. (1986)a. Transport of molecules and organelles in meroistic ovarioles of insects. *Differentiation* **31,** 155-165.

Gutzeit, H.O. (1986)b. The role of microfilaments in cytoplasmic streaming in *Drosophila* follicles. *J. Cell Sci.* **80**, 159-169.

Gutzeit, H.O., Haas-Assenbaum, A. (1991). The somatic envelopes around the germ-line cells of polytrophic insect follicles: structural and functional aspects. *Tissue Cell* **23**, 853-865.

Gutzeit, H.O., Huebner, E. (1986). Comparison of microfilament patterns in nurse cells of different insects with polytrophic and telotrophic ovarioles. *J. Embryol. Exp. Morphol.* **93,** 291-301.

Hajnoczky, G., Csordas, G., Madesh, M., Pacher, P. (2000). The machinery of local Ca^{2+} signalling between sarco-endoplasmic reticulum and mitochondria. *J. Physiol.* **529**, 69-81.

Haley, C.A., O'Donnell, M.J. (1997). K^+ reabsorption by the lower Malphigian tubule of *Rhodnius prolixus*: inhibition by Ba^{2+} and blockers of H^+/K^+ ATPases. *J. Exp. Biol.* **200,** 139-147.

Hamaguchi, M.S., Hamaguchi, Y. (2001). Measurement of the intracellular pH threshold for sperm aster formation in sea urchin eggs. *Dev. Growth Differ.* **43,** 447-458.

Hamel, E., Batra, J.K., Huang, A.B., Lin, C.M. (1986). Effects of pH on tubulin-nucleotide interactions. *Arch. Biochem. Biophys.* **245**, 316-330.

Hardingham, G.E., Bading, H. (1998). Nuclear calcium: a key regulator of gene expression. *Biometals* **11**, 345-358.

Hardingham, G.E., Bading, H. (1999). Calcium as a versatile second messenger in the control of gene expression. *Microsc. Res. Tech.* **46**, 348-355.

Hardingham, G.E., Chawla, S., Johnson, C.M., Bading, H. (1997). Distinct functions of nuclear and cytoplasmic calcium in the control of gene expression. *Nature* **385**, 260-265.

Hardingham, G.E., Cruzalegui, F.H., Chawla, S., Bading, H. (1998). Mechanisms controlling gene expression by nuclear calcium signals. *Cell Calcium* **23**, 131-134.

Harris, P.J., Clason, E.L. (1992). Conditions for assembly of tubulin-based structures in unfertilized sea urchin eggs. Spirals, monasters and cytasters. *J. Cell Sci.* **102**, 557-567.

Harrison, R.E., Huebner, E. (1997). Unipolar microtubule array is directly involved in nurse cell-oocyte transport. *Cell Motil. Cytoskel.* **36,** 355-362.

Harvey, W.R. (1992). Physiology of V-ATPases. *J. Exp. Biol.* **172**, 1-17.

Harvey, W.R., Wieczorek, H. (1997). Animal plasma membrane energization by chemiosmotic H^+ V-ATPases. *J. Exp. Biol.* **200,** 203-216.

Hatano, S., Kondo, H., Miki-Noumura, T. (1969). Purification of sea urchin egg actin. *Exp.Cell Res.* **55**, 275-277.

Heberlein, U., Moses, K. (1995). Mechanisms of *Drosophila* retinal morphogenesis: the virtues of being progressive. *Cell* **81**, 987-990.

Hisanaga, S., Sakai, H. (1983). Cytoplasmic dynein of the sea urchin egg. II. Purification, characterization, and interactions with microtubules and Ca-calmodulin. *J. Biochem. (Tokyo)* **93**, 87-98.

Hoth, M., Fanger, C.M., Lewis, R.S. (1997). Mitochondrial regulation of store-operated calcium signalling in T lymphocytes. *J. Cell Biol.* **137**, 633-648.

Huebner, E. (1981)a. Nurse cell-oocyte interaction in the telotrophic ovarioles of an insect, *Rhodnius prolixus*. *Tissue Cell* **13,** 105-125.

Huebner, E. (1981)b. Oocyte-follicle cell interaction during normal oogenesis and atresia in an insect. *J. Ultrastruct. Res.* **74,** 95-104.

Huebner, E. (1984). The ultrastructure and development of the telotrophic ovary. In "Insect Ultrastructure", Vol. 2. (R.C.King and H. Akai, Eds.). Plenum Press, New York, p. 3-48.

Huebner, E., Anderson, E. (1972)a. A cytological study of the ovary of *Rhodnius prolixus*. I. The ontogeny of the follicular epithelium. *J. Morph.* **136,** 459-494.

Huebner, E., Anderson, E. (1972)b. A cytological study of the ovary of *Rhodnius prolixus*. II. Oocyte differentiation. *J. Morph.* **137,** 385-416.

Huebner, E., Anderson, E. (1972)c. A cytological study of the ovary of *Rhodnius prolixus*. III. Cytoarchitecture and development of the trophic chamber. *J. Morph.* **138,** 1-40.

Huebner, E., Bjornsson, C.S. (2002). Follicle cell specialization during oogenesis: F-actin and ionic aspects. *Mol. Biol. Cell* (Suppl.).

Huebner, E., Harrison, R.E., Yeow, K. (1994). A new feeding technique for experimental and routing culturing of the insect, *Rhodnius prolixus*. *Can. J. Zool.* **72,** 2244-2247.

Huebner, E., Injeyan, H. (1980). Patency of the follicular epithelium in *Rhodnius prolixus*: a re-examination of the hormone response and technique refinement. *Can. J. Zool.* **58**, 1617-1625.

Huebner, E., Injeyan, H. (1981). Follicular modulation during oocyte development in an insect: formation and modulation of septate and gap junctions. *Dev. Biol.* **83,** 101-113.

Huebner, E., Sigurdson, W.J. (1986). Extracellular currents during insect oogenesis: special emphasis on telotrophic ovarioles. In "Ionic Currents in Development" (R. Nuccitelli, Ed.). New York, Alan R. Liss Inc. 2, 210: 155-164.

Huebner, E., Tobe, S.S., Davey, K.G. (1975.). Structural and functional dynamics of oogenesis in *Glossina austeni*: vitellogenesis with special reference to the follicular epithelium. *Tissue Cell* **7**, 535-558.

Huotari, V., Vaaraniemi, J., Lehto, V.P., Eskelinen, S (1996). Regulation of the disassembly/assembly of the membrane skeleton in Madin-Darby canine kidney cells. *J. Cell Physiol.* **167**, 121-130.

Hurst, S., Talbot, N.J., Stebbings, H. (1999). A staufen-like RNA-binding protein in translocation channels linking nurse cells to oocytes in *Notonecta* shows nucleotide-dependent attachment to microtubules. *J. Cell Sci.,* **112**, 2947-2955.

Hyams, J.S., Stebbings, H. (1979). The formation and breakdown of nutritive tubes - massive microtubular organelles associated with cytoplasmic transport. *J. Ultrastruct. Res.* **68,** 46-57.

Hyams, J.S., Stebbings, H. (1977). The distribution and function of microtubules in nutritive tubes. *Tissue Cell* **9,** 537-545.

Isaac, P.G., Bownes, M. (1982). Ovarian and fat-body vitellogenin synthesis in *Drosophila melanogaster*. *Eur. J. Biochem.* **123**, 527-534.

Jaffe, L.F. (1956). Effects of polarized light on polarity of *Fucus*. *Science* **123**, 1081-1082.

Jaffe, L.F. (1986). Ion currents in development: an overview. *Prog. Clin. Biol. Res.* **210**, 351-357.

Jaffe, L.F. (1993). Classes and mechanisms of calcium waves. *Cell Calcium* **14**, 736-745.

Jaffe, L.F. (1999). Organization of early development by calcium patterns. *BioEssays* **21**, 657-667.

Jaffe, L.F., Creton, R. (1998). On the conservation of calcium wave speeds. *Cell Calcium* **24**, 1-8.

Jaffe, L.F., Nuccitelli, R. (1974). An ultrasensitive vibrating probe for measuring steady extracellular currents. *J. Cell Biol.* **63,** 614-628.

Jaffe, L.F., Woodruff, R.I. (1979). Large electrical currents traverse developing *cecropia* follicles. *Proc. Natl. Acad. Sci. USA* **76,** 1328-1332.

Jeng, R.L., Welch, M.D. (2001). Cytoskeleton: actin and endocytosis – no longer the weakest link. *Curr. Biol.* **11**, R691-694.

Johnson, R.A. (1982). Changes in pH sensitiviy of adenylate cyclase specifically induced by fluoride and vanadate. *Arch. Biochem. Biophys.* **218**, 68-76.

Jordan, P., Karess, R. (1997). Myosin light chain-activating phosphorylation sites are required for oogenesis in *Drosophila*. *J. Cell Biol.* **139**, 1805-1819.

Jouaville, L.S., Ichas, F., Holmuhamedov, E.L., Camacho, P., Lechleiter, J.D. (1995). Synchronization of calcium waves by mitochondrial substrates in *Xenopus laevis* oocytes. *Nature* **377**, 438-441.

Kamp, T.J., Hell, J.W. (2000). Regulation of cardiac L-type calcium channels by protein kinase A and protein kinase C. *Circ. Res.* **87**, 1095-1102.

Kane, R.E. (1976). Actin polymerization and interaction with other proteins in temperature-induced gelation of sea urchin egg extracts. *J. Cell Biol.* **71**, 704-714.

King, R.C., Buning, J. (1985). The origin and functioning of insect oocytes and nurse cells. In "Comprehensive Insect Physiology, Biochemistry and Pharmacology, Vol 1. Embryogenesis and Reproduction". (G.A. Kerkut and L.I Gilbert, Eds.). Pergamon Press, New York, p. 37-82.

Koch, G.L. (1990). The endoplasmic reticulum and calcium storage. *BioEssays* **12**, 527-531.

Kramerova, I.A., Kramerov, A.A. (1999). Mucinoprotein is a universal constituent of stable intercellular bridges in *Drosophila melanogaster* germ line and somatic cells. *Dev. Dyn.* **216**, 349-360.

Kropf, D.L. (1997). Induction of polarity in fucoid zygotes. *The Plant Cell* **9**, 1011-1020.

Kubota, K., Gay, N.J. (1995). Calcium destabilizes *Drosophila* cactus protein and dephosphorylates the dorsal transcription factor. *Biochem. Biophys. Res. Commun.* **214**, 1191-1196.

Kuhtreiber, W.M., Jaffe, L.F. (1990). Detection of extracellular calcium gradients with a calcium-specific vibrating electrode. *J. Cell Biol.* **110,** 1565-1574.

Kume, S., Muto, A., Inoue, T., Suga, K., Okano, H., Mikoshiba, K. (1997). Role of inositol 1,4,5-trisphosphate receptor in ventral signaling in *Xenopus* embryos. *Science* **278**, 1940-1943.

Kunkel J.G., Faszewski, E. (1995). Pattern of potassium ion and proton currents in the ovariole of the cockroach, *Periplaneta americana*, indicates future embryonic polarity. *Biol. Bull.* **189,** 197-198.

Kurieshy, N., Sapountzi, V., Prag, S., Anilkumar, N., Adams, J.C. (2002). Fascins, and their roles in cell structure and function. *BioEssays* **24**, 350-361.

Lamb, J.A., Allen, P.G., Tuan, B.Y., Janmey, P.A. (1993). Modulation of gelsolin function: Activation at low pH overrides calcium requirement. *J. Biol. Chem.* **268**, 8999-9004.

Larson, R.E., Goldenring, J.R., Vallano, M.L., DeLorenzo, R.J. (1985). Identification of endogenous calmodulin-dependent kinase and calmodulin-binding proteins in cold-stable microtubule preparations from rat brain. *J. Neurochem.* **44**, 1566-1574.

Leitch, B., Finbow, M.E. (1990). The gap junction-like form of a vacuolar proton channel component appears not to be an artifact of isolation: an immunocytochemical localization study. *Exp. Cell Res.* **190**, 218-226.

Leite, M.F., Hirata, K., Pusl, T., Burgstahler, A.D., Okazaki, K., Ortega, J.M., Goes, A.M., Prado, M.A., Spray, D.C., Nathanson, M.H. (2002). Molecular basis for pacemaker cells in epithelia. *J. Biol. Chem.* **277**, 16313-16323.

Levin, M. (2002). Isolation and community: a review of gap-junctional communication in embryonic patterning. *J. Membr. Biol.* **185,** 177-192.

Lin, H. Yue, L., Spradling, A.C. (1994). The *Drosophila* fusome, a germline-specific organelle, contains membrane skeletal proteins and functions in cyst formation. *Development* **120**, 947-956.

Lipp, P., Bootman, M.D. (1997). To quark or to spark, that is the question. *J. Physiol.* **502**, 1.

Liu, S., Taffet, S., Stoner, L., Delmar, M., Vallano, M.L., Jalife, J. (1993). A structural basis for the unequal sensitivity of the major cardiac and liver gap junctions to intracellular acidification: the carboxy tail length. *Biophys. J.* **64**, 1422-1433.

Liu, L., Hammar, K., Smith, P.J., Inoue, S., Keefe, D.L. (2001). Mitochondrial modulation of calcium signaling at the initiation of development. *Cell Calcium* **30**, 423-433.

Lodish, H., Berk, A., Zipursky, S.L., Matsudaira, P., Baltimore, D., Darnell, J. (2000). Molecular Cell Biology. 4th Ed. W. H. Freeman and Company. New York.

Loewenstein, A. (1999). The touchstone of life. New York, Oxford University Press.

Lutz, D.A., Huebner, E. (1980). Development and cellular differentiation of an insect telotrophic ovary (*Rhodnius prolixus*). *Tissue Cell* **12,** 773-794.

Lutz, D.A., Huebner, E. (1981). Development of nurse cell-oocyte interactions in the insect telotrophic ovary (*Rhodnius prolixus*). *Tissue Cell* **13,** 321-335.

Macgregor, H.C., and Stebbings, H. (1970). A massive system of microtubules associated with cytoplasmic movement in telotrophic ovarioles. *J. Cell Sci.* **6**, 431-439.

Machesky, L.M., Way, M. (1998). Actin branches out. *Nature*, **394**, 125-126.

Mahowald, A.P. (1971). The formation of ring canals by cell furrows in *Drosophila. Z. Zellforsch Mikrosk. Anat.* **118**, 162-167.

Maslanski, J.A., Leshko, L., Busa, W.B. (1992). Lithium-sensitive production of inositol phosphates during amphibian embryonic mesoderm induction. *Science* **256**, 243-245.

McDonald, J.M., Bruns, D.E., Jarett, L. (1976). The ability of insulin to alter the stable calcium pools of isolated adipocyte subcellular fractions. *Biochem. Biophys. Res. Commun.* **71**, 114-121.

McPherson, S.M.G., Huebner, E. (1993). Dynamics of the oocyte cortical cytoskeleton during oogenesis in *Rhodnius prolixus*. *Tissue Cell* **25,** 399-421.

Means, A.R. (1994). Calcium, calmodulin, and cell cycle regulation. *FEBS Lett.* **347**, 1-4.

Melo, A.C., Valle, D., Machado, E.A., Salerno, A.P., Paiva-Silva, G.O., Cunha, E., Silva, N.L., de Souza, W., Masuda, H. (2000). Synthesis of vitellogenin by the follicle cells of *Rhodnius prolixus*. *Insect Biochem. Mol. Biol.* **30**, 549-557.

Meyer, T., Streyer, L. (1991). Calcium spiking. *Annu. Rev. Biophys. Biophys. Chem.* **20**, 153-174.

Miller, A.L., Fluck, R.A., McLaughlin, J.A., Jaffe, L.F. (1993). Calcium buffer injections inhibit cytokinesis in Xenopus eggs. *J. Cell Sci.* **106**, 523-534.

Milner, R.E., Famulski, K.S., Michalak, M. (1992). Calcium binding proteins in the sarcoplasmic/endoplasmic reticulum of muscle and nonmuscle cells. *Mol. Cell Biochem.* **112**, 1-13.

Miyazaki, S., Hagiwara, S. (1976). Electrical properties of the *Drosophila* egg membrane. *Dev. Biol.* **53**, 91-100.

Mohler, P.J., Gramolini, A.O., Bennett, V. (2002). Ankyrins. *J. Cell Sci.* **115**, 1565-1566.

Montero, M., Brini, M., Marsault, R., Alvarez, J., Sitia, R., Pozzan, T., Rizzuto, R. (1995). Monitoring dynamic changes in free Ca^{2+} concentration in the endoplasmic reticulum of intact cells. *EMBO J.* **14**, 5467-5475.

Mostov, K.E., Cardone, M.H. (1995). Regulation of protein traffic in polarized epithelial cells. *BioEssays* **17**, 129-138.

Mooseker, M.S., Cheney, R.E. (1995). Unconventional myosins. *Annu. Rev. Cell Dev. Biol.* **11**, 633-675.

Moreno, D. H. (1999). Molecular and functional diversity of voltage-gated calcium channels. *Ann. NY Acad. Sci.* **868**, 102-117.

Munz, A. (1988). Heterologous gap junctions between oocyte and follicle cells of an insect, *Dysdercus intermedius*, and their potential roles as ion current pathways. *Cell Tissue Res.* **252**, 147-155.

Munz, A., Dittmann, F. (1987). Voltage gradients and microtubules both involved in intracellular protein and mitochondria transport in the telotrophic ovariole of *Dysdercus intermedius*. *Dev. Biol.* **196**, 391-396.

Nelson, M.T., Cheng, H., Rubart, M., Santana, L.F., Bonev, A.D., Knot, H.J., Lederer, W.J. (1995). Relaxation of arterial smooth muscle by calcium sparks. *Science* **270**, 633-637.

Nelson, N. (1991). Structure and pharmacology of the proton-ATPases. *Trends Pharmacol. Sci.* **12**, 71-75.

Nelson, W.J., Veshnock, P.J. (1987). Ankyrin binding to $(Na^+ + K^+)$ATPase and implications for the organization of membrane domains in polarized cells. *Nature*, **328**, 533-536.

Nordin, J.H., Beaudoin, E.L., Liu, X. (1990). Coincident expression of the processing proteinase for an insect vitellin with acidification of yolk granules. *J. Cell Biol.* **111,** 485a.

Nordin, J.H., Beaudoin, E.L., Liu, X. (1991). Acidification of yolk granules in *Blattella germanica* eggs coincident with proteolytic processing of vitellin. *Arch. Insect Biochem. Physiol.* **18,** 177-192.

Nuccitelli, R. (1986). A two-dimensional vibrating probe with computerized graphics display. In Ion Currents in Development. Alan R. Liss, New York. pp. 13-20.

O'Donnell, M.J. (1985). Calcium action potentials in the developing oocytes of an insect, *Rhodnius prolixus*. *J. Exp. Biol.* **119,** 287-300.

O'Donnell, M.J. (1986). Action potentials in *Rhodnius* oocytes: repolarization is sensitive to potassium channel blockers. *J. Exp. Biol.* **126**, 119-132.

O'Donnell, M.J. (1988). Potassium channel blockers unmask electrical excitability of insect follicles. *J. Exp. Zool.* **245**, 137-143.

O'Donnell, M.J., Sharda, R.K. (1994). Membrane potential and pH regulation in vitellogenic follicles of an insect, *Rhodnius prolixus*. *Physiol. Zool.* **67,** 7-28.

Ogawa, Y., Tanokura, M. (1984). Calcium binding to calmodulin: effects of ionic strength, Mg^{2+}, pH and temperature. *J. Biochem. (Tokyo)* **95**, 19-28.

Okamura, H., Yashuhara, J.C., Fambrough, D.M., Takeyasu, K. (2003). P-type ATPases in *Caenorhabditis* and *Drosophila*: Implications for evolution of the P-type ATPase subunit families with special reference to the Na,K-ATPase and H,K-ATPase subgroup. *J. Membr. Biol.* **191**, 13-24.

Olmsted, J.B., Borisy, G.G. (1975). Ionic and nucleotide requirements for microtubule polymerization in vitro. *Biochemistry* **14**, 2996-3005.

Ono, S., Yamakita, Y., Yamashiro, S., Matsudaira, P.T., Gnarra, J.R., Obinata, T., Matsumura, F. (1997). Identification of an actin-binding region and a protein kinase C phosphorylation site on human fascin. *J. Biol. Chem.* **272**, 2527-2533.

Overall, R. Jaffe, L.F. (1985). Patterns of ionic current through *Drosophila* follicles and eggs. *Dev. Biol.* **108,** 102-119.

Parton, R.G., Dotti, C.G., Bacallao, R., Kurtz, I., Simons, K., Prydz, K. (1991). pH-induced microtubule-dependent redistribution of late endosomes in neuronal epithelial cells. *Cell Biol.* **113,** 261-274.

Pederson, P.L., Carafoli, E. (1987). Ion motive ATPases. I. Ubiquity, properties and significance to cell function. *Trends Biochem. Sci.* **12**, 146-150.

Perrachia, C., Perrachia, L.L. (1980)a. Gap junction dynamics: reversible effects of divalent cations. *J. Cell Biol.* **87**, 708-718.

Perrachia, C., Perrachia, L.L., (1980)b. Gap junction dynamics: reversible effects of hydrogen ions. *J. Cell Biol.* **87,** 719-727.

Peterson, O.H., Burdakov, D., Tepikin, A.V. (1999). Polarity in intracellular calcium signaling. *BioEssays* **21**, 851-860.

Petersen, O.H., Gerasimenko, O.V., Gerasimenko, J.V., Mogami, H., Tepikin, A.V. (1998). The calcium store in the nuclear envelope. *Cell Calcium* **23**, 87-90.

Phelan, P., Bacon, J.P., Davies, J.A., Stebbings, L.A., Todman, M.G., Avery, L., Baines, R.A., Barnes, T.M., Ford, C., Hekimi, S., Lee, R., Shaw, J.E., Starich, T.A.,

Curtin, K.D., Sun, Y.A., Wyman, R.J. (1998). Innexins: a family of invertebrate gap-junction proteins. *Trends Genet.* **14**, 348-349.

Pollard, T.D., Weihing, R.R. (1974). Actin and myosin in cell movements. *Crit. Rev. Biochem.* **2,** 1-65.

Pozzan, T., Magalhaes, P., Rizzuto, R. (2000). The comeback of mitochondria to calcium signalling. *Cell Calcium* **28**, 279-283.

Pratt, G.E., Davey, K.G. (1972). The corpus allatum and oogenesis in *Rhodnius prolixus* (Stal). I. The effects of allatectomy. *J. Exp. Biol.* **56,** 201-214.

Pu, R., Robinson, K.R. (1998). Cytoplasmic calcium gradients and calmodulin in the the early development of the fucoid alga, *Pelvetia compressa. J. Cell Sci.* **111**, 3197-3207.

Quist, A.P., Rhee, S.K., Lin, H., Lal, R. (2000). Physiological role of gap-junctional hemichannels. Extracellular calcium-dependent isosmotic volume regulation. *J. Cell Biol.* **148**, 1063-1074.

Rappaport, R. (1996). Cytokinesis in Animal Cells. Cambridge University Press.

Rasmussen, H. (1981). Synarchic regulation and sensitivity modulation in hormone action. *Bull. Schweiz Akad. Med. Wiss.* **82**, 131-147.

Regula, C.S., Pfeiffer, J.R., Berlin, R.D. (1981). Microtubule assembly and disassembly at alkaline pH. *J. Cell Biol.* **89,** 45-53.

Reynolds, R.C., Haugaard, N. (1967). The effect of variations of pH upon the activation of phosphorylase by epinephrine in perfused contracting heart, liver slices, and skeletal muscle. *J. Pharm. Exp. Ther.* **156,** 417-425.

Riparbelli, M.G., Callaini, G. (1995). Cytoskeleton of the *Drosophila* egg chamber: new observations on microfilament distribution during oocyte growth. *Cell Motil. Cytoskel.* **31,** 298-306.

Rizzuto, R., Pinton, P., Carrington, W., Fay, F.S., Fogarty, K.E., Lifshitz, L.M., Tuft, R.A., Pozzan, T. (1998). Close contacts with the endoplasmic reticulum as determinants of mitochondrial Ca^{2+} responses. *Science* **280**, 1763-1766.

Robinson, D.N., Cant, K., Cooley, L. (1994). Morphogenesis of *Drosophila* ovarian ring canals. *Development* **120**, 2105-2025.

Robinson, D.N., Cooley, L. (1997). *Drosophila* kelch is an oligomeric ring canal actin organizer. *J. Cell Biol.* **138**, 799-810.

Robinson, D.N., Smith-Leiker, T.A., Sokol, N.S., Hudson, A.M., Cooley, L. (1997). Formation of the *Drosophila* ovarian ring canal inner rim depends on cheerio. *Genetics* **145**, 1063-1072.

Robinson, K.R. (1996). Calcium and the photopolarization of *Pelvetia* zygotes. *Planta* **198**, 378-384.

Robinson, K.R., Jaffe, L.F. (1975). Polarizing fucoid eggs drive a calcium current through themselves. *Science* **187**, 70-72.

Rozental, R., Srinivas, M., Spray, D.C., (2001). How to close a gap junction channel. Efficacies and potencies of uncoupling agents. *Methods Mol. Biol.* **154,** 447-476.

Rutter, G.A., Theler, J.M., Murgia, M., Wollheim, C.B., Pozzan, T., Rizzuto, R. (1993). Stimulated Ca^{2+} influx raises mitochondrial free Ca^{2+} to supramicromolar levels in a pancreatic beta-cell line. Possible role in glucose- and agonist-induced insulin secretion. *J. Biol. Chem.* **268**, 22385-22390.

Rutter, G.A., Fasolato, C., Rizzuto, R. (1998). Calcium and organelles: a two-sided story. *Biochem. Biophys. Res. Commun.* **253**, 549-557.

Saini, Y., Kung, C. (1994). Ion channel regulation by calmodulin. *FEBS Lett.* **350**, 155-158.

Sanderson, M.J., Charles, A.C. Boitano, S., Dirksen, E.R. (1994). Mechanisms of intercellular calcium signaling. *Mol. Cell Endocrinol.* **98**, 173-187.

Sanderson, M.J., Charles, A.C., Dirksen, E.R. (1990). Mechanical stimulation and intercellular communication increases intracellular Ca^{2+} in epithelial cells. *Cell Regul.* **1**, 585-596.

Santella, L. (1996). Calcium regulation and calcium function in the nucleus of starfish oocytes. *Invert. Reprod. Dev.* **30**, 7-15.

Santella, L. (1998). The role of calcium in the cell cycle: facts and hypothesis. *Biochem. Biophys. Res. Commun.* **244**, 317-324.

Santella, L., Carafoli, E. (1997). Calcium signaling in the cell nucleus. *FASEB J.* **11**, 1091-1109.

Santella, L., Kozyuka, K. (1994). Reinitiation of meiosis in starfish oocytes requires an increase in nuclear Ca^{2+}. *Biochem. Biophys. Res. Commun.* **203**, 674-680.

Santella, L., Kozyuka, K. (1997). Effects of 1-methyladenine on nuclear Ca^{2+} transients and meiosis resumption in starfish oocytes are mimicked by the nuclear injection of inositol 1,4,5-trisphosphate and cADP-ribose. *Cell Calcium* **22**, 11-20.

Schatten, G., Bestor, T., Balczon, R., Henson, J., Schatten, H. (1985). Intracellular pH shift leads to microtubule assembly and microtubule-mediated motility during sea urchin fertilization: correlations between elevated intracellular pH and

microtubule activity and depressed intracellular pH and microtubule disassembly. *Eur. J. Cell Biol.* **36,** 116-127.

Schatten, G., Bestor, T., Balczon, R., Henson, J., Schatten, H. (1986). Intracellular pH shift initiates microtubule-mediated motility during sea urchin fertilization. *Ann. NY Acad. Sci.* **466,** 940-944.

Serras, F., Buultjens, T.E., Finbow, M.E. (1988). Inhibition of dye-coupling in *Patella* (Mollusca) embryos by microinjection of antiserum against *Nephrops* (Arthropoda) gap junctions. *Exp. Cell Res.* **179**, 282-288.

Setlow, B., Setlow, P. (1980). Measurements of the pH within dormant and germinated bacterial spores. *Proc. Natl. Acad. Sci. USA* **77,** 2474-2476.

Sevala, V.L., Davey, K.G. (1993). Juvenile hormone dependent phosphorylation of a 100 kDa polypeptide is mediated by protein kinase C in the follicle cells of *Rhodnius prolixus*. *Invert. Reprod. Dev.* **23**, 189-193.

Sevala, V.L., Davey, K.G. (1989). Action of juvenile hormone on the follicle cells of *Rhodnius prolixus*: Evidence for a novel regulatory mechanism involving protein kinase C. *Experentia (BASEL)* **45**, 355-356.

Shapiro, B.M., Cook, S., Quest, A.F., Oberdorf, J., Wothe, D. (1990). Molecular mechanisms of sea-urchin sperm activation before fertilization. *J. Reprod. Fertil. Suppl.* **42,** 3-8.

Shen, S.S., Steinhardt, R.A. (1978). Direct measurement of intracellular pH during metabolic derepression of the sea urchin egg. *Nature London* **272,** 253-254.

Shen, S.S., Steinhardt, R.A. (1980). Intracellular pH controls the development of new potassium conductance after fertilization of the sea urchin egg. *Exp. Cell Res.* **125**, 55-61.

Shore, G.C., Tata, J.R. (1977). Two fractions of rough endoplasmic reticulum from rat liver. I. Recovery of rapidly sedimenting endoplasmic reticulum in association with mitochondria. *J. Cell Biol.* **72**, 714-725.

Sigurdson, W.J. (1984). Bioelectric aspects of the *Rhodnius prolixus* ovariole: extracellular current mapping during oogenesis. Master's Thesis, Department of Zoology, University of Manitoba, Winnipeg, Canada.

Silver, R.A., Lamb, A.G., Bolsover, S.R. (1990). Calcium hotspots caused by L-channel clustering promote morphological changes in neuronal growth cones. *Nature* **343**, 751-754.

Simon, J.R., Parsons, S.F., Salmon, E.D. (1992). Buffer conditions and nontubulin factors critically affect the microtubule dynamic instability of sea urchin egg tubulin. *Cell Motil. Cytoskel.* **21**, 1-14.

Singleton, K., Woodruff, R.I. (1994). The osmolarity of adult *Drosophila* hemolymph and its effect on oocyte-nurse cell electrical polarity. *Dev. Biol.* **161**, 154-167.

Sokol, N.S., Cooley, L. (1999). *Drosophila* filamin encoded by the cheerio locus is a component of ovarian ring canals. *Curr. Biol.* **9**, 1221-1230.

Somiesky, P., Nagel, W. (2001). Measurement of pH gradients using an ion-sensitive vibrating probe technique (IP). *Pflugers Arch. Eur. J. Physiol.* **442,** 142-149.

Sommer, J.R., Johnson, E.A. (1970). Comparative ultrastructure of cardiac cell membrane specializations. A review. *Am. J. Cardiol.* **25**, 184-194.

Southwick, F.S., (2000). Gelsolin and ADF/cofilin enhance the actin dynamics of motile cells. *Proc. Natl. Acad. Sci. USA* **97,** 6936-6938.

Speksnijder, J.E., Miller, A.L., Weisenseel, M.H., Chen, T.H., Jaffe, L.F. (1989). Calcium buffer injections block fucoid egg development by facilitating calcium diffusion. *Proc. Natl. Acad. Sci. (USA)* **86**, 6607-6611.

Speksnijder, J.E., Sardet, C., Jaffe, L.F. (1990). The activation wave of calcium in the ascidian and its role in ooplasmic segregation. *J. Cell Biol.* **110**, 1589-1590.

Spudich, J.A. (1974). Biochemical and structural studies of actomyosin-like proteins from non-muscle cells. II. Purification, properties, and membrane association of actin from amoebae of *Dictyostelium discoideum. J. Biol. Chem.* **249**, 6013-6020.

Stachel, S.E., Grunwald, D.J., Myers, P.Z. (1993). Lithium perturbation and goosecoid expression identify a dorsal specification pathway in the pregastrula zebrafish. *Development* **117**, 1261-1274.

Stebbings, H. (1971). Influence of vinblastine sulphate on the deployment of microtubules and ribosomes in telotrophic ovarioles. *J. Cell Sci.* **8**, 111-125.

Stebbings, H. (1981). Observations on cytoplasmic transport along ovarian nutritive tubes of polyphagous coleopterans. *Cell Tissue Res.* **220**, 153-161.

Stebbings, H. (1997). Direct evidence for the nature of the binding of mitochondria to microtubules in ovarian nutritive tubes of an hemipteran insect. *Cell Tissue Res.* **289**, 333-337.

Stebbings, H. (2001). Cytoskeleton-dependent transport and localization of mRNA. *Int. Rev. Cytol.* **211**, 1-31.

Stebbings, H., Hunt, C. (1987). The translocation of mitochondria along insect ovarian microtubules from isolated nutritive tubes: a simple reactivated model. *J. Cell Sci.* **88**, 641-648.

Stebbings, L.A., Todman, M.G., Phillips, R., Greer, C.E., Tam, J., Phelan, P., Jacobs, K., Bacon, J.P., Davies, J.A. (2002). Gap junctions in *Drosophila*: developmental expression of the entire innexin gene family. *Mech. Dev.* **113**, 197-205.

Stephen, S., Talbot, N.J., Stebbings, H. (1999). Poly(A) mRNA is attached to insect ovarian microtubules *in vivo* in a nucleotide-sensitive manner. *Cell Motil. Cytoskeleton* **43**, 159-166.

Steinhardt, R.A., Mazia, D. (1973). Development of K-conductance and membrane potentials in unfertilized sea urchin eggs after exposure to NH_4OH. *Nature London* **241**, 400-401.

Stricker, S.A. (1999). Comparative biology of calcium signaling during fertilization and egg activation in animals. *Dev. Biol.* **211**, 157-176.

Strogatz, S.H., Stewart, I. (1993). Coupled oscillators and biological synchronization. *Sci. Am.* **269**, 102-107.

Stynen, D., Woodruff, R.I., Telfer, W.H. (1988). Effects of ionophores on vitellogenin uptake by *Hyalophora* oocytes. *Arch. Insect Biochem. Physiol.* **8,** 261-276.

Sun, T.Q., Wyman, R.J. (1987). Lack of an oocyte to nurse cell voltage difference in *Drosophila*. *Neurosci.* **13**, 1139.

Sun, T.Q., Wyman, R.J. (1989). The *Drosophila* egg chamber: external ionic currents and the hypothesis of electrophoretic transport. *Biol. Bull.* **176(S)**, 79-85.

Sun, Y., Wyman, R.J. (1993). Reevaluation of electrophoresis in the *Drosophila* egg chamber. *Dev. Biol.* **155**, 206-215.

Suprenant, K.A. (1989). Alkaline pH favors microtubule self-assembly in surf clam, *Spisula solidissima*, oocyte extracts. *Exp. Cell Res.* **184,** 167-180.

Suprenant, K.A. (1991). Unidirectional microtubule assembly in cell-free extracts of *Spisula solidissima* oocytes is regulated by subtle changes in pH. *Cell Motil. Cytoskel.* **19,** 207-220.

Svitkina, T.M., Borisy, G.G., (1998). Arp2/3 complex and actin depolymerizing factor/cofilin in dendritic organization and treadmilling of actin filament array in lamellopodia. *J. Cell Biol.* **145,** 1009-1026.

Swerdlow, B.M., Setlow, B., Setlow, P. (1981). Levels of H^+ and other monovalent cations in dormant and germinating spores of *Bacillus megaterium*. *J. Bacteriol.* **148,** 20-29.

Telfer, W.H., (1965). The mechanism and control of yolk formation. *Annu. Rev. Entomol.* **10,** 161-184.

Telfer, W.H. (1975). Development and physiology of the oocyte-nurse cell syncytium. *Adv. Insect Physiol.* **11,** 223-319.

Telfer, W.H., Woodruff, R.I., Huebner, E. (1981). Electrical polarity and cellular differentiation in insect meroistic ovaries. *Am. Zool.* **21,** 675-686.

Telfer, W.H., Huebner, E., Smith, D.S., (1982). The cell biology of vitellogenic follicles in *Hyalophora* and *Rhodnius*. In "Insect Ultrastructure" (RC King and H Akai, Eds.). New York, Plenum Press. 1: 118-149.

Thayer, S.A., Miller, R.J. (1990). Regulation of the intracellular free calcium concentration in single rat dorsal root ganglion neurons in vitro. *J. Physiol.* **425**, 85-115.

Theriot, J.A. (1997). Accelerating on a treadmill: ADF/cofilin promotes rapid actin filament turnover in the dynamic cytoskeleton. *J. Cell Biol.* **136,** 1165-1168.

Therkauf, W.E. (1994). Microtubules and cytoplasm organization during *Drosophila* oogenesis. *Dev. Biol.* **165**, 352-360.

Tilney, L.G., Connelly, P., Smith, S., Guild, G.M. (1996)a. F-actin bundles in *Drosophila* bristles are assembled from modules composed of short filaments. *J. Cell Biol.* **135**, 1291-1308.

Tilney, L.G., Jaffe, L.A. (1980). Actin, microvilli, and the fertilization cone of sea urchin eggs. *J. Cell Biol.* **87,** 771-782.

Tilney, L.G., Kiehart, D.P., Sardet, C., Tilney, M. (1978). Polymerization of actin IV. Role of Ca^{++} and H^{+} in the assembly of actin and in membrane fusion in the acrosomal reaction of echinoderm sperm. *J. Cell Biol.* **77,** 536-550.

Tilney, L.G., Tilney, M.S., Guild, G.M. (1996)b. Formation of actin filament bundles in the ring canals of developing *Drosophila* follicles. *J. Cell Biol.* **133**, 61-74.

Tinel, H., Cancela, J.M., Mogami, H., Gerasimenko, J.V., Gerasimenko, O.V., Tepikin, A.V., Petersen, O.H. (1999). Active mitochondria surrounding the pancreatic acinar granule region prevent spreading of inositol trisphosphate-evoked local cytosolic Ca^{2+} signals. *EMBO J.* **18**, 4999-5008.

Tkachuk, V.A., Men'shikov, M. (1981). Effect of pH on Ca-binding properties of calmodulin and on its interaction with Ca-dependent phosphodiesterase of cyclic nucleotides. *Biokhimiia* **46**, 963-973.

Toker, A. (1998). Signaling through protein kinase C. *Frontiers Biosci.* **3**, 1134-1147.

Trivedi, B., Dansforth, W.H. (1966). Effect of pH on the kinetics of frog muscle phosphofructokinase. *J. Biol. Chem.* **241,** 4110-4114.

Valdimarsson, G. (1987). The development of microtubular arrays in the germ tissue of an insect telotrophic ovary. M. Sc. Thesis. University of Manitoba. Winnipeg, MB, Canada.

Valdimarsson, G., Huebner, E. (1989). The development of microtubular arrays in the germ tissue of an insect telotrophic ovary. *Tissue Cell* **21**, 123-138.

van Eldik, L.J., Hertzberg, E.L., Berdan, R.C., Gilula, N.B. (1985). Interaction of calmodulin and other calcium-modulated proteins with mammalian and arthropod junctional membrane proteins. *Biochem. Biophys. Res. Commun.* **126**, 825-832.

Vanderberg, J.P. (1963). Synthesis and transfer of DNA, RNA, and protein during oogenesis in *Rhodnius prolixus* (Hemiptera). *Biol. Bull.* **125,** 556-575.

Verachtert, B., DeLoof, A. (1986). Electric currents around the polytrophic ovarian follicles of *Sarcophaga bullata* and the panoistic follicles of *Locusta migratoria.* In "Ionic Currents Currents in Development". (R. Nuccitelli, Ed.). New York, AR Liss. pp. 173-180.

Verhey, K.J., Lizotte, D.L., Abramson, T., Barenboim, L., Schnapp, B.J., Rapoport, T.A. (1998). Light chain-dependent regulation of kinesin's interaction with microtubules. *J. Cell Biol.* **143**, 1053-1066.

Voet, D., Voet, J.G. (1990). Biochemistry. John Wiley & Sons. New York.

Vogel, H.J. (1994). Calmodulin: a versatile calcium mediator protein. *Biochem Cell Biol.* **72**, 357-376.

Wallmark, B., Lorentzon, P., Sachs, G. (1990). The gastric H^+,K^+-ATPase. *J. Intern. Med. Suppl.* **732**, 3-8.

Warn, R.M., Gutzeit, H.O., Smith, L., Warn, A. (1985). F-actin rings are associated with the ring canals of the *Drosophila* egg chamber. *Exp. Cell Res.* **157**, 355-363.

Watson, A.J., Huebner, E. (1986). Modulation of cytoskeletal organization during insect follicle cell morphogenesis. *Tissue Cell* **18,** 741-752.

Webb, S.E., Lee, K.W., Karplus, E., Miller, A.L. (1997). Localized calcium transients accompany furrow positioning, propagation, and deepening during the early cleavage period of zebrafish embryos. *Dev. Biol.* **192**, 78-92.

Welch, M.D., Mallavarapu, A., Rosenblatt, J., Mitchison, T.J. (1997). Actin dynamics in vivo. *Curr. Opin. Cell Biol.* **9**, 54-61.

Werth, J.L., Thayer, S.A. (1994). Mitochondria buffer physiological calcium loads in cultured rat dorsal root ganglion neurons. *J. Neurosci.* **14**, 348-356.

Wigglesworth, V.B. (1936). The function of the corpus allatum in the growth and reproduction of *Rhodnius prolixus* (Hemiptera). *Q. J. Micr. Sci.* **79**, 91-121.

Wieczorek, H., Brown, D., Grinstein, S., Ehrenfeld, J., Harvey, W.R. (1999). Animal plasma membrane energization by proteon-motive V-ATPases. *BioEssays* **21**, 637-648.

Winkler, M.M. (1982). Regulation of protein synthesis in sea urchin eggs by intracellular pH. In "Intracellular pH: Its Measurement, Regulation, and Utilization in Cellular Functions". (R. Nuccitelli and D.W. Deamer, Eds). New York: Liss, pp. 325-240.

Winkler, M.M., Steinhardt, R.A. (1981). Activation of protein synthesis in a sea urchin cell-free system. *Dev. Biol.* **84,** 432-439.

Wollberg, Z., Cohen, E., Kalina, M. (1976). Electrical properties of developing oocytes in the migratory locust, *Locusta migratoria. J. Cell Physiol.* **88**, 145-158.

Woodruff, R.I. (1989). Charge-dependent molecular movement through intercellular bridges in *Drosophila* follicles. *Biol. Bull. Woods Hole* **176(S)**, 110-117.

Woodruff, R.I., Dittmann, F., Telfer, W.H. (1998). Ca^{2+} current from oocyte to nurse cells and suppression of uridine incorporation in the germinal vesicle of *Hyalophora cecropia. Invert. Reprod. Dev.* **34**, 157-164.

Woodruff, R.I., Huebner, E., Telfer, W.H. (1986)a. Electrical properties of insect ovarian follicles: some challenges of a multicellular system. In "Ion Currents in Development". (R. Nuccitelli, Ed.). New York, AR Liss. pp. 147-154.

Woodruff, R.I., Huebner, E., Telfer, W.H. (1986)b. Ion currents in *Hyalophora* ovaries: the role of the epithelium and the intercellular spaces of the trophic cap. *Dev. Biol.* **117,** 405-416.

Woodruff, R.I., Kulp, J.H., LaGaccia, E.D. (1988). Electrically mediated protein movement in *Drosophila* follicles. *Roux's Arch. Dev. Biol.* **197**, 231-238.

Woodruff, R.I., Telfer, W.H. (1973). Polarized intercellular bridges in ovarian follicles of the cecropia moth. *J. Cell Biol.* **58**, 172-188.

Woodruff, R.I., Telfer, W.H. (1980). Electrophoresis of proteins in intercellular bridges. *Nature* **286**, 84-86.

Woodruff, R.I., Telfer, W.H. (1990). Activation of a new physiological state at the onset of vitellogenesis in *Hyalophora* follicles. *Dev. Biol.* **138,** 410-420.

Woodruff, R.I., Telfer, W.H. (1994). Steady-state gradient in calcium ion activity across the intercellular bridges connecting oocytes and nurse cells in *Hyalophora cecropia*. *Arch. Insect Biochem. Physiol.* **25**, 9-20.

Xia, S.L., Gelband, C.H., Wingo, C.S. (1999). Cation channels of the rabbit outer medullary collecting duct. *Semin. Nephrol.* **19**, 472-476.

Yajima, M., Ui, M. (1975). Hydrocortisone restoration of the pH-dependent metabolic responses to catecholamines. *Am. J. Physiol.* **228,** 1053-1059.

Yamakita, Y., Ono, S., Matsumura, F., Yamashiro, S. (1996). Phosphorylation of human fascin inhibits its actin binding and bundling activities. *J. Biol. Chem.* **271,** 12632-12638.

Yeow, K. (1996). Development and dynamics of F-actin in the germ tissue of the telotrophic ovariole of *Rhodnius prolixus*. M. Sc. Thesis. University of Manitoba. Winnipeg, MB, Canada.

Yoshida, T., Kamiya, T., Imanaka-Yoshida, K., Sakakura, T. (1999). Low cytoplasmic pH causes fragmentation and dispersal of the Golgi apparatus in human hepatoma cells. Int. *J. Exp. Pathol.* **80**, 51-57.

Zimmermann, B. (2000). Control of $InsP_3$-induced Ca^{2+} oscillations in permeabilized blowfly salivary glands: contribution of mitochondria. *J. Physiol. (London)* **525**, 707-719.